Identification, Optimization, and Evaluation of Inositol Phosphorylceramide Synthase Inhibitors as New Antileishmanials

COURTNEY NICOLE COVINGTON

Identification, Optimization, and Evaluation of Inositol Phosphorylceramide Synthase Inhibitors as New Antileishmanials

A thesis submitted in partial fulfilment of the requirements for the degree of Doctor of Philosophy from the University of Durham

Courtney Nicole Covington

January 2021

Department of Chemistry

Abstract

COVINGTON, Courtney Nicole. **Identification, Optimization, and Evaluation of Inositol Phosphorylceramide Synthase Inhibitors as New Antileishmanials**

Leishmaniasis is a Neglected Tropical Disease caused by the protozoan parasites of the genus *Leishmania*. Globally, an estimated 350 million are at risk of infection, and more than 12 million people are directly affected by the disease. With no effective vaccines available, the control strategy relies solely on chemotherapy. Current treatments for this disease suffer from multiple toxicities, increasing parasitic resistance, and are often expensive. Thus, there is an urgent need for the development of novel drug therapies with improved pharmacokinetic and safety profiles. *Leishmania major* inositol phosphorylceramide synthase (*Lmj*IPCS), an essential enzyme involved in the biosynthesis of sphingolipids, has been identified as an attractive drug target. As this enzyme has no mammalian equivalent, selective drug candidates can be created with minimal host toxicity. A 1.8 million compound library was screened for activity against *Lmj*IPCS and the parasite. Two 3H-benzazepine analogues, found to be potent *Lmj*IPCS inhibitors, were selected for further investigation. Initial efforts focused on the synthesis of a series of 4-fluoroindole substituted benzazepine analogues, primarily with variations of the amine substituent and modifications of the N-alkyl linker. These compounds were most active against *L. major* promastigotes and several were identified as selective inhibitors of *Lmj*IPCS. In an attempt to improve metabolic stability, the N-alkyl linker was extended providing benzazepine **74**. With an EC_{50} of 1.42 μM, this analogue which exceed the inhibition of lead benzazepine **33a** (EC_{50} = 3.23 μM) while maintaining *Lmj*IPCS selectivity. In an effort to explore the necessity of the heterocycle on antileishmanial activity, phenethylamine based acyclic analogues were prepared. Although this more easily accessible acyclic series displayed moderate promastigote growth inhibition, the acyclic analogues more exhibited less species-dependent variation in activity. Overall, this investigation shows that 4-fluoroindole substituted benzazepine analogues are good candidates for further development of new antileishmanials.

Table of Contents

Abbreviations

π	Hansch partition coefficient
σ	Hammett substituent constant
4 Å MS	4 Å molecular sieves
AbA	Aureobasidin A
AIDS	Acquired Immunodeficiency Syndrome
Amp B	Amphotericin B
Ar	Aromatic group
ASAP	Atmospheric sample analysis probe
AUR1	Inositol phosphorylceramide synthase catalytic subunit
CDase	Ceramidase
Cdes	Ceramide Desaturase
CerS	Ceramide Synthase
CHN	Elemental analysis
CI	Confidence interval
CL	Cutaneous Leishmaniasis
CL_{int}	Intrinsic clearance
cLogP	Calculated logarithm of the 1-octanol−water partition coefficient
CoA	Coenzyme A
COSY	^{1}H-^{1}H correlation spectroscopy
CYP450	Cytochrome P450
DAG	Diacylglycerol
DALY	Disability-adjusted life year
DCM	Dichloromethane
DDQ	2,3-dichloro-5,6-dicyano-1,4-benzoquinone
dec.	Decomposition
DMF	Dimethylformamide
DMSO	Dimethylsulfoxide
DNUAC	Dose normalized area under the curve
EC_{50}	Median effective concentration
EDC-Cl	N-(3-dimethylamino)propyl-N-ethylcarbodiimide hydrochloride
FDGlu	Fluorescein di-(β-D-glucopyranoside)
eq.	Equivalent(s)
E_s	Taft size parameter
GCase	Glycosidases
GCS	Glucosylceramide Synthase
GSK	GlaxoSmithKline
h	Hour

HepG2	Human liver cancer cell line
HIV	Human immunodeficiency virus
HOBt	Hydroxybenzotriazole
HRMS	High-resolution mass spectrometry
HSQC	Heteronuclear single quantum coherence
HTS	High throughput screening
HMBC	^{1}H-^{13}C Heteronuclear multiple bond correlation
HTS	High-throughput screening
IL	Intralesional
IM	Intramuscular
IPC	Inositol phosphorylceramide
IPCS	Inositol phosphorylceramide synthase
IR	Infrared
IL	intralesional
ISCL	Inositol phosphosphingolipid phospholipase C-like
IV	Intravenous
KSR	3-Ketosphinganine reductase
LCMS	Liquid chromatography-mass spectrometry
lit.	Literature value
Lam	*Leishmania amazonensis*
Lmj	*Leishmania major*
Lmx	*Leishmania mexicana*
LPP	Lipid phosphate phosphatase
LCMS	Low resolution mass spectroscopy
MCL	Mucocutaneous Leishmaniasis
min	Minute
mp	melting point
Ms	Methanesulfonyl
mw	Microwave
NADPH	Nicotinamide adenine dinucleotide phosphate
NMR	Nuclear Magnetic Resonance
NOE/NOSEY	Nuclear Overhauser Effect in ^{1}H-NMR spectroscopy
NTD	Neglected Tropical Diseases
PC	Phosphatidylcholine
PFI	Property forecast index
PI	Phosphatidylinositol
PKDL	Post Kala Azar Dermal
R&D	Research and Development
rt	Room temperature
S1P	Sphingosine-1-phosphate

S1Plyase	Sphingosine-1-phosphate lyase
SAR	Structure-activity relationship
SK	Sphingosine Kinase
SL	Sphingolipid
SM	Sphingomyelin
SMase	Sphingomyelinase
SMS	Sphingomyelin synthase
SPT	Serine palmitoyltransferase
THF	Tetrahydrofuran
THP-1	Human leukemia monocytic cell line
TLC	Thin layer chromatography
Troc-Cl	Trichloroethyl chloroformate
VL	Visceral Leishmaniasis
WHO	World Health Organization
WT	Wild Type

Declaration

The work presented in this thesis was carried out in the Department of Chemistry, Durham University between November 2016 and March 2020. All work is the author's own, unless otherwise stated. No part of this work has been submitted for a degree at this or any other University.

Statement of Copyright

Acknowledgements

I would first like to express my greatest appreciation and sincere gratitude to my supervisor, Prof. Patrick Steel, for the opportunity to work on this project. The door to your office was always open whenever I had a question or needed help. You not only offered me invaluable advice, continuous support, and patience during my Ph.D. study, but you also pushed me when I needed it. I would also like to thank Dr. Paul Denny for providing insightful feedback and Prof. Angelo de Lira Machado for discussing all of the beautiful chemistry with me.

Thanks are also owed to the staff at Durham University, especially everyone in the NMR, mass spec, and chromatography service for their assistance and helpful discussions.

I would like to thank everyone in CG001, past and present, for a cherished time spent together in the lab, and social settings. Bex and Jay, thank you for welcoming me to Durham and for continuing to support me, even now. Victor, Michaela, and Vanessa, I have enjoyed learning from you all but, mostly I thank you for keeping me sane and entertained. We've had some good laughs. I am lucky to have worked with you all.

I would also like to thank my friends and family. Dr. Fazio, your wise counsel and sympathetic ear always lifted my spirits. You have been a great confidant to me and a true friend. Finally, I must express my very profound gratitude to my mom and for providing me with unfailing support and continuous encouragement throughout all of my years of study and through the process of researching and writing this thesis. This accomplishment would not have been possible without you. Thank you.

1 Introduction

1.1 Overview

The work within this thesis is aimed at using the anti-leishmanial drug target inositol phosphorylceramide synthase (IPCS), an enzyme in the sphingolipid biosynthetic pathway, in the development of potential chemotherapeutic agents for the treatment of the parasitic disease leishmaniasis (caused by *Leishmania spp.*). This thesis is comprised of five chapters. This chapter presents a review of the fundamental areas of work central to this project, beginning with an overview of the disease. Following this, the structure and function of sphingolipids will be summarized along with the development of *Leishmania major* IPCS (*Lmj*IPCS) as a drug target.

Previous work within the group identified two 3H-benzazepine analogues as potent inhibitors of *Lmj*IPCS. Chapter 2 will therefore give an overview of this previous work and outline the aims of this investigation. Chapter 3 will discuss the work undertaken to develop synthetic routes to 3H-benzazepine analogues and construct structure-activity relationship (SAR) data which can be used to probe *Lmj*IPCS and identify a more potent drug candidate. Conclusions and future work are discussed in Chapter 4 while Chapter 5 will detail the chemical and biological experimental procedures developed in these studies.

1.2 Neglected Tropical Diseases

Neglected Tropical Diseases (NTDs) are a select group of communicable infections which are classified due to their prevalence in tropical and subtropical geographical locales. They are some of the oldest afflictions known to humankind and have been described in the ancient texts of Hippocrates, the Talmud, and the Bible.[1,2] Although they have been largely eliminated in the more developed parts of the world, these diseases are designated as neglected because of the low research priority given to them despite the

global demand for improved treatments and their continued persistence in the most marginalized communities.[3–5] NTDs thrive in developing regions of the world where sanitation, hygiene, the provision of safe water, adequate nutrition, and access to medical care are substandard, thus making these populations more vulnerable to infection.[1,6]

In fact, NTDs are among the most common infectious diseases affecting impoverished regions and can most commonly be found in low and middle-income countries of Africa, Asia, and Latin America. The World Health Organization (WHO) estimates more than one billion of the 2.7 billion poorest people – those living on less than two dollars a day – suffer from at least one NTD.[7,8] Although NTDs do not typically lead to death, they can impair childhood growth, intellectual development, and cause disabilities that persist for a lifetime; this substantially impacts the productivity and economic prospects of these populations.[9]

NTDs take a tremendous toll on global health, resulting in impaired development, poor pregnancy outcomes, reduced productivity, and disfigurement.[1,3,6,10,11] The disability burden of NTDs is 25% of the HIV disability burden and is almost equal to that of malaria. Despite the fact that academic and grey literature both highlight NTDs as a global health crisis, there is a disparity in the allocation of funds by global health entities. In 2010, for example, HIV/AIDS programs received approximately 40% of total international development assistance whereas NTDs received a meager 0.6%.[1]

Furthermore, as these diseases are primarily concentrated within marginalized populations and the risk to wealthier populations is minimal, there is little incentive to invest in the research and development (R&D) of drugs and vaccines.[9] This lack of interest in the R&D of new drugs for NTDs reflects their market failure and, as a consequence, there are few treatments available for NTDs.[1,3,12] Evidently, of the 1,233 new drugs brought to market between 1975 and 1997, only four were specifically developed for the treatment of NTDs.[1]

1.3 Leishmaniasis

Leishmaniasis is one of the most common and costly NTDs.[1,13] The worldwide prevalence of leishmaniasis is estimated to be approximately 12 million cases, with an incidence of more than 1.5-2 million new cases per year, and approximately 350 million people at risk of infection and disease.[1,10,14–17] Furthermore, the disease burden continues to increase due to deforestation, urbanization, migration, tourism, militarized conflicts, and HIV, which causes a disruption in the healthcare systems of endemic areas.[2,3,6,11,18–21]

Leishmaniasis is not a single entity but is comprised of several illnesses caused by members of the dimorphic intracellular kinetoplastid protozoan parasite of the genus *Leishmania*. The disease is transmitted by the bite of infected female phlebotomine sandflies which inoculate *Leishmania* promastigotes into mammalian hosts.[10,15,17,22] It can be anthroponotic, transmissible through a human reservoir, or zoonotic, transmissible through an animal reservoir.[6,10,15,23]

The disease not only has a wide geographical distribution but is also an extensive epidemiological diversity. There are more than ninety sandfly species known to transmit *Leishmania* parasites and approximately twenty *Leishmania* species which are responsible for the disease manifestation in humans (Table 1.1).[6] It can also show marked regional differences in the sandfly vector, the parasite species, the route of transmission, and the clinical profile. Moreover, radically different pathologies can be caused by different species of *Leishmania* or even by different isolates of the same species.[6,10,14,22,24,25]

Leishmania Species Found in Humans				
Tropism (subgenera)	Viscerotropic (*L. Leishmania*)	Dermotropic (*L. Leishmania*)	Dermotropic (*L. Viannia*)	Mucotropic (*L. Viannia*)
Old World	*L. donovani* *L. infantum*	*L. major* *L. tropica* *L. killickia* *L. aethiopica* *L. infantum*		
New World	*L. infantum*	*L. infantum* *L. mexicana* *L. pifanoia* *L. venezuelensis* *L. garnhamia* *L. amazonensis*	*L. braziliensis* *L. guyanensis* *L. panamensis* *L. shawi* *L. naïffi* *L. lainsoni* *L. lindenbergi* *L. peruviana* *L. colombiensis*	*L. braziliensis* *L. panamensis*

Table 1.1: *Leishmania* species found in humans, adapted from WHO with permission[6]

The clinical spectrum ranges from asymptomatic infections to infections which carry a high mortality; lesions which may be confined to the skin, or those that result in mucocutaneous destruction; or a visceral disease which begins insidiously but, in the absence of specific therapy, can be fatal. There are three main clinical forms of leishmaniasis: cutaneous leishmaniasis (CL); mucocutaneous leishmaniasis (MCL); and visceral leishmaniasis (VL). Occasionally, diffuse cutaneous leishmaniasis and disseminated cutaneous leishmaniasis, additional forms of CL are described as separate entities.[10,15,22,26]

Asymptomatic leishmaniasis could be considered a final type of leishmaniasis as the majority of people infected by the parasite are without symptoms. These infections are characterized by low parasite titers that persist for the patient's lifetime. Furthermore, the infections also offer protective immunity against subsequent leishmanial infections.[3,10,22,27–29]

1.3.1 Cutaneous Leishmaniasis

Cutaneous leishmaniasis (CL) is the most common and least severe form of leishmaniasis.[30] Old World CL can be found in North Africa, the Mediterranean, the Middle East, the Indian Subcontinent, and Central Asia (Figure 1.1).[31] Its primary etiological agents are *L. major*, *L. tropica,* and *L. aethiopica*, however, in the Mediterranean Basin, *L. infantum* and *L. donovani* are occasionally found to be the cause of CL. New World or American CL is found in Central and South America. It is primarily caused by *L. braziliensis*, *L. guyanensis*, *L. amazonensis*, *L. panamensis*, *L. mexicana,* and *L. peruviana*.[1,6,19,20,22,32–34]

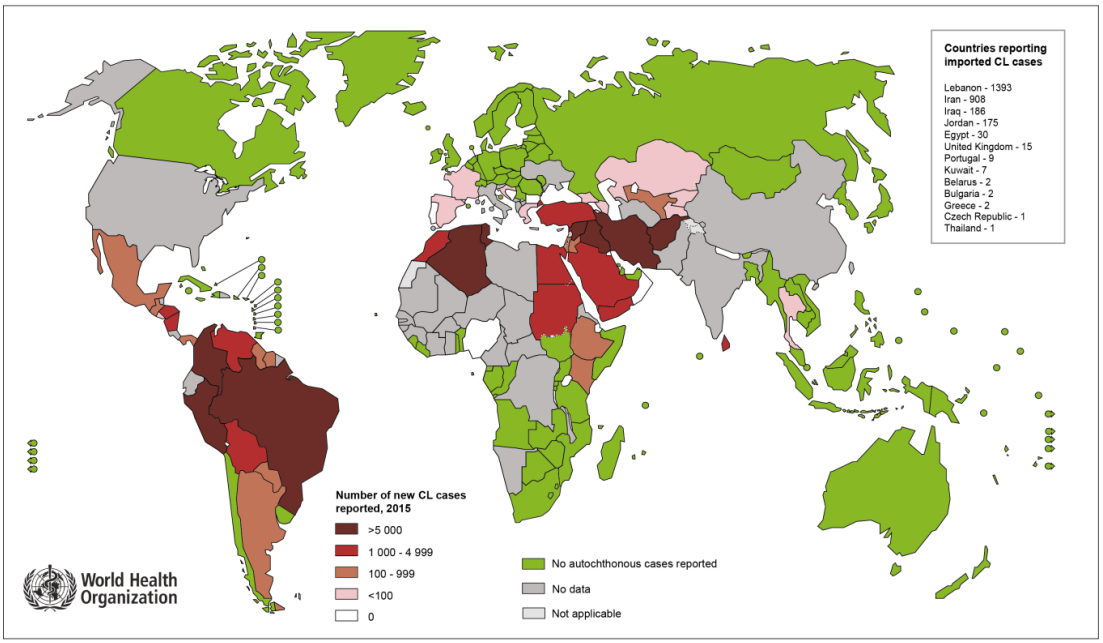

Figure 1.1: Global distribution of Cutaneous leishmaniasis (CL), reproduced from WHO with permission[31]

The clinical features of CL vary, depending on the region, the vector species, parasitic species, and the reservoir. It can be anthroponotic or zoonotic, with a wide variety of rodents and big mammals acting as reservoirs. CL has been subdivided into four different clinical forms: localized-CL, leishmania recidivans, diffuse-CL, and disseminated-CL.[1,6,35]

Localized-CL is the most prevalent form of CL in both the Old World and New World. In localized-CL, the parasite is confined to the skin where it causes the formation of a slow-growing lesion at the site of inoculation. The lesions are generally painless and frequently multiple; it is not unusual for satellite nodules to develop at the edge of the lesion. Secondary bacterial infections are a common occurrence with localized-CL infections and can result in severe pain and disability. This type of CL can heal without treatment, over the course of several months or years, but often results in permanent scarring and altered pigmentation.[6,10,19,20,34]

Leishmania recidivans, also known as lupoid or tuberculoid leishmaniasis, is a chronic, relapsing form of CL that resembles tuberculosis of the skin.[6,15,34] This manifestation of leishmaniasis caused by *L. tropica* is rarely found in the Old World.[27,33,36] It is characterized by the recrudescence of microsatellite lesions which form near the site of previous scars.[15] It is also found to have a scarcity of amastigotes in the lesion which often leads to misdiagnosis.[34] Unfortunately, leishmanial recidivnans has a lower tendency for spontaneous healing than localized CL and rarely responds to treatment. Thus, as leishmanial recidivans can persist for many years, it can become destructive and extremely disfiguring.[6,11]

Occasionally, leishmanial infections may diffuse to other areas of the body where the parasite reproduces and causes diffuse-CL or disseminated-CL. In the Old World, diffuse-CL is caused by *L. aethiopica* and *L. major* while in the New World *L. amazonensis* and *L. mexicana* are the main causative agents.[18,22,33] Diffuse-CL is characterized by a primary lesion which widely disseminates until the entire body is affected. The resulting lesions, which resemble lepromatous leprosy, are extremely disfiguring. Mucosal involvement is absent in these infections. Diffuse-CL infections are chronic and although responding to initial treatment, post-treatment relapses are frequent. Moreover, successive treatments are usually unsuccessful.[6,18,19,30]

Disseminated-CL is a New World affliction that has been described in association with *L. braziliensis*, *L. panamensis*, and *L. guyanensis* infections. It is characterized by numerous lesions in two or more parts of the body. Unlike diffuse-CL where the parasite reproduces widely, very few parasites are found in the disseminate-CL lesions. However, mucosal

involvement is frequently found in these cases. Disseminated-CL is more responsive to treatment than diffuse-CL.[6,10,19,34]

1.3.2 Mucocutaneous Leishmaniasis

Mucocutaneous leishmaniasis (MCL) is a New World disease as it is rarely seen in the Old World. Ninety percent of MCL cases occur in Brazil, Bolivia, and Peru. The main causative agents of MCL are *L. braziliensis* and *L. panamensis* in the New World and *L. aethiopica* in the Old World.[6,10,11,34]

MCL is a sequelae of CL that is not self-healing, frequently reoccurring, and difficult to treat. It progresses similarly to that of CL, and the two infections can be concurrent, but it is not uncommon for MCL to develop many years after the recovery of a cutaneous lesion. The characteristic feature of this disease is metastasis of cutaneous lesions to the mucosal tissues of the mouth, nasal, and pharyngeal cavities. MCL lesions may multiply and increase in size, resulting in severe disfiguration and the gradual obstruction and destruction of the respiratory tract.[6,10,20,37,38]

Because of the extensive tissue damage caused by MCL, secondary bacterial infections are commonplace and can be fatal. In fact, a simultaneous pneumonia infection is a common cause of death in these cases. Furthermore, with prolonged infection, this form of leishmaniasis can be fatal. Death can also be caused by respiratory compromise and malnutrition.[3,6,11,15,19]

1.3.3 Visceral Leishmaniasis

Visceral leishmaniasis (VL), also known as kala-azar and black fever, is the most fatal form of leishmaniasis. In the Old World, VL can be found in Africa, the Mediterranean, the Middle East, Central Asia, and the Indian subcontinent (Figure 1.2).[39] In Asia and Africa, the main parasitic agent is *L. donovani*. The VL in these areas is anthroponotic with humans acting as the parasitic reservoir. In the Mediterranean, *L. infantum* is responsible for the majority of VL infections. Mediterranean VL is zoonotic where mammals such as

dogs and foxes act as the main reservoirs. Although it has traditionally been associated with CL, *L. tropica* has been linked to several cases of VL in the Old World.[6,10,11,19,22,29,33,34,40]

New World VL is comparable to that found in the Mediterranean. It is endemic in Central and South America and as in the Mediterranean, the primary causative agent is *L. infantum*. VL has generally been a disease of rural areas with the natural reservoirs being domestic dogs and foxes.[6,15,41] However, as urbanization has progressed, peri-urban regions have become affected. Infectious rates are observed to eventually decrease as urbanization completes. In the New World, *L. amazonensis* has been seen to occasionally cause VL.[6,20,34]

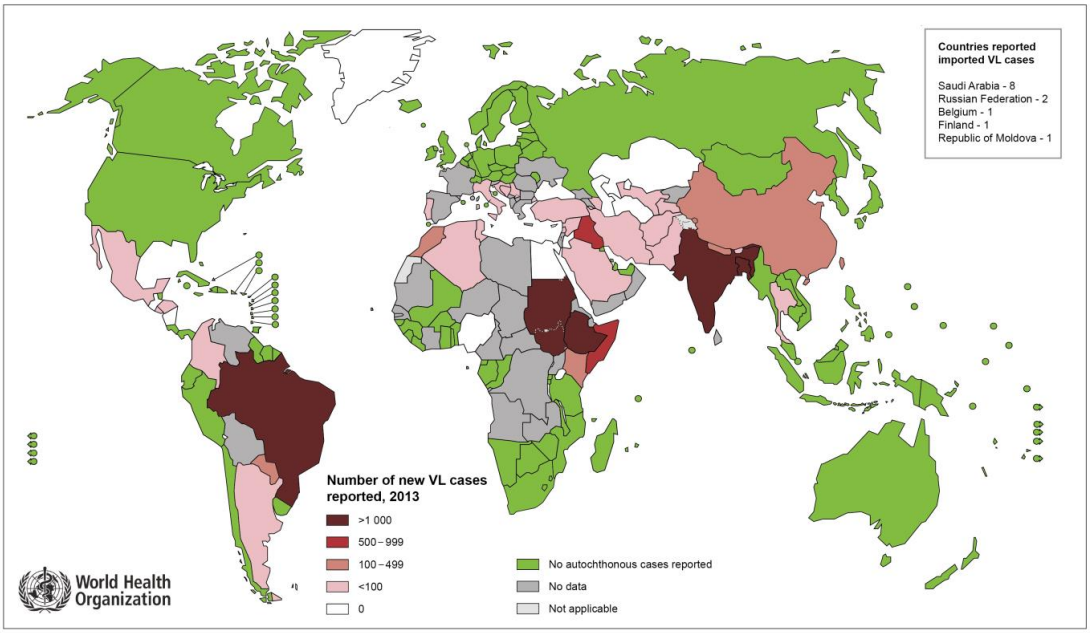

Figure 1.2: Global distribution of Visceral leishmaniasis (VL), reproduced from WHO with permission[39]

The clinical features of VL can vary based on its classification: endemic, sporadic, or epidemic. For example, VL may be prevalent in a particular region or with a particular population. In these endemic areas, VL is more of a chronic illness which particularly affects children. Sporadic VL may infect travelers to an endemic region or can overlap with environmental changes such as urbanization or disforestation. Acute forms that occur with high mortality rates are observed with epidemic VL. Epidemic VL has no correlation with population.[6,10,20,35,42]

Although most infections may be mild or asymptomatic, it has been witnessed that some patients eventually develop clinical VL. In general, the disease presents with a gradual onset, but for people visiting endemic areas, onset may be acute. The most common symptoms of clinical VL are fever, dramatic weight loss, anemia, fatigue, discomfort, and abdominal distention of the spleen and liver. Additionally, enlargement of the lymph nodes is described in some parts of Africa while in India, patients with prolonged disease often develop hyperpigmentation.[3,4,5,10,14,18,22,33,34]

These symptoms are largely due to the parasite attacking the reticuloendothelial system, an important part of the immune system that helps fight foreign bodies and clear old and abnormal cells.[6,10,15,32,34] Consequentially, VL patients are susceptible to intercurrent infections. If left untreated, VL is generally fatal within two years. Oftentimes, death is from secondary infections, but disease-related complications such as gastrointestinal bleeding, liver, or heart failure are common causes of death.[6,10,29,19,32]

Occasionally, a skin sequelae of VL may be followed by the successful treatment and resolution of VL in some patients. This disease, known as Post Kala-Azar Dermal Leishmaniasis (PKDL), is characterized by a hypopigmented rash or multiple nodular lesions which begins around the mouth then spreads to the rest of the body. PKDL is most common to East Africa where *L. donovani* is the primary causative agent, although it may also sporadically occur in endemic areas of South America from *L. infantum* and the Mediterranean from *L. chagasi*. Approximately 50% of treated patients in East Africa suffer from PKDL while in South Asia, the disease is relatively rare. Less than 10% of treated patients in that area are seen with the disease.[6,22,27,28,33,34]

1.3.4 Leishmaniasis and HIV

Due to the use of immunosuppression drugs for transplantation and the rise of the HIV/AIDS epidemic, there has been an increased incidence of more severe forms of leishmaniasis, which are difficult to manage and show resistance to currently available treatments. As immuno-compromised patients are particularly vulnerable to opportunistic infections, the burden of leishmaniasis has been able to move into new populations and geographic areas.[2,6,11,29,43]

For example, children under 5 were previously the most affected by endemic VL caused by *L. infantum* in the Mediterranean. However, HIV infection has caused about half of the current cases to present in adults.[6] Similar changes have been seen in Africa, Asia, and South America. *Leishmania*–HIV coinfection has been reported in 35 countries and while the number of new cases in the Mediterranean has now declined due to the use of antiretroviral therapy, the prevalence is still high in countries where this treatment option is limited.[4,33,45]

Leishmania–HIV coinfection poses a major challenge to disease management. Not only does VL hasten HIV replication and progression to AIDS, but these patients are also more likely to develop severe, life-threatening complications. Fortunately, antiretroviral therapy can improve the survival rates of co-infected patients by reducing the development of the disease and preventing relapses.[6]

1.3.5 *Leishmania* lifecycle

Leishmania parasites have a dimorphic lifecycle that is divided into two hosts: the extracellular promastigote stage which occurs in the sandfly vector and the intracellular amastigote stage which occurs in mammalian hosts (Figure 1.3).[15,46,47]

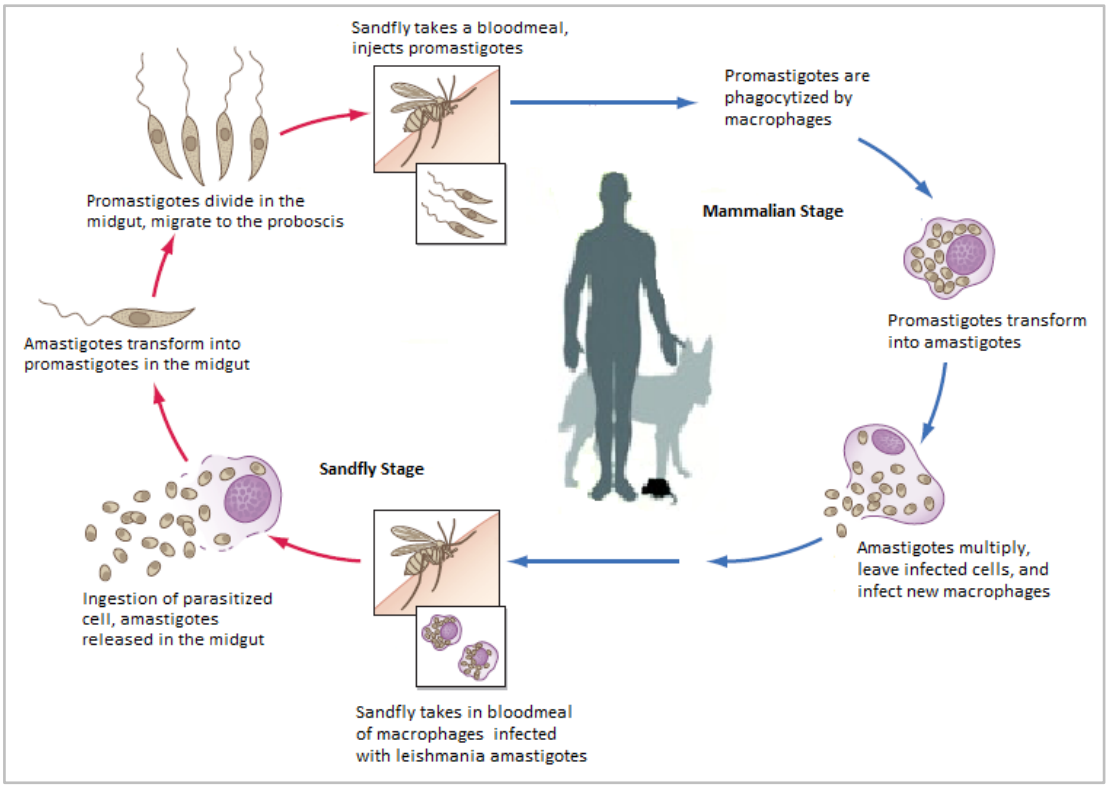

Figure 1.3 Life cycle of *Leishmania* infection

Infection begins when a feeding sandfly takes in macrophages infected with *Leishmania* amastigotes while ingesting the blood from an infected host. The infected bloodmeal then undergoes developmental differentiation as it migrates through the digestive tract. The sandflies then inject the infective promastigotes into the host bloodstream where they are taken up by macrophages via phagocytosis.

The mammalian stage of the life cycle is dependent upon the phagocytic activity of the host cell as the parasite cannot independently invade host cells. Within the macrophage phagolysosome, the promastigote converts to its non-motile amastigote form. The amastigotes multiply by binary fission and accumulate in the macrophage until they are released from the host cell. Free amastigotes are then taken up by new macrophages where they begin another replicative cycle, ultimately resulting in one of the clinical forms of Leishmaniasis.[14,23,29,48–50]

1.3.6 Antiparasitic Agents

There are a limited number of antileishmanial agents available (Figure 1.4) and the preferences for first-line treatment not only depend on the clinical manifestation of the disease but are often guided by regional practice.[6,15]

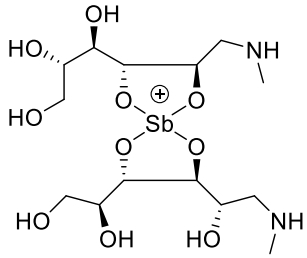

Meglumine antimoniate **1**

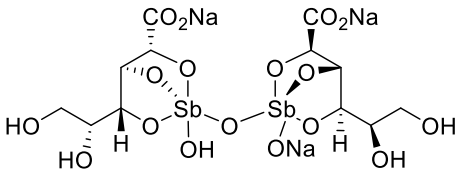

Sodium stibogluconate **2**

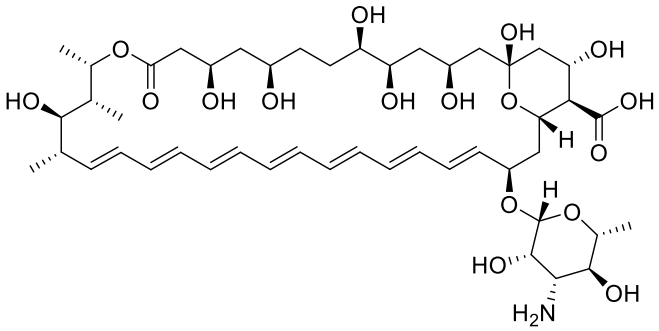

Amphotericin B **3**

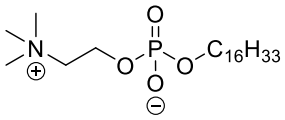

Miltefosine **4**

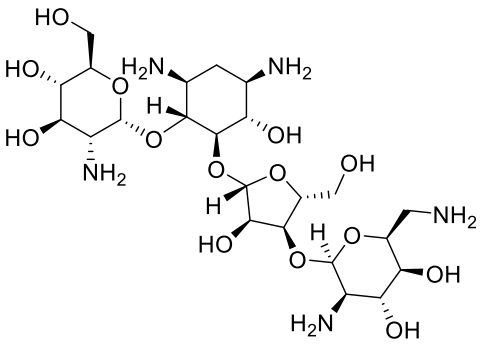

Paromomycin **5**

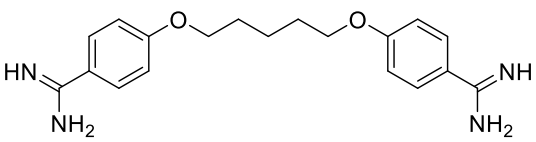

Pentamidine **6**

Figure 1.4: Current leishmanial therapies

Unfortunately, the increasing incidence of HIV co-infection and the expense of current therapeutic methods further limit the treatments available and the chances of an effective cure.[28,34,51,52] There are also several obstacles in the treatment of patients with current antileishmanial drugs as most suffer from several drawbacks including a long course of intramuscular or intravenous therapy, significant toxicity, and variable efficacy (Table 1.2). Accordingly, disease recrudescence is common.[3,6,10,15,19]

Drug	Mode of action	Mode of administration	Efficacy	Advantages	Adverse effects and Limitations
Pentavalent antimonials **1, 2**	Prodrug, trypanothoine reductase inhibitor which increases oxidative stress	IV, IM IL	35 – 95%	Low cost; easy availability	Abdominal pain, erythema, nausea, exceedingly toxic, parasite resistance, requires hospitalization and patient monitoring
Amphotericin B **3**	Ergosterol binding changes parasitic membrane permeability and stability	IV	> 90%	High safety and efficacy; 1st line treatment in case of Sb(V) resistance	Fever, nausea, severe nephrotoxicity, electrolyte abnormalities, infusion-related reactions, requires hospitalization and patient monitoring
Liposomal Amphotericin B **3**	Targeted delivery of drug to infected macrophages and kills parasite as with AmpB	IV	> 97%	High safety and efficacy, Less toxic than AmB, No need for hospitalization	Rigors and chills during infusion, occasional mild nephrotoxicity, costly, requires maintenance of cool temperature
Miltefosine **4**	Interferes with phospholipid metabolism and biosynthesis; disrupts membrane integrity; induces an apoptosis-like death	Oral	60 – 94%	Safe in HIV-VL co-infection, non-invasive route, no need for hospitalization	Nausea, vomiting, diarrhea, nephrotoxicity, hepatotoxicity, teratogenic, costly, parasitic resistance, efficacy dependent on parasitic species
Paromomycin **5**	Inhibits parasitic protein biosynthesis; disrupts mitochondrial membrane potential	IM, topical	46 – 94%	Low cost, non-invasive route	Erythema, oedema, severe nephrotoxicity, ototoxicity, hepatotoxicity
Pentamidine **6**	Inhibit DNA transcription; modifies parasite morphology	IM, IL	35 – 96%	Effective in combination therapy	Gastointestinal adverse effects, hypertension, hypoglycemia as a result of pancreatic damage, parasite resistance, largely abandoned in endemic areas

Table 1.2: Drugs used for the treatment of leishmaniasis; IV: intravenous administration; IM: intramuscular administration; IL: intralesional administration[10,22,53,54]

While preferential pricing agreements exist between health organizations like WHO and pharmaceutical companies, many of these treatments are accompanied by the additional cost of hospitalization, travel, and lost wages which adds an additional burden.[6,10,33] Generics can mitigate the expense, but even cheaper drugs such as Sb(V) **1** and **2** and paromomycin **5** can be roughly equivalent to a year's income in some developing countries. These factors can deter patients from completing their treatment regimen.[3,11,12,28]

Thermotherapy and cryotherapy have been used to resolve CL lesions with variable success. Unfortunately, these nontraditional therapies are not only limited by the availability of equipment, but there is also the risk of parasite dissemination and secondary infections.[6,10,27,33]

The emergence and spreading of drug resistance is also of concern for the treatment of leishmaniasis as a long-term cure is not always achieved. WHO has recommended several multidrug regimens which would improve treatment compliance and reduce the spread of drug resistance, but this can also make treatment more costly.[6,28,33,55]

Although there are several canine vaccines available, progress in developing protective immunization against leishmaniasis in humans has proven to be a difficult task. There has been research into many different vaccination approaches; however, there is still no vaccine available.[19,40,54–56] Control of leishmaniasis, then, depends on the effective chemotherapy.

1.4 Sphingolipids and Leishmaniasis

1.4.1 Spingolipids – Structure and Function

There is a growing need for the discovery and optimization of antileishmanial agents which are affordable, lower in toxicity, and are active against resistant parasitic strains. The sphingolipid synthetic pathway has been identified as a potential drug target for leishmaniasis.[57,58]

Sphingolipids (SLs) are an essential class of lipid species found in eukaryotic membranes. These compounds, first identified in the 1870s, have seen a recent upsurge of interest due to the wide range of biological processes ascribed to them. Many complex SLs are highly bioactive in cellular signaling and membrane structure and have also been shown to be regulators of growth, differentiation, migration, survival, and stress.[49,50,51]

SLs are amphipathic compounds composed of three main structural elements: a long-chain amino alcohol sphingoid base comprises the central moiety, a fatty acyl group attached to the C-2 via an amide bond, and a hydrophilic head group at the C-1 hydroxyl (Figure 1.5). Structurally, SLs show great diversity throughout nature with unique variations in chain lengths, hydroxylation, and conjugation.[59,62,63]

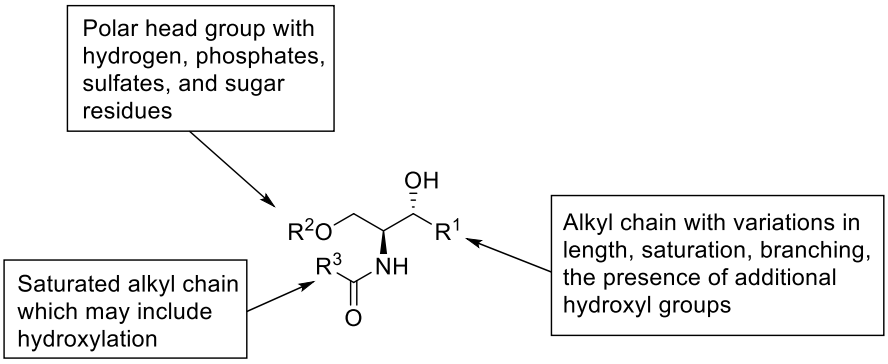

Figure 1.5: Structural variation of sphingolipids.

1.4.2 Sphingolipid Biosynthetic Pathway

The biosynthetic pathway for the formation of SLs, particularly the first two steps, is largely conserved for all eukaryotes. *De novo* biosynthesis of SLs (Scheme 1.1) is initiated by the condensation of palmitoyl CoA **7** and serine **8** to produce 3-ketodihydrosphingosine **9**. This reaction occurs in the endoplasmic reticulum and is catalyzed by the serine palmitoyltransferase (SPT), the rate-limiting enzyme of the sphingolipid biosynthetic pathway. Next, 3-ketodihydrosphingosine **9** is reduced to sphinganine (dihydrosphingosine) **10** by 3-ketosphinganine reductase (KSR) in an NADPH dependent manner.[64–66]

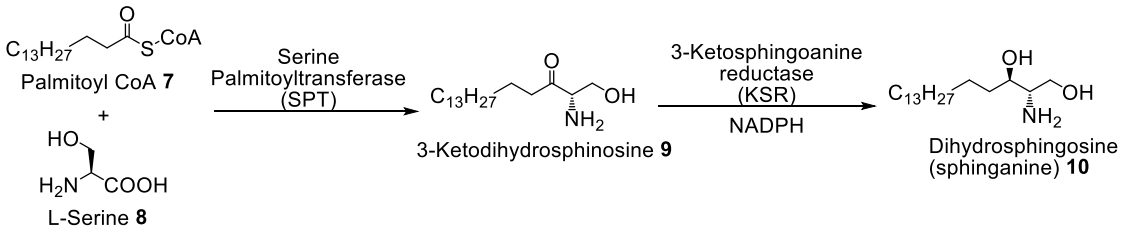

Scheme 1.1: *De novo* sphingolipid biosynthetic pathway

Following the formation of sphinganine **10**, SLs synthesis exhibits a divergence in the metabolic pathway (Scheme 1.2). In mammalian cells, sphinganine **10** is first N-acylated to form dihydroceramide **11** then desaturated at C-4 to form ceramide **12**. However, in fungi and higher plants, sphinganine **10** is hydroxylated at C-4 to form phytosphingosine **13** and then N-acylated to form phytoceramide **14**.[64,65,67]

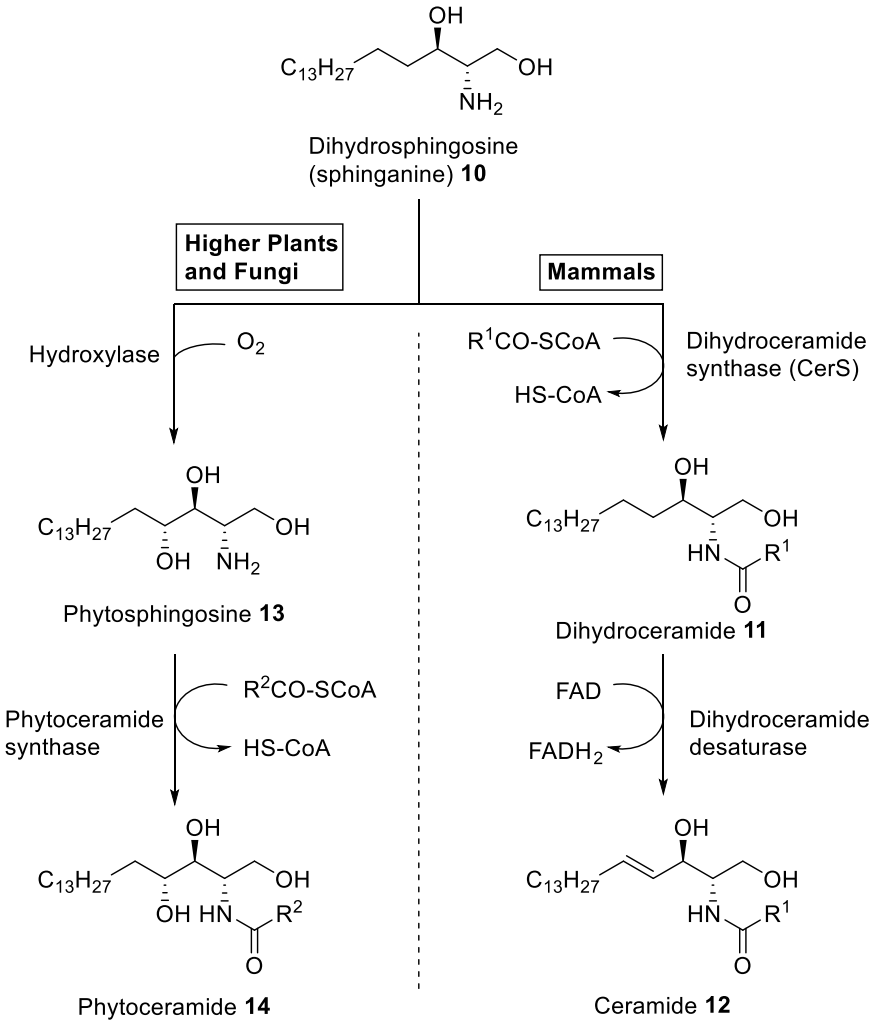

Scheme 1.2: Divergence in the sphingolipid biosynthetic pathway

Ceramides are simple SLs that are considered to be the central hub of SL synthesis. They have been found to serve as secondary messengers in eukaryotic cell signaling mechanisms and act as a regulator of several cellular processes including proliferation, and apoptosis.[61,66] These unmodified SLs are trafficked from the endoplasmic reticulum to the Golgi apparatus, where the synthesis of more complex SLs takes place.

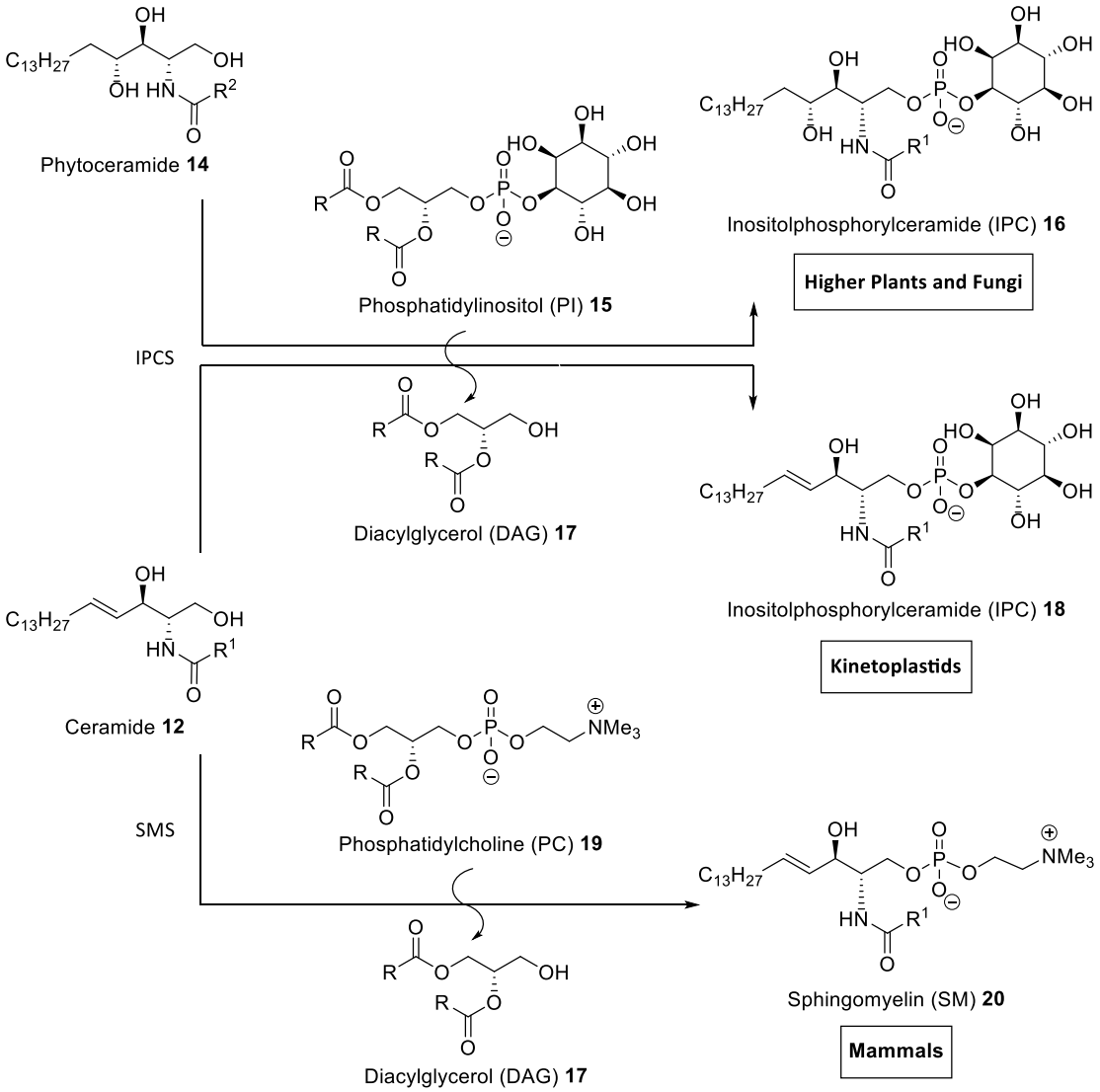

Scheme 1.3: Post ceramide divergence in the sphingolipid biosynthetic pathway

In mammalian cells, a phosphocholine head group is transferred from the phospholipid phosphatidylcholine (PC) **19** to ceramide **12** by sphingomyelin synthase (SMS) to produce the predominant sphingolipid sphingomyelin (SM) **20**. Conversely, fungi and higher plants use inositol phosphorylceramide synthase (IPCS) to attach a phosphoinositol head group onto phytoceramide **14** from phosphatidylinositol (PI) **15** to produce inositol

phosphorylceramide (IPC) **16**. Like fungi and higher plants, kinetoplastids such as Leishmania use the IPCS pathway. In this case, a phosphoinositol head group is attached to ceramide **12** to produce IPC **18**, the predominant kinetoplastid SL (Scheme 1.3). The newly synthesized SLs are finally transported to the plasma membrane (PM) where they participate in cellular maintenance.[67–69]

1.4.3 Sphingolipid Salvage and Degradation

In addition to *de novo* synthesis, SLs can be produced following a salvage and degradation pathway (Figure 1.6). During this event, ceramide **12** can be recycled into the SL biosynthetic pathway or degraded to sphingosine. Sphingosine, the core moiety of many sphingolipids, is not an intermediate in SL biosynthesis, but is a product of sphingolipid degradation. It can then be recycled into the SL biosynthetic pathway or further degraded to sphingosine-1-phosphate (S1P). The penultimate SL in the degradation pathway, S1P, can be permanently degraded, providing the only exit from the SL metabolic pathway.[65,68]

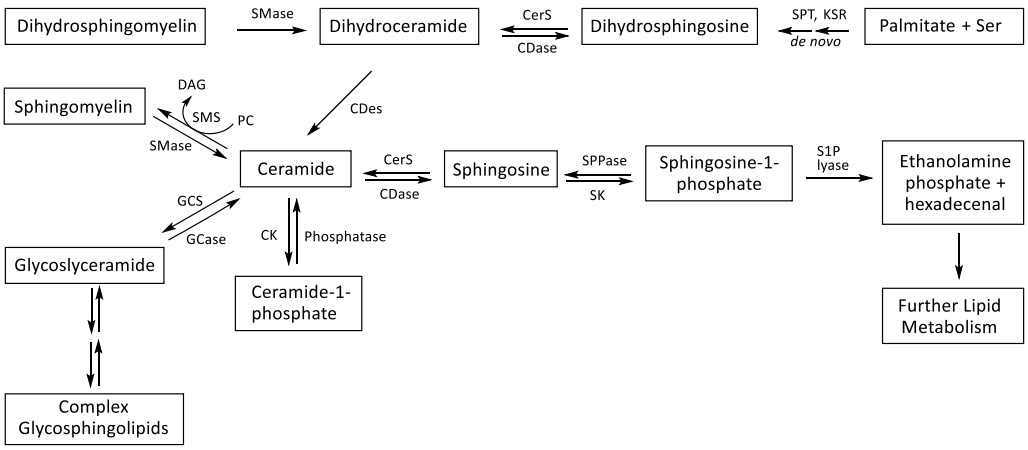

Figure 1.6: *De novo*, salvage, and degradation pathways of mammal sphingolipid metabolism, adapted from Hannun *et al.* with permission[68]

Leishmania parasites possess a potent, neutral sphingomyelinase that aids in the process of SL salvage and degradation pathway – inositol phosphosphingolipid phospholipase C-like (ISCL). This enzyme is responsible for the degradation of both host SM and parasite IPC. It is suggested that the degradation of host SM, and the production of ceramide through this salvage pathway, is essential for amastigote proliferation and virulence in

mammals.[24,70–72] Furthermore, IPC degradation plays an important role in allowing the parasite to adapt to the acidic phagolysosome environment. In this respect, SL salvage and degradation are essential processes in amastigote survival.[70,73]

1.4.4 Sphingolipid biosynthesis as a drug target

Several steps of the SL biosynthetic pathway have been tested as potential *Leishmania* drug targets. In particular, *L. major* infections of macrophages were treated with myriocin **21**, an inhibitor of SPT that mediates the first step in SL biosynthesis, and fumonisin B1 **22**, an inhibitor of CerS which mediates the third step in SL biosynthesis (Figure 1.7). While these drugs were found to disrupt *de novo* SL biosynthesis in mammalian cells, they showed no activity against *Leishmania* – neither promastigote survival nor amastigote replication.[46,74]

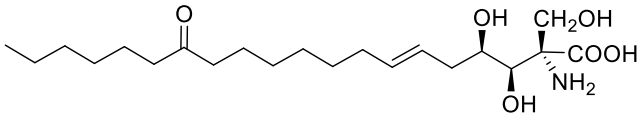

Myriocin **21**

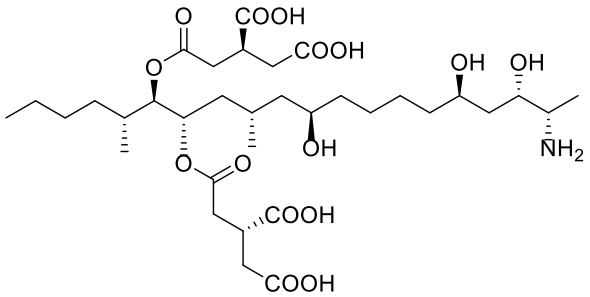

Fumonisin B1 **22**

Figure 1.7: Inhibitors of sphingolipid biosynthesis

SPT was further examined using an SL-null mutant, *L. major* (*spt2*$^{-}$), created by deleting the SPT2 subunit gene. It was observed that *spt2*$^{-}$ remained fully functional and maintained wild type (WT) growth rates, however, they failed to differentiate into the infective metacyclic form. This is because *de novo* biosynthesis is the dominant pathway for promastigotes and is essential to establish infection in the host. Accordingly, *spt2*$^{-}$

promastigotes showed reduced infectivity even though *spt2*$^-$ amastigotes showed no change in virulence.

Despite being defective in *de novo* SL synthesis, analysis of *spt2*$^-$ amastigotes showed WT levels of an active IPCS. It is suggested that this is due to amastigote dependence on host SL salvage for parasite survival. Indeed, further investigation showed that parasites carry out head-group remodeling through salvage of host SLs. It has also been shown that *L. donovani* stimulates host macrophages to upregulate the production of ceramide **12**, creating a pool of host SL available for scavenging.[46]

Together, these studies suggest that while *de novo* SL synthesis is important for initial infection and differentiation by metacyclic promastigotes, it is not essential for survival and pathogenesis within host macrophages.[46] Unfortunately, these studies also show that disrupting the SL pathway prior to the generation of ceramide **12** will not be curative. However, it is clear that complex SLs are necessary for survival. The synthesis of IPC, the primary complex sphingolipid of *Leishmania*, is therefore, a promising drug target.

1.4.5 IPCS as a Drug Target

The SL biosynthetic pathway is conserved until the synthesis of ceramide **12**. Therefore, inhibitors that target enzymes in the initial stages of pathway are not good drug targets. At these stages, the generation of complex SLs through the salvage pathway would not be inhibited. Additionally, selectivity would not be attained and any drug action would result in host toxicity. IPCS, an enzyme functioning after the synthesis of ceramide **12**, has no mammalian equivalent, making it a good drug target.

Precedence for the use of IPCS as a drug target comes from several fungal studies. In pathogenic fungi, IPCS is believed to be encoded by the AUR1 gene.[58] Mutations to this gene confers resistance to the potent fungal IPCS inhibitor Aureobasidin A **23** (AbA, Figure 1.8) and renders cells incapable of proper growth and division.[75] Additionally, a mutant *S. cerevisiae* yeast strain lacking IPCS activity accumulated ceramide **12** when fed exogenous phytosphingosine **13**. This ceramide **12** accumulation led to cell death.[76]

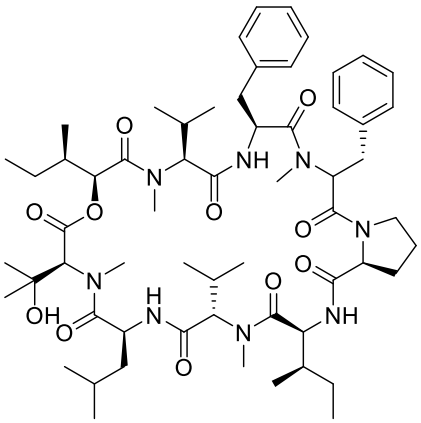

Aureobasidin A (AbA) **23**

Figure 1.8: Fungal IPCS inhibitor Aureobasidin A

When tested as a potential leishmanial parasitic inhibitor, AbA **23** showed growth inhibition in several species of leishmanial promastigotes.[77] AbA **23** inhibition of *L. major* promastigote growth is observed at 0.6 µM. It is similarly toxic to *spt2*$^{-}$ parasites where parasitic IPCS would be redundant.[72] However, when tested against *L. major* IPCS expressed in a mutant yeast system, AbA **23** shows no inhibitory effect until 100 µM.[58] It has been suggested, then, that the AbA **23** inhibitory effect is not simply due to IPCS inhibition. [69,78]

Although AbA **23** does not display a favorable pharmacokinetic profile, this research helps to demonstrate that IPCS is necessary for fungal viability and that in its absence, cell death occurs from ceramide **12** accumulation.[79] It also points to the difference between IPCS found in yeast and *Leishmania*. Thus, IPCS represents an attractive pharmaceutical target that would result in drugs with high pathogen specificity and minimal host toxicity.

1.4.6 Discovery and Characterization of Kinetoplastid IPCS

Recent research by Denny *et al.* isolated a single copy gene encoding a functional orthologue of the fungal *AUR1* in *L. major* (*Lmj*IPCS, *Lmj*F35.4990) through the use of bioinformatics and functional genetics. Orthologues of LmjIPCS were also identified in the parasitic kinetoplastids *T. cruzi* and *T. brucei* (Figure 1.9).

T. cruzi has been found to synthesize IPC as its major complex sphingolipid and is known to possess IPCS activity. Accordingly, the *T. cruzi* orthologues share more than 50% sequence identity and approximately 70% similarity with *Lmj*IPCS.[58]

Where *T. cruzi* and *L. major* have a single gene encoding for IPC, *T. brucei* has four tandemly arrayed genes encoding for sphingolipid synthases (TbSLS1-4).[69] Variation in a single residue adjacent to the catalytic histidine has been shown to influence TbSLS enzymatic specificity. Only gene product TbSLS1 (Ser_{252}) is an IPC synthase whereas TbSLS2 (Phe_{252}) is an ethanolamine phosphorylceramide (EPC) synthase and TbSLS3 and TbSLS4 (Phe_{252}) are bifunctional SM/EPC synthases.[80,81] These orthologues were found to share approximately 45% identity and more than 60% similarity with *Lmj*IPCS. This shows that there is a high level of conservation within the kinetoplastid species.[58]

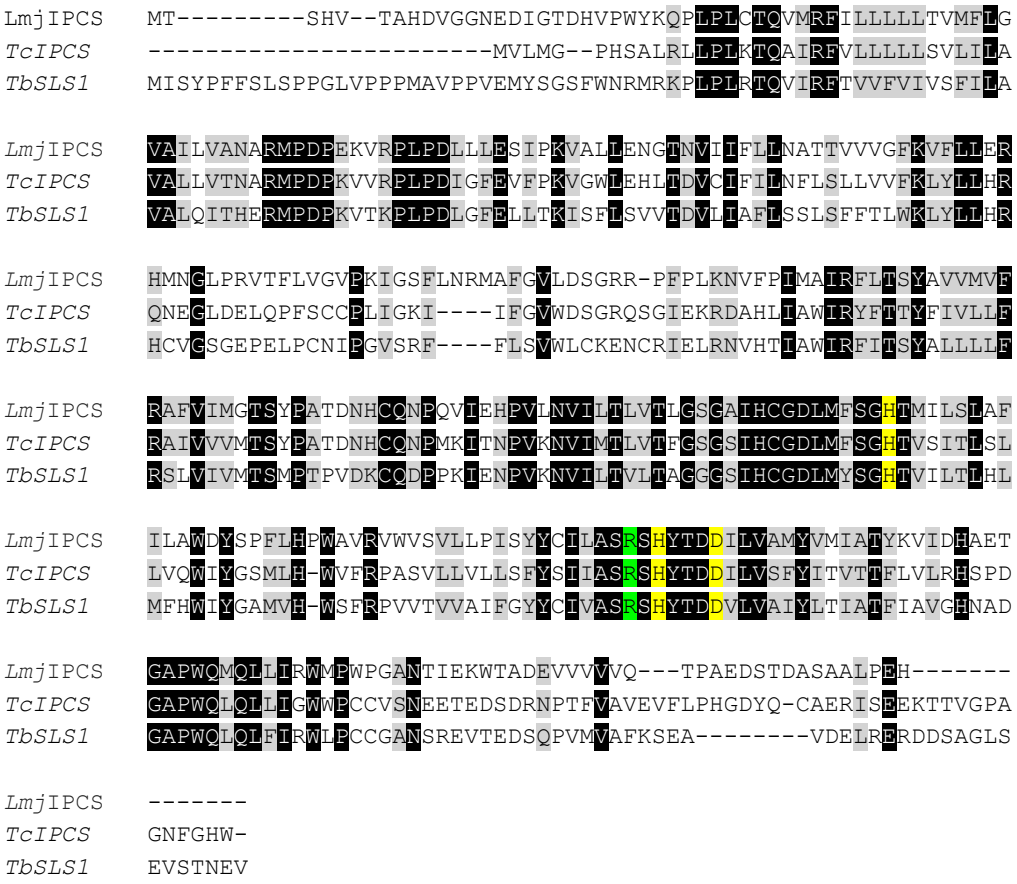

Figure 1.9: Clustal Omega alignment of protein sequences from *L. major* IPCS (LmjF35.4990), *T. cruzi* SLS (Tc00.1047053506885.124), and *T. brucei* SLS1 (Tb09.211.1030). Shaded black, sequence identity; Shaded grey, sequence similarity; Shaded yellow, catalytic triad His_{220}, His_{264}, Asp_{268}; Shaded green, stabilizing residue Arg_{262}.

*Lmj*IPCS is predicted to have six transmembrane (TM) helices.[82] Two regions of the identified kinetoplastid orthologues showed the conserved histidine and aspartate residues in a motif shared by the lipid phosphate phosphatase (LPP) family, fungal AUR1p proteins, and mammalian SMS. These residues, located in the luminal domains of D3 and D4,[80,82] make up the catalytic triad that that mediates the nucleophilic attack of ceramide **12** on the phosphate ester of phosphatidylinositol (PI) **15** (Figure 1.10, a).[58,67] In the proposed mechanism, nucleophilic attack is initiated by His_{220} while His_{264} and Asp_{268} operate as a charge relay system. Arg_{262} is thought to stabilize the transition state during the transfer of the phosphorylinositol group by *Lmj*IPCS (Figure 1.10, b).[67] Interestingly, mutagenesis of the these conserved histidine and aspartate residues have been shown to inactivate fungal IPCS activity.[58]

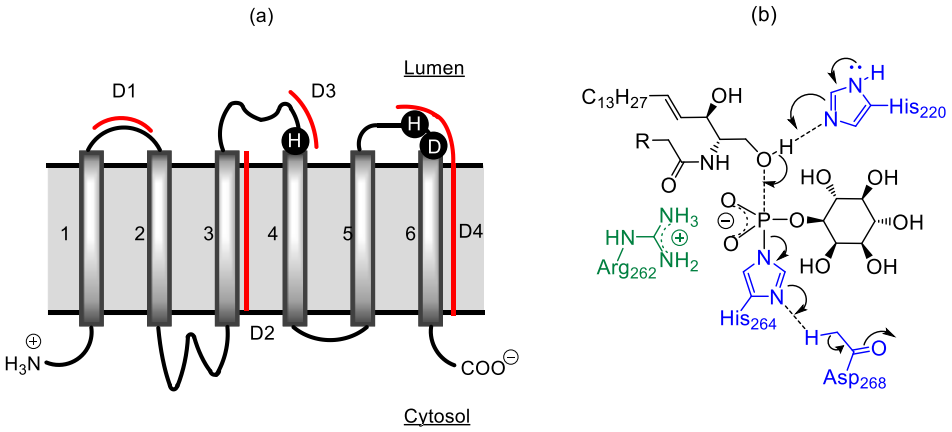

Figure 1.10: (a) Diagram of the predicted topology of kinetoplastid IPCS, adapted from Sutterwala *et al.* with permission.[82] Four domains of SMS sequences (D1–D4) proposed by Huitema *et al*. are highlighted with red lines.[82,83] Key residues of the HHD catalytic triad (*Lmj*IPCS, His_{220}, His_{264}, Asp_{268}) in TM4 and TM6 are indicated in the model. (b) Proposed mechanism of action of *Lmj*IPCS, adapted from Mina *et al.* with permission.[67]

Kinetic studies have shown that *Lmj*IPCS proceeds through a double displacement model (Scheme 1.11). *Lmj*IPCS first transfers the phosphorylinositol group from PI **15** to the catalytic histidine residue, His_{264}. The phosphorylinositol group is then transferred by *Lmj*IPCS to the acceptor ceramide **12** to give IPC **18**. In these reactions, the mitogenic byproduct DAG **17** is released concomitantly. Therefore, the synthesis of complex SLs through the IPCS pathway plays an essential role important in maintaining cellular homeostasis as they regulate the concentrations of pro-apoptotic ceramide **12** and of the

mitogenic DAG **17**. Consequently, compounds which inhibit IPCS would reduce parasitic survival and virulence.

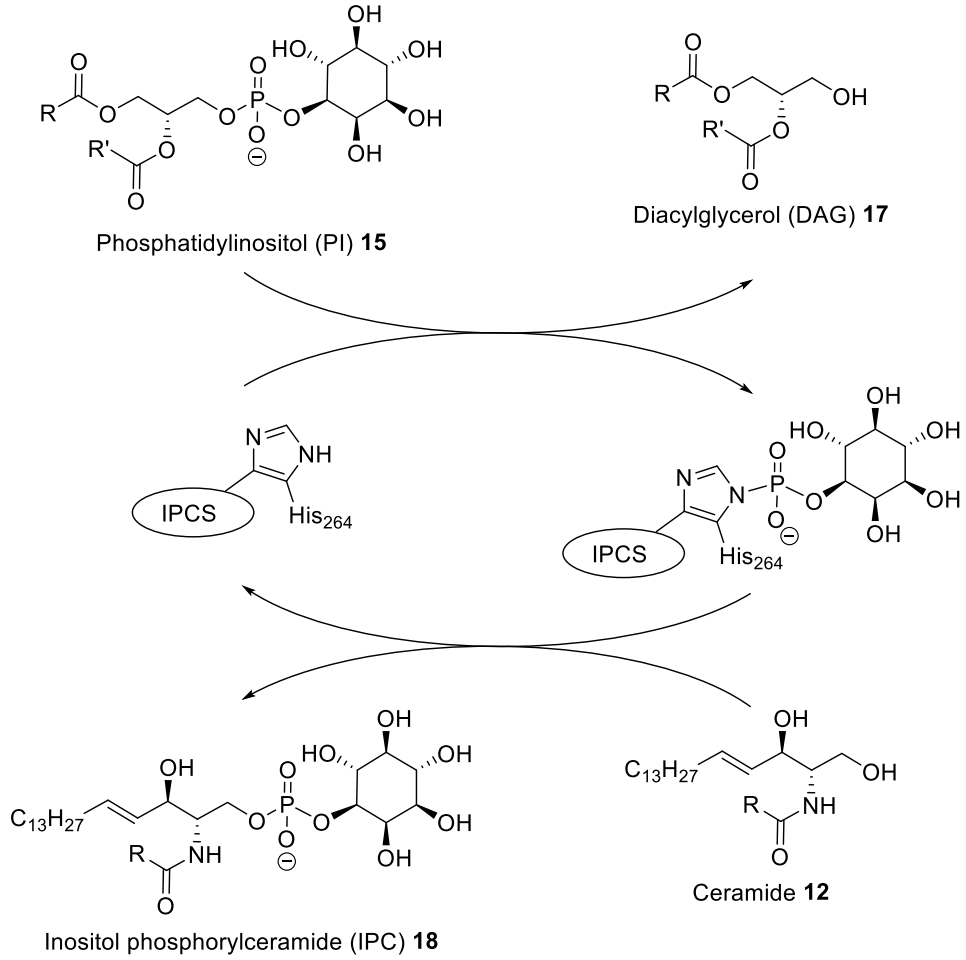

Scheme 1.11: Double displacement mechanism of action of *Lmj*IPCS

Further experimentation showed that the expression of *Lmj*IPCS in a mammalian cell line led to the synthesis of IPC-like lipids. This suggests that *Lmj*IPCS is able to establish IPC synthase activity in a system where IPC is not naturally present. In fact, the protozoan *Lmj*IPCS shares more similarity with the mammalian SMS than it does with fungal IPCS despite having equivalent functions. Evidently, phylogenetic analysis showed that *Lmj*IPCS belongs to a new class of kinetoplastid sphingolipid synthases that are distinct from fungal and mammalian orthologues.[58]

*Lmj*IPCS, which is largely confined to the Golgi apparatus, is a membrane-bound protein comprised of 338 amino acids and a mass of 38 kDa.[58,84] Like many other membrane-

bound proteins, *Lmj*IPCS is difficult to characterize thus, the true structure of *Lmj*IPCS remains unknown. In an effort to contribute to the development of a pharmacophore model of *Lmj*IPCS, Mina created a small library of ceramide analogues with which to explore the binding domain. This was done using a microtitre plate-based assay in which *Lmj*IPCS enriched microsomal membranes were used to measure the analogues ability to inhibit the IPCS mediated conversion of the fluorescent NBD-C_6-ceramide **24** to NBD-C_6-IPC **25** (Scheme 1.12).[67]

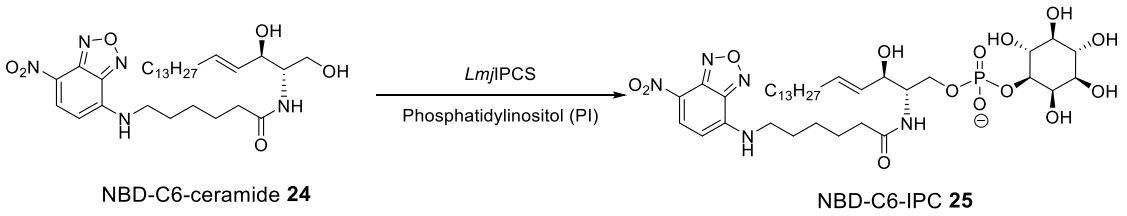

Scheme 1.12: *Lmj*IPCS biochemical assay

It was previously suggested that the *trans*- double bond affects the strength of the hydrogen bonding interactions of the C-3 hydroxyl group in ceramide **12**.[63] A structure-activity relationship (SAR) of the ceramide analogues (Figure 1.13) supports this theory, revealing that the C-3 hydroxyl group enhances enzyme binding affinity. While the amide linkage was not found to be essential, the presence of an N-acyl chain also contributed to binding affinity. Furthermore, a long hydrocarbon ceramide tail and steric bulk at the N-acyl group improve inhibition of IPC synthesis. In general, structural components which increase hydrophobicity have been found to favor affinity and improve inhibition. These findings are expected due to the hydrophobic nature of the membrane-bound enzyme.[67]

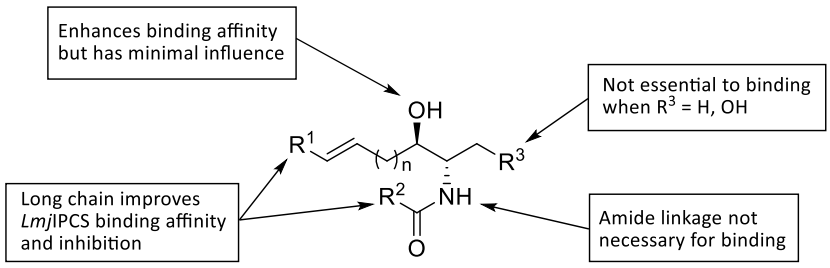

Figure 1.13: SAR of ceramide analogues on the *Lmj*IPCS binding domain

2 Previous work and aims

2.1 Previous work

High throughput screening (HTS) was used by Norcliffe to screen GSK's 1.8 million compound library against *Lmj*IPCS expressed in a mutant yeast system.[85,86] The initial screen was carried out through the development of an HTS-compatible fluorescence output assay which exploits the extracellular enzyme, exo-β-glucanase, as a measure of growth. This was done by exposing mutant yeast to fluorescein di-(β-D-glucopyranoside) **26** (FDGlu) which hydrolyzes to fluorescein **27**, a product that fluoresces in the presence of exo-β-glucanase (Scheme 2.1). Accordingly, compounds which inhibited *Lmj*IPCS and prevented growth showed little fluorescence due to the decreased production of exo-β-glucanase.

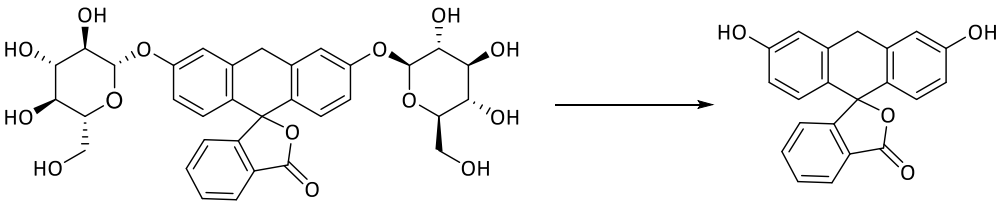

Scheme 2.1: The hydrolysis of FDGlu 26, used in HTS to identify hits

A total of 216 hit compounds, found to be highly active against *Lmj*IPCS and selective for *Lmj*IPCS when compared with fungal IPCS (AUR1p), were submitted for further screening. The compounds were first subjected to a parasite cytotoxicity assay against *L. major* promastigotes.[85,86] *L. major* is the predominant species the most clinically prevalent form of leishmaniasis, CL. However, its clinical manifestation is generally self-healing;[19,38,87] making it is less of a priority for drug discovery. As the London Declaration on NTDs had identified VL as a target for elimination,[41] a change was made in the HTS process to select compounds that showed inhibitory activity against *L. donovani*, the main causative species for VL. Amastigotes are the more clinically relevant parasitic life stage that is observed in the mammalian host.[88,89] However, due to the ease of implementation, axenic parasites

were used in the HTS process. Subsequently, the 216 compounds were subjected to a dose-response assay against *L. donovani* axenic amastigotes. Both of these assays used resazurin **28**, which is reduced *in celluo* to the highly fluorescent resorufin **29** (Scheme 2.2). A compound which gave a lower fluorescent output indicated a reduction in parasite viability and was therefore a more active antileishmanial. This led to a subset of 53 compounds which retained inhibitory activity greater than 50% at a 10 μM concentration against *L. major* promastigotes and *L. donovani* axenic amastigotes.[85,86]

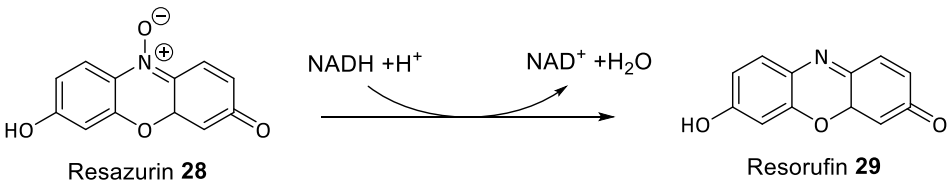

Scheme 2.2: The reduction of resazurin 28, used to determine parasite cytotoxicity

Next, the 216 compounds were subjected to preliminary host cytotoxicity tests using HepG2 cells, derived from human hepatocellular carcinoma. Here, cytotoxicity was measured by the addition of CellTiter-Glo to HepG2 cells which were incubated with the hit compounds. The CellTiter-Glo assay uses the luciferase reaction which converts luciferin **30** into the highly luminescent oxiluciferin **31** in the presence of adenosine triphosphate (ATP) (Scheme 2.3). As seen in the previous assays, a low luminescence output indicated a reduction in cell growth and therefore a cytotoxic compound. Following this assay, 53 compounds were found to have an SI (selectivity index) greater than or equal to 1.0, where an SI of 1.0 indicates a compound which is 10 times more potent against *L. donovani* axenic amastigotes than HepG2 cells.[85,86]

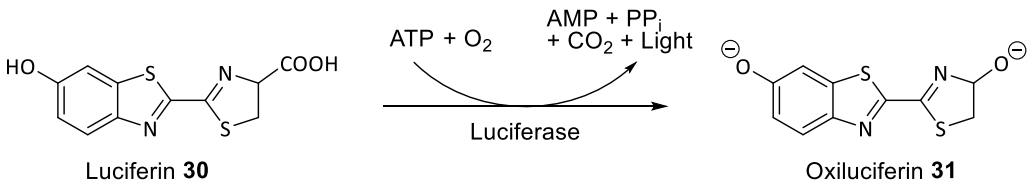

Scheme 2.3: The oxidative decarboxylation of luciferin 30, used to determine host cytotoxicity

The set of 53 compounds was then examined on the basis of several key physicochemical properties that are used to evaluate the hydrophobicity of a compound. This measurement, known as the property forecast index (PFI), is calculated as the sum of the

cLogP and the number of aromatic rings in a compound. This led to a set of 30 compounds, with a maximum of 4 aromatic rings and a PFI less than or equal to 8.0, which were selected for further investigation. These compounds were tested against intramacrophage *L. donovani* amastigotes to more accurately mimic the disease state and then subjected to a final cytotoxicity screen against macrophages using a human derived THP-1 premonocytes cell line.[85,86]

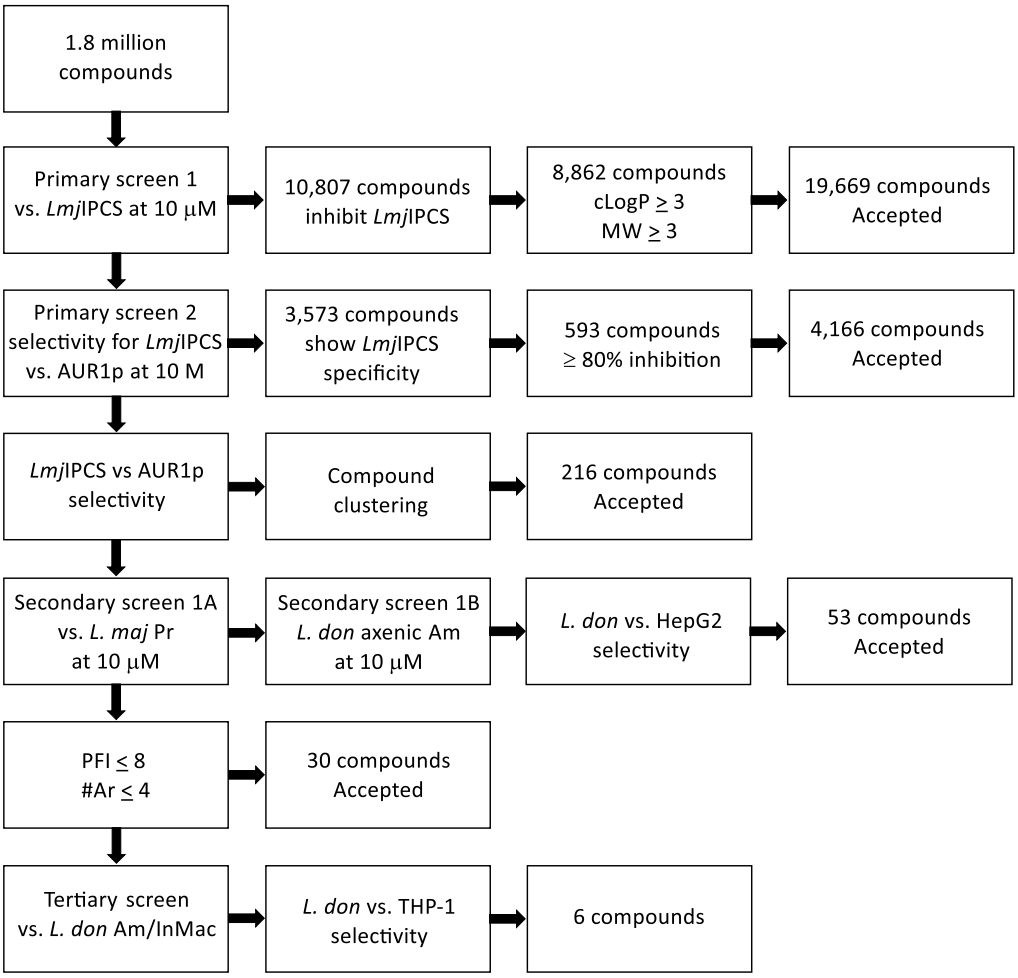

Figure 2.1: Schematic of the HTS workflow; Pr: promastigote, Am: amastigote

Using a selection criteria of compounds that show an inhibitory activity greater than 50% at a 10 μM concentration and a 10 fold greater potency against the *L. donovani* intramacrophage (InMac) amastigotes yielded a small set – six compounds which demonstrated high activity, low mammalian cytotoxicity, and favorable physiochemical properties. Two of the compounds identified as potent *Lmj*IPCS inhibitors, **32a** and **32b**,

contained a benzazepine core (Figure 2.2).[85,86] Figure 2.1 provides a schematic of the HTS process completed by Norcliffe.

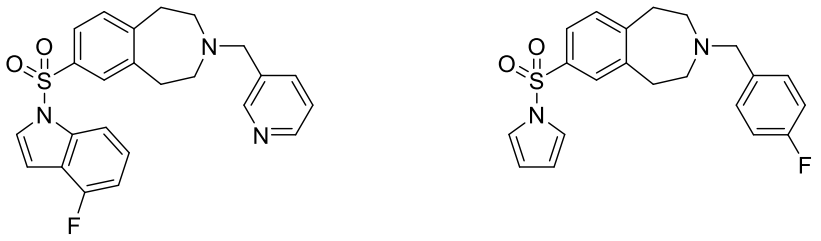

32a **32b**

Figure 2.2: Benzazepines found to be potent LmjIPCS inhibitors

To optimize the lead benzazepine compounds, a number of additional analogues were prepared. The initial focus was on a set of chimeric compounds **33a** and **33b**, which were created by exchanging the 4-fluoroindole and pyrrole substituents of the lead compounds. (Figure 2.3). Compound **33b** showed good parasitic inhibition with an EC_{50} of 2.5 µM. However, with an EC_{50} of 68 µM, it was not very active against the target enzyme (Table 2.1) when compared with lead compounds **32a** and **32b** (*Lmj*IPCS EC_{50} = 2.0 µM and 0.8 µM respectively).[85,86] Chimeric lead **33b** was subsequently submitted to metabolic stability testing. After incubating the inhibitor with human and mouse liver microsomes, the compound intrinsic clearance level (CL_{int}) was determined. While a favorable 2.3 $mL \cdot min^{-1}$ was found for human microsomes, mouse microsomes showed a high clearance level of 29 $mL \cdot min^{-1}$. It was thought that the high clearance levels were due to CYP450 oxidation of the metabolically labile benzylic position.[85]

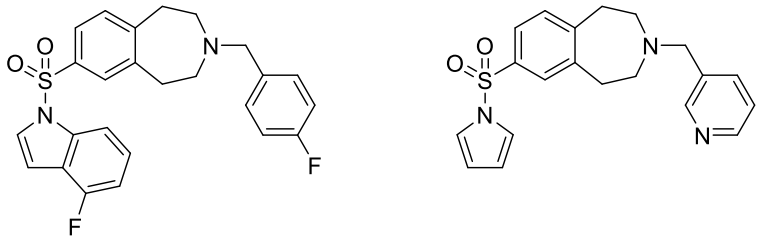

33a **33b**

Figure 2.3: Chimeric benzazepines in which the 3-substituent of lead compounds 32a and 32b are exchanged

To examine this theory, a deuterated version of **33b** was prepared and submitted for metabolic stability testing (Table 2.1). For **33b-d_2**, a reduced clearance level would be

expected as C-D bonds are more difficult to cleave than C-H bonds.[90–92] However, the intrinsic clearance levels of **33b-d_2** were similar to that of **33b**, suggesting that the benzylic position was not being oxidized by CYP450. Despite the similarity in activity and clearance level, **33b** and **33b-d_2** displayed very different pharmacokinetic properties. Namely, **33b-d_2** reached a maximum concentration (C_{max}) that was three times more than **33b** in less than half the time (t_{max}). Additionally, the total drug exposure, expressed as the dose normalized area under the curve (DNAUC), of **33b-d_2** was two times more than **33b**. These measurements show that the parasites were exposed to a higher concentration of **33b-d_2** for a longer period of time.[85] Furthermore, these results serve as an indicator that **33b-d_2** is engaged in deuterium-induced metabolic switching, where the primary pathway for metabolism is altered as a consequence of the increased energy barrier to CYP450 oxidation caused by the stronger C-D bond.[92]

	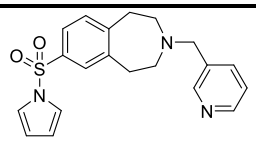 **33b**	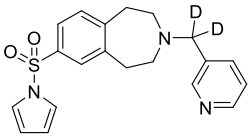 **33b-d_2**
*Lmj*IPCS EC_{50} (µM)	68	59
L. major EC_{50} (µM)	2.5	2.0
L. donovani Am/InMac EC_{50} (µM)	0.5	0.4
CL_{int} – human (mL/min·g)	2.3	5.0
CL_{int} – mouse (mL/min·g)	29	30
C_{max} (ng/mL)	1091	3043
t_{max} (h)	1.00	0.42
DNAUC (ng.h/mL per mg/kg)	71	150

Table 2.1: Parasitic activity and metabolic stability of 33b and 33b-d_2

Additional analogues containing the pyrrole ring were also tested for inhibitory effects. However, the majority of these compounds were poor inhibitors of *Lmj*IPCS. A summary of the structure-activity relationship is given below (Figure 2.4). Upon further analysis, **33a** was found to have an EC_{50} of 2.0 µM against *L. major* promastigotes. Additionally, **33a** displayed on target effects when tested against *Lmj*IPCS.[85,86] This work leaves

benzazepines **33a** available for further development and provides the basis of this investigation.

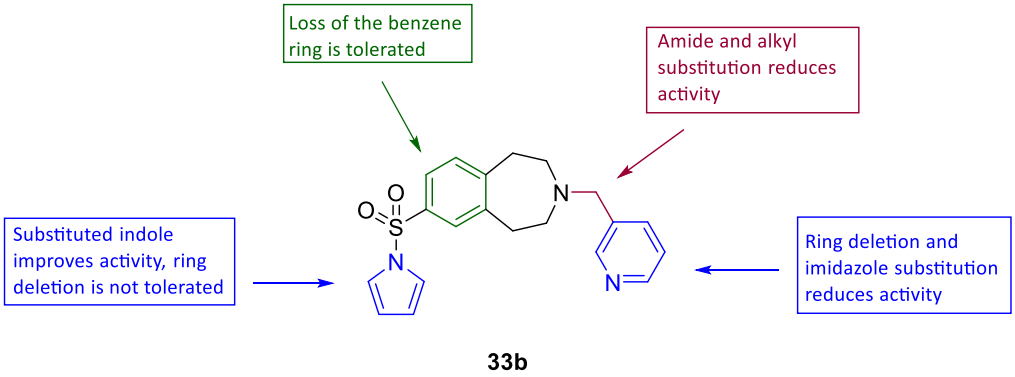

Figure 2.4: Summary of early structure-activity relationships

2.2. Project Aims

Taking into consideration the data that was obtained from the GSK high throughput screen, the primary objective of this project was to develop an efficient method to prepare 3-, 7- substituted 3H-benzazepines analogues. As analogues of lead compound **32b** were previously explored, initial work would focus on the synthesis of **32a** analogues with a focus on the substituent in the 3- position, the alkyl linker, and the azapane ring (Figure 2.5). These compounds would then be tested for activity and selectivity against *Leishmania spp.*

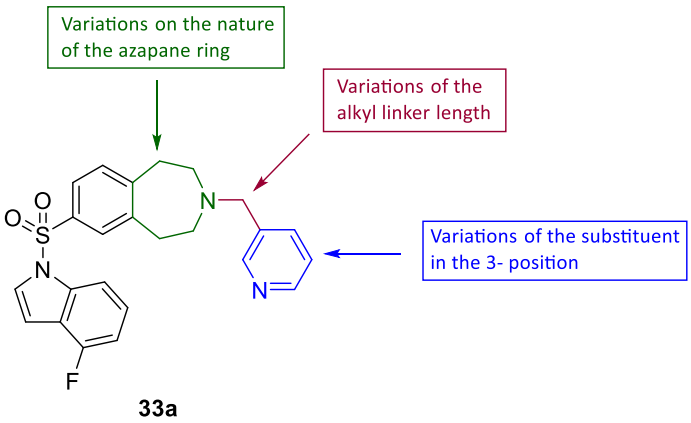

Figure 2.5: Investigation of benzazepine 32a

Subsequent work would then focus on elaboration of the chemical structure of the most promising compounds, with a view to generating structure activity data that could be used to validate IPCS as a drug target.

3. Results and Discussion

3.1 Chemical Synthesis

As discussed in section 2.1, 3H-benzazepines have been shown to be potent *Lmj*IPCS inhibitors. Past studies in the group concerning the lead optimization has shifted the interest to indole substituted 3H-benzazepines. Therefore, it was of interest to synthesize analogues in order to develop structure activity relationships (SAR).

3.1.1 3H-Benzazepines

A disconnection strategy of lead compound **32a** results in the identification of four key groups: a 3-methylpyridine head group **34**, a 4-fluoroindole tail group **35**, a sulfonyl group, and the core 3H-benzazepine **37** (Scheme 3.1).

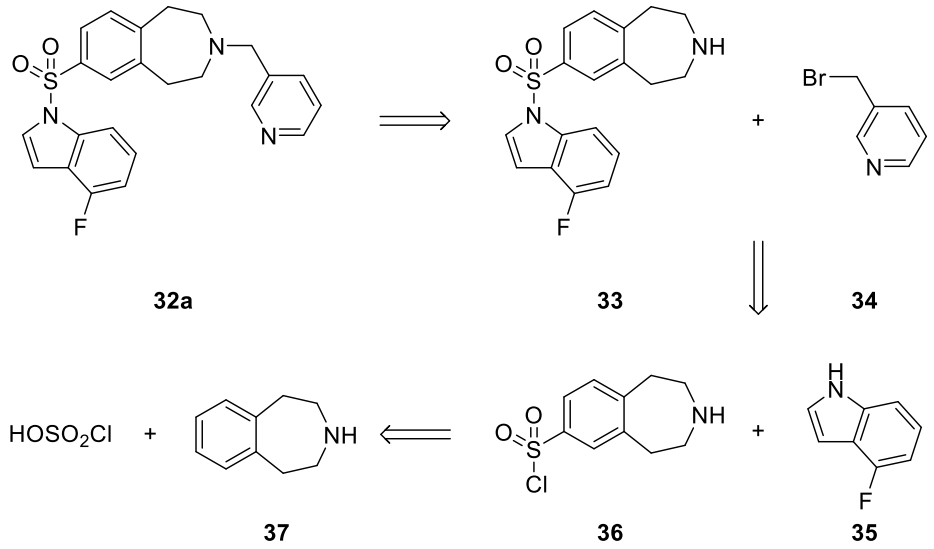

Scheme 3.1: Disconnection strategy of lead benzazepine 32a

Functionalized 3H-benzazepines have become a versatile class of compounds used in the development of molecules of pharmaceutical and biological interest. Drug products such as those in Figure 3.1 have a wide range of applications and biological activities. For example varenicline,[93] lorcaserin,[94,95] and fenoldopam[96,97] are used in the treatment of smoking cessation, weight management, and hypertension, respectively. Ivabradine[98,99] and related compounds form a family of hyperpolarization-activated cyclic nucleotide-gated (HCN) channel inhibitors.

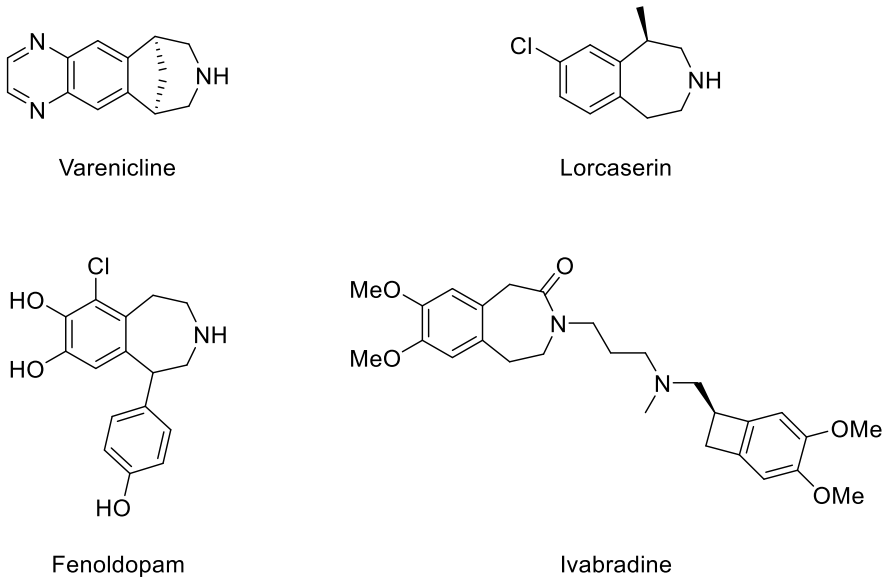

Figure 3.1: Drug products containing a functionalized 3H-benzazepine

While 3H-benzazepine is commercially available, it is expensive as a core building block. The biological relevance of the benzazepine framework has prompted the development of novel methodologies for the synthesis of such ring systems. Generally, these nitrogen-containing heterocycles are formed at a late stage in a synthetic route. This is exemplified in the synthesis of varenicline and fenoldopam. Key transformations through which benzazepines are constructed include cycloaddition, electrophilic aromatic substitution, cross-coupling reactions, ring expansions, and rearrangements.[94,96,99–102]

3.1.1.1 Synthesis of 1,2,4,5-tetrahydro-1H-3-benzazepine

In order to make the target compound and derivatives based on this key group, it was imperative to develop a synthetic route which would produce large quantities of the core molecule and allow for variation at the 3- and 7- positions. An analysis of this structure suggests two possible approaches which start from the readily available 1,2-phenylenediacetic acid **38** (Scheme 3.3). Both were initially explored concurrently.

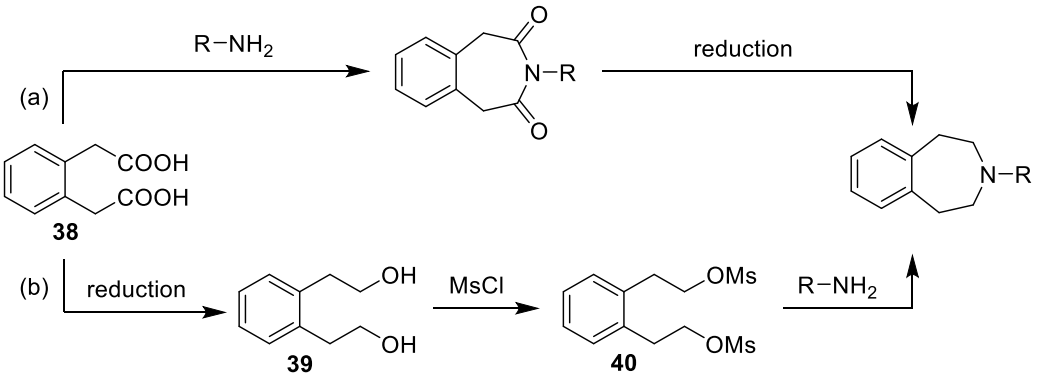

Scheme 3.2: Routes to 3H-benzazepine from 1,2-phenylenediacetic acid 38

The potentially shorter route involved cyclization to the imide followed by reduction (Scheme 3.2, a). A method described by Flaih *et al.* provides for the one pot synthesis of cyclic imides (Scheme 3.3). This procedure involves the activation of the carboxyl groups of compound **38** with N-(3-dimethylamino)propyl-N-ethylcarbodiimide hydrochloride (EDC-HCl) and hydroxybenzotriazole (HOBt), to produce an activated ester. Finally, nucleophilic attack by trifluoroacetamide produces the cyclic imide **40**.[103]

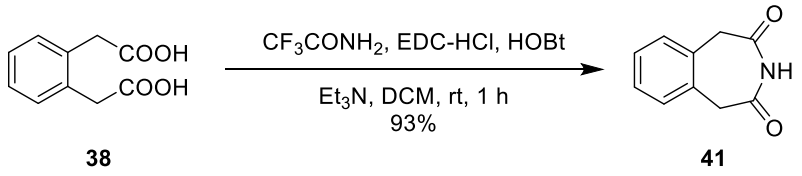

Scheme 3.3: Synthesis of cyclic imide 41 by Flaih *et al.*[103]

Attempts to replicate this method were not successful, with reaction monitoring by TLC showing no product formation even after 6 hours. Although modified conditions could be

successful, this work was not pursued further as the alternative approach proved to be more promising. The alternative strategy of initial reduction of 1,2-phenylenediacetic acid **38** followed by the mesylation of the resulting diol **39** was explored (Scheme 3.2, b). This method, first described by Harvey *et al.* in the synthesis of polyaromatic systems (Scheme 3.4),[104] has since been used in several patents in the synthesis of 3H-benzazepines.[105,106]

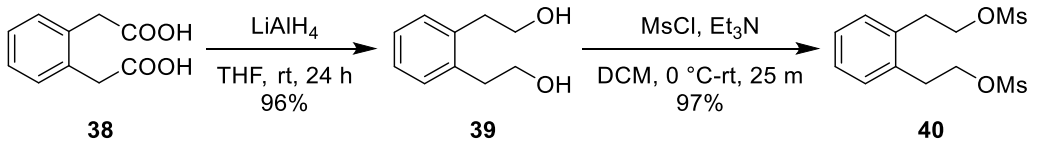

Scheme 3.4 Synthesis of 1,2-bis-[2'-(methanesulfonyloxy)ethyl]benzene 40 by Harvey *et al.*[104]

Following this precedent, the reduction of 1,2-phenylenediacetic acid **38** with $LiAlH_4$ in THF at reflux followed by aqueous workup afforded the pure product 2,2'-(1,2-phenylene)diethanol **39** in 98% yield in a fraction of the time reported by Harvey. The formation of the desired diol **39** was confirmed by the loss of the carbonyl stretch in the IR spectrum and appearance of the newly formed carbinol CH_2 group in the ^{1}H-NMR spectrum at 3.81 ppm. Subsequent treatment of the diol **39** with MsCl produced the pure desired 1,2-bis-[2'-(methanesulfonyloxy)ethyl]benzene **40** in 99% yield as determined by a shift in the carbinol CH_2 signal to 4.41 ppm and the appearance of the CH_3 signal characteristic of the mesyl group at 2.90 ppm in the ^{1}H-NMR spectrum. The replicated yield over these two steps was generally quantitative and lead to products that were sufficiently pure and could be used directly without further purification (Scheme 3.5).

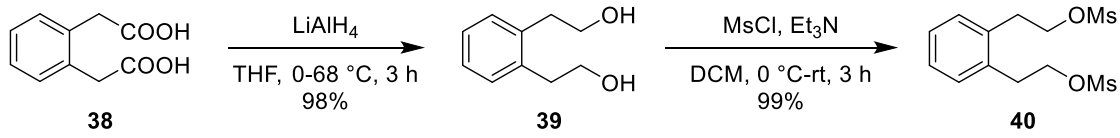

Scheme 3.5: Synthesis of 2,2'-(1,2-phenylene)diethanol 39 and 1,2-bis-[2'-(methanesulfonyloxy)ethyl]benzene 40

With the bis-mesylated product **40** readily available, attention was turned to the key cyclisation step. Previous work in the group showed that *N*-allyl protected pyrrolidines **42**

could be prepared through the reaction of a similarly bis-mesylated substrate **41** with allylamine. Subsequent deprotection using Wilkinson's catalyst then afforded the pyrrolidine **43** (Scheme 3.6).[107]

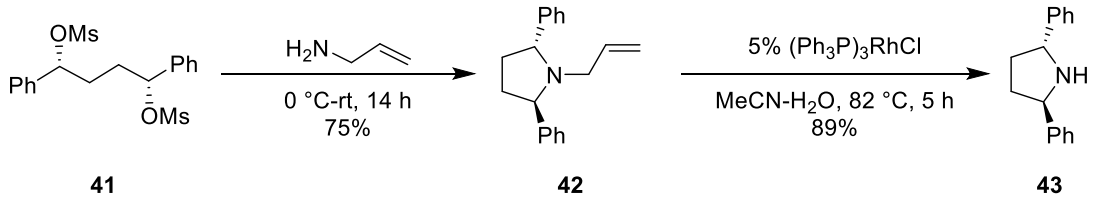

Scheme 3.6: Cyclization and N-allylic deprotection of a pyrrolidine by Dutton[107]

This was an attractive approach as the allylic protecting group is a robust system which will withstand chlorosulfonation. Blocking the amine with a protecting group that is both acid and base resistant and inert to nucleophiles would allow for the subsequent directed substitution of the benzene ring. Based on this, the bis-mesylated product **40** was reacted with allylamine in order to arrive at the protected heterocycle (Scheme 3.7). Following reaction optimization, it transpired that generating the benzazepine required 48 hours at room temperature to reach completion. With this change, the reaction afforded the desired allyl protected benzazepine **44** in 81% yield after aqueous workup and purification by column chromatography. Formation of the protected benzazepine was confirmed by the corresponding peak in the LCMS spectrum (*m/z* (ES^+) found $[M+H]^+$ 188.2).

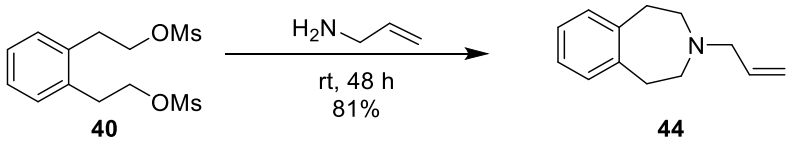

Scheme 3.7: Synthesis of allyl protected benzazepine 44

Following the protocol from the group application of a Laguzza and Ganem procedure, Wilkinson's catalyst was used to deprotect benzazepine **44** (Scheme 3.8).[108] Surprisingly, this reaction did not give the desired product and lead to extensive decomposition. Further attempts with larger catalytic loads of 10% and 15% gave the same result.

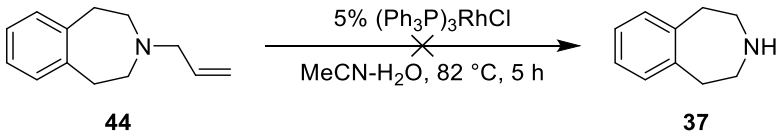

Scheme 3.8: Attempted deprotection of 3-(prop-2'-en-1'-yl)-1,2,4,5-tetrahydro-1H-3-benzazepine 44 using Wilkinson's catalyst

A review of the literature revealed that a more effective deprotection can be obtained by increasing the catalytic load to 25% in the presence of 1 molar equivalent of trifluoroacetic acid as an allyl scavenger and by changing the solvent system to refluxing ethanol.[109,110] Unfortunately, attempts to apply these conditions were also unsuccessful. It remains unclear as to why this process is not effective for the 3H-benzazepine scaffold. Given these difficulties, alternative methods were pursued.

A method described by Kumar *et al.* showed that an N-allylic group could be cleaved from a variety of amines using the high oxidation potential of 2,3-dichloro-5,6-dicyano-1,4-benzoquinone (DDQ) (Scheme 3.9).[111]

Scheme 3.9: N-allylic deprotection by Kumar *et al.*[111]

Following this precedent, deprotection of the N-allylic benzazepine **44** was attempted in the presence of DDQ (Scheme 3.10). Although this method has been shown to work well on various tertiary allyl amines, it proved to be unsuccessful in this investigation and lead to loss of the starting material. The original report gave no precedence for the deprotection of cyclic amines suggesting that the allyl protected benzazepine is not a suitable substrate for this reaction, which works most efficiently in aliphatic or benzylic allyl amine substrates.[111]

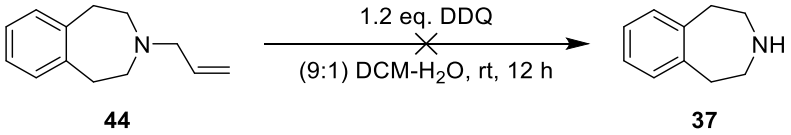

Scheme 3.10: Attempted DDQ deprotection of 3-(prop-2'-en-1'-yl)-1,2,4,5-tetrahydro-1H-3-benzazepine 37

With the difficulties in deprotecting the allyl group, attention then turned towards directly synthesizing the unsubstituted 3H-benzazepine. A review of the literature revealed two protocols in which the mesylate **40** was reacted with ammonium hydroxide to directly produce the unsubstituted 3H-benzazepine **37** (Scheme 3.11).[105,106]

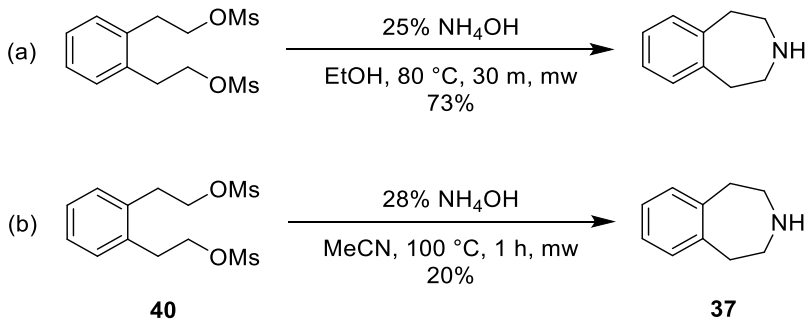

Scheme 3.11: Synthesis of 1,2,4,5-tetrahydro-1H-3-benzazepine 37 by (a) Braje *et al.*[106] and (b) Zhang *et al.*[105]

First, a screen was done to determine whether the difference in product yield could be attributed to the change in reaction conditions. The results of the screen are summarized in Table 3.1 where the isolated yield of the product is reported. The screen confirmed the significant difference in the amount of product formed, despite the scale of the reaction. For reasons that are not obvious, ethanol improved yields by 25% while allowing the reaction to be performed at a lower temperature.

Entry	Solvent System (v/v)	Scale (mmol)	Time (h)	Yield (%)[c]
1	EtOH – 28% NH_4OH (1:1)[a]	0.25	0.5	75
2	EtOH – 28% NH_4OH (1:1)[a]	0.80	0.5	73
3	MeCN – 28% NH_4OH (1:1)[b]	0.25	1	58
4	MeCN – 28% NH_4OH (1:1)[b]	0.80	1	41

Table 3.1: Comparison of microwave protocols for the synthesis of benzazepine 37; [a]Reacted at 80 °C; [b]Reacted at 100 °C; [c]Isolated yield.

Completing this synthetic step in the microwave would limit the scale of the reaction. In an attempt to avoid doing several dozen microwave reactions, a secondary screen was undertaken. This screen would determine the optimal scale and concentration of this reaction, the results of which are summarized in Table 3.2.

Unfortunately, product yield was negatively affected as the system became more concentrated (Table 3.2, Entries 2 and 3). While it is not surprising that decreasing the concentration of ammonia gave a reduction in product formation (Table 3.2, Entries 5 and 6), a reduction in yield was also seen when the ethanol concentration was reduced (Table 3.2, Entry 4). This is likely due to a reduced solubility of the bis-mesylated substrate **40**. The results of these optimization trials suggest that carrying out this reaction in a 1:1 ethanol-ammonium hydroxide solvent system at 0.15 M (Table 3.2, Entry 1) was found to be ideal.

Entry	Solvent System (v/v)	Concentration (M)[a]	Yield (%)[b]
1	EtOH – 28% NH_4OH (1:1)	0.15 M	83
2	EtOH – 28% NH_4OH (1:1)	0.30 M	48
3	EtOH – 28% NH_4OH (1:1)	0.60 M	43
4	EtOH – 28% NH_4OH (1.2)	0.40 M	22
5	EtOH – 28% NH_4OH (2:1)	0.40 M	16
6	EtOH – 28% NH_4OH (2.5:1)	0.80 M	37

Table 3.2: Optimization of microwave reaction conditions for the synthesis of benzazepine 37. [a]Concentration based on total volume, reactions performed on 0.80 mmol scale. [b] Isolated yield.

Following the two condition screenings, the original conditions from the Braje protocol (Scheme 3.11, a) was chosen for this investigation. The appearance of a broad peak at 2.32 ppm in the ^{1}H NMR spectrum, assigned to the N-*H* group and the and the corresponding peak in the LC-MS chromatogram (*m/z* (ES^+) = 148.3 $[M+H]^+$) confirmed the formation of 1,2,4,5-tetrahydro-1H-3-benzazepine **37.**

3.1.1.2 Functionalization of 1,2,4,5-tetrahydro-1H-3-benzazepine

Functionalization of 1,2,4,5-tetrahydro-1H-3-benzazepine **37** began with the protection of the azepane N-atom with trichloroethyl chloroformate (Troc-Cl, Scheme 3.12) as this protecting group is impervious to the strongly acidic conditions of chlorosulfonylation. After 18 h, analysis by thin layer chromatography (TLC) showed that all starting material was consumed. Initial attempts to purify the Troc-protected benzazepine **47** by silica column chromatography led to product decomposition, as determined by 2D TLC, and would be impractical on a large scale. Therefore, crystallization from ethanol was undertaken and proved to be optimal, giving a 68% yield of 2',2',2'-trichloroethyl-1,2,4,5-tetrahydro-1H-3-benzazepine-3-carboxylate **47**. Formation of the Troc protected benzazepine **47** was confirmed by the strong carbonyl stretch in the IR spectrum at 1707 cm^{-1} and by the distinctive 27:27:9:1 isotope pattern observed in the ASAP chromatograph of triply chlorinated molecules.

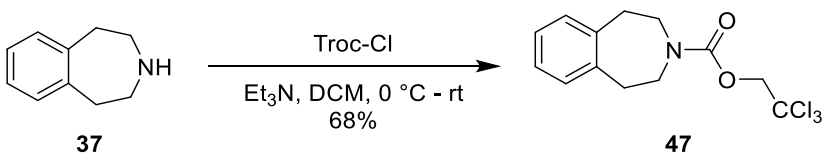

37 47

Scheme 3.12: Troc protection of 1,2,4,5-tetrahydro-1H-3-benzazepine 37

With the now protected benzazepine in hand, the next step was the introduction of the sulfonyl group. Chlorosulfonic acid is a powerful sulfonating agent which can give sulfonic acids, sulfones, and sulfonyl chlorides, therefore reaction conditions can vary widely depending on the nature of the substrate and the desired product. In light of this, a method by Liu *et al.* (Scheme 3.13) was used in this investigation where the trichloroacetyl protected substrate **48** is added to three equivalents of chlorosulfonic acid in dichloromethane at 0°C and the mixture slowly warmed to room temperature. The sulfonyl chloride **49** was then readily isolated by addition to ice-DCM mixture followed by extraction.[112]

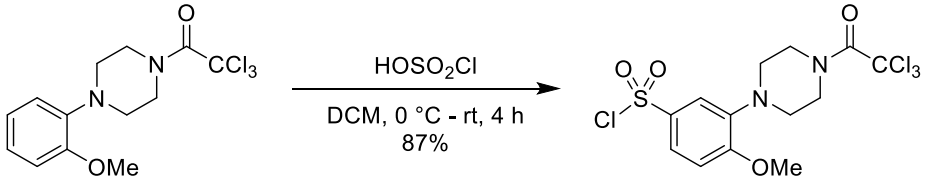

48 49

Scheme 3.13: Chlorosulfonation of a trichloroacetyl protected amine by Liu *et al.*[112]

As sulfonyl chlorides are sensitive to traces of heat and moisture, this investigation found that the acid chloride could easily convert to the sulfonic acid **48** during aqueous workup if the temperature did not remain cold (Scheme 3.14). Additionally, attempts at further purification lead to product decomposition. Confirmation of the acid product **48** was obtained from the LCMS (ES^+) analysis, where the corresponding peak showed the molecular ion *m/z* 402.1. Further supporting evidence was gained from infrared analysis which showed a broad peak characteristic of the hydroxyl group at δ 3230 cm^{-1}.

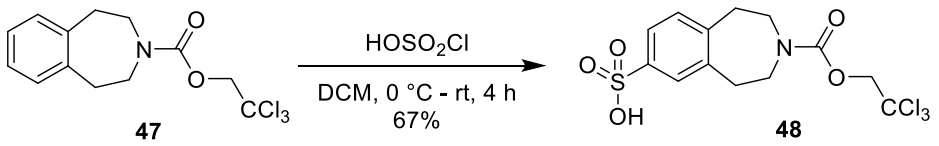

Scheme 3.14: Attempted chlorosulfonation of Troc-protected benzazepine 47

Even though **48** was not the desired product, as the sulfonic acid **48** had been obtained after a five-step route, an attempt was made to convert it to the sulfonyl chloride **49** rather than lose all progress in the synthesis of the target molecule. The first attempt was to react the acid in neat thionyl chloride. Unfortunately, analysis by LCMS did not show the formation of product (Scheme 3.15). Further attempts to convert acid **48** to the sulfonyl chloride were made with the addition of a catalytic amount of chlorosulfonic acid, performing the reaction in DMF, and increasing the temperature and the reaction time also failed. In all of these cases, the substrate degraded.

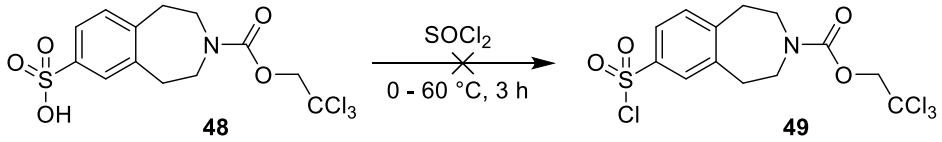

Scheme 3.15: Attempted acid chloride formation using thionyl chloride

A literature search suggested another method in which heating a sulfonic acid with phosphorous pentachloride in trichlorophosphate would generate an acid chloride (Scheme 3.16). However, applying these conditions to acid **48** also failed to give the desired product and lead to complete decomposition of the substrate. Further attempts to convert **48** to the sulfonyl chloride **49** were abandoned.

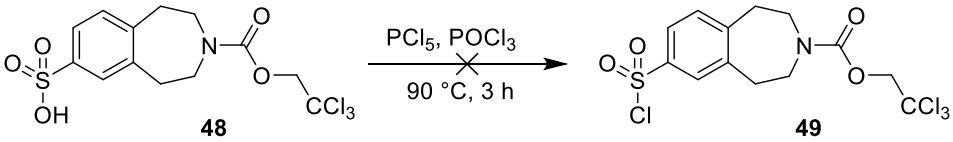

Scheme 3.16: Attempted acid chloride formation using a $PCl_5/POCl_3$ system

Ultimately, after considerable experimentation, ensuring that a large volume of cold ether was used during the workup of the chlorosulfonation of **47** lead to a 61% yield of the desired 7-chlorosulfonyl-2,3,4,5-tetrahydro-1H-3-benzazepine-3-carboxylate **49** that was sufficiently pure after workup (Scheme 3.17).

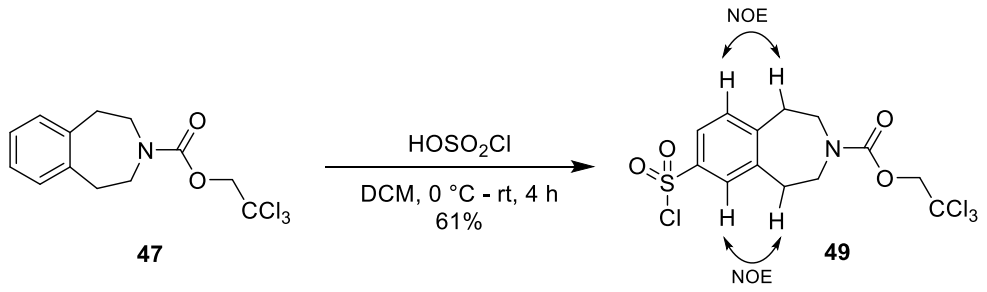

Scheme 3.17: Chlorosulfonation of Troc-protected benzazepine 47

Chlorosulfonation occurs selectively at the 7- position of the benzazepine, as confirmed by the strong NOE correlations of H_2-1 and H_2-5 with *H*-9 and *H*-6, respectively. Infrared analysis showing the lack of a characteristic -OH stretch provided confirmation that the product was not the sulfonic acid. Further evidence that the sulfonyl chloride was indeed made came from the LRMS chlorine isotope pattern of 81:108:54:12:1 observed from quadrupole chlorination as well as from HRMS-ASAP, where $[M+H]^+$ was found to be 419.9405 *m/z*.

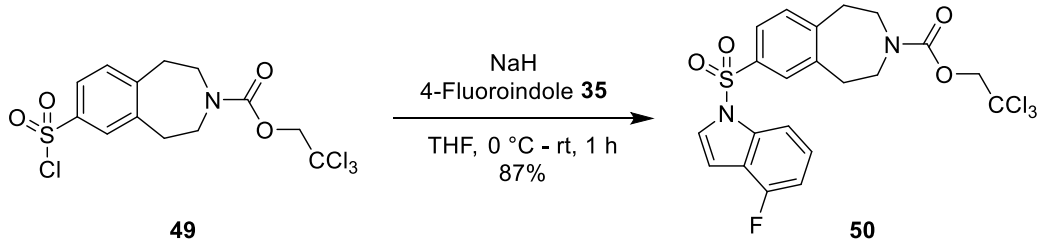

Scheme 3.18: Sulfamidation of benzazepine 49 with 4-fluoroindole 35

Initially, the retrosynthesis of benzazepine **32a** requires coupling with 4-fluoroindole **35**. Previous work in the group had shown that sulfamidation of the benzazepine substrate could be completed with an indole in the presence of NaH.[113] Following this precedent, the 4-fluoroindole substituted benzazepine **50** was generated in 87% yield (Scheme 3.18). The product was confirmed by HRMS-ASAP, where $[M+H]^+$ was found to be 518.0036 *m/z* as well

as by the appearance of a peak at 120.70 ppm corresponding to the indole fluorine in the ^{19}F-NMR.

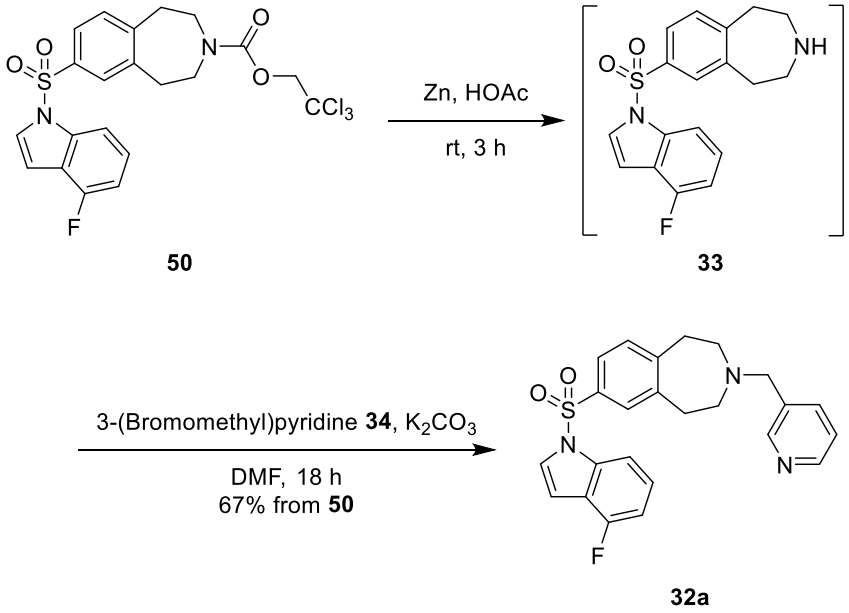

Scheme 3.19: Synthesis of lead benzazepine 32a from sulfonyl indole 50

Cleavage of the Troc protecting group to reveal the free secondary amine **33** was performed using excess zinc powder in the presence of acetic acid as previously reported by Boudreault and Leblanc.[114] TLC analysis confirmed reaction completion through the consumption of starting material. Further evidence of the formation of **33** was confirmed by the corresponding peak in the LCMS spectrum (*m/z* (ES^+) found $[M+H]^+$ 345.16). In order to avoid difficulties in isolating the pure secondary amine **33**, the product was used directly in the subsequent N-alkylation with 3-(bromomethyl)pyridine **34** in the presence of potassium carbonate to give the target compound **32a** in 67% yield over two steps (Scheme 3.19). The product was confirmed by the loss of the Troc CH_2 group at 4.77 ppm and the appearance of the pyridyl CH_2 group at 3.60 ppm. Further confirmation could be found from the corresponding peak in the LCMS (ES^+) chromatogram, where $[M+H]^+$ was found to be 436.350 *m/z*.

Despite the use of new batches of reactant, all subsequent attempts to reliably replicate the zinc mediated Troc deprotection showed a reduction in product formation, even over an

extended period of time. For these reasons, the use of a new protecting group was explored. A literature research revealed a procedure described by Macdonald *et al.* which gives access to sulfonylchloride **52** via acetamide protected benzazepine **51** (Scheme 3.20).[115]

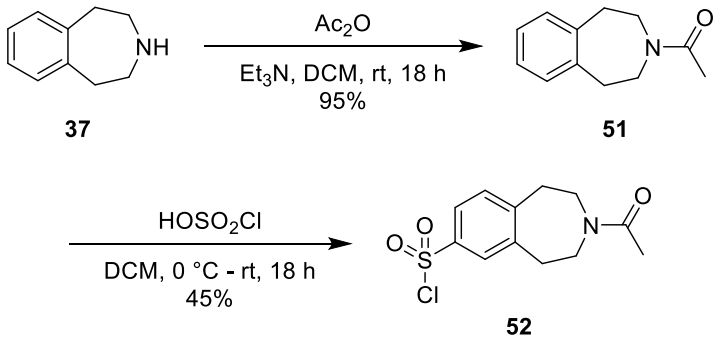

Scheme 3.20: Acetamide protection and chlorosulfonation of 1,2,4,5-tetrahydro-1H-3-benzazepine 37 by Macdonald *et al.*[115]

Using this method, the pure 1'-(1,2,4,5-tetrahydro-1H-3-benzazepin-3-yl)ethan-1'-one **51** was successfully obtained in 95% yield after aqueous workup. This was evident by the presence of a characteristic singlet at 2.18 ppm corresponding to the acetamide C*H*$_3$ and loss of the azepine N-*H* in the ^{1}H-NMR spectrum. Subsequent chlorosulfonation of the acetemide protected benzazepine **51** afforded the desired 3-acetyl-1,2,4,5-tetrahydro-1H-3-benzazepine-7-sulfonylchloride **52** in 60% yield (Scheme 3.21). As with the Troc protected benzazepine **47**, substitution was only observed at the 7- position. The rotameric structure complicated the NMR spectrum as evidenced by ^{1}H-NMR spectroscopic analysis which now showed the acetamide C*H*$_3$ as two peaks at 2.23 and 2.08 ppm. The chlorine isotope pattern of 3:1 observed was also observed in the LCMS (ES$^+$) analysis, where 288.192 [M(^{35}Cl)H]$^+$ and 290.130 [M(^{37}Cl)H]$^+$ *m/z* were found in the corresponding peak.

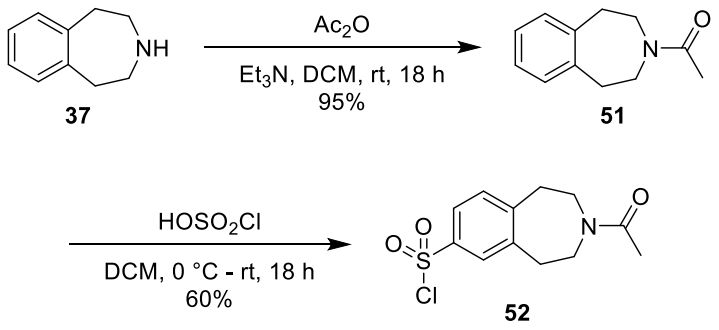

37 51 52

Scheme 3.21: Acetamide protection and chlorosulfonation of 1,2,4,5-tetrahydro-1H-3-benzazepine 37

As yields for the sulfamidation of Troc protected benzazepine **49** in the presence of NaH had steadily declined due to the presence of water in the reaction, a new method for the synthesis of benzazepine **56** was needed. A literature search presented a mild method for the synthesis of N-Arylsulfonylindoles described by Xu and Wang which uses sodium hydroxide and triethylbenzylammonium chloride (TEBA-Cl) as a phase transfer catalyst (Scheme 3.22).[116] These conditions were applied to the synthesis of **56**.

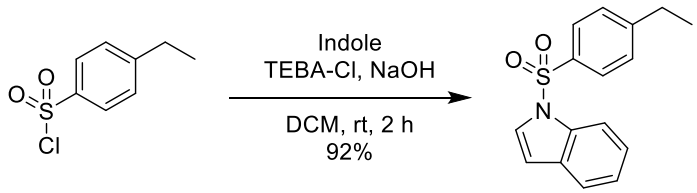

53 54

Scheme 3.22: N-Arylsulfonylindole Synthesis by Xu and Wang[116]

Powdered NaOH and TEBA-Cl was added to a solution of 4-fluoroindole **35** and **52** in anhydrous dichloromethane. After 20 h, analysis by TLC showed that all starting material was consumed. Aqueous workup and column chromatography gave the desired sulfonylindole **55** in 63% yield**,** which was confirmed by the corresponding peak in LCMS (*m/z* (ES^+) = 387.226 $[M+H]^+$). Further evidence of the formation of this molecule was also evident by the appearance of two peaks in the ^{19}F-NMR spectrum at -120.66 and -120.69 ppm (Scheme 3.23).

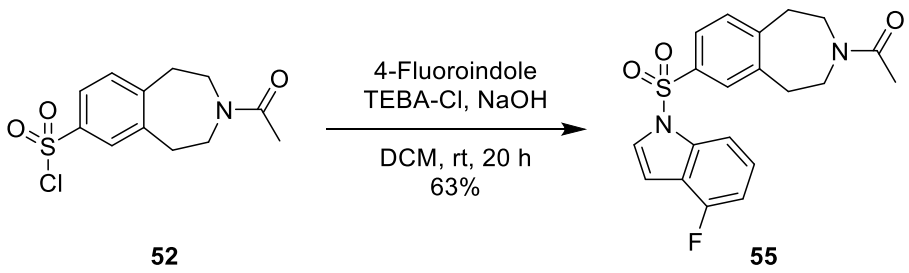

Scheme 3.23: Synthesis of sulfonylindole 56

3.1.1.3 Variations of the substituent in the 3-position

Deprotection of sulfonylindole **55** in refluxing HCl lead to benzazepine **33** as evidenced by the return of the broad N-*H* peak in the ^{1}H NMR spectrum and the signal in the LCMS (ES^{+}) spectrum with a *m/z* = 345.32 corresponding to the $[M+H]^{+}$ molecular ion. Due to the difficulty in obtaining good chromatographic purification, **33** was then subjected to N-alkylation to afford benzazepine analogues **32a** and **56** in good isolated yields (Table 3.3, Entries 1 – 2).

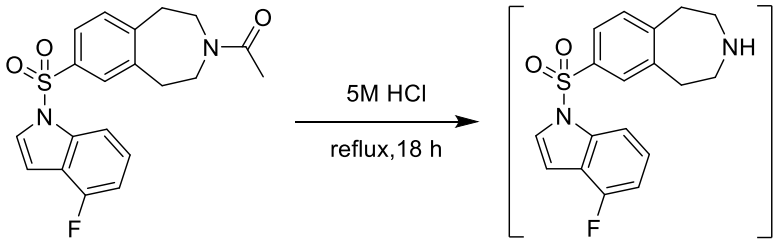

55 **33**

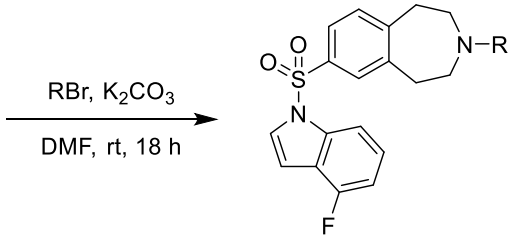

32a, 56 - 58

Entry	Starting material	Product	R	Yield (%)[a]
1	3-(Bromomethyl)pyridine **34**	**32a**	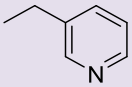	78
2	4-(Bromomethyl)benzonitrile	**56**	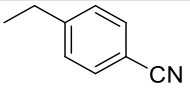	74
3	2-(Bromomethyl)pyridine	**57**	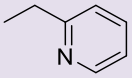	–
4	3-(2-Bromoethyl)pyridine **61**	**58**	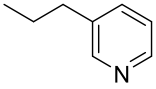	–

Table 3.3: Synthesis of benzazepines analogues (32a, 56 – 58); [a]Reported yield is over two steps

In an effort to explore the electronic environment of the binding pocket, the position of the nitrogen atom in lead compound **32a** was manipulated. This was first done by alkylating with 4-(Bromomethyl)benzonitrile, thereby removing the nitrogen atom from the ring (Table 3.3, Entry 2). In an effort to examine the position of the nitrogen on the ring, an attempt to alkylate **33** with 2-(Bromomethyl)pyridine was also made. Unfortunately, after extending the reaction time to 24 h, no product was observed in the crude NMR (Table 3.3, Entry 3).

In order to synthesize **58**, it was necessary to first synthesize the 3-(Bromoethyl)pyridine **61**. Ethyl 3-pyridylacetate **59** was reduced with $LiAlH_4$ to form 2-(pyridin-3'-yl)ethan-1-ol **60** in 30% yield after aqueous workup and column chromatography (Scheme 3.24). A triplet at 3.88 ppm in the ^{1}H-NMR spectrum assigned to the carbinol CH_2 group and a triplet at 2.86 ppm assigned to the two protons of the CH_2-group next to it confirmed the formation of the product. The loss of the carbonyl stretch in the IR spectrum gave further confirmation of the product. The low yield is possibly due to the poor solubility of ethyl 3-pyridylacetate **59** in THF.

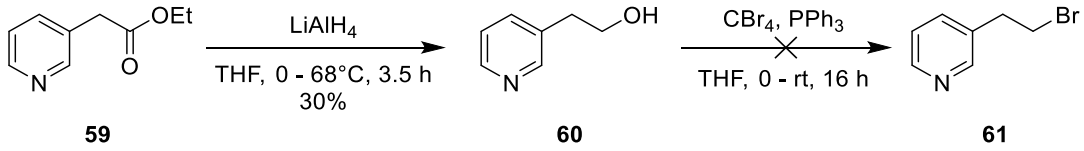

59 **60** **61**

Scheme 3.24: Attempted synthesis of 3-(Bromoethyl)pyridine 61

An initial attempt to generate 3-(2-Bromoethyl)pyridine **61** began by treating alcohol **60** with triphenylphosphine and carbon tetrabromide for 16 h at room temperature. No evidence for the brominated product was observed by LCMS and NMR analysis of the crude. Consequently, a second attempt was made by heating **60** in HBr under reflux until LCMS analysis showed complete conversion of the starting material. Aqueous workup and column chromatography gave the desired 3-(2-Bromoethyl)pyridine **61** in 52% yield (Scheme 3.25). Evidence of this product was found in the in the LCMS (ES^+) spectrum, with a peak showing a 1:1 ratio characteristic of the bromine isotope pattern of 186.162 and 188.100 *m/z* attributed to $[M(^{79}Br)H]^+$ and $[M(^{81}Br)H]^+$.

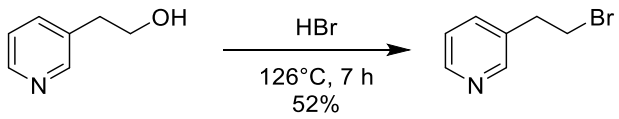

60 **61**

Scheme 3.25: Synthesis of 3-(Bromoethyl)pyridine 61

Alkylation of **33** with 3-(2-Bromoethyl)pyridine **61** using potassium carbonate showed no product formation after 18 h at room temperature (Table 3.3, Entry 4). Further attempts

were made to generate **58** by heating the reaction to 80°C, adding 10 mol % tetrabutylammonium iodide (TBAI), and extending the reaction time. However, product **58** could not be detected under these modified conditions.

As there are several methods for N-alkylation with carbonyl compounds, a screen of different conditions was conducted using azepane **62** as a model for the benzazepines made in this investigation. The results of the screen are in Table 3.4 which reports the isolated yields. Most of the conditions worked in low to moderate yields to produce 1-[(4-fluorophenyl)methyl]azepane **64**, which was confirmed by the newly formed singlet at 3.59 ppm in the ^{1}H-NMR corresponding to the benzylic CH_2.

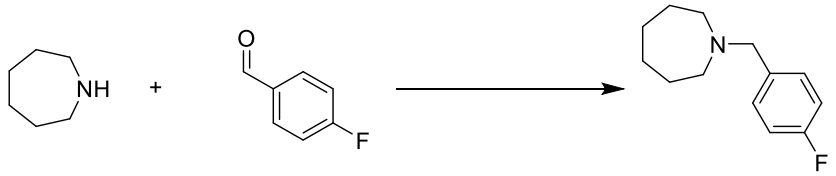

62 **63** **64**

Entry	Conditions for Reductive Amination[a]	Yield (%)[b]
1	$NaCNBH_3$ (3 eq), 4Å MS MeOH, rt, 8 h	50
2	$Na(OAc)_3BH$ (1.4 eq) DCE, rt, 15 h	64
3	$Na(OAc)_3BH$ (1.4 eq), AcOH (2 drops) DCE, rt, 24 h	17
4	$Na(OAc)_3BH$ (1.4 eq), Et_3N (1.1 eq) DCE, rt, 24 h	–
5	10 % Pd/C (5 mol %), TESH (2 eq) EtOH, rt, 1.5 h	24
6	$NaBH_4$ (2 eq) MeOH, rt, 18 h	–

Table 3.4: Reductive amination conditions screen. [a] 1 mmol scale. [b] Isolated yield.

A weakly acidic additive can be used to increase the reaction rate of reductive aminations, but in this instance, a catalytic amount of acetic acid led to a more sluggish reaction and a

decreased yield. Conversely, adding triethylamine completely stopped the reaction (Table 3.4, Entries 3 – 4). Catalytic hydrogenation is generally an effective method of reductive amination, and although the system used here gave the fastest reaction, the yield was low (Table 3.4, Entry 5). Ultimately, using sodium cyanoborohydride and sodium triacetoxyborohydride (STAB) as reducing agents gave the highest yields of 50% and 64%, respectively (Table 3.4, Entries 1 – 2). Unsurprisingly, these conditions are known to work well for reductive aminations and are often employed for this type of reaction.

Conditions from entry 1, using sodium cyanoborohydride was chosen for further reactions and a library of compounds was synthesized to afford benzazepines **33a** and **65** – **74** in moderate yields (Table 3.5, entries 1 – 8, 11).

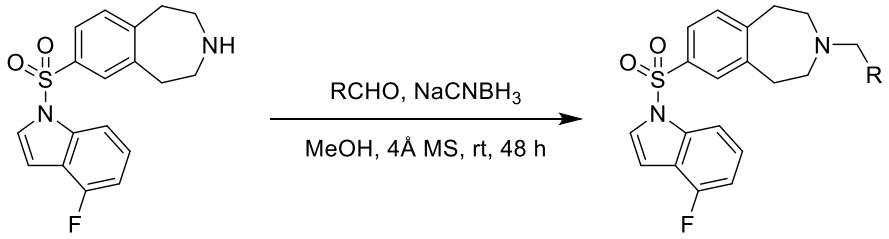

33 **33a, 65 - 74**

Entry	Starting material	Product	R	Yield (%)
1	4-Fluorobenzaldehyde **63**	**33a**	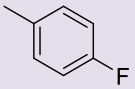	22
2	3-Fluorobenzaldehyde	**65**	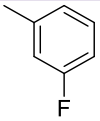	21
3	4-(Trifluoromethyl)benzaldehyde	**66**	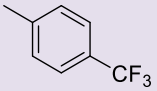	28
4	4-Pyridinecarboxaldehyde	**67**	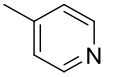	73
5	p-Tolualdehyde	**68**	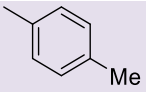	39
6	Benzaldehyde	**69**		25
7	4-Chlorobenzaldehyde	**70**	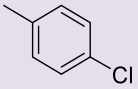	38
8	p-Anisaldehyde	**71**	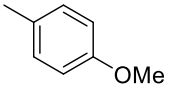	37
9	2-Fluoro-5-formylpyridine	**72**	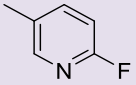	–
10	5-Formyl-2-pyridinecarbonitrile	**73**	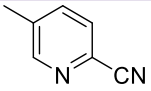	–
11	2-(4-fluorophenyl)acetaldehyde **76**	**74**	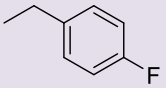	50

Table 3.5: Synthesis of benzazepine analogues 33a and 65 – 74

The N-alkylation with 2-fluoro-5-formylpyridine was successful but attempts to isolate the product using silica gel chromatography failed and the pure compound **72** could not be

obtained (Table 3.5, Entry 9). The reaction with 5-formyl-2-pyridinecarbonitrile was not successful, with the LCMS chromatograph showing mostly unreacted starting material **33** (Table 3.5, Entry 10).

As discussed in Chapter 2.1, the metabolically labile benzylic position of benzazepine **33b** lead to high clearance levels in mouse microsomes. As an addition the structure activity relationship investigations, the alkyl chain of **33a** was extended in an effort to improve metabolic stability.

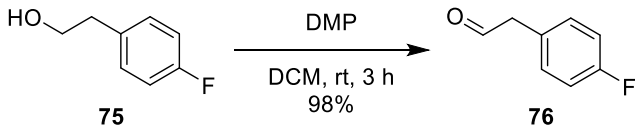

Scheme 3.26: Snythesis of 2-(4'-fluorophenyl)acetaldehyde 76

Aldehyde **76** had to be synthesized, as it is not commercially available. Following a simple protocol by Szcześniak *et al.* for the preparation of aldehydes, 4-fluorophenethyl alcohol **75** was oxidized with Dess–Martin periodinane (DMP) to form, after aqueous workup, the pure 2-(4'-fluorophenyl)acetaldehyde **76** in 98% yield (Scheme 3.26).[117] A triplet at 9.75 ppm in the ^{1}H-NMR spectrum, assigned to the carbonyl C*H,* and the carbonyl stretch in the IR spectrum at 1726 cm^{-1} confirmed the formation of the product. Subsequent N-alkylation of benzazepine **33** with aldehyde **76** afforded **74** in good yield (Table 3.5, Entry 11).

3.1.2 *para*- Acyclic analogues

The secondary goal of this study was to determine the necessity of the benzazepine core in regards to antileishmanial activity and LmjIPCS inhibition. As an addition to the structure activity investigation, *para*- substituted acyclic analogues derived from phenethylamine **77**, were synthesized.

3.1.2.1 Synthesis of *para*- Acyclic analogues

Initial attempts began with the protection of the primary amine **77** with 2,3-dimethylmaleic anhydride to afford the pure maleimide **78** in 92% yield (Scheme 3.27). Product formation was confirmed by a singlet at 1.94 ppm in the ^{1}H-NMR spectrum, assigned to the two methyl groups, and by LCMS (*m/z* (ES^{+}) = 230.241 $[M+H]^{+}$).

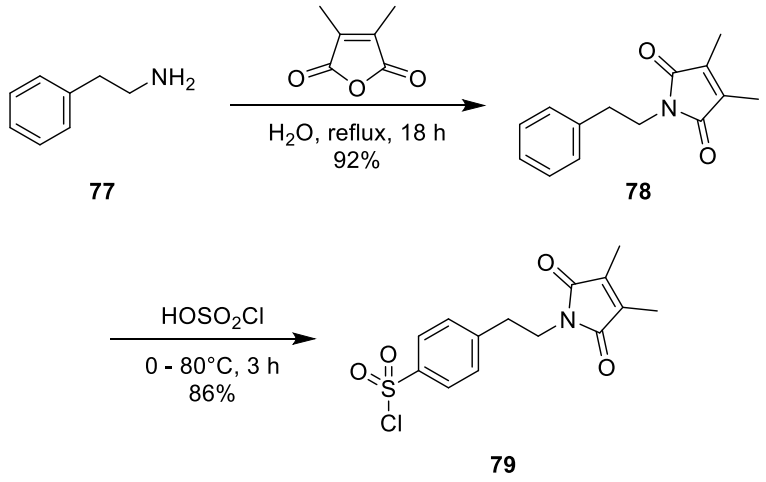

Scheme 3.27: Synthesis of chlorosulfonylphenyl maleimide 79.

The chlorosulfonation of N-phenylmaleimides had previously been reported by by Corrêa *et al.*[118,119] Following this precedent, maleimide **78** was treated with neat chlorosulfonic acid at 80°C for 3 h, when TLC analysis showed that the starting material was consumed. The pure chlorosulfonylphenyl maleimide **79** was obtained after aqueous workup in 86% yield (Scheme 3.28). *para*-Substitution was confirmed by the AA'BB' pattern of the aromatic protons in the ^{1}H-NMR spectrum which resonated as two double doublets at 7.47 and 7.96 ppm. Formation of the desired sulfonyl chloride **79** was confirmed by LCMS analysis, which showed the expected 3:1 molecular ions 328.1 and 330.2 *m/z* attributed to $[M(^{35}Cl)H]^{+}$ and $[M(^{37}Cl)H]^{+}$. Additionally, product formation was evident from the IR spectrum, which displayed absorptions at 1386 and 1175 cm^{-1} characteristic of a sulfonyl stretching frequency.

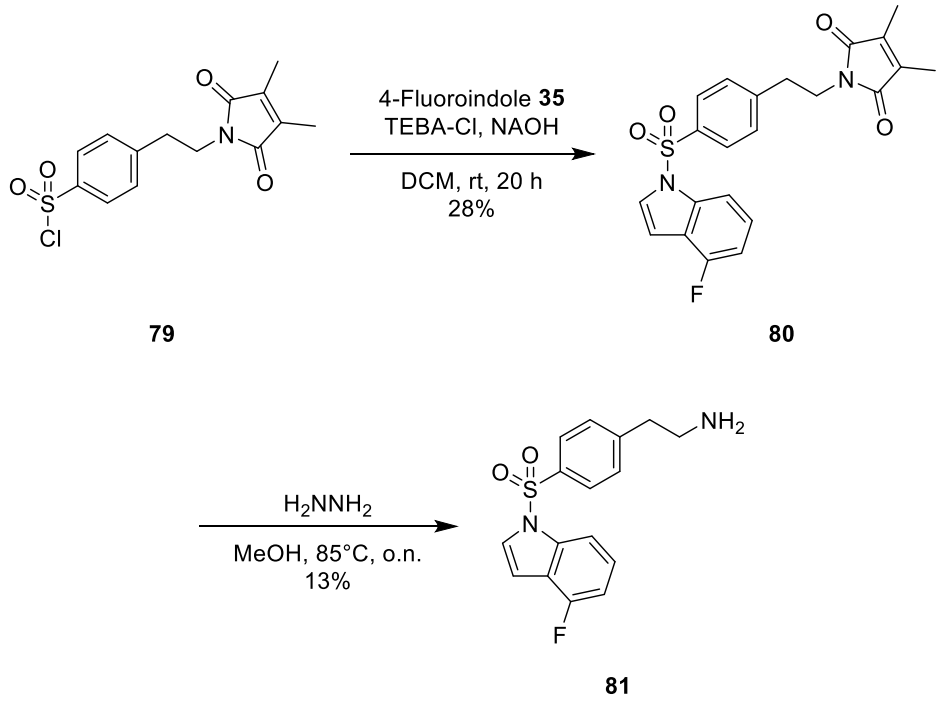

Scheme 3.28: Synthesis and deprotection of sulfonylindole 80

Following the Xu and Wang method previously described in Scheme 3.22, chlorosulfonylphenyl maleimide **79** was reacted with 4-fluoroindole **35** to give sulfonylindole **80** in 28% yield. Confirmation of the structure was found in the ES^+ mass spectrum, which showed the expected $[M+H]^+$ molecular ion at 427.205 *m/z*. Deprotection of sulfonylindole **80** was performed in refluxing methanolic hydrazine to give amine **81** in 13% yield as confirmed by LCMS (*m/z* (ES^+) = 319.2 $[M+H^+]$) (Scheme 3.28). The low yield is likely due to the poor solubility of the maleimide **80** in MeOH. Attempts to improve the deprotection conditions of **80** using a variety of solvents including EtOH, dioxane, and H_2O similarly led to low conversion.

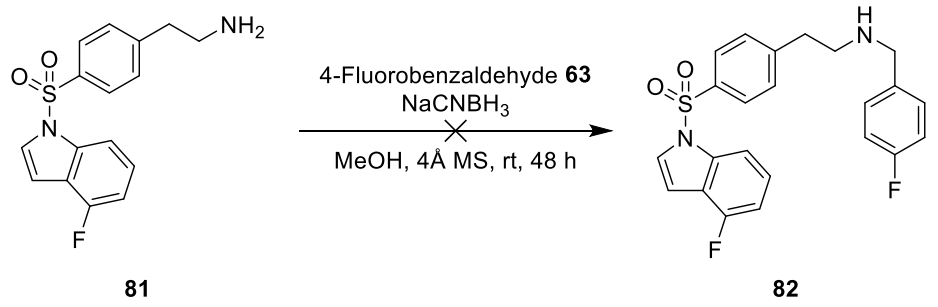

81 **82**

Scheme 3.29: Attempted synthesis of acyclic analogue 82

As with deprotected benzazepine **33**, chromatographic purification of **81** could not be obtained. Therefore, the crude material was globally subjected to reductive amination with 4-fluorobenzaldehye **63**. The formation of monosubstituted product **82** was found in LCMS chromatograph (*m/z* (ES^+) = 427.2 [$M+H^+$]) along with the maleimde **80**, the doubly substituted amine, and several other materials. Attempts to find conditions to isolate **82** were ineffective (Scheme 3.29). Due to the poor solubility of maleimide **80** and the difficulty in the deprotection step, another protecting group was necessary.

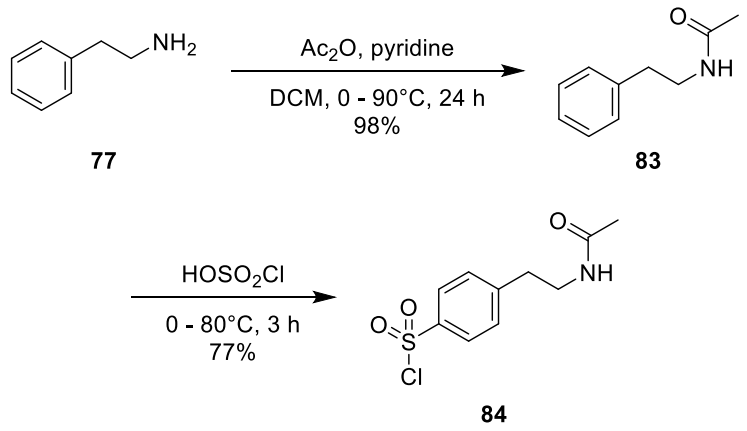

77 **83** **84**

Scheme 3.30: Acetamide protection and chlorosulfonation of phenethylamine 77

In this iteration, phenethylamine **77** was treated with acetic anhydride at 90°C for 24 h. Aqueous workup followed by recrystallization from petroleum ether afforded the pure N-(2'-phenylethyl)acetamide **83** in 98% yield. A singlet at 1.94 ppm in the ^{1}H-NMR spectrum, assigned to the methyl group, and the amide stretch in the IR spectrum at 1659 cm^{-1} confirmed the formation of the product. Chlorosulfonation of the acetamide **83**, completed

according to the Corrêa *et al.* method previously described in Scheme 3.27, afforded sulfonyl chloride **84** in 77% yield (Scheme 3.30). The AA'BB' pattern of the aromatic protons which resonated as two doublets at 7.45 and 7.98 ppm in the 1H-NMR spectrum confirmed *para*-substitution. Furthermore, the chlorine isotope pattern of 3:1 was observed in the ASAP mass spectrum, where 262.0 $[M(^{35}Cl)H]^+$ and 264.0 $[M(^{37}Cl)H]^+$ *m/z* were found in the corresponding peak.

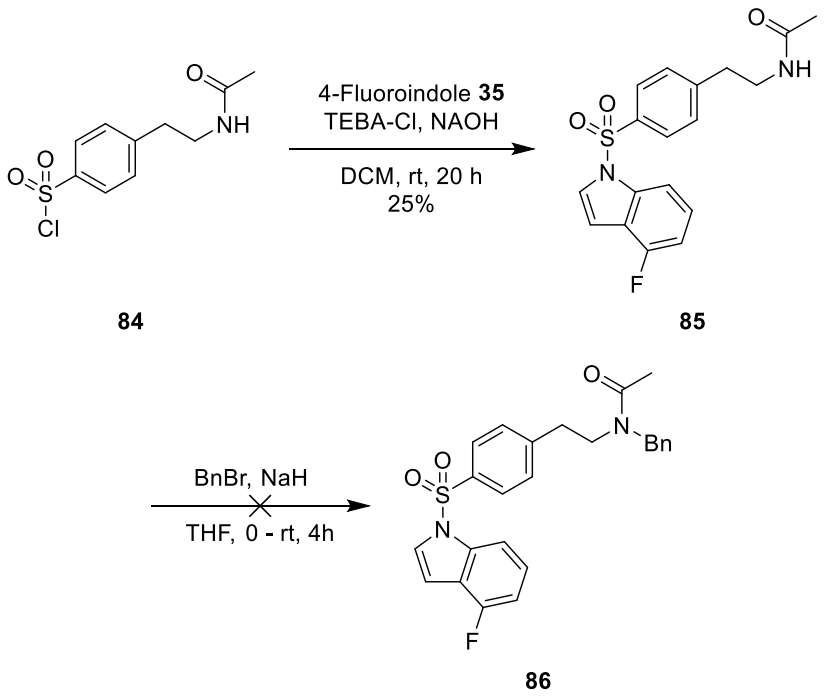

Scheme 3.31: Attempted N-alkylation of amide 85

Sulfamidation of amide **84** was completed with 4-fluoroindole **35** in the presence of NaOH and TEBA-Cl to give sulfonylindole **85** in 25% yield. Formation of the desired product was confirmed by LCMS analysis (*m/z* (ES^+) = 361.5 $[M+H^+]$). In addition, confirmation of the rotameric nature of this molecule was determined by ^{19}F-NMR spectroscopic analysis which showed two peaks at -120.71 and -121.24 ppm. NaH mediated N-alkylation of amide **85** with benzyl bromide was attempted. Reaction monitoring by TLC and LCMS showed that while all of the benzyl bromide had been consumed, the starting amide remained unchanged. Additionally, no product formation could be observed (Scheme 3.31). This was presumably due to the failure of the NaH to deprotonate the amide. Consequently, the approach for the

synthesis of *para*-substituted acyclic analogues was modified. Since the amide **85** was difficult to alkylate, it was suggested to begin with N-Methyl-N-phenethylamine **87** which could be deprotected to generate a secondary amine, a species which is simpler to alkylate. Furthermore, analogues produced using this new substrate would also retain the tertiary amine present in the lead benzazepine compounds.

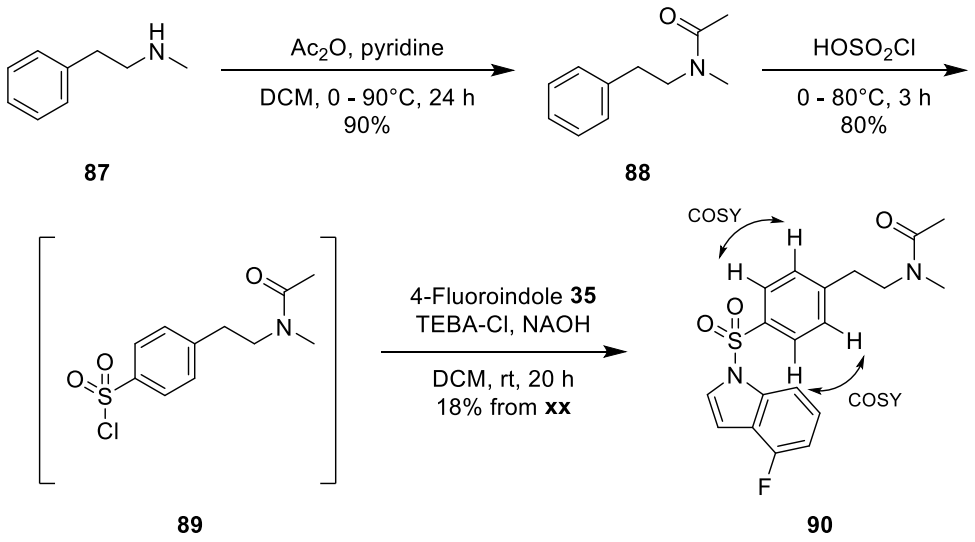

Scheme 3.32: Synthesis of sulfonylindole 90

Acetylation of N-Methyl-N-phenethylamine **87** was completed as previously described in Scheme 3.30. Treatment of **87** with acetic anhydride followed by aqueous workup afforded the pure N-methyl-N-(2-phenylethyl)acetamide **88** in 90% yield. As the generation of the acetamide group initiated rotamerism, two singlets at 1.86 and 2.06 ppm in the ^{1}H-NMR spectrum, assigned to the acetamide C*H*$_3$, and shift in the amino C*H*$_3$ from 2.47 to 2.87 and 2.95 ppm confirmed the product. Chlorosulfonation of the acetemide **88**, completed according to the Corrêa *et al.* method previously described, afforded sulfonyl chloride **89** in 80% yield. Due to the difficulty in obtaining a spectroscopically pure compound, **89** was immediately subjected to sulfamidation with 4-fluoroindole **35** to afford **90** in 18% yield over two steps (Scheme 3.32). Formation of the desired sulfonylindole **90** was confirmed by LCMS analysis (*m/z* (ES$^+$) = 375.327 [M+H$^+$]). Additionally, *para*- substitution was confirmed by the strong COSY correlations of *H*-2' and *H*-6' with *H*-3' and *H*-5' respectively.

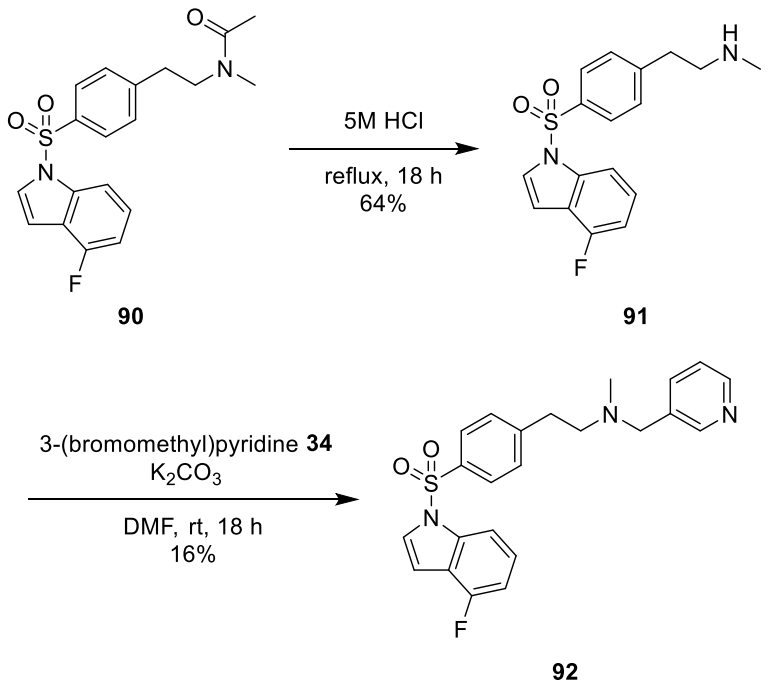

Scheme 3.33: Deprotection and N-alkylation of sulfonylindole 90

Deprotection of sulfonylindole **90** was performed in refluxing 5M HCl to give N-methyl amine **91** in 64% yield. The product was confirmed by the loss of rotamerism in the ^{1}H-NMR spectrum as well as the appearance of the broad N*H* peak at 1.44 ppm. Furthermore, a signal corresponding to 333.205 *m/z* was found in the LCMS (ES^{+}) mass spectrum, and this was attributed to the $[M+H]^{+}$ molecular ion. N-methyl amine **91** was treated with 3-(bromomethyl)pyridine **34** in DMF for 18 h to afford the *para*-acyclic analogue **92** in 16% yield (Scheme 3.33). A signal attributed to the $[M+H]^{+}$ molecular ion at 424.303 *m/z* found in the LCMS (ES^{+}) mass spectrum confirmed the formation of the product. Furthermore, the presence of a singlet at 3.48 ppm in the ^{1}H-NMR corresponding to the two α-pyridyl hydrogens provided additional evidence of the desired analogue.

3.1.2.2 Variations of the amine substituent

In order to investigate the influence of the alkyl chain length on antileishmanial activity, 4-fluoro and pyridyl analogues with two and three carbons were also synthesized. Reductive

amination of **91** with a variety of aldehydes led to acyclic analogues **93** – **97** in moderate isolated yields (Table 3.6, Entries 1 – 5). With the exception of 4-fluorobenzaldehyde **63**, which was commercially available, all other aldehydes had to be prepared.

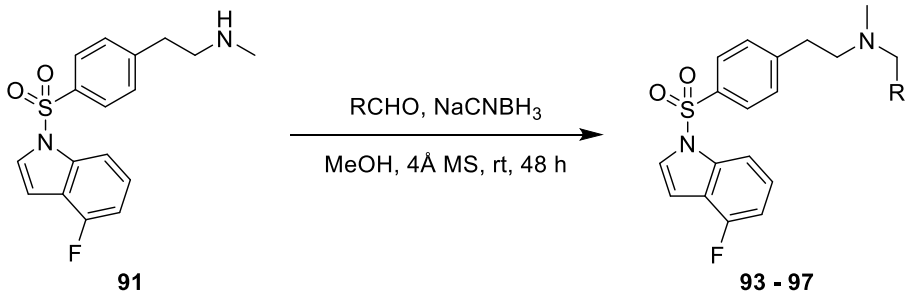

Entry	Starting material	Product	R	Yield (%)
1	4-Fluorobenzaldehyde **63**	**93**	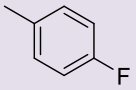	34%
2	2-(4'-fluorophenyl)acetaldehyde **76**	**94**	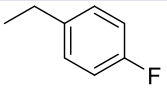	20%
3	3-(4'-fluorophenyl)propanal **100**	**95**	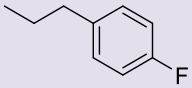	21%
4	2-(pyridin-3-yl)acetaldehyde **102**	**96**	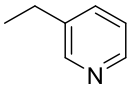	–
5	3-(pyridin-3'-yl)propanal **104**	**97**	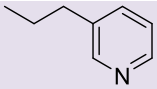	16%

Table 3.6: Synthesis of acyclic analogues (93 – 97)

3-(4'-fluorophenyl)propanal **100** was accessed following a two-step sequence. 3,4-fluorophenylpropionic acid **98** was reduced by $LiAlH_4$ to afford, after chromatographic purification, 3-(4'-fluorophenyl)propan-1-ol **99** in 99% yield. The appearance of a triplet at 2.69 ppm assigned to the O*H* proton in the ^{1}H-NMR confirmed the formation of the product. This was then treated with DMP to form 3-(4'-fluorophenyl)propanal **100** (Scheme 3.34).

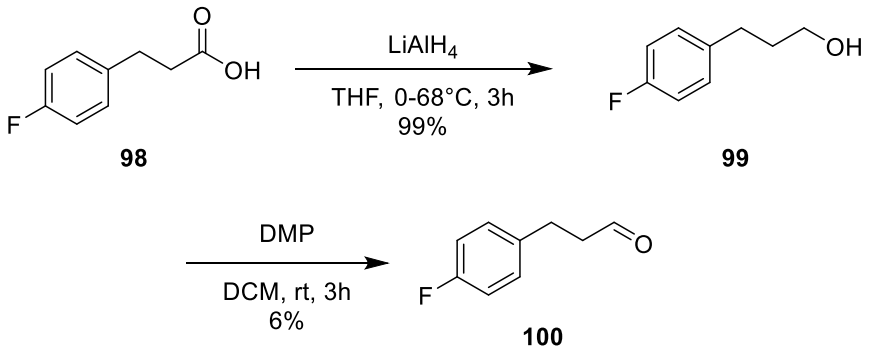

Scheme 3.34: Synthesis of 3-(4'-fluorophenyl)propanal 100

On the basis of NMR analysis, aldehyde **100** underwent rapid oxidation to the acid, evidenced by a singlet at 11.30 ppm in the ^{1}H-NMR corresponding to the COO*H* proton. Although the aldehyde was isolated by washing the crude material with sodium metabisulfite and sodium bicarbonate leaving a mere 6% yield, 10% degradation is still observed in the NMR spectra. The reappearance of the carbonyl signal at 1708 cm^{-1} in the infrared spectrum as well as a triplet at 9.81 ppm in the ^{1}H-NMR corresponding to the carbonyl C*H* confirmed the formation of the product. Due to the instability of aldehyde **100**, it was immediately reacted with N-methyl amine **91** to give product **95** in 21% yield (Table 3.6, Entry 3).

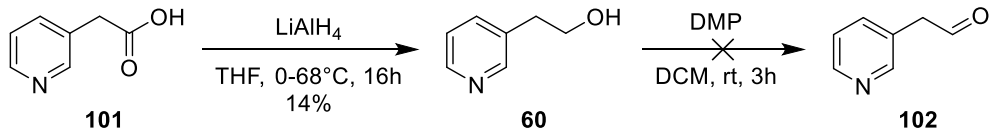

Scheme 3.35: Attempted synthesis of 2-(pyridin-3-yl)acetaldehyde 102

Following the same strategy, preparation of 2-(pyridin-3-yl)acetaldehyde **102** was undertaken starting from ethyl 3-pyridylacetate **101**. The rather low reduction yield (14%) can be attributed to the poor solubility of the acid **101** in THF. During the oxidation of the resulting 2-(pyridin-3'-yl)ethan-1-ol **60**, LCMS analysis showed complete consumption of alcohol **60** and formation of aldehyde **102** however, aqueous workup and removal of excess DCM under reduced pressure led to decomposition of the aldehyde (Scheme 3.35). Consequently, N-methyl amine **91** was reacted with **102** in DCM. Unfortunately, this reaction was also unsuccessful (Table 3.6, Entry 4).

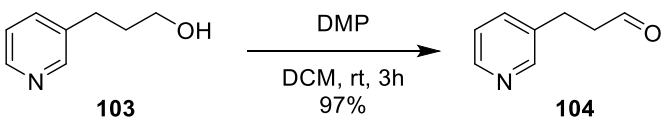

Scheme 3.36: Aynthesis of 3-(pyridin-3'-yl)propanal 104

DMP mediated oxidation of 3-pyridinepropanol **103** afforded 3-(pyridin-3'-yl)propanal **104** in an excellent yield of 97% as confirmed by LCMS analysis (*m/z* (ES^+) = 136.0 $[M+H]^+$ (Scheme 3.36). Subsequent reductive amination with deprotected N-methylamine **91** afforded analogue **97** in 16% yield (Table 3.6, Entry 5).

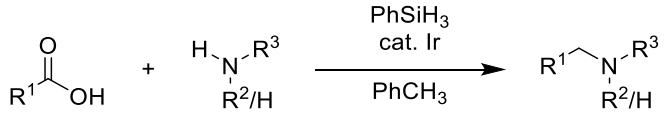

Scheme 3.37: Andrews *et al.* catalytic reductive N-alkylation[120]

The dual failures of preparing 2-(pyridin-3-yl)acetaldehyde **102** (Scheme 3.35) and of the previous attempt to N-alkylate with 3-(2-Bromoethyl)pyridine **61** (Table 3.3, Entry 4) suggested that another approach was needed to prepare analogue **96**. A review of the literature revealed a catalytic reductive alkylation of amines with carboxylic acids described by Andrews *et al.*[120] In this two-step reaction, a carbon-nitrogen bond is formed using the reactivity of phenylsilane followed by an iridium catalyzed reduction (Scheme 3.37).

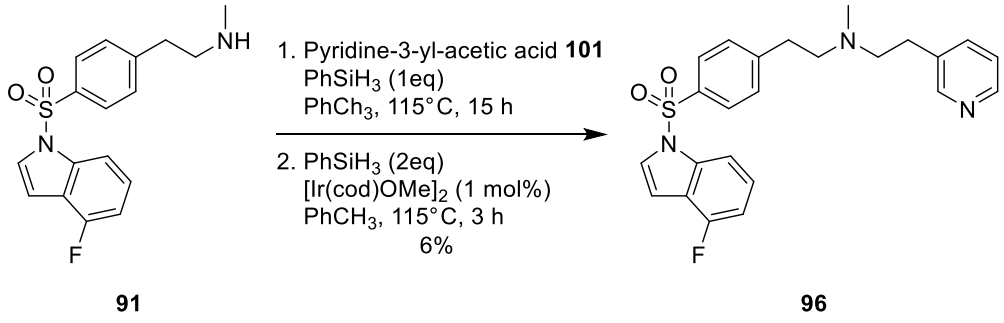

Scheme 3.38: Synthesis of 105 using a $PhSiH_3$/$[Ir(cod)OMe]_2$ catalytic catalytic system

Using the conditions reported by Andrews *et al.*, ethyl 3-pyridylacetate **101** was treated with phenylsilane and amine **101** in refluxing toluene for 15 h. Subsequent addition of

$[Ir(cod)OMe]_2$ and additional phenylsilane followed by aqueous workup and chromatographic purification afforded **96** in 6% yield. Confirmation of the product was determined by a peak in the LCMS (ES^+) spectrum which found 438.3 *m/z* attributed to the $[M+H]^+$ ion (Scheme 3.38). The low yield is likely due to steric hindrance which would impede amide formation in the first step. A similar result is observed by Andrews *et al.*

3.1.3 Efforts Towards the Synthesis of *meta*- Acyclic Analogues

As *para*- substituted acyclic analogues exhibited antileishmanial activity (*cf*. Chapter 3.2), it was decided to also synthesize *meta*- substituted acyclic analogues to more fully explore the special arrangement created by the azepane ring system. Along with determining the necessity of the benzazepine core in regards to antileishmanial activity, the importance of the position of the alkyl amine in relation to the sulfonyl group could be determined.

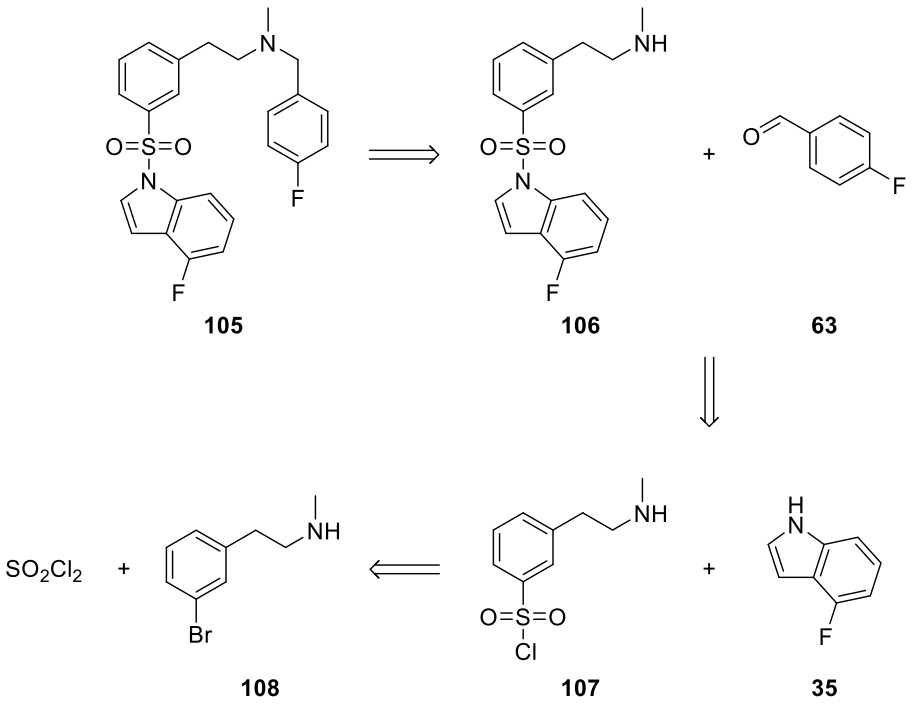

Scheme 3.39: Disconnection strategy of *meta*- acyclic analogue 105

A disconnection strategy of target compound **105** results in the identification of [2-(3' bromophenyl)ethyl](methyl)amine **108** as a key fragment. Although a majority of aryl sulfonyl chlorides are prepared by electrophilic aromatic substitution via an excess of chlorosulfonic acid, aryl lithiums prepared from the corresponding aryl halides have been shown to be an effective method in the preparation of aryl sulfonyl chlorides.[121] It was therefore postulated that an aryl bromide could be activated via a metal-halogen exchange reaction to add the sulfonyl functionalization seen in the target compound (Scheme 3.39).

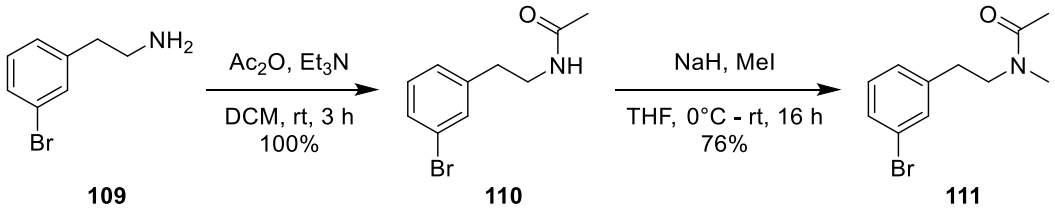

109 **110** **111**

Scheme 3.40: Synthesis of N-[2-(3'-bromophenyl)ethyl]-N-methylacetamide 111

Following a similar strategy used in the preparation of *para*- acyclic analogues, 2-(3'-bromophenyl)ethanamine **109** was subjected to acetamide protection to afford N-[2-(3'-bromophenyl)ethyl]acetamide **110** as confirmed by LCMS (ES^+) (*m/z* = 242.131 $[M(^{79}Br)H]^+$; 244.118 $[M(^{81}Br)H]^+$). Subsequent methylation in the presence of NaH afforded N-[2-(3'-bromophenyl)ethyl]-N-methylacetamide **111** in 76% yield over two steps. The loss of the N*H* peak and the appearance of two singlets at 1.93 and 2.08 ppm in the ^{1}H-NMR spectrum, corresponding to the acetamide and N-methyl group respectively, gave confirmation of the product (Scheme 3.40).

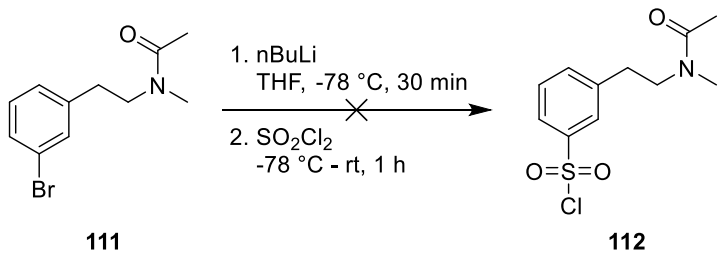

111 **112**

Scheme 3.41: Attempted lithiation and chlorosulfonation of N-methylacetamide 111

Applying a procedure described by Hale *et al.*, initial attempts to generate sulfonyl chloride **112** began by treating N-methylacetamide **111** with n-butyllithium followed by sulfuryl chloride.[122] NMR analysis of the crude material showed the decomposition of aryl bromide **111** to unknown materials. On a second attempt, complexing reagent TMEDA (N,N,N',N'-tetramethylethylenediamine) was added to improve the lithium-halogen exchange.[123] However, this also failed to generate the sulfonyl chloride **112** and again led to decomposition (Scheme 3.41). It was speculated that the acetamide protecting group impeded the lithium-halogen exchange therefore it was decided to synthesize di-aryl amine **113**.

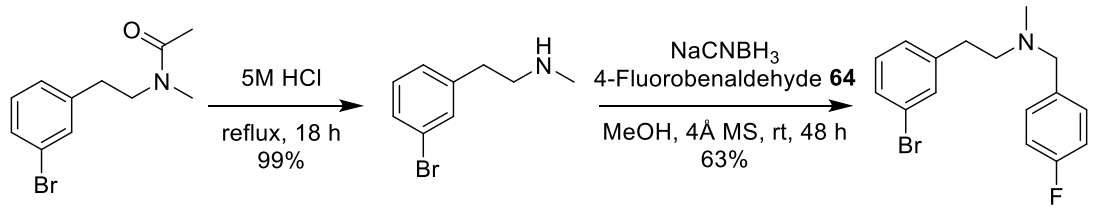

111 **108** **113**

Scheme 3.42: Deprotection and N-alkylation of acetamide 111

Applying the same reaction conditions as described in Chapter 3.1.1.3, N-methylacetamide **111** was converted to the N-methyl amine **108** in 99% yield via an acid catalyzed hydrolysis as confirmed by the appearance of an N*H* peak at 4.05 ppm in the ^{1}H-NMR spectrum. Subsequent alkylation with 4-fluorobenzaldehyde **63** afforded [2-(3'-bromophenyl)ethyl][(4''-fluorophenyl)methyl]methylamine **113** in 63% yield. The product was confirmed by LCMS (ES^{+}) (*m/z* = 322.284 [M(^{79}Br)H]$^{+}$; 324.260 *m/z* [M(^{81}Br)H]$^{+}$) and by ^{1}H-NMR analysis with the characteristic singlet 3.29 ppm corresponding to the benzylamine protons (Scheme 3.42).

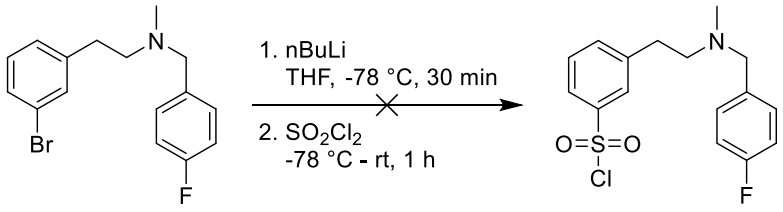

113 **114**

Scheme 3.43: Attempted lithiation and chlorosulfonation of methylamine 113

With methylamine **113** in hand, a new attempt at the lithium-halogen exchange reaction could be undertaken. Unfortunately, applying the Hale *et al.* lithiation conditions similarly led to no product formation and decomposition of the substrate. The addition of TMEDA also failed to generate the sulfonyl chloride **114** (Scheme 3.43). The reasons for this result could not be determined. Accordingly, an alternative method for the metal-halogen exchange was sought.

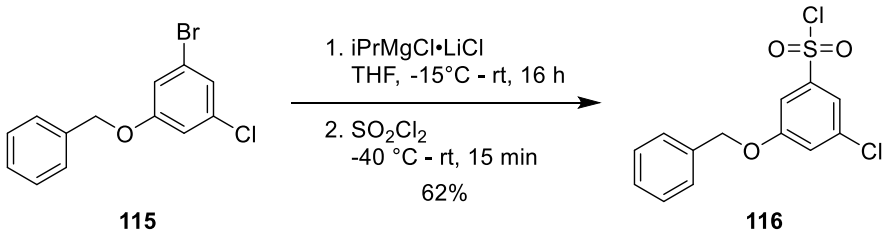

115 116

Scheme 3.44: Grignard mediated exchange reaction for the preparation of sulfonyl chloride by Loevezijn *et al.*[124]

A literature search presented a method for the synthesis of sulfonyl chlorides described by Loevezijn *et al.* which uses the bimetallic reagent iPrMgCl·LiCl to convert aryl bromide **115** to the corresponding Grignard reagent. Quenching with sulfuryl chloride furnishes the product **116** in 62% yield (Scheme 3.44).[124] This Grignard reagent, which also allows the use of highly functionalized aryl and heteroaryl bromides, has been shown to considerably improve the bromine-magnesium exchange.[125,126]

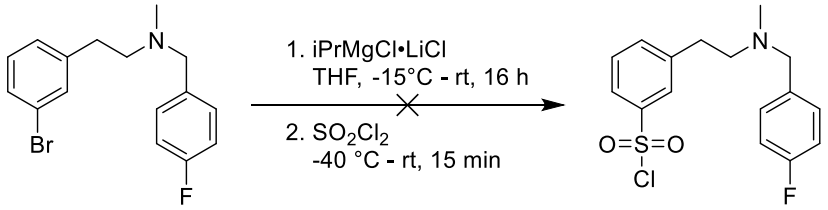

113 114

Scheme 3.45: Attempted Grignard mediated chlorosulfonation of methylamine 114

Using the conditions described by Loevezijn *et al.*, a further examination of the metal-halogen exchange reaction was undertaken. However, treating methylamine **113** with iPrMgCl·LiCl

followed by a sulfuryl chloride quench did not produce sulfonyl chloride **114**. Analysis of the crude reaction by NMR and LCMS showed an intractable mixture of unknown materials (Scheme 3.45). This route was not investigated further.

3.2 Biological Testing

3.2.1 Dose-response assay for EC_{50} determination

L. major, an Old World species, is recognized as causing the majority of cases of cutaneous leishmaniasis (CL) across Asia, Europe, and Africa[127] whereas *L. amazonensis* and *L. mexicana* are two of the primary causative agents for New World CL.[15,128] One of the challenges for the development of anti-leishmanial therapeutics is that multiple and phylogenetically distinct *Leishmania spp.* cause a range of clinical manifestations. This is most evident in cases of New World CL.[6,87,129] Unfortunately, there is a lack of information relating treatment outcomes for the *Leishmania* species and the clinical manifestations of leishmaniasis they cause. In fact, most of the literature is focused on the treatment of CL caused by Old World species.[130] However, there have been reports of multiple treatment outcomes for CL caused by different New World species of *Leishmania* in the Americas.[129,131] Therefore, it is important that a drug candidate is active against several *Leishmania spp*. For this reason, benzazepine analogues were tested against New World species, *L. amazonensis* and *L. mexicana,* in addition to Old World species, *L. major*.

As discussed in Chapter 2 lead compounds **32a** and **33a** were identified as potent inhibitors of *Lmj*IPCS with high activity against *L. major* promastigotes.[85,86] In order to understand the inhibitory effects of the benzazepine analogues, a dose-response assay which determined the growth inhibition of *Leishmania* promastigotes was performed in this investigation. As previously discussed, this dose-response assay is based on the NADH mediated reduction of resazurin **28** which is weakly fluorescent (Scheme 2.2). The reaction forms the highly fluorescent product, resorufin **29**, which can be fluorometrically detected at 585 nm (ex. 570 nm). All compounds were tested in a dilution by 3 series over a 0.05 – 100 μM concentration range. Examples of the dose-response curves are shown in Figure 3.2. Promastigote inhibitory effects are reported as EC_{50} and are summarized in Table 3.7. The results are discussed in more detail below.

(a)

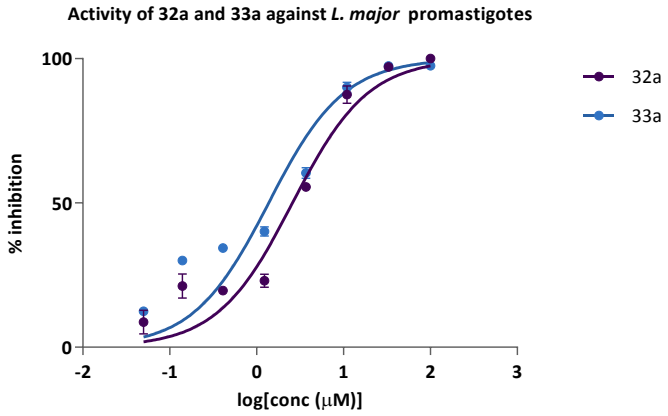

(b)

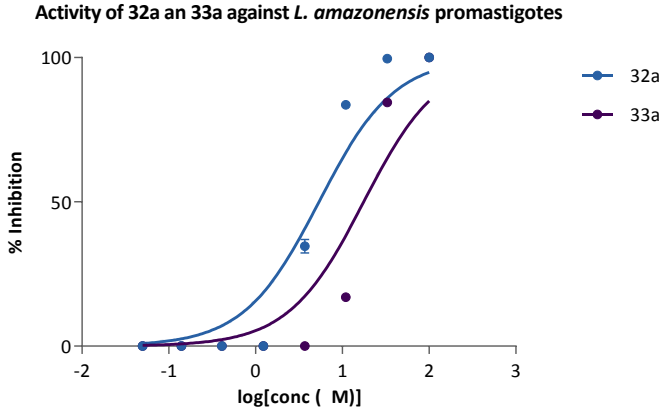

(c)

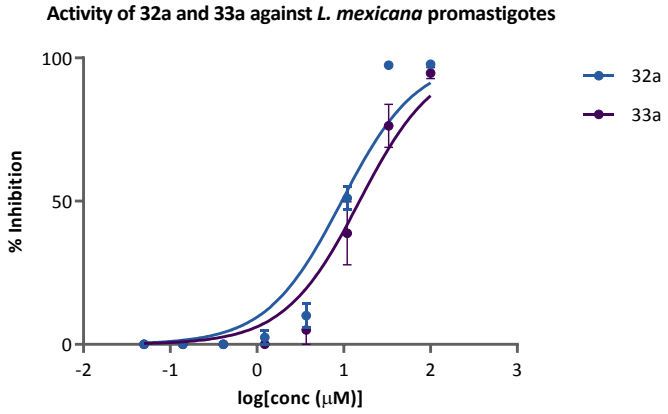

Figure 3.2: Dose-response curves for 32a and 33a against (a) *L. major*, (b) *L. amazonensis*, (c) *L. mexicana*; assays were performed in triplicate and each curve shows a representative experiment.

Compound Number	Structure	*L. major* EC_{50} (μM)	*L. amazonensis* EC_{50} (μM)	*L. mexicana* EC_{50} (μM)	*ΔLCB2* EC_{50} (μM)	*pX* EC_{50} (μM)	clogP
32a	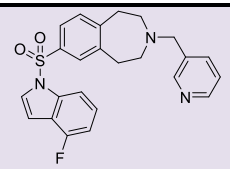	0.57 ± 0.03	6.38 ± 0.47	8.37 ± 0.75	5.16 ± 0.01	0.50 ± 0.01	2.91
33a	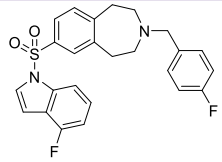	3.23 ± 0.63	20.23 ± 2.62	18.78 ± 2.28	7.98 ± 1.94	3.36 ± 0.09	4.01
56	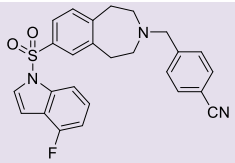	2.29 ± 0.35	11.62 ± 4.61	8.40 ± 0.94	--	--	3.75
65	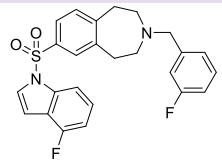	5.30 ± 0.58	33.49 ± 4.28	6.45 ± 2.58	--	--	4.01
66	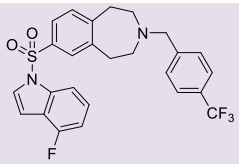	13.76 ± 0.29	30.84 ± 10.37	16.49 ± 2.40	--	--	4.76
67	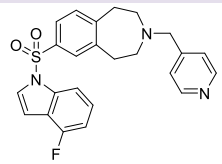	2.06 ± 0.79	14.45 ± 3.34	7.64 ± 1.47	--	--	2.91

Compound Number	Structure	*L. major* EC_{50} (μM)	*L. amazonensis* EC_{50} (μM)	*L. mexicana* EC_{50} (μM)	*ΔLCB2* EC_{50} (μM)	*pX* EC_{50} (μM)	clogP
68	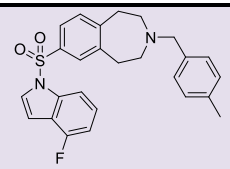	2.03 ± 0.97	17.65 ± 2.16	3.82 ± 0.58	--	--	4.26
69	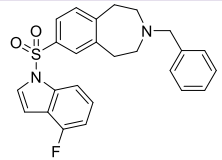	2.52 ± 1.15	14.09 ± 4.84	8.87 ± 0.89	--	--	3.91
70	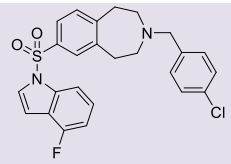	13.84 ± 1.25	80.33 ± 17.98	6.77 ± 0.87	--	--	4.52
71	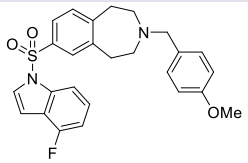	1.27 ± 0.49	14.71 ± 4.39	4.19 ± 1.25	2.34 ± 0.23	1.13 ± 0.12	3.84
74	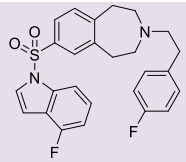	1.42 ± 0.37	7.92 ± 1.53	5.69 ± 0.28	2.56 ± 0.43	1.31 ± 0.01	4.44
92	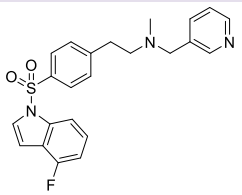	17.73 ± 1.36	13.24 ± 3.50	--	--	--	2.52

Compound Number	Structure	*L. major* EC_{50} (μM)	*L. amazonensis* EC_{50} (μM)	*L. mexicana* EC_{50} (μM)	*ΔLCB2* EC_{50} (μM)	*pX* EC_{50} (μM)	clogP
93	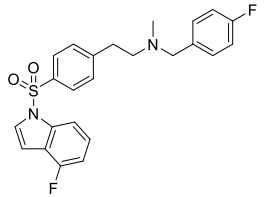	7.40 ± 0.44	8.04 ± 0.81	--	--	--	3.62
94	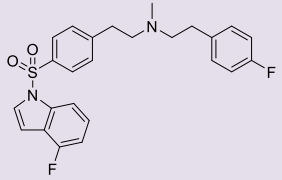	2.43 ± 0.21	1.49 ± 0.23	--	--	--	4.05
95	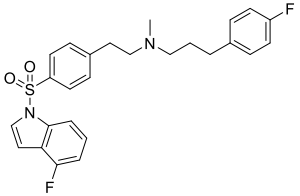	9.90 ± 2.07	14.45 ± 2.96	--	--	--	4.51
96	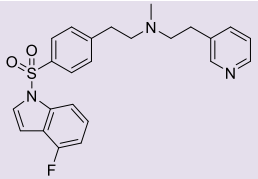	11.97 ± 2.29	10.20 ± 0.21	--	--	--	2.95
97	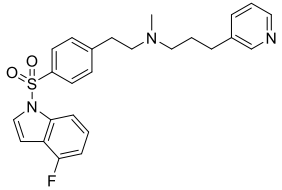	6.77 ± 1.06	6.05 ± 0.69	--	--	--	3.41

Table 3.7 Results of the dose-response assay for promastigote growth inhibition. Values are reported as EC_{50} and are mean ± 95% confidence interval from three experiments. clogP values are predicted using Osiris Property Explorer.

3.2.2 Activity of benzazepine analogues

As a confirmation of the results obtained from the previous investigation by Norcliffe, lead compound **32a** was subjected to a dose-response assay against *L. major* promastigotes. The results from this assay show sub-micromolar levels of activity for **32a** (EC_{50} of 0.57 ± 0.03 μM). Lead benzazepine **32a** was also tested against *L. amazonensis* promastigotes where a significant loss in activity (EC_{50} of 6.28 ± 0.47 μM) was seen when compared with *L. major* promastigotes (Figure 3.4).

One possibility for this variation could be because of the difference in the IPCS active site due to the difference in the providence of the *Leishmania* species – Old World *L. major* compared with New World *L. amazonensis*. Orthologues of *Lmj*IPCS have been identified in *L. amazonensis*[1] *and L. mexicana*[132] (Figure 3.3). *Lama*IPCS and *Lmx*IPCS were found to share approximately 97% sequence identity with each other. Accordingly, *Lama*IPCS and *Lmx*IPCS both share an 87% sequence identity with *Lmj*IPCS. This shows that there is a genetic basis for disease tropism and a variation in drug response.

[1] Unpublished *L. amazonensis* gene sequence by Douglas Escrivani (Federal University of Rio de Janeiro)

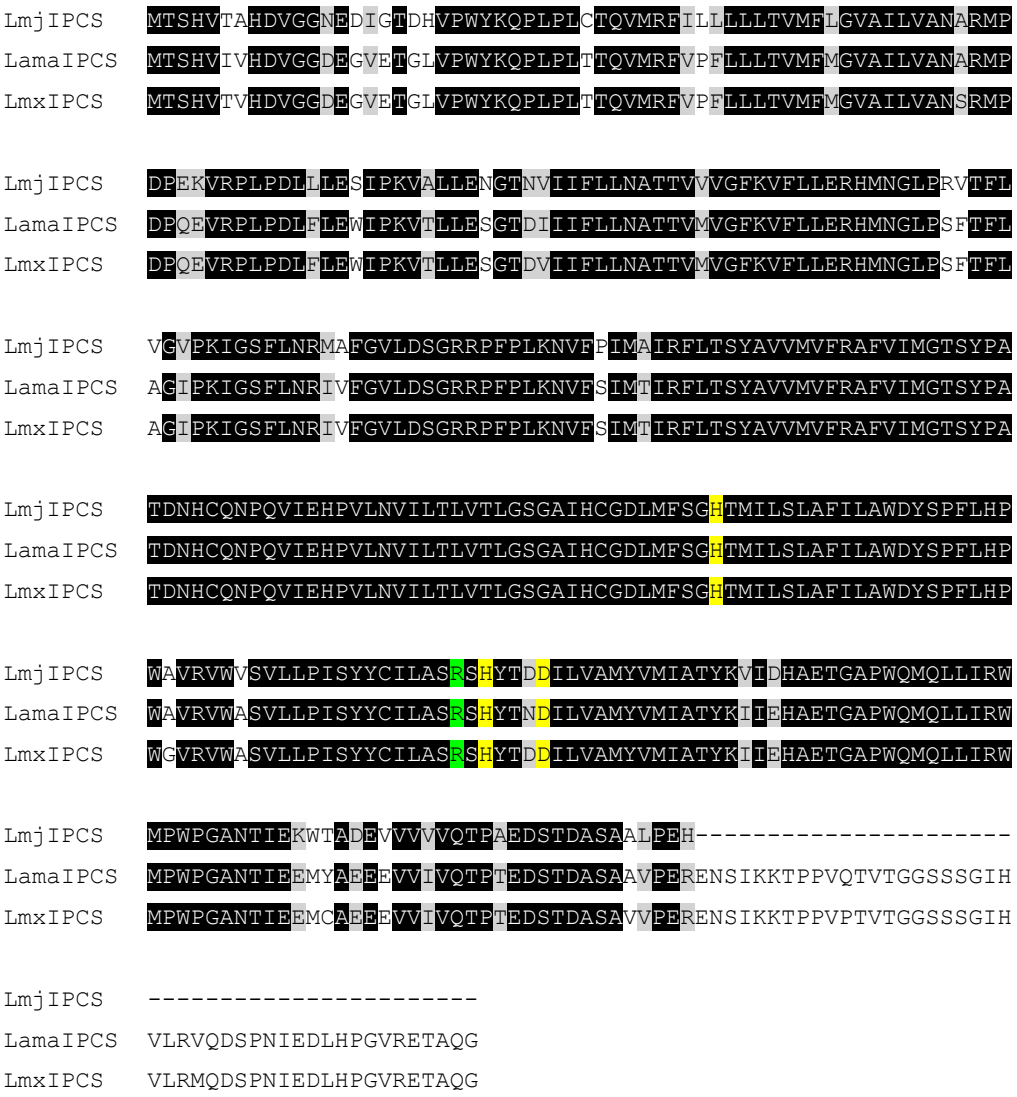

Figure 3.3: Clustal Omega alignment of protein sequences from *L. major* IPCS (LmjF35.4990), *L. amazonensis* IPCS (LAMA_000816400), and *L. mexicana* IPCS (LmxM.34.4990.1). Shaded black, sequence identity; Shaded grey, sequence similarity; Shaded yellow, catalytic triad His_{224}, His_{264}, Asp_{268}; Shaded green, stabilizing residue Arg_{262}.

To further test this theory, New World species, *L. mexicana* was included in the dose-response assays. In this case, **32a** was moderately more potent against *L. amazonensis* than *L. mexicana* (Figure 3.4). Although there is a high level of conservation across *Leishmania* species, alterations in gene expression can occur in response to environmental conditions. This is further evidence of the polymorphism of cutaneous leishmaniasis.

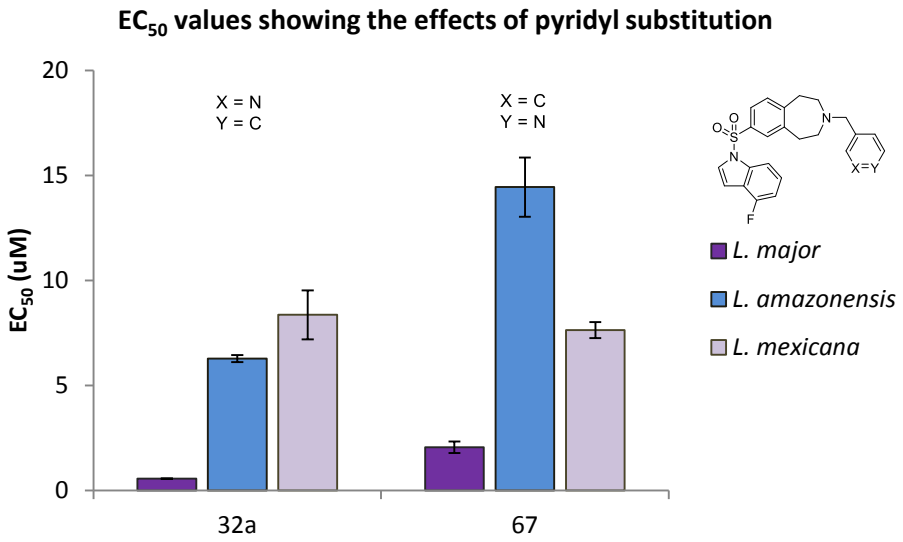

Figure 3.4: EC_{50} values for 32a (*meta*-pyridyl) and 67 (*para*-pyridyl) against *L. major, L. amazonensis*, and *L. mexicana*; values are mean ± 95% confidence interval from three experiments.

The *para*-pyridyl analogue **67** was less potent than the lead *meta*- analogue **32a** against *L. major* and *L. amazonensis*. Additionally, the *para*- analogue shows a slight increase in activity against *L. mexicana* when compared with the lead compound (Figure 3.4). Although the reason for this is not clear, this suggests that there are significant differences in the binding site across the species.

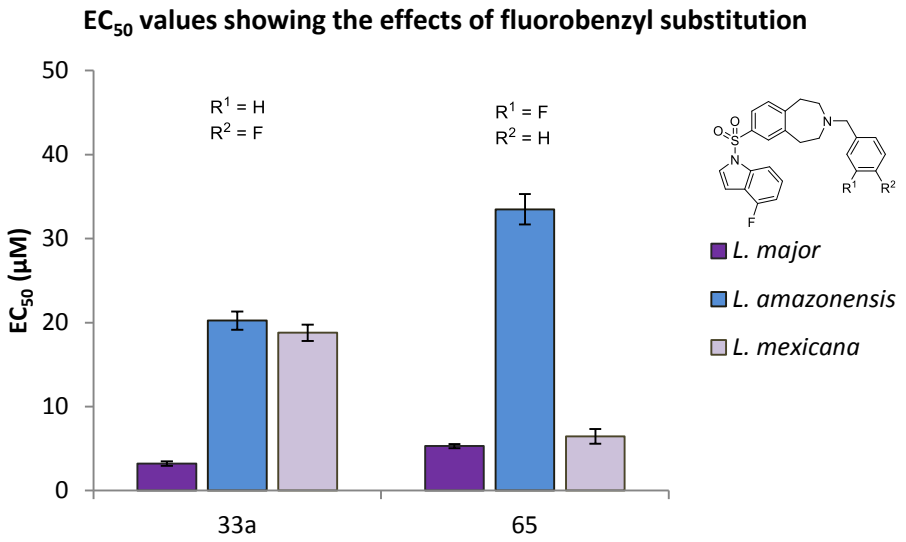

Figure 3.5: EC_{50} values for 33a (*para*-fluoro) and 66 (*meta*-fluoro) against *L. major, L. amazonensis*, and *L. mexicana*; values are mean ± 95% confidence interval from three experiments.

Chimeric lead **33a** was also verified in this investigation. The results from this assay show a less potent inhibitor against *L. major* promastigote growth (EC_{50} of 3.23 ± 0.63 µM). The activity dropped to 20.23 ± 2.62 µM and 18.78 ± 2.28 µM when **33a** was tested against *L. amazonensis* and *L. mexicana* promastigotes, respectively. This trend was also observed with analogue **32a**. In relation to the chimeric lead **33a**, the *meta*-fluorinated analogue **65** displayed a reduction in activity against *L. major* (EC_{50} of 5.30 ± 0.58 µM). Interestingly, this compound maintained a similar activity for *L. major* and *L. mexicana* while it exhibited a major decrease in activity for *L. amazonensis* (33.49 ± 4.28 µM, Figure 3.5).

The Topliss method is a systematic approach to analyze aromatic structures by means of quantitative data used to express biological activity. It is constructed from the knowledge of how biological activity is influenced by the physiochemical properties of the substituents of a phenyl ring. These properties include electron withdrawing or donating character represented by the Hammett substituent constant σ; the lipophilic character represented by the Hansch partition coefficient π; and the size of the substituent represented by the Taft size parameter E_s.[133] The Topliss method is often used to support the design of highly active compounds. Although this method was not used in the development of analogues in this investigation, its parameters are useful in their analysis. For this fluorinated set of compounds, the higher potency of **33a** suggests that improved

bioactivity can be related to the electron-donating character of the fluorine atom in the *para*- position (via positive mesomerism) when compared with the *meta*- position (σ = 0.06 and 0.34, respectively).

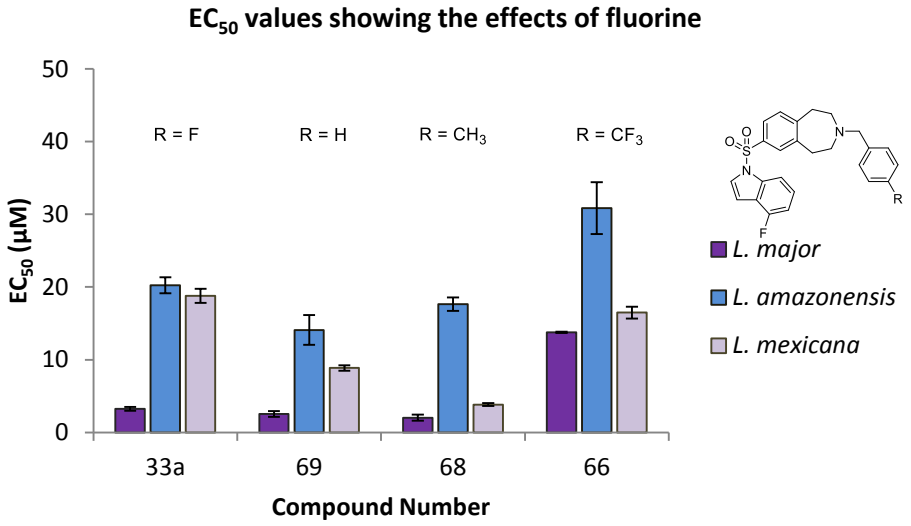

Figure 3.6: EC_{50} values for 33a (-F), 69 (-H), 68 (-CH_3), 66 (-CF_3) against *L. major, L. amazonensis*, and *L. mexicana*; values are mean ± 95% confidence interval from three experiments.

The electronics and small size of the fluorine atom can influence a wide range of biochemical properties including lipophilicity, conformational preferences, and activity of a molecule. Exchanging the fluorine in lead **33a** for hydrogen in **69** improved inhibitory activity in all species tested, particularly in *L. mexicana* which displayed a 2-fold increase in potency (Figure 3.6). This is possibly due to the fact that the C-H bond is more hydrophilic than the C-F bond, leading to analogue **69** having a reduced lipophilicity and an increased membrane penetration. Using a Topliss approach, the lipophilic and electronic contribution of **69** decreased (π = 0.00 and σ = 0.00, respectively) supporting this theory. Accordingly, the lipophilicity (clogP) for **33a** and **69** are predicted to be 4.01 and 3.91 respectively.

The *para*-methyl analogue **68** showed a further improvement in activity in *L. mexicana promastigotes*. While exchanging a single hydrogen atom with fluorine only had a modest effect on activity, the replacement of a CH_3 (**68**, clogP =4.26) with a CF_3 (**66**, clogP = 4.76) had a more significant effect. The trifluoromethyl group, which has a more pronounced

electronegative character than both the fluorine atom and the methyl group (**66**, σ = 0.54; **68**, σ = 0.17; **33a,** σ = 0.06), showed a significant drop in potency across all species when compared to its methyl bioisostere **68** (Figure 3.6). Additionally, the CF_3 group is more efficient in its hydrophobicity than the CH_3 group (π = 0.88 and 0.52, respectively). Finally, the CF_3 group adds the most steric bulk in this group of inhibitors (**33a**, E_s = -0.46; **69**, E_s = 0.00; **66**, E_s = -2.40; **68**, E_s = -1.24); therefore it is also possible that **66** does not fit into the binding pocket well, contributing to a reduction in activity. In general, the variations in activities seen in this group of compounds could be due to the effect of the fluorine atom.

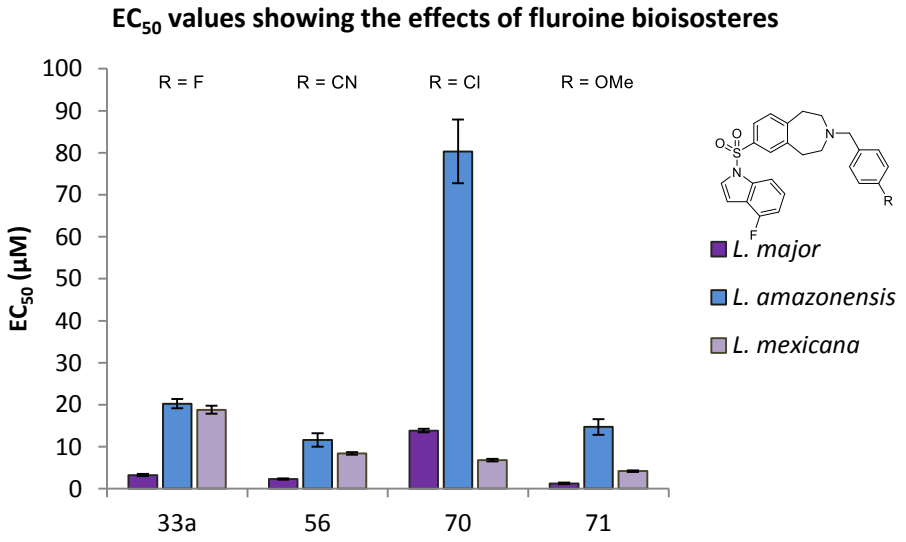

Figure 3.7: EC_{50} values for 33a (-F), 56 (-CN), 70 (-Cl), 71 (-OMe) against *L. major, L. amazonensis*, and *L. mexicana*; values are mean ± 95% confidence interval from three experiments.

Several examples of a bioisosteric relationship between the aryl-fluoride and aryl-nitrile moieties have been described as the nitrile group mimics the polarization of the fluorine atom. Nitriles are often favored for their stability, decreased lipophilicity, and favorable pharmacokinetic properties.[134,135] With the added capability for hydrogen bonding, the introduction of the nitrile group in analogue **56** improved activity to levels that better align with meta-pyridine **67** (EC_{50} = 2.29 ± 0.35 μM and 1.77 ± 0.78 μM against *L. major*, respectively) (Figure 3.7). The higher potency of the nitrile analogue can be related to the improved hydrophilicity when compared with the aryl-fluoride (π = -0.57 and 0.14, respectively).

It is often not possible to replace a fluorine atom with another halogen. This is evident with the chlorine-containing analogue **70** which shows a significant loss of activity against *L. amazonensis* promastigotes. As with the CF_3 analogue **66**, it is possible that increased bulk (**70**, E_s = 0.97) and reduced lipophilicity (**70**, clogP = 4.52) may contribute to the low inhibition displayed by **70**. Surprisingly, the methoxy analogue **71** showed gains in activity against all species. This is most noticeable when compared with **33a** against *L. major* (EC_{50} = 1.27 ± 0.49 μM for **71**; 3.23 ± 0.63 μM for **33a**), which is 2 times more active, and *L. mexicana* (EC_{50} = 4.12 ± 1.25 μM for **71**; 18.87 ± 2.28 μM for **33a**) (Figure 3.7). Interestingly, the non-classical fluorine bioisostere **71** is the only analogue that donates electron density to the aromatic ring (σ = -0.02) and has hydrogen bonding capability (π = -0.27).

As the structure of the IPCS protein is not known, these findings may offer clues as to the nature of the active site. For example, the results of the various benzazepine analogues suggest that hydrogen bonding capability improves antiparasitic activity. Additionally, increased steric bulk and electron-withdrawing effects may be tolerated when combined with properties, such as hydrogen bonding, which makes the inhibitor more biocompatible. Finally, electron-donating substituents could improve π-stacking interactions with aromatic amino acids in the binding site.

3.2.3 Activity of benzazepine analogue with extended linker

In the previous investigation (*cf.* Chapter 2.1), Norcliffe found that chimeric benzazepine **33b** displayed low activity and high clearance levels in mouse microsomes. It was postulated that this was due to metabolic instability, possibly by CYP450 oxidation of the metabolically labile benzylic position. Although the results from the subsequent metabolic stability assay were inconclusive,[85] it was suggested that extending the alkyl chain length could improve both metabolic stability and antileishmanial activity. This is because one of the ways to improve metabolic stability is to reduce the potential for enzymatic oxidation by CYP450.[136,137] Kinetic isotope studies have shown that the benzylic position is easily oxidized by CYP450.[90,91] Further studies on the effects of alkyl linkers on CYP450 oxidation demonstrated that catalytic activity is dramatically reduced as the

length of the alkyl chain increases.[138,139] Therefore, modifying the labile linkage from an oxidizable methyl group to a more stable ethyl group would result in a more potent inhibitor.

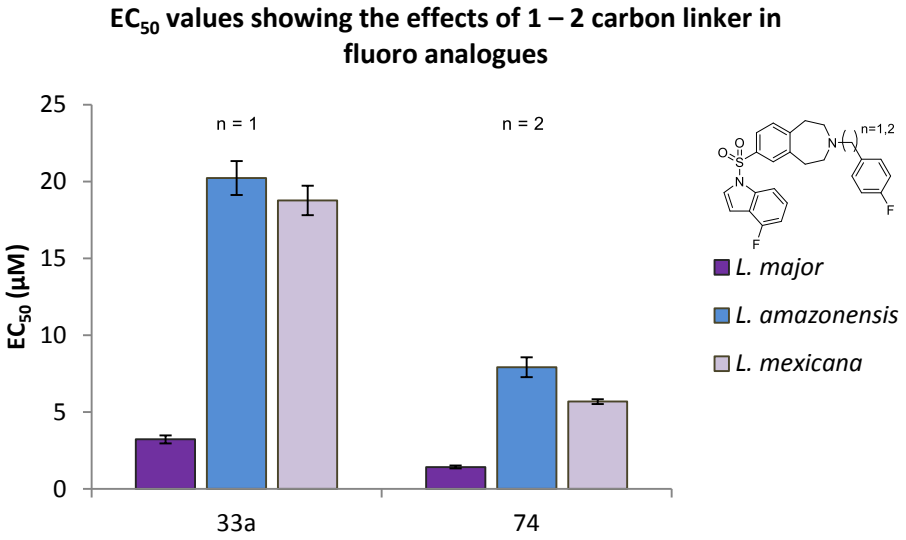

Figure 3.8: EC_{50} values for 33a and 74 against *L. major, L. amazonensis*, and *L. mexicana*; values are mean ± 95% confidence interval from three experiments.

Pleasingly, adding one carbon to the alkyl chain of **33a** to create **74** displayed a significant improvement in activity in all *Leishmania* species tested. As an example, **74** displayed EC_{50} values of 1.42 ± 0.28 µM and 7.92 ± 1.53 µM, whereas **33a** displayed EC_{50} values of 3.23 ± 0.63 µM and 20.23 ± 2.62 µM against *L. major* and *L. amazonensis*, respectively (Figure 3.8). This finding suggests that increasing flexibility and reducing the potential for CYP450 oxidation has a positive impact on inhibitor potency.

3.2.4 Activity of acyclic analogues

The previous investigation into the necessity of the benzazepine core included an azapane analogue **117** (Figure 3.9). Norcliffe found that the azapane analogue was a potent inhibitor of *L. major* promastigote growth with an EC_{50} of 0.79 µM. This shows that the benzene ring is not necessary for antiparasitic activity. Additionally, **117** displayed on-target effects, suggesting that the benzene ring was not necessary for *Lmj*IPCS inhibitory activity.[85]

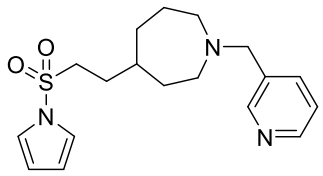

117

Figure 3.9: Azapane analogue

Due to the difficulty in preparing analogues of **117**, this investigation focused on phenethylamine based acyclic analogues. Therefore, with several acyclic analogues in hand, attention was turned towards measuring their activity against *Leishmania* promastigotes in an effort to discover the essentiality of the azepine ring. Dose-response studies for these compounds were accomplished through growth inhibition *of L. major* and *L. amazonensis* promastigotes.[2]

Acyclic pyridyl analogue **92** showed a significant drop in potency when compared to lead benzazepine **32a**. This is particularly evident against *L. major* as **92** was 30 times less active compared to the sub-micromolar activity of **32a** (EC_{50} = 17.73 ± 1.36 µM and 0.57 ± 0.03 µM, respectively). However, the variation in the activity levels between *L. major* and *L. amazonensis* was less pronounced for analogue **92** (Figure 3.10).

[2] EC_{50} testing was conducted in collaboration with Vanessa Lyne (Durham University).

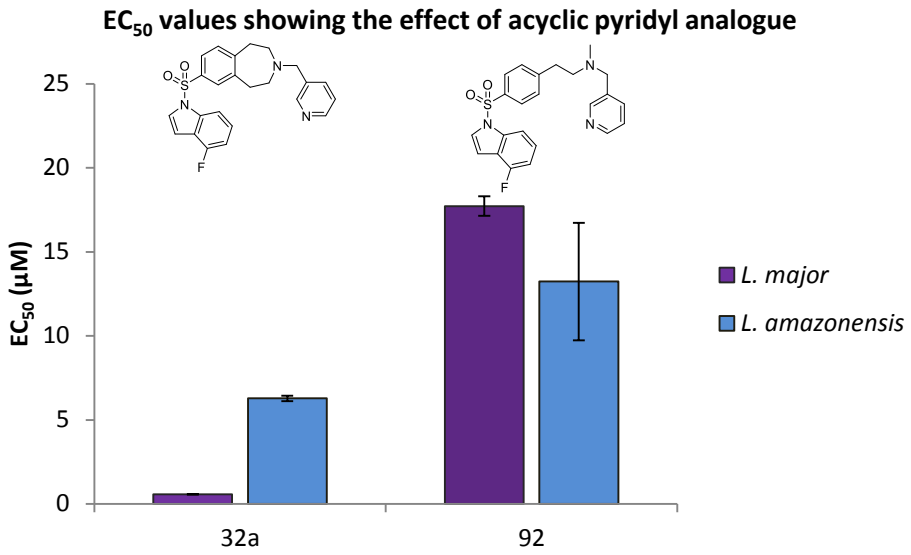

Figure 3.10: EC_{50} values for 32a and 92 against *L. major* and *L. amazonensis*; values are mean ± 95% confidence interval from three experiments.

Although **93** was less active against *L. major* promastigotes than the chimeric lead **33a**, the acyclic analogue showed an improvement in activity against *L. amazonensis* promastigotes (EC_{50} = 7.40 ± 0.44 µM for **93** and 3.225 ± 0.63 µM for **33a**). Additionally, the activity of **93** remained stable across the species tested (Figure 3.11). This phenomenon, which was previously unseen for the benzazepine analogues, could be due to off-target effects or the increased flexibility of the molecule which is better able to accommodate variations in the binding site.

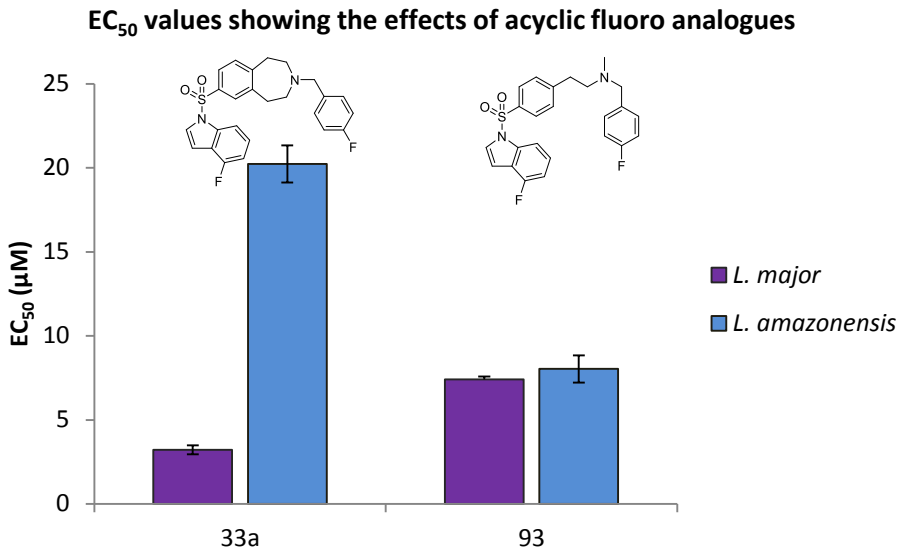

Figure 3.11: EC_{50} values for 33a and 93 against *L. major* and *L. amazonensis*; values are mean ± 95% confidence interval from three experiments.

In general, the acyclic analogues were not as active as their benzazepine partners. However, the slightly shorter synthetic route and the loss of variation in activity across species make the acyclic compounds attractive leads as general antileishmanial inhibitors.

3.2.5 Activity of acyclic analogues with extended linker

Although the initial set of acyclic analogues, **92** and **93**, were not as active as lead benzazepines, the preparation of additional acyclic analogues was validated in the dose-response assay by the moderate levels of activity displayed. Based on the increased potency of **74**, which was prepared by extending the linker of benzazepine **33a** to 2-carbon units, it was suggested that extending the linker of **93** would similarly improve its activity and metabolic stability. Gratifyingly, compound **94** was 5 times more active than **74** against *L. amazonensis* against promastigotes (EC_{50} = 1.49 ± 0.24 µM) making it the best inhibitor for this species (Figure 3.12).

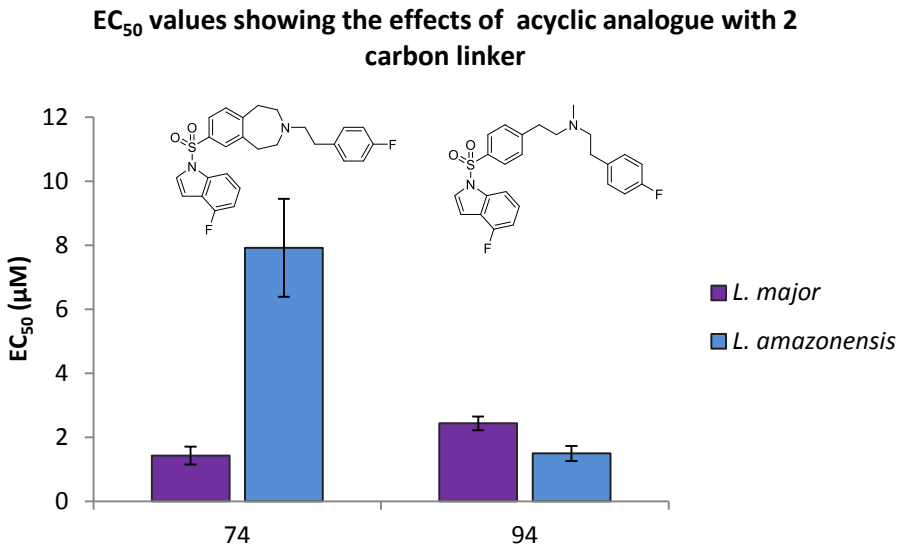

Figure 3.12: EC_{50} values for 74 and 94 against *L. major* and *L. amazonensis*; values are mean ± 95% confidence interval from three experiments.

The fluorophenyl substituted acyclic analogues did not display a clear tread for the relationship between linker length and activity. The 2-carbon linked fluorophenyl analogue **94** showed a marked increase in potency compared to **93**. With an EC_{50} of 1.49 ± 0.23 µM, the ethyl fluorophenyl analogue is the most active compound against *L. amazonensis*. Furthermore, it exhibited better inhibition than the chimeric lead **33a** for both species tested.

On the other hand, a sharp drop in potency, as well as more variation in activity across the species, was seen for 3-carbon linked analogue **95** (Figure 3.13). The reason for the fluctuation in activity of the fluorophenyl analogues as the linker increases in carbon units is unclear. A different trend might be seen with *ortho*- and *meta*- fluorophenyl analogues therefore, the relationship between linker length and substituent position could be investigated further.

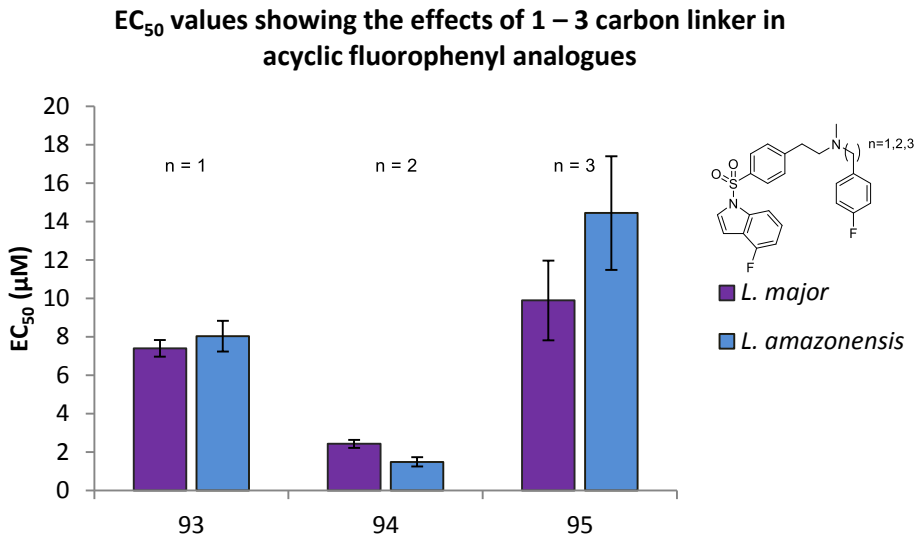

Figure 3.13: EC_{50} values for 93 (1C), 94 (2C), 95 (3C) against *L. major* and *L. amazonensis*; values are mean ± 95% confidence interval from three experiments.

The pyridyl substituted acyclic analogues demonstrated an overall drop in potency when compared with the lead benzazepine **32a**. Analogues **93**, **96**, and **97** were 10 – 30 times less active against *L. major*. However, growth inhibition improved as the length of the linker increased for this pyridyl substituted acyclic series. The 3-carbon linked analogue **97** completely regained activity against *L. amazonensis* when compared with **32a** (EC_{50} = 6.05 ± 0.69 μM and 6.28 ± 0.47 μM for **97** and **32a**, respectively) (Figure 3.14).

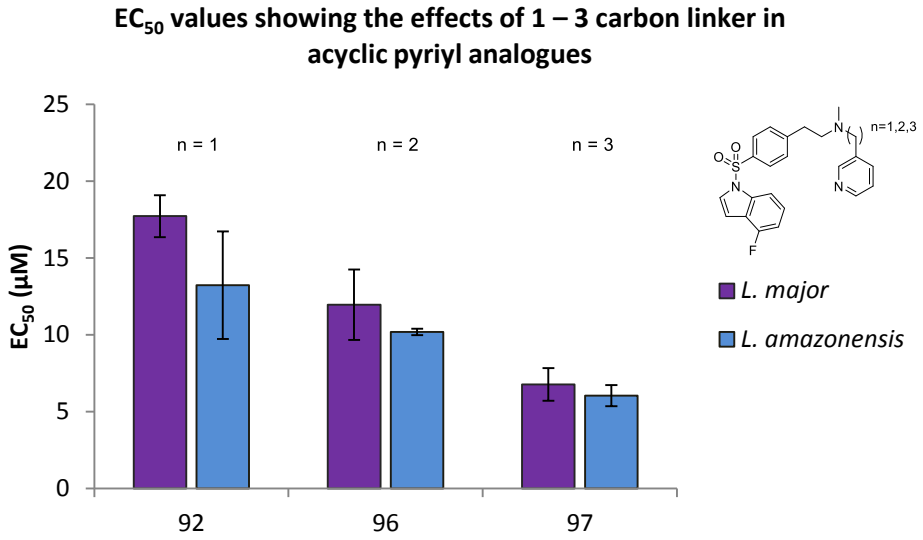

Figure 3.14: EC_{50} values for 92, 96, 97 against *L. major* and *L. amazonensis*; values are mean ± 95% confidence interval from three experiments.

The 2-carbon linked fluorophenyl analogue **94** is the most active inhibitor of the acyclic series. However, unlike its closest related benzazepine analogue **74** and lead benzazepine **33a**, this compound did not show increased potency against *L. major* promastigotes. Additionally, the submicromolar level of activity demonstrated by lead benzazepine **32a** against *L. major* was not found in any of the acyclic pyridyl analogues prepared in this investigation. Overall, the acyclic pyridyl series showed the most effect against *L. amazonensis* promastigotes. Further optimization would be needed to see a similar effect against *L. major* promastigotes.

3.2.6 *Lmj*IPCS On-target effects

As described in Chapter 2, benzazepines **32a** and **33a** were identified as *Lmj*IPCS inhibitors by Norcliffe through the use of *Lmj*IPCS enriched microsomes.[85,86] However, due to technical problems with the method, these results could not be reproduced in this investigation. Instead, a sphingolipid–free *L. major* mutant (*ΔLCB2*) cell line was used to perform a dose-response assay to assess if these molecules were acting on the sphingolipid biosynthetic pathway. These parasites were created through the removal of an essential SPT subunit, *Lm*LCB2. Although the *L. major ΔLCB2* mutants maintain

functional IPCS, they are compromised in their ability to form *de novo* synthesized ceramide and sphingolipids rendering IPCS activity redundant.[140–142]

As described by Denny, a plasmid coding for *Lm*LCB2 [*pX NEO Lm*LCB2] was transfected into the chromosomal null *L. major ΔLCB2* parasites, reintroducing the *Lm*LCB2 gene and restoring sphingolipid production by the cell.[140,142] For the purposes of this investigation, this 'add-back' cell line will be called *L. major pX*. As a control, dose-response assays against unaltered *L. major* wild type (WT) promastigotes and the mutant *L. major pX* cell line were also performed. Compounds which target the sphingolipid biosynthetic pathway should show reduced activity against *L. major ΔLCB2* promastigotes when compared with the *L. major* WT and *pX* cell lines.

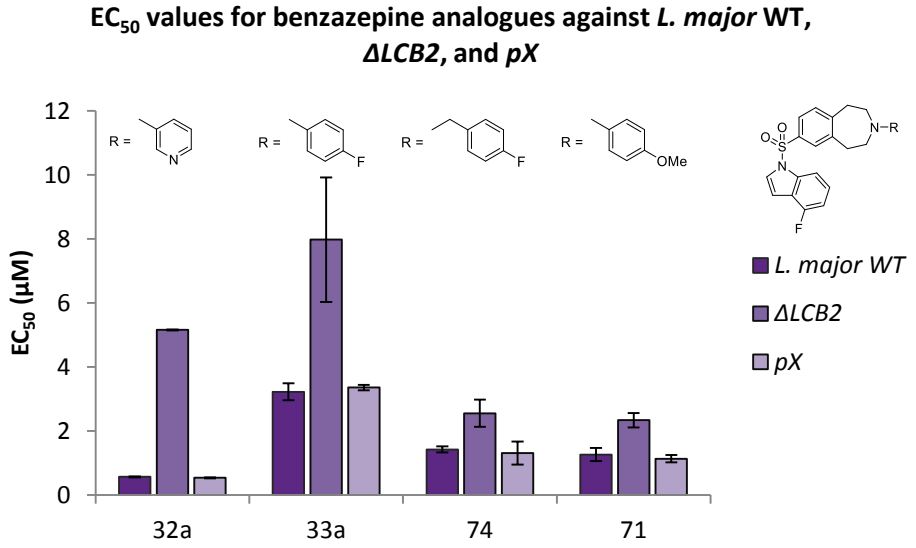

Figure 3.15: EC_{50} values for 32a, 33a, 74, and 71 against *L. major WT, ΔLCB2*, and *pX* promastigotes; values are mean ± 95% confidence interval from three experiments.

Results of the dose-dependent growth inhibition assay showed an EC_{50} of 5.16 ± 0.01 μM and 7.98 ± 1.94 μM against *L. major ΔLCB2* for lead compounds **32a** and **33a**, respectively. This is significantly less active than what is seen for WT promastigotes. Additionally, activity against the pX cell line was maintained at the same levels seen in WT promastigotes (EC_{50} = 0.54 ± 0.01 μM and 3.36 ± 0.08 μM for **32a** and **33a**, respectively) (Figure 3.15).

The selectivity of benzazepines **32a** and **33a** for the wild type parasite over the *ΔLCB2* cell line supports the finding that these compounds are having on-target effects. Like benzazepines **32a** and **33a**, analogues **74** and **71** are also more active against the WT and *pX* cell lines than the sphingolipid-free *L. major* mutant, *ΔLCB2*. This suggests that **74** and **71** are also disrupting the sphingolipid biosynthetic pathway.

Overall, the activity of the benzazepine analogues tested against *ΔLCB2* parasites is lower than that observed against WT and *pX* parasites. This supports the hypothesis that 4-fluoroindole benzazepine analogues are having an effect on the sphingolipid pathway. Interestingly, lead compound **32a** is approximately 9 times more active against the WT and *pX* cell lines than the mutant *ΔLCB2* promastigotes whereas benzazepines **33a**, **74**, and **71** are only 2 – 3 times more active. This suggests that **32a** is a more selective *Lmj*IPCS inhibitor.

3.3 Structure-activity relationship analysis

The inhibition activity of the benzazepine analogues is shown in Figures 3.16 and 3.17. When viewed collectively, a number of structure-activity relationships can be drawn from the biological data introduced in this investigation and provide clues into the nature of the *Lmj*IPCS binding site.

Overall, the benzazepine compounds were most active against *L. major* promastigotes with EC_{50} values generally less than 5 μM. The exceptions to this are the chlorobenzyl **70** and trifluoromethylbenzyl **66** analogues which saw a significant decrease in *L. major* activity. This suggests that the increased bulk and reduced lipophilicity of these compounds is affecting the activity of the inhibitor. Lead benzazepine **32a** remains the most active compound of this investigation. However, ethyl fluorophenyl analogue **74** shows that extending the alkyl linker of fluorobenzyl analogue **33a** improves metabolic stability and antileishmanial activity. Additionally, *Lmj*IPCS selectivity is retained (Figure 3.16).

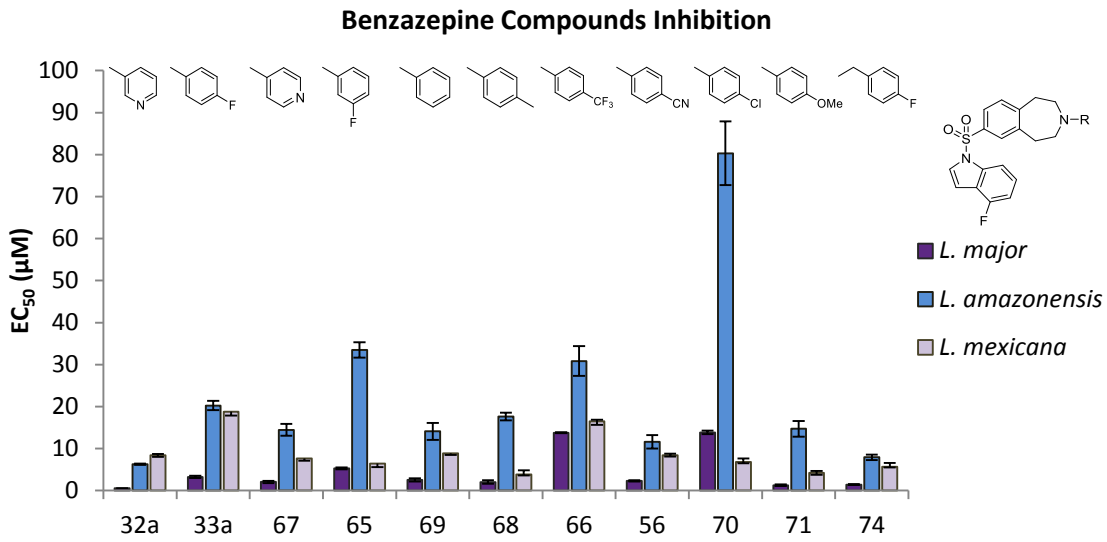

Figure 3.16: EC_{50} values for all benzazepine analogues; values are mean ± 95% confidence interval from three experiments.

The acyclic analogues were generally less active and showed less species selectivity than the benzazepine parent compounds. As the length of the alkyl chain increased, the inhibition activity of the acyclic pyridyl analogues (**92**, **96**, and **97**) also increased. This trend is not seen with the acyclic fluorophenyl analogues where inhibition activity varied as the alkyl chain length increased. The ethyl analogue **94** was significantly more active than the methyl compound **93**. This result is possibly due to the improved metabolic stability of analogue **94**. Further extending the linker by an additional carbon in **95**, however, led to a substantial reduction in potency (Figure 3.17).

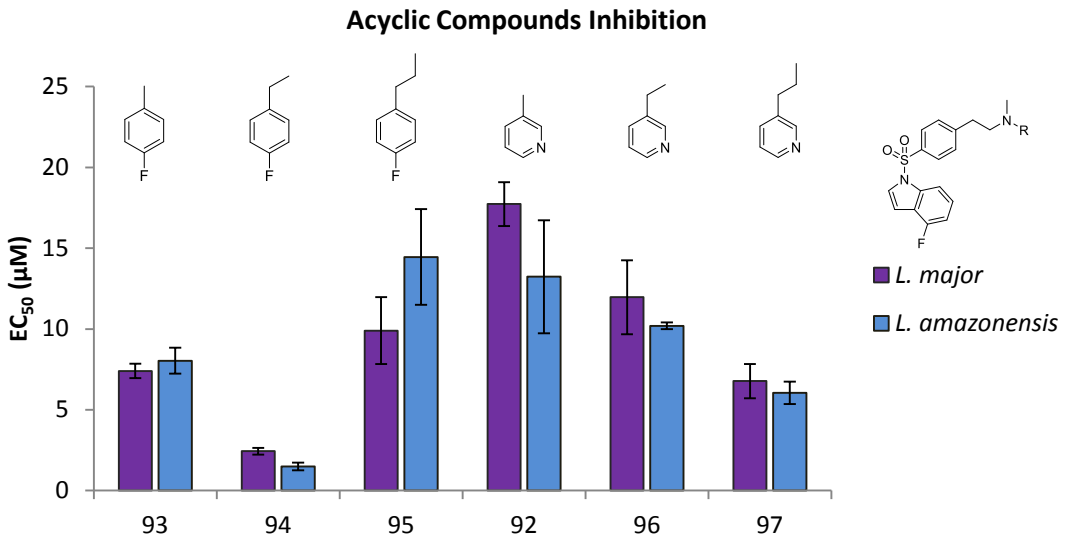

Figure 3.17: EC_{50} values for all acylic analogues; values are mean ± 95% confidence interval from three experiments.

One of the more noteworthy observations in this investigation was the use of benzyl substituents with hydrogen bonding capability lead to more potent inhibitors. Additionally, studies on the alkyl linker revealed that increasing flexibility also improved activity for the benzazepine series and the acyclic pyridyl series. These modifications preserve *Lmj*IPCS inhibition.

3.3.1 Benzazepine series SAR

A number of benzazepine analogues were explored, including pyridyl, alkyl pyridyl, benzyl, and alkyl benzyl, substituted compounds. As these compounds are most active against *L. major* promastigotes, the focus of this section will be on *L. major*.

The pyridyl analogues were generally more active than benzylic analogues. This is likely due to an increased solubility and bioavailability of these high polarity compounds (clogP = 2.91). The dose-response assay revealed a preference for the *meta*-pyridyl substituted benzazepine, with **32a** displaying sub-micromolar activity when tested against *L. major* (Figure 3.18). A complementary analogue bearing an *otho*- pyridyl substituent was not tested dues to synthetic difficulties. Consequently, there is a limitation to these findings as an *ortho*- analogue has an unknown effect on *Leishmania* promastigotes.

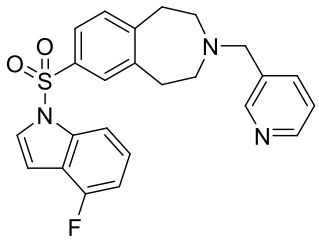

32a

Lmj EC_{50}: 0.57 ± 0.03 µM

Lama EC_{50}: 6.38 ± 0.47 µM

Lmx. EC_{50}: 8.37 ± 0.75 µM

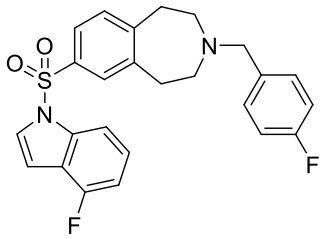

33a

Lmj EC_{50}: 3.23 ± 0.63 µM

Lama EC_{50}: 20.23 ± 2.62µM

Lmx EC_{50}: 18.78 ± 2.28 µM

Figure 3.18: Lead benzazepine analogues showing preferred substitution patterns

The majority of benzyl analogues tested against *L. major* were found to have EC_{50} values in the range of 1 – 5 µM, with the exception of the moderately active chloro **70** and trifluoromethyl **66** analogues. A study of the position of the benzyl substitution revealed an increased potency for *para*- substituted analogues as seen with fluorobenzyl **33a** (Figure 3.18). However, as with the pyridyl substituted benzazepines, the *ortho*-fluorobenzyl analogue was not obtained.

Further analysis of the *para*- substituted analogues led to the more active methoxybenzyl **71** and benzylnitrile **56** substituted benzazepines (Figure 3.19). These analogues feature substituents that can engage in hydrogen bonding. Hydrogen bonding capability in the *para*- position may be an important factor for improving antileishmanial activity, however further experimentation and structure optimization based on these analogues would help to expound on this observation.

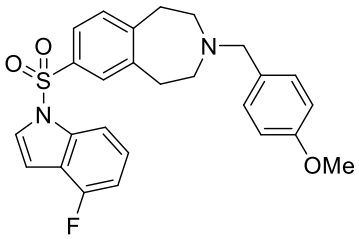

71

Lmj EC_{50}: 1.27 ± 0.49 µM

Lama EC_{50}: 14.71 ± 4.39 µM

Lmx EC_{50}: 4.19 ± 1.25 µM

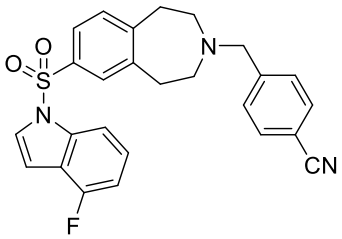

56

Lmj EC_{50}: 2.29 ± 0.35 µM

Lama EC_{50}: 11.62 ± 4.61 µM

LmxEC_{50}: 8.40 ± 0.94 µM

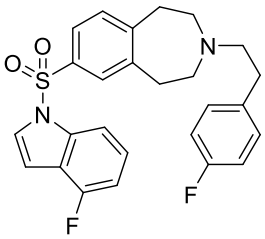

74

Lmj EC_{50}: 1.42 ± 0.37 µM

Lama EC_{50}: 7.92 ± 1.53 µM

LmxEC_{50}: 5.69 ± 0.28 µM

Figure 3.19 Example benzazepine analogues with H-bonding capability and extended alkyl linkeer

An investigation into extending the alkyl chain length was also undertaken. The use of a 2-carbon linker, as seen in benzazepine **74**, introduced flexibility and resulted in a 3-fold improvement in activity (Figure 3.19). While further analysis would be needed to determine if this modification stabilized **74** towards metabolic attack and reduced metabolic clearance, it appeared sufficient to afford in itself a superior antileishmanial profile.

3.3.2 Acyclic series SAR

An assessment of analogues with acyclic functionality was undertaken. With EC_{50} values in the range of 2 – 18 µM, the acyclic series was moderately active against *Leishmania* promastigotes. The loss of heterocyclic functionality of parent benzazepines **32a, 33a,** and **74** resulted in comparatively weak inhibitors of *L. major*. However, dose-response measurements revealed that these compounds showed less species-dependent variation in activity. This is a significant feature of the acyclic series that could lead to a broad leishmanial inhibitor. While the influence of the alkyl linker is unclear for benzyl substituted analogues, antileishmanial activity of the pyridyl substituted compounds improved as the length of the alkyl linker increased (Figure 3.20).

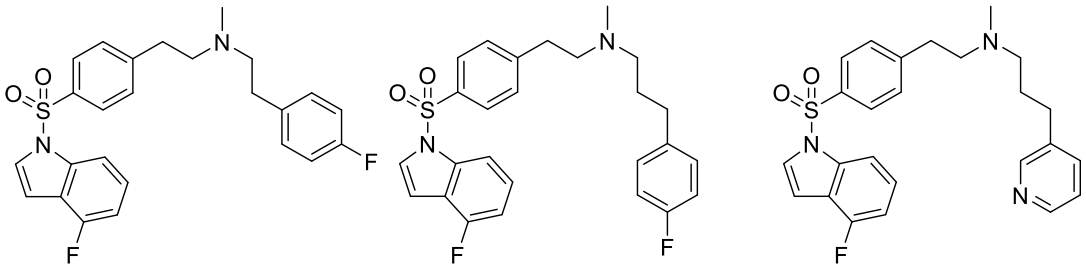

94	**95**	**97**
Lmj EC_{50}: 2.43 ± 0.21 µM	*Lmj* EC_{50}: 9.90 ± 2.07 µM	*Lmj* EC_{50}: 6.77 ± 1.06 µM
Lama EC_{50}: 1.49 ± 0.23 µM	*Lama* EC_{50}: 14.45 ± 2.96 µM	*Lama* EC_{50}: 6.05 ± 0.69 µM

Figure 3.20 Example acyclic analogues showing the effects of an extended alkyl linker

3.4 Conclusion

The work described in this chapter involved developing a synthetic route to 3-,7-substituted benzazepine analogues. These analogues were then submitted for biological testing against Leishmania promastigotes. Lead benzazepine **32a** demonstrated sub-micromolar activity against *L. major* promastigotes (0.57 ± 0.03 µM). With a 2-carbon linker, the ethylfluorophenyl analogue **74** was 3 times more active against *L. major* promastigotes than lead benzazepine **33a** (1.42 ± 0.37 µM and 3.23 ± 0.63µM, respectively). This improvement in activity was also observed for *L. mexicana* and *L. amazonensis* promastigotes. Progression of benzazepines **33a**, **32a**, **74**, and **71** to drug target validation, through analyses of dose-response assays using *L. major* WT, *ΔLCB2* and p*X* promastigotes, revealed that each of these compounds displayed on-target effects for LmjIPCS. A route to the more easily accessed phenethylamine based acyclic analogues was also developed. Although the acyclic compounds were not as active as the benzazepine series, analogue **94** was identified as a potent inhibitor of *L. major* and *L. amazonensis* promastigote growth (2.43 ± 0.21 µM and 1.49 ± 0.23 µM, respectively).

4 Conclusions and Future Work

4.1 Conclusions

The work presented in this thesis comprises efforts made towards the development of novel *Lmj*IPCS inhibitors as new therapeutic agents for leishmaniasis. Following a screening campaign of GSK's 1.8 million compound library revealed that benzazepine analogues **32a** and **33a** were potent anti-leishmanial compounds and selective *Lmj*IPCS inhibitors.

A small library of 3-,7- substituted benzazepine analogues was synthesized, focusing on variations of the amine substituent and modifications of the N-alkyl linker. Several phenethylamine based acyclic analogues were also prepared in an effort to explore the necessity of the azapane ring. In order to understand the inhibitory effects of these analogues, each compound was submitted to a dose-response assay to determine its ability to inhibit the growth of *Leishmania* promastigotes. The data collected from the biological screening lead to several interesting SAR discoveries. These findings, alongside features learned from the previous investigation, are summarized below (Figure 4.1).

A series of benzazepine analogues were prepared by modifying the substituent in the 3-position of the benzazepine scaffold **33**. These compounds were most active against *L. major* promastigotes. Although most of the amine substituents were tolerated, improved activity appeared to be inherent in substitutions that could engage in hydrogen bonding. This suggests that hydrogen bonding may play a role in enzyme-drug complexation.

With a view towards improving the metabolic stability observed for benzazepine **33b**, the alkyl linker of the fluorobenzyl substituted **33a** was extended. Pleasingly, the ethyl linker introduced in the corresponding analogue **77** improved *L. major* parasitic inhibition from 3.23 ± 0.63 μM for the fluorobenzyl substituted **33a** to 1.42 ± 0.37 μM for the ethyl fluorophenyl substituted **77**. Additionally, initial testing of these compounds revealed that activity against *Lmj*IPCS was maintained.

A series of acyclic analogues bearing alkyl fluorophenyl and alkyl pyridyl substitutions were successfully prepared. Increasing the linker length of the alkyl fluorophenyl analogues revealed no discernable trend. However, activity for the alkyl pyridyl analogues improved with increasing chain length, from an inhibition of only 17.73 ± 1.36 µM for the methyl pyridyl analogue **93** to 6.77 ± 1.06 µM for the propyl pyridyl analogue **98**. Even though the potency of the initial lead molecules **32a** and **33a** could not be improved upon in the acyclic series, dose-response measurements revealed that compounds of this series showed less species-dependent variation in activity. This observation is crucial for the development of a broad leishmanial inhibitor.

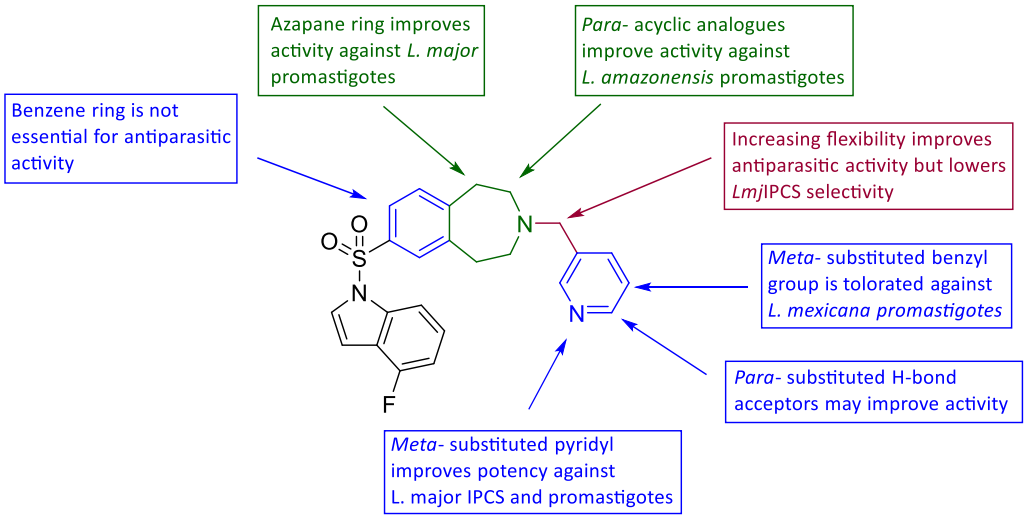

Figure 4.1: SAR observations

4.2 Future Work

Although several effective antileishmanial compounds were identified from this investigation, SAR analysis has highlighted areas for additional investigation. An in-depth study of analogues with various heterocycles may reveal different activity profiles and shed light on potential hydrogen bonding and pi-stacking interactions. Further optimization of the alkyl linker could improve antileishmanial activity in both the benzazepine series as well as the acyclic series. As described in Chapter 3.1, a continuation of efforts towards the synthesis of *meta*- acyclic analogues represents

another area for further investigation. The addition of this series of compounds will give a more complete understanding of the antileishmanial effects of the benzazepine scaffold.

The new analogues should be submitted for biological testing against intramacrophage amastigotes to more accurately mimic the disease state and against THP-1 cells to explore any cytotoxic effects. Additionally, a biochemical *Lmj*IPCS assay would determine the enzymatic target of these compounds. This could help provide more information on the interaction of the inhibitor with *Lmj*IPCS and lead to the creation of a more potent antileishmanial.

Another area for additional investigation would include structural studies of the *Lmj*IPCS enzyme. Obtaining the crystal structure of *Lmj*IPCS would provide information on the enzyme binding pocket which could be exploited to improve drug design. As previously mentioned, *Lmj*IPCS is a membrane-bound protein[67] – one of the more challenging classes of proteins that crystallographers face.[143,144] Although a few crystallization methods have been presented for membrane-bound proteins, their amphiphilic nature and the difficulties of crystal formation in the absence of their membrane environments makes obtaining an X-ray crystal structure of this class of proteins challenging.[143–146]

Therefore, instead of crystallographic information, further investigation could focus on developing a photoaffinity labeled ligand based on the benzazepine pharmacophore. In general, three main photoreactive moieties are used for photoaffinity labeling: azides, diazirines, and benzophenones. The photogroup can be directly incorporated into pharmacophore[147] used as a chemical probe which will covalently bind to its target upon irradiation (Figure 4.2,b).[148,149] Following tryptic digestion and mass spectrometry based analysis, important structural details about the binding site can be elucidated (Figure 4.2,a).[149]

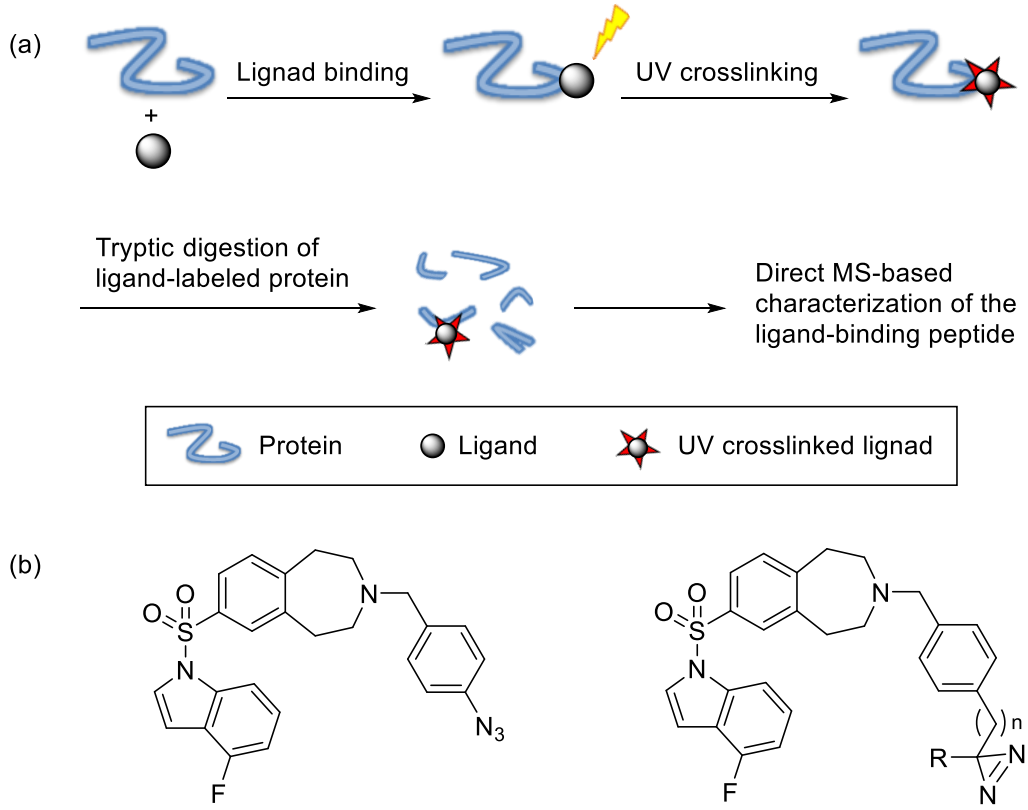

4.2 (a) General method of photoaffinity labeling experiments combined with MS-based characterization of protein–ligand complexes (adapted from Robinette *et al.*)[149] (b) Potential benzazepine-based photoaffinity probe

This information could allow for compound modifications which would generate a more potent antileishmanial. Additionally, the target of the benzazepine compounds could be validated as IPCS. Therefore, subsequent work should include the synthesis of benzazepine derivatives featuring aryl azide and diazirine photoreactive groups (Figure 4.2,b).

5 Experimental

5.1 Chemical Experimental Details

5.1.1 General Experimental Details

SOLVENTS AND REAGENTS: All solvents and reagents were purchased from commercial suppliers. Methanesulfonyl chloride was distilled from P_2O_5 and allylamine was distilled from $CaCl_2$ prior to use. All other chemicals were used without further purification. All dry reaction solvents were obtained dry from an Innovative Technology Solvent Purification System and stored under an atmosphere of argon.

CHROMATOGRAPHY: Thin layer chromatography (TLC) was performed on Merck Silica Gel 60 F254 aluminum-backed plates pre-coated with silica gel. Compounds were visualized under a 254 nm and 365 nm UV-light, then stained using the appropriate reagent, and heated. Purification via flash column chromatography was performed on a CombiFlash® System from Teledyne Isco equipped with a UV-light detector using prepacked RediSep Rf cartridges with the stated solvent gradient. Crude mixtures to be purified were dry loaded onto silica prior to loading onto the column.

NMR SPECTROSCOPY: NMR spectra were recorded on a Bruker Advance-400 (^{1}H at 400 MHz, ^{13}C at 101 MHz, ^{19}F at 376 MHz), Varian Inova-600 (^{1}H at 600 MHz, ^{13}C at 151 MHz), and a Varian VNMRS-700 (^{1}H at 700 MHz, ^{13}C at 176 MHz) instruments at room temperature and were referenced relative to $CDCl_3$ (δ_H = 7.26 ppm, δ_C = 77.16 ppm) and CD_3OD: (δ_H = 3.31 ppm, δ_C = 49.00 ppm). For some spectra, tetramethylsilane was used as an internal standard. ^{13}C spectra were run in proton decoupled mode. Assignments were made with the aid of 2D NMR experiments: COSY, NOESY, TOSEY, HSQC and HMBC. Chemical shifts (δ) are reported in parts per million (ppm); coupling constants (J) are given in Hertz (Hz); and multiplicity is indicated as singlet (s), doublet (d), triplet (t), quartet (q), pentet (p), multiplet (m), broad (br), or a combination thereof. In the case of rotameric

compounds, where elucidation of the separate rotamers is possible, proton and carbon resonances of the major and minor rotamers are assigned as A and B respectively, and their relative integration values reported.

IR SPECTROSCOPY: Infrared (IR) spectra were recorded on a Perkin Elmer Paragon 1000 FT-IR Spectrometer or a Perkin Elmer RX I FT-IR Spectrometer equipped with a Golden Gate Diamond ATR (attenuated total reflection) apparatus in the range of 3500 - 600 cm^{-1}. Absorption maxima (ν_{max}) are reported in wavenumbers (cm^{-1}).

MASS SPECTROSCOPY: Low resolution mass spectra (LRMS) analyses were on a recorded via electrospray ionization (ES^+), on a Waters TQD mass spectrometer which was equipped with an Acquity UPLC using an Acquity UPLC BEH C18 (2.1 mm x 50 mm, 1.7 µm) column. Absorbance data was collected from 210 to 400 nm using an Acquity photodiode array detector. Mass to charge ratios (*m/z*) are reported in Daltons with the corresponding fragment ion, where known. ASAP analyses were performed on a Waters ZCT Premier XE mass spectrometer with an ASAP ion source. High resolution mass spectra (HRMS) analyses were recorded on a Waters LCT Premier XE mass spectrometer with an ASAP ion source or a Waters QTOF Premier mass spectrometer with an electrospray ion (ES^+) source.

MELTING POINTS: Melting points were measured in open capillary tubes using a Fisher Scientific™ Electrothermal IA9100 Digital Melting Point Apparatus and are uncorrected. Dec. refers to material that decomposed upon heating.

MICROWAVE-ASSISTED REACTIONS: Reactions under microwave irradiation conditions were performed using a Personal Chemistry Emrys™ Optimizer in septum-containing, crimp capped, and sealed microwave process vials. The reported times are fixed hold times, the time that the reaction mixture was maintained at the designated temperature by varying irradiation power.

5.1.2 General Procedures

General Procedure: $LiAlH_4$ Reduction

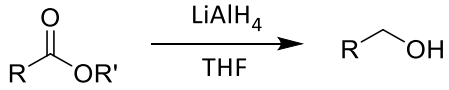

Procedure:[104] An oven-dried two-neck round-bottom flask fit with a condenser, an argon balloon, and a pressure-equalizing dropping funnel was charged with $LiAlH_4$ (1.5 eq) suspended in anhydrous THF (1 mL·mmol^{-1}) and cooled to 0 ˚C. A solution of the SM (1 eq) in anhydrous THF (2 mL·mmol^{-1}) was added dropwise maintaining the reaction temperature at 0 ˚C. After the addition was complete and the vigorous evolution of gas subsided, the mixture was stirred and heated under reflux for 3 h. The reaction was cooled to 0 °C, and the base was carefully quenched with the sequential dropwise addition of water (1 mL·mol^{-1}), 3M NaOH (1 mL·mol^{-1}), and water (3 mL·mol^{-1}) to afford a white precipitate. The resulting mixture was filtered through Celite® and the residue washed with EtOAc. The organic layer was separated, dried with $MgSO_4$, and concentrated *in vacuo* to give the product.

General Procedure: **Sulfamidation**

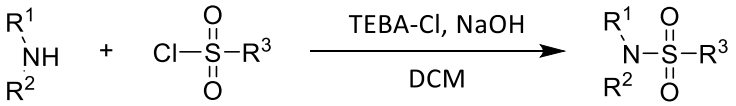

Procedure:[116] The sulfonyl chloride (1 eq), amine (1.1 eq), NaOH (3 eq), and benzyltriethylammonium chloride (TEBA-Cl) (13 mol%) were dissolved in anhydrous DCM (2 mL·mmol^{-1}) in a round bottom flask under an argon atmosphere. The resulting mixture was stirred at room temperature for 20 h, when TLC analysis revealed complete consumption of the starting material. The reaction mixture was partitioned between water (50 mL) and DCM (50 mL) and the aqueous layer separated and extracted with DCM (4 x 20 mL). The combined organic extracts were washed with water (3 x 50 mL) and brine

(20 mL), dried over $MgSO_4$ and concentrated *in vacuo* The crude residue was then purified by silica column chromatography to provide the product.

General Procedure: **Acetyl Protection**

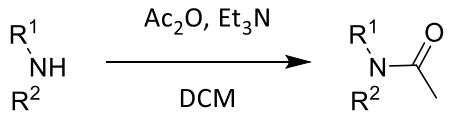

Procedure:[150] Ac_2O (1.1 eq) was added portionwise to a cooled (0 ˚C) solution of the amine (1 eq) and Et_3N (1.1 eq) in anhydrous DCM (3 mL·mmol^{-1}) under an argon atmosphere. After the addition was complete, the reaction was stirred at room temperature for 3 – 18 h until TLC analysis indicated complete consumption of the starting material. The reaction mixture was washed with 0.5 M HCl (2 x 20 mL), $NaCO_3$ (2 x 20 mL), and water (2 x 20 mL). The organic layer was separated, dried with $MgSO_4$, and concentrated *en vaccuo* to give the product.

General Procedure: **Acetamide Deprotection**

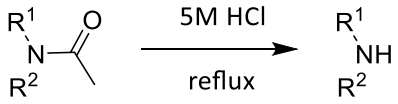

Procedure:[115] A round-bottom flask fit with a condenser was charged with the amide (1 eq). 5 M HCl (10 mL·mmol^{-1}) was then added and the solution refluxed at 110 °C for 18 h. The reaction mixture was then cooled to room temperature and basified to pH 12 with solid K_2CO_3 in an ice-cooling bath. The amine was extracted from the basified solution with EtOAc (5 × 20 mL). The combined organic extracts were dried over $MgSO_4$. The solvent was then removed *in vacuo* to give the product which was used without further purification.

General Procedure: **DMP Oxidation**

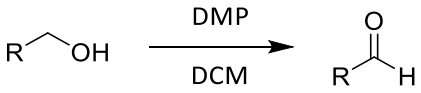

Procedure:[117] Dess-Martin periodinane (1.2 eq) was added in one portion to a cooled (0 ˚C) solution of the alcohol (1 eq) in anhydrous DCM (10 mL·mmol^{-1}) under inert atmosphere. The reaction mixture was stirred at room temperature for 3 h. Saturated $Na_2S_2O_3$ (10 mL·mmol^{-1}) was then added and the reaction stirred for an additional 15 minutes. The aqueous layer was separated and extracted with DCM (2 x 20 mL). The combined organic layers were then washed with brine (20 mL), dried over $MgSO_4$ and concentrated *in vacuo* to give the aldehyde.

General Procedure: Reductive Amination

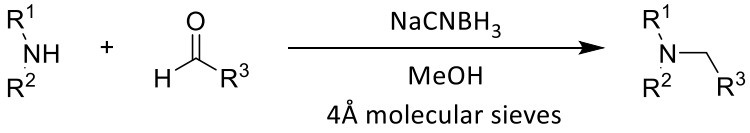

Procedure:[151] A round bottom flask was charged with the amine (1 eq) and 5 x 4Å molecular sieves under an argon atmosphere. A solution of the aldehyde (1 eq) in anhydrous MeOH (2 mL·mmol^{-1}) was then added and the resulting mixture stirred at room temperature for 5 min when $NaCNBH_3$ (3 eq) was added in a single portion. The reaction mixture was then stirred at room temperature for 48 h. After this time, the reaction mixture was partitioned between water (20 mL) and DCM (10 mL). The aqueous layer was separated and extracted with DCM (2 x 10 mL). The combined organic layers were washed with brine (20 mL), dried with $MgSO_4$ and concentrated *in vacuo*. The crude residue was purified by silica column chromatography to provide the product.

General Procedure: N-alkylation

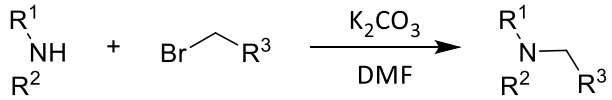

Procedure:[152] A round bottom flask was charged with the bromide (1 eq), K_2CO_3 (1.5 eq), and the amine (1 eq) dissolved in anhydrous DMF (2 mL·mmol^{-1}) under an argon atmosphere. The reaction was stirred at room temperature for 18 h until TLC analysis indicated complete consumption of the starting material. The reaction mixture was then partitioned between water (20 mL) and DCM (10 mL) and the aqueous layer extracted with DCM (3 x 10 mL). The combined organic layers were washed with water (3 x 20 mL) and brine (20 mL), dried over $MgSO_4$, and concentrated *in vacuo. T*he crude residue was purified by silica column chromatography to provide the product.

General Procedure: Catalytic N-alkylation

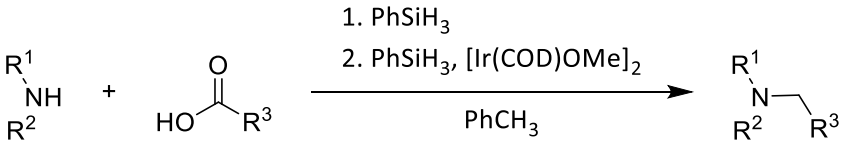

Procedure:[120] Phenylsilane (1 eq) was added to a solution of the carboxylic acid (1.5 eq) in anhydrous toluene (1 mL·mmol^{-1}) under an inert atmosphere and the resulting solution heated under reflux at 115 °C until the acid had completely dissolved. The reaction was removed from the heat and the amine (1 eq) was added portionwise. Once the addition was complete and the vigorous evolution of gas subsided, the reaction was then heated and stirred under reflux for 15 h. $[Ir(COD)OMe]_2$ (1 mol%) and phenylsilane (2 eq) were then added and the reaction mixture continued to stir at reflux for an additional 3 h. The toluene was then removed *in vacuo* and the residue partitioned between water (10 mL) and EtOAc (10 mL). The organic layer was then extracted with 3 M HCl (3 x 10 mL). The combined acid washings were basified to pH 9 with NaOH maintaining the temperature at 0 ˚C. The aqueous layer was extracted with DCM (3 x 10 mL) and the combined organic layers were washed brine (20 mL), dried over $MgSO_4$, and concentrated *in vacuo.* The crude residue purified by silica column chromatography to provide the product.

5.1.3 Compound synthesis and characterization

2,2'-(1,2-phenylene)diethanol[153] **39**

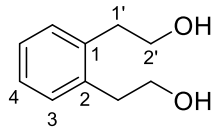

Following the general procedure for $LiAlH_4$ reduction, 1,2-phenylenediactic acid (7.82 g, 40.3 mmol) was reduced to give the title compound (6.54 g, 39.4 mmol, 98% yield) as a yellow oil which solidified on standing and was sufficiently pure to be used without any further purification.

mp 67 – 68 °C (lit.[154] mp 61 – 63 °C); ν_{max} (ATR): 3328 (br, *OH*), 2959, 2886, 1488, 1441, 1334, 1272, 1038, 1003, 756, 640, 611 cm^{-1}; δ_H (600 MHz, $CDCl_3$): 7.24 – 7.11 (4H, m, Ar-*H*), 3.81 (2H, t, J = 6.8 Hz, 2'-H_2), 2.91 (2H, t, J = 6.8 Hz, 1'-H_2), 2.74 (1H, s, O*H*); δ_C (151 MHz, $CDCl_3$): 137.3 (C-1), 130.1 (C-3), 126.8 (C-4), 63.5 (C-2'), 35.7 (C-1'); CHN calculated for $C_{10}H_{14}O_2$: C, 72.26%; H, 8.49%. Found: C, 71.96%; H, 8.42%.

1,2-bis-[2'-(methanesulfonyloxy)ethyl]benzene[106] **40**

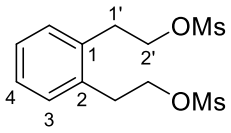

Methanesulfonyl chloride (8.1 g, 5.5 mL, 71.1 mmol) was added dropwise to a solution of **39** (5.01 g, 30.1 mmol) in anhydrous DCM (100 mL) and Et_3N (6.9 g, 9.5 mL, 68.2 mmol) cooled to 0° C. The reaction was stirred for 1 hour at 0°C then warmed to room temperature with stirring over 2 hours. The organic layer was washed with 1M HCl (3 x 20 mL), $NaHCO_3$ (20 mL), and brine (20 mL). The organic layer was then dried over $MgSO_4$ and concentrated under reduced pressure to give the title compound (9.63g, 29.9 mmol, 99%) as a brown oil which solidified on standing and was sufficiently pure to be used without any further purification.

mp 67 – 68 °C; ν_{max} (ATR): 3023, 2939, 1341, 1329 (S=O), 1174 (S=O), 1163, 973, 914, 803 cm^{-1}; δ_H (600 MHz, $CDCl_3$): 7.25 – 7.22 (4H, m, Ar-*H*), 4.41 (4H, t, J = 7.1 Hz, 2'-H_2), 3.13 (t, J = 7.1 Hz, 4H, 1'-H_2), 2.90 (6H, s, CH_3); δ_C (151 MHz, $CDCl_3$): 134.6 (C-1), 130.1 (C-3), 127.5 (C-4), 69.6 (C-2'), 37.2 (C-1'), 32.1 (*C*H_3); CHN calculated for $C_{12}H_{18}O_6S_2$: C, 44.7%; H, 5.63%. Found: C, 44.63%; H, 5.57%.

3-(prop-2'-en-1'-yl)-1,2,4,5-tetrahydro-1H-3-benzazepine **44**

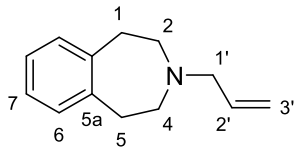

To **40** (1.02 g, 3.17 mmol), allylamine (1 mL) was added. The reaction was stirred for 48 hours at room temperature. When the reaction was complete by TLC, the organic layer was washed with 1M HCl (3 x 20 mL), $NaHCO_3$ (20 mL), and brine (20 mL). The organic layer was then dried over $MgSO_4$ and concentrated under reduced pressure. Purification by column chromatography (2% - 10% EtOAc/Hexane) gave title compound as a yellow oil (0.48 g, 2.56 mmol, 81% yield).

ν_{max} (ATR): 3303, 2929, 2801, 1641, 1493, 1451, 1110, 1049 cm^{-1}; δ_H (700 MHz, $CDCl_3$): 7.14 – 7.07 (4H, Ar-*H*), 5.93 (1H, ddt, *J* = 16.9, 10.2, 6.6 Hz, 2'-*H*), 5.22 – 5.14 (2H, m, 3'- H_2), 3.14 (2H, dt, *J* = 6.5, 1.3 Hz, 1'-H_2), 2.98 – 2.89 (4H, m, 2-H_2, 4-H_2), 2.65 (4H, s, 1-H_2, 5-H_2); δ_C (151 MHz, $CDCl_3$): 142.2 (C-5a), 135.5 (C-2'), 129.0 (C-6), 126.4 (C-7), 118.0 (C-3'), 62.6 (C-1'), 55.4 (C-2), 36.6 (C-1); *m/z* (ES^+) 188.2 $[M+H]^+$; HRMS (ES^+) found $[M+H]^+$ 188.1447; $C_{13}H_{18}N$ requires *M,* 188.1439.

1,2,4,5-tetrahydro-1H-3-benzazepine[106] **37**

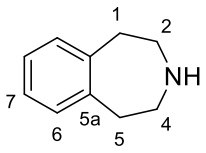

A solution of **40** (1.94 g, 6.02 mmol) in EtOH (20 mL) and 28% aqueous ammonia (20 mL) was stirred at 80 °C in a microwave for 30 minutes. The organic solvent was then evaporated and the aqueous residue acidified to pH 4 with HCl (4 M) and extracted with Et_2O (4 x 20 mL). The aqueous phase was then basified to pH 14 with NaOH (4 M) and extracted with DCM (4 x 20 mL). The combined organic extracts were washed with water, dried with $MgSO_4$, and concentrated under reduced pressure to give the title compound (75 mg, 5.1 mmol, 85%) as a brown oil which was used without any further purification.

ν_{max} (ATR): 3294 (br, NH), 2935, 1577, 1490, 1454, 1375, 1307, 1276, 1128, 1045 cm^{-1}; δ_H (600 MHz, $CDCl_3$): 7.15 – 7.07 (4H, m, Ar-*H*), 3.01 – 2.92 (8H, m, 1-*H₂,* 2-*H₂, 4-H₂,* 5-*H₂*), 2.32 (1H, br, N*H*); δ_C (151 MHz, $CDCl_3$): 142.1 (C-5a), 129.2 (C-6), 126.2 (C-7), 48.5 (C-2), 39.8 (C-1); *m/z* (ES^+) 148.3 $[M+H]^+$; HRMS (ES^+) found $[M+H]^+$ 148.1126; $C_{10}H_{14}N$ requires *M*, 148.1137.

2',2',2'-trichloroethyl-1,2,4,5-tetrahydro-1H-3-benzazepine-3-carboxylate **47**

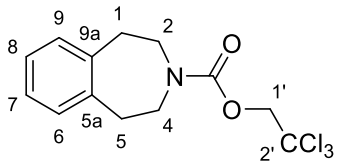

2,2,2-trichlorethoxycarbonyl chloride (1.57 g, 1.02 mL, 7.41 mmol) was added dropwise to a stirred solution of benzazepine **37** (0.99 g, 6.73 mmol) in anhydrous DCM (35 mL) and Et_3N (0.68 g, 0.94 mL, 6.73 mmol) cooled to 0° C under an argon atmosphere. On completion of the addition, the mixture was warmed to room temperature and stirred for a further 18 h. When the reaction was complete by TLC, the organic layer was washed with water (20 mL) and brine (20 mL) then dried with $MgSO_4$. Evaporation of the solvent under reduced pressure gave a brown oil which solidified on standing. Purification was

completed by recrystallization from EtOH to give the title compound (1.47 g, 4.58 mmol, 68%) as flat beige crystals.

mp 74 – 76 °C; ν_{max} (ATR): 2925, 1707 (C=O), 1457, 1435, 1209, 1106 cm^{-1}; δ_H (700 MHz, $CDCl_3$, mixture of rotamers A,B, 1:1): 7.18 – 7.08 (4H, m, Ar-*H*), 4.80 (2H, s, 1'-H_2), 3.71 – 3.63 (4H, m, 2-H_2), 2.99 – 2.93 (4H, m, 1-H_2); δ_C (176 MHz, $CDCl_3$, mixture of rotamers A,B, 1:1): 154.0 (C=O), 140.7 (C-9a, C-5a), 140.7 (C-9a, C-5a), 130.1 (C-9, C-6), 130.0 (C-9, C-6), 126.8 (C-8, C-7), 126.8 (C-8, C-7), 96.0 (C-2'), 75.3 (C-1'), 47.6 (C-2, C-4), 47.4 (C- 2, C-4), 38.1 (C-1, C-5), 37.8 (C-1, C-5); *m/z* (ASAP) 322.01 $[M(^{35}Cl_3)+H]^+$ (41%); 324.01 $[M(^{35}Cl_2{}^{37}Cl)+H]^+$ (41%); 326.12 $[M(^{35}Cl^{37}Cl_2)+H]^+$ (16%); 328.01 $[M(^{37}Cl_3)+H]^+$ (2%). HRMS ASAP found $[M+H]^+$ 322.0162; $C_{13}H_{15}NO_2{}^{35}Cl_3$ requires *M*, 322.0168. CHN calculated for $C_{13}H_{14}NO_2Cl_3$: C, 48.4%; H, 4.37%, N, 4.34%. Found: C, 48.25%; H, 4.36%, N, 4.32%.

2',2',2'-trichloroethyl 7-chlorosulfonyl-2,3,4,5-tetrahydro-1H-3-benzazepine-3-carboxylate **49**

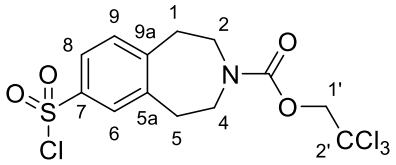

To a stirred solution of chlorosulfonic acid (0.3 mL, 4.51 mmol) in DCM (5 mL), **47** (0.47 g, 1.48 mmol) in DCM (2 mL) was added dropwise at 0 °C under an argon atmosphere. On completion of the addition, the mixture was slowly warmed to room temperature and stirred at this temperature for a further 4 h. The reaction was then slowly poured over an ether-ice mixture. The resultant mixture was separated and the aqueous layer extracted with cold Et_2O (3 × 100 mL). The combined organic extracts were dried with $MgSO_4$ and concentrated to give the title compound (0.38 g, 0.90 mmol, 61%) as a white solid which was used directly without any further purification.

mp 120 – 123 °C; ν_{max} (ATR): 2925, 1707 (C=O), 1457, 1435, 1377 (S=O), 1209, 1175 (S=O), 1188 cm^{-1}; δ_H (600 MHz, $CDCl_3$ A,B, 1:1): 7.85 – 7.79 (2H, m, 8-*H*, 6-*H*), 7.38 (1H, m, 9-*H*), 4.81 (2H, s, 1'-H_2), 3.78-3.68 (4H, m, 2-H_2, 4-H_2), 3.13 – 3.07 (4H, m, 1-H_2, 5-H_2); δ_C NMR (151 MHz, $CDCl_3$, mixture of rotamers A,B, 1:1): 153.9 (C=O), 153.9 (C=O), 149.1(C-9a),

149.1 (C-9a), 142.8 (C-7, C-5a), 142.7 (C-7, C-5a), 142.8 (C-7, C-5a), 142.7 (C-7, C-5a), 131.4 (C-9), 131.2 (C-9), 128.2 (C-6), 128.1 (C-6), 125.6 (C-8), 125.6 (C-8), 95.8 (C-2'), 75.3 (C-1'), 46.9 (C-2, C-4), 46.6 (C-2, C-4), 46.6 (C-2, C-4), 46.4 (C-2, C-4), 38.3 (C-1, C-5), 37.9 (C-1, C-5), 37.8 (C-1, C-5), 37.7 (C-1, C-5); *m/z* (ASAP) 419.96 $[M(^{35}Cl_4)+H]^+$ (31%); 421.94 $[M(^{35}Cl_3{}^{37}Cl)+H]^+$ (40%); 432.94 $[M(^{35}Cl_2{}^{37}Cl_2)+H]^+$ (22%); 425.93 $[M(^{35}Cl^{37}Cl_3)+H]^+$ (6%); 427.39 $[M(^{37}Cl_4)+H]^+$ (1%). HRMS ASAP found $[M+H]^+$ 419.9405; $C_{13}H_{14}NO_4S^{35}Cl_4$ requires *M*, 419.9389. CHN calculated for $C_{13}H_{13}NO_4SCl_4$: C, 37.08%; H, 3.11%; N, 3.33%. Found: C, 36.66%; H, 3.15%; N, 3.25%.

2",2",2"-trichloroethyl 7-[(4'-fluoro-1'H-indol-1'-yl)sulfonyl]-1,2,4,5- tetrahydro-1H-3-benzazepine-3-carboxylate **50**

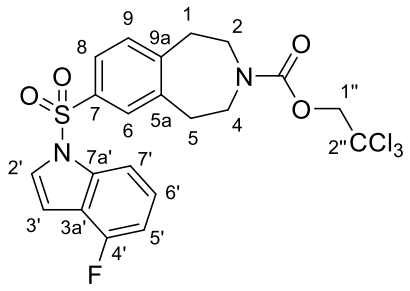

A solution of 4-fluoroindole **35** (52.5 mg, 0.4 mmol) in anhydrous THF (0.5 mL) was added to a suspension of NaH (60% in mineral oil) (15.3 mg, 0.64 mmol) in anhydrous THF (0.5 mL) under an argon atmosphere. The resulting solution was allowed to stir at 0 °C for 30 min when a solution of **49** (106 mg, 0.25 mmol) dissolved in anhydrous THF (1 mL) was added. The reaction mixture was warmed to room temperature and allowed to stir for 30 minutes until the reaction was judged complete by TLC. The reaction was carefully quenched by the dropwise addition of NH_4Cl followed by removal of the solvent under reduced pressure. The resultant mixture extracted with Et_2O (3 x 5 mL) and the combined organic layers dried with $MgSO_4$ and concentrated to give a pink oil. Purification by column chromatography (70% - 100% Hexane/$CHCl_3$) gave the title compound as a pink solid (114 mg, 0.22 mmol, 87%).

mp 114 – 117 °C dec.; ν_{max} (ATR): 3145, 3117, 2948, 1714 (C=O), 1489, 1464, 1432, 1375 (S=O), 1237, 1180 (S=O), 1126 cm^{-1}; δ_H (600 MHz, $CDCl_3$, mixture of rotamers A,B, 1:1):

7.77 (1H, d, *J* = 8.4 Hz 7'-*H*), 7.70 – 7.61 (2H, m, 6-*H*, 8-*H*), 7.54 (1H, m, 2'-*H*), 7.26 – 7.18 (2H, m, 6'-*H,* 9-*H*), 6.92 (1H, dd, $J_{H,F}$ = 9.5 Hz, $J_{H,H}$ = 8.1 Hz, 5'-*H*), 6.76 (1H, d, *J* = 3.7 Hz, 3'-*H*), 4.77 (2H, s, 1''-H_2), 3.70 – 3.57 (4H, m, 2-H_2, 4-H_2), 3.00 – 2.93 (4H, m, 1-H_2, 5-H_2); δ_C (151 MHz, $CDCl_3$, mixture of rotamers A,B, 1:1): 156.0 (d, $J_{C,F}$ = 249.5 Hz, C-4'), 153.9 (C=O), 153.8 (C=O), 147.6 (C-9a), 142.3 (d, $J_{C,F}$ = 14.4 Hz, C-7a'), 137.0 (C-5a), 137.0 (C-5a), 136.4 (C-7), 136.3 (C-7), 131.1 (C-9), 131.1 (C-9), 131.0 (C-2'), 128.1 (C-6), 127.9 (C-6), 126.4 (C-2'), 125.6 (d, $J_{C,F}$ = 7.5 Hz, C-6'), 125.5 (C-8), 125.4 (C-8), 119.9 (d, $J_{C,F}$ = 22.3 Hz, C-3a'), 109.7 (d, $J_{C,F}$ = 2.1 Hz, C-7'), 108.8 (d, $J_{C,F}$ = 18.5 Hz, C-5'), 104.8 (C-3'), 95.8 (C-2''), 75.3 (C-1''), 46.8 (C-2, C-4), 46.6 (C-2, C-4), 46.5 (C-2, C-4), 46.4 (C-2, C-4), 38.1 (C-1, C-5), 37.9 (C-1, C-5), 37.7 (C-1, C-5), 37.7 (C-1, C-5); δ_F (376 MHz, $CDCl_3$): - 120.70; *m/z* (ASAP) 519.00 $[M(^{35}Cl_3)+H]^+$ (40%); 521.00 $[M(^{35}Cl_2{}^{37}Cl)+H]^+$ (40%); 523.01 $[M(^{35}Cl\ {}^{37}Cl_2)+H]^+$ (18%); 525.01 $[M(^{37}Cl_3)+H]^+$ (3%); HRMS ASAP found $[M]^+$ 518.0036; $C_{21}H_{18}N_2O_4SF^{35}Cl_3$ requires *M*, 518.0037; CHN calculated for $C_{21}H_{18}N_2O_4SFCl_3$: C, 48.52%; H, 3.49%; N, 5.39%. Found: C, 48.56%; H, 3.56%; N, 5.25%.

7-(4''-fluoroindol-1''-ylsulfonyl)-3-(pyridin-3'-ylmethyl)-1,2,4,5-tetrahydro-3-benzazepine **32a**

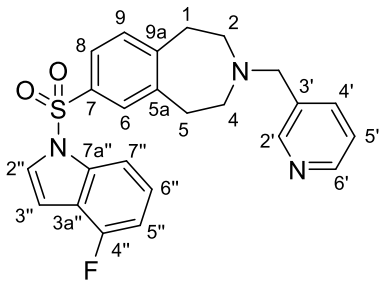

A solution of **50** (139.5 mg, 0.27 mmol) and zinc powder (106.3 mg, 1.63 mmol) in HOAc (1.5 mL) was allowed to stir at room temperature for 3 hours. The completed reaction was filtered, and the residue was diluted with water. The resultant mixture was extracted with DCM (3 x 5 mL) and the combined organic layers dried with $MgSO_4$. The combined filtrate was concentrated under reduced pressure to afford **33** (68.2 mg, 0.20 mmol, 74%) as a brown oil which was used without further purification.

Next, following the general procedure for N-alkylation, amine **33** (68.2 mg, 0.20 mmol) was combined with 3-(bromomethyl)pyridine hydrobromide (57.5 mg, 0.23 mmol) to afford, after purification by silica column chromatography (0 – 40% MeOH/Et_2O), the title compound (79.8 mg, 0.18 mmol, 93%) as a brown oil.

ν_{max} (ATR): 3160, 2932, 1663, 1486, 1429, 1384 (S=O), 1294, 1177 (S=O), 1163, 1129 cm^{1}; δ_H (600 MHz, $CDCl_3$): 8.54 (1H, s, 2'-*H*), 8.51 (1H, d, *J* = 4.8 Hz, 6'-*H*), 7.77 (1H, d, *J* = 8.4 Hz, 7''-*H*), 7.67 (1H, d, *J* = 7.7 Hz, 4'-*H*), 7.63 (1H, dd, *J* = 8.0, 2.1 Hz, 8-*H*), 7.58 (1H, d, *J* = 2.1 Hz, 6-*H*), 7.54 (1H, d, *J* = 3.7 Hz, 2''-*H*), 7.27 – 7.20 (2H, m, 5'-*H,* 6''-*H*), 7.15 (1H, d, *J* = 8.0 Hz, 9-*H*), 6.91 (1H, dd, $J_{H,F}$ = 9.6 Hz, $J_{H,H}$ = 8.1 Hz, 5''-*H*), 6.75 (1H, d, *J* = 3.7 Hz, 3''-*H*), 3.60 (2H, s, NCH_2Ar), 2.91 (4H, m, 1-H_2, 5-H_2), 2.57 (4H, m, 2-H_2, 4-H_2); δ_C (151 MHz, $CDCl_3$): 156.0 (d, $J_{C,F}$ = 249.7 Hz, C-4''), 150.5 (C-2'), 148.9 (C-6'), 143.9 (C-5a), 143.5 (C-9a), 137.0 (d, $J_{C,F}$ = 9.7 Hz, C-7a''), 136.7 (C-4'), 135.9 (C-7), 130.2 (C-3'), 129.9 (C-9), 127.0 (C-6), 126.4 (C-2''), 125.5 (d, $J_{C,F}$ = 7.0 Hz, C-6''), 125.2 (C-8), 123.54 (C-5'), 119.9 (d, $J_{C,F}$ = 22.3 Hz, C-3a''), 109.7 (d, $J_{C,F}$ = 3.6 Hz, C-7''), 108.6 (d, $J_{C,F}$ = 18.5 Hz, C-5''), 104.6 (C-3''), 60.7 (NCH_2Ar), 54.8 (C-2, C-4), 54.39 (C-2, C-4), 36.8 (C-1, C-5), 36.7 (C-1, C-5); δ_F (376 MHz, $CDCl_3$): -123.9; *m/z* (ES^+) 436.350 $[M+H]^+$; HRMS (ES^+) found $[M+H]^+$ 436.1495; $C_{24}H_{23}N_3O_2FS$ requires *M*, 436.1501.

1'-(1,2,4,5-tetrahydro-1H-3-benzazepin-3-yl)ethan-1'-one[115] **51**

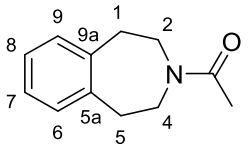

Following the general procedure for acetamide protection, amine **37** (6.37 g, 43.30 mol) was converted, after 18 h, to the title compound (10.24 g, 54.10 mmol, 95%) and isolated as a yellow oil which was sufficiently pure to be used without any further purification.

ν_{max} (ATR): 2932, 1643 (C=O), 1427, 1247, 1032, 948, 758 cm^{-1}; δ_H (600 MHz, $CDCl_3$, mixture of rotamers A,B, 1:1): 7.20 – 7.10 (m, 4H, Ar-*H*), 3.74 – 3.70 (m, 4H, 2-H_2, 4-H_2, *A*), 3.60 – 3.56 (m, 4H, 2-H_2, 4-H_2, *B*), 2.96 – 2.92 (m, 4H, 1-H_2, 5-H_2, *B*), 2.92 – 2.89 (m, 4H, 1-H_2, 5-H_2, *A*), 2.18 (s, 3H, CH_3); δ_C (151 MHz, $CDCl_3$, mixture of rotamers A,B, 1:1):

169.4(C=O), 141.0 (C-5a, C-9a), 139.9 (C-5a, C-9a), 129.9 (C-6, C-9), 129.7 (C-6, C-9), 126.8 (C-7, C-8), 126.4 (C-7, C-8), 49.2 (C-2, C-4, B), 44.8 (C-2, C-4, A), 38.2 (C-1, C-5, B), 37.4 (C-1, C-5, A), 21.8 (CH_3); *m/z* (ES^+) 190.190 $[M+H]^+$; HRMS (ES^+) found $[M+H]^+$ 190.1237; $C_{12}H_{16}NO$ requires *M*, 190.1232.

3-acetyl-1,2,4,5-tetrahydro-1H-3-benzazepine-7-sulfonylchloride[115] **52**

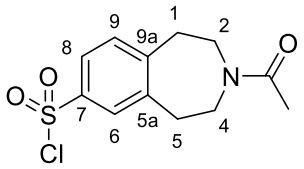

While maintaining the reaction temperature of 0 °C, chlorosulfonic acid (7.63 g, 4.36 mL, 65.46 mmol) was added dropwise to a solution of benzazepine **51** (4.13 g, 21.82 mmol) in anhydrous DCM (45 mL) in a round bottom flask under an argon atmosphere. After the addition was complete, the reaction was stirred at room temperature for 18 h. The reaction was then poured onto an ice/Et_2O slurry and extracted with Et_2O (3 × 20 mL). The combined organic extracts were dried over $MgSO_4$ and concentrated *in vacuo* to give the title compound (3.79 g, 13.20 mmol, 60%) as a yellow semi-solid which was used directly without further purification.

ν_{max} (ATR): 2930, 1644 (C=O), 1433, 1376 (S=O), 1249, 1172 (S=O), 1037, 950 cm^1; δ_H (700 MHz, $CDCl_3$, mixture of rotamers A,B, 2:1): 7.85 – 7.79 (2H, m, 6-*H*, 8-*H*), 7.39 (1H, d, J = 8.0 Hz, 9-*H*), 3.71 (4H, m, 2-H_2, 4-H_2), 3.06 (4H, s, 1-H_2, 5-H_2), 2.23 (3H, s, CH_3, A), 2.08 (3H, s, CH_3, B); δ_C (176 MHz, $CDCl_3$, mixture of rotamers A,B, 2:1): 175.7 (C=O, B), 170.2 (C=O, A), 149.6 (C-9a), 148.3 (C-9a), 143.3 (C-7, C-5a), 142.8 (C-7, C-5a), 142.5 (C-7, C-5a), 141.9 (C-7, C-5a), 131.3 (C-9) , 131.2 (C-9), 128.1 (C-6), 128.0 (C-6), 125.8 (C-8), 125.4 (C-8), 48.7 (C-2, C-4), 48.4 (C-2, C-4), 44.5 (C-2, C-4), 44.1 (C-2, C-4), 38.4 (C-1, C-5), 38.0 (C-1, C-5), 37.5 (C-1, C-5), 37.3 (C-1, C-5), 21.6 (CH_3, A), 20.8 (CH_3, B); *m/z* (ES^+) 288.154 $[M+H]^+$; HRMS (ES^+) found $[M+H]^+$ 288.0478; $C_{12}H_{15}NO_3SCl$ requires *M*, 288.0461.

1’-(7-[(4”-fluoro-1”H-indol-1”-yl)sulfonyl]-1,2,4,5-tetrahydro-1H-3-benzazepin-3-yl)ethan-1’-one **55**

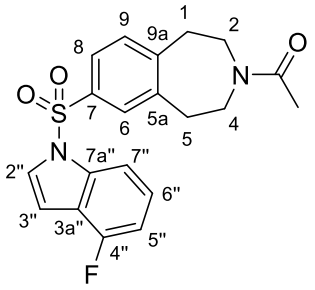

Following the general procedure for sulfamidation, sulfonylchloride **52** (3.55 g, 12.3 mmol) was combined with 4-fluoroindole (1.67 g, 12.3 mmol) to afford, after purification by silica column chromatography (0 – 100% EtOAc/Hexane), the title product (2.99 g, 7.74 mmol, 63%) as a yellow oil.

ν_{max} (ATR): 2923, 1641 (C=O), 1491, 1430, 1376 (S=O), 1250, 1183 (S=O), 1166, 1130, 948, cm^1; δ_H (600 MHz, $CDCl_3$, 1:1 mixture of rotamers A,B): 7.79 – 7.73 (1H, m, 7’’-*H*), 7.69 – 7.60 (2H, m, 6-*H*, 8-*H*), 7.55 – 7.52 (1H, m, 2’’-*H*), 7.37 – 7.17 (2H, m, 9-*H*, 6’’-*H*), 6.91 (1H, dd, $J_{H,F}$ = 9.6 Hz, $J_{H,H}$ = 8.0 Hz, 5’’-*H*), 6.77 – 6.74 (1H, m, 3’’-*H*), 3.69 – 3.49 (4H, m, 2-H_2, 4-H_2), 2.96 – 2.85 (4H, m, 1-H_2, 5-H_2), 2.14 (3H, CH_3, B), 2.12 (3H, CH_3, A); δ_C (151 MHz, $CDCl_3$, 1:1 mixture of rotamers A,B): 169.5 (C=O, B), 169.4 (C=O, A), 156.0 (d, $J_{C,F}$ = 249.6 Hz, C-4’’), 148.3 (C-5a), 147.0 (C-5a), 143.0 (C-9a), 141.6 (C-9a), 136.9 (d, $J_{C,F}$ = 9.5 Hz, C-7a’’), 136.4 (C-7), 136.1 (C-7), 131.1 (C-9), 130.9 (C-9), 128.7 (d, $J_{C,F}$ = 7.7 Hz, C-6’’), 128.0 (C-6), 127.7 (C-6), 126.4 (C-2’’), 126.3 (C-2’’), 125.6 (C-8), 125.2 (C-8), 119.8 (d, $J_{C,F}$ = 21.5 Hz, C-3a’’), 109.6 (d, $J_{C,F}$ = 3.3 Hz, C-7’’), 109.6 (d, $J_{C,F}$ = 3.3 Hz, C-7’’), 108.7 (d, $J_{C,F}$ = 18.6 Hz, C-5’’), 108.6 (d, $J_{C,F}$ = 18.6 Hz, C-5’’), 104.8 (C-3’’), 104.8 (C-3’’), 48.6 (C-2, C-4, A), 48.4 (C-2, C-4, B), 44.1 (C-2, C-4), 43.7 (C-2, C-4), 38.4 (C-1, C-5), 38.1 (C-1, C-5), 37.5 (C-1, C-5, B), 37.5 (C-1, C-5, A), 21.8 (CH_3, B), 21.8 (CH_3, A); δ_F (376 MHz, $CDCl_3$, 1:1 mixture of rotamers A,B): -120.66, -120.69; *m/z* (ES^+) 387.226 $[M+H]^+$; HRMS (ES^+) found $[M+H]^+$ 386.1180 $C_{20}H_{20}N_2O_3SF$ requires *M,* 387.1179.

4’-{[7-(4”-fluoroindol-1”-ylsulfonyl)-1,2,4,5-tetrahydro-3-benzazepin-3-yl]methyl}benzonitrile **56**

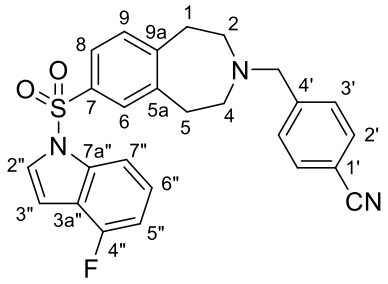

Following the general procedure for acetamide deprotection, amide **55** (72.3 mg, 0.19 mmol) was hydrolyzed to afford the crude amine **33** (64.4 mg, 0.29 mmol, 100%) as a brown oil which was used without further purification.

Next, following the general procedure for N-alkylation, amine **33** (93.6 mg, 0.27 mmol) was combined with 4-(bromomethyl)benzonitrile (53.5 mg, 0.27 mmol) to afford, after purification by silica column chromatography (0 – 100% EtOAc/Hexane), the title product (93.8 mg, 0.20 mmol, 74%) as a white solid.

mp: 123 – 124 °C; ν_{max} (ATR): 3044, 2950, 2813, 2231 (C≡N), 1490, 1435, 1376 (S=O), 1180 (S=O), 1167, 1129, 1032 cm^{1}; δ_H (600 MHz, $CDCl_3$): 7.77 (1H, d, *J* = 8.3 Hz, 7’’-*H*), 7.64 (1H, dd, *J* = 8.1, 2.1 Hz, 8-*H*), 7.61 (2H, d, *J* = 8.0 Hz, 2’-*H*, 6’-*H*), 7.58 (1H, d, *J* = 2.1 Hz, 6-*H*), 7.54 (1H, d, *J* = 3.7 Hz, 2’’-*H*), 7.45 (2H, d, *J* = 8.0 Hz, 3’-*H*, 5’-*H*), 7.25 – 7.21 (1H, m, 6’’-*H*), 7.15 (1H, d, *J* = 8.1 Hz, 9-*H*), 6.91 (1H, dd, $J_{H,F}$ = 9.6 Hz, $J_{H,H}$ = 8.0 Hz, 5’’-*H*), 6.75 (1H, d, *J* = 3.7 Hz, 3’’-*H*), 3.62 (2H, s, NCH_2Ar), 2.96 – 2.87 (4H, m, 1-H_2, 5-H_2), 2.61 – 2.50 (4H, m, 2-H_2, 4-H_2); δ_C (151 MHz, $CDCl_3$): 155.8 (d, $J_{C,F}$ = 249.3 Hz, C-4’’), 149.0 (C-5a), 144.4 (C-4’), 143.5 (C-9a), 136.8 (d, $J_{C,F}$ = 9.6 Hz, C-7a’’), 135.7 (C-7), 132.2 (C-2’, C-6’), 129.8 (C-9), 129.2 (C-3’, C-5’), 126.8 (C-6), 126.2 (C-2’’), 125.3 (d, $J_{C,F}$ = 7.4 Hz, C-6’’), 125.1 (C-8), 119.7 (d, $J_{C,F}$ = 22.5 Hz, C-3a’’), 118.9 (C≡N), 111.0 (C-1’), 109.5 (d, $J_{C,F}$ = 3.9 Hz, C-7’’), 108.5 (d, $J_{C,F}$ = 18.8 Hz, C-5’’), 104.4 (C-3’’), 62.8 (NCH_2Ar), 54.8 (C-2, C-4), 54.4 (C-2, C-4), 36.7 (C-1, C-5), 36.6 (C-1, C-5); δ_F (376 MHz, $CDCl_3$): -120.8; *m/z* (ES^+) 460.799 $[M+H]^+$; HRMS (ES^+) found $[M+H]^+$ 460.1511; $C_{26}H_{23}N_3O_2FS$ requires *M,* 460.1495.

2-(pyridin-3'-yl)ethan-1-ol[155,156] **60**

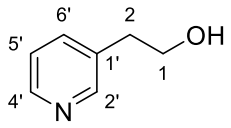

Following the general procedure for $LiAlH_4$ Reduction, ethyl 3-pyridylacetate (2.09 g, 12.6 mmol) was stirred under reflux for 16 hours to afford, after purification by silica column chromatography (5% MeOH/ 95% $CHCl_3$), the title compound (0.22 g, 1.8 mmol, 14%) as a yellow oil.

ν_{max} (ATR): 3251 (br, OH), 2946, 2871, 1740, 1428, 1242, 1049 cm^{-1}; δ_H (700 MHz, $CDCl_3$): 8.45 (1H, d, *J* = 2.1 Hz, 2'-*H*), 8.43 (1H, dd, *J* = 4.8, 1.6 Hz, 4'-*H*), 7.57 (1H, ddd, *J* = 7.8, 2.1, 1.6 Hz, 6'-*H*), 7.22 (1H, ddd, *J* = 7.8, 4.8, 0.9 Hz, 5'-*H*), 3.88 (2H, t, *J* = 6.5 Hz, 1-CH_2), 2.86 (2H, t, *J* = 6.5 Hz, 2-CH_2); δ_C (176 MHz, $CDCl_3$): 150.4 (2'-C), 147.9 (4'-C), 136.8 (C-6'), 134.2 (1'-C), 123.5 (C-5'), 63.2 (C-1), 36.4 (C-2); *m/z* (ES^+) 124.189 $[M+H]^+$; HRMS ES^+ found $[M+H]^+$ 124.0761 $C_7H_{10}NO$ requires *M,* 124.0762.

3-(2-bromoethyl)pyridine[157] **61**

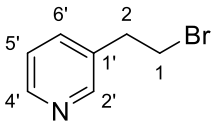

A round-bottom flask fit with a condenser was charged with alcohol **61** (0.25 g, 2.05 mmol). 48% HBr (4.1 g, 2.8 mL, 50.8 mmol) was then added and the solution refluxed at 126 °C for 9 h. The reaction mixture was then cooled to room temperature and basified to pH 12 with a solution of saturated $NaHCO_3$ in an ice-cooling bath. The crude product was extracted from the basified solution with DCM (3 × 10 mL). The combined organic extracts were washed with water, dried with MgSO4, and concentrated under reduced pressure to afford, after purification by silica column chromatography (0 – 10% MeOH/DCM), the title compound (0.20 g, 1.07 mmol, 52%) as a yellow oil.

ν_{max} (ATR): 2930, 2856, 1723, 1412, 1245, 1043 cm^{-1}. δ_H (400 MHz, MeOD): 8.76 (1H, s, 2'-*H*), 8.72 (1H, d, *J* = 5.8, 4'-*H*), 8.56 (1H, dt, *J* = 8.1, 1.8 Hz, 6'-*H*), 8.03 (1H, dd, *J* = 8.1, 5.8 Hz,

5'-*H*), 3.85 (2H, t, *J* = 6.0 Hz, 1-CH_2), 3.04 (2H, t, *J* = 6.0 Hz, 2-CH_2). δ_C (101 MHz, MeOD): 148.9 (C-2'), 128.2 (C-5'), 62.0 (C-1), 36.5 (C-2); *m/z* (ES^+) 186.162 $[M(^{79}Br)H]^+$, 188.100 $[M(^{81}Br)H]^+$.

7-(4''-fluoroindol-1''-ylsulfonyl)-3-[(4'-fluorophenyl)methyl]-1,2,4,5-tetrahydro-3-benzazepine **33a**

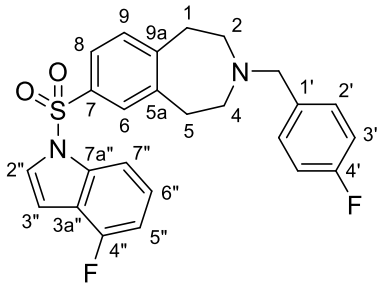

Following the general procedure for reductive amination, amine **33** (40.1 mg, 0.12 mmol) was combined with 4-flurobenzaldehyde (15.7 mg, 0.13 mmol) to afford, after purification by silica column chromatography (0 – 100% Hexane/EtOAc), the title compound (11.7 mg, 0.026 mmol, 22%) as a yellow oil.

ν_{max} (ATR): 3132, 2936, 2815, 1490, 1434, 1377 (S=O), 1179 (S=O), 1033 cm^1. δ_H (700 MHz, $CDCl_3$): 7.77 (1H, dt, *J* = 8.4, 0.8 Hz 7''-*H*), 7.63 (1H, dd, *J* = 8.0, 2.1 Hz, 8-*H*), 7.58 (1H, d, *J* = 2.1 Hz, 6-*H*), 7.54 (1H, d, *J* = 3.7 Hz, 2''-*H*), 7.30 – 7.26 (2H, m, 2'-*H*, 6'-*H*), 7.25 – 7.22 (1H, m, 6''-*H*), 7.14 (1H, d, *J* = 8.0 Hz, 9-*H*), 7.00 (1H, td, $J_{H,F}$ = 9.5 Hz, $J_{H,H}$ = 8.6, 2.0 Hz, 3'-*H*, 5'-*H*), 6.91 (1H, ddd, $J_{H,F}$ = 9.6 Hz, $J_{H,H}$ = 8.1, 0.8 Hz, 5''-*H*), 6.75 (1H, dd, *J* = 3.7, 0.8 Hz, 3''-*H*), 3.54 (2H, s, NCH_2Ar), 2.92 – 2.86 (4H, m, 1-H_2, 5-H_2), 2.60 – 2.48 (4H, m, 2-H_2, 4-H_2). δ_C (176 MHz, $CDCl_3$): 162.0 (d, $J_{C,F}$ = 245.2 Hz, C-4'), 155.8 (d, $J_{C,F}$ = 249.3 Hz, C-4''), 149.3 (C-5a), 143.8 (C-9a), 136.9 (d, $J_{C,F}$ = 9.6 Hz, C-7a''), 135.6 (C-7), 134.1 (d, $J_{C,F}$ = 3.2 Hz, C-1'), 130.3 (d, $J_{C,F}$ = 7.9 Hz, C-2', C-6'), 129.8 (C-9), 126.8 (C-6), 126.2 (C-2''), 125.3 (d, $J_{C,F}$ = 7.5 Hz, C-6''), 124.9 (C-8), 119.7 (d, $J_{C,F}$ = 22.3 Hz, C-3a''), 115.1 (d, $J_{C,F}$ = 21.2 Hz, C-3', C-5'), 109.5 (d, $J_{C,F}$ = 4.0 Hz, C-7''), 108.4 (d, $J_{C,F}$ = 18.6 Hz, C-5''), 104.40 (C-3''), 62.5 (NCH_2Ar), 54.5 (C-2, C-4), 54.1 (C-2, C-4), 36.7 (C-1, C-5), 36.6 (C-1, C-5); δ_F (376 MHz, $CDCl_3$): -115.7 (F-4'), -120.9 (F-4''); *m/z* (ES^+) 453.141 $[M+H]^+$; HRMS (ES^+) found $[M+H]^+$ 453.1436 $C_{25}H_{23}N_2O_2F_2S$ requires *M,* 453.1448.

7-(4''-fluoroindol-1''-ylsulfonyl)-3-[(3'-fluorophenyl)methyl]-1,2,4,5-tetrahydro-3-benzazepine **65**

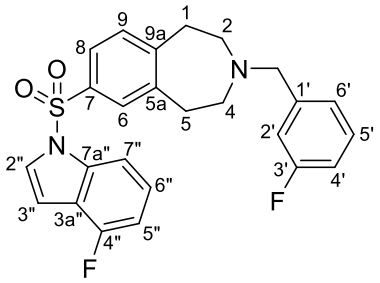

Following the general procedure for reductive amination, amine **33** (114.9 mg, 0.33 mmol) was combined with 3-fluorobenzaldehyde (41.9 mg, 0.34 mmol) to afford, after purification by silica column chromatography (0 – 50% Hexane/Et_2O), the title compound (31.8 mg, 0.070 mmol, 21%) as a yellow oil.

ν_{max} (ATR): 3159, 2947, 2816, 1587, 1488, 1433, 1375 (S=O), 1251, 1178 (S=O), 1166, 1125, 1087 cm^1; δ_H (600 MHz, $CDCl_3$): 7.77 (1H, d, *J* = 8.4 Hz, 7''-*H*), 7.63 (1H, dd, *J* = 8.0, 2.1 Hz, 8-*H*), 7.59 (1H, d, *J* = 2.1 Hz, 6-*H*), 7.54 (1H, d, *J* = 3.7 Hz, 2''-*H*), 7.29 – 7.22 (3H, m, 5'-*H*, 6''-*H*), 7.15 (1H, d, *J* = 8.0 Hz, 9-*H*), 7.10 – 7.05 (2H, m, 6'-*H*, 2'-*H*), 6.95 (1H, td, $J_{H,F}$ = 8.2 Hz, $J_{H,H}$ = 6.2, 2.1 Hz, 4'-*H*), 6.93 – 6.88 (1H, m, 5''-*H*), 6.75 (1H, d, *J* = 3.7 Hz, 3''-*H*), 3.57 (2H, s, NCH_2Ar), 2.94 – 2.88 (4H, m, 1-H_2, 5-H_2), 2.59 – 2.53 (4H, m, 2-H_2, 4-H_2); δ_C (176 MHz, $CDCl_3$): 163.1 (d, $J_{C,F}$ = 245.5 Hz, C-3'), 156.0 (d, $J_{C,F}$ = 249.3 Hz, C-4''), 149.4 (C-5a), 143.9 (C-9a), 141.5 (d, $J_{C,F}$ = 6.3 Hz, C-1'), 137.0 (d, $J_{C,F}$ = 9.5 Hz, C-7a''), 135.7 (C-7), 130.0 (C-9), 129.8 (d, $J_{C,F}$ = 8.2 Hz, C-5'), 127.0 (C-6), 126.4 (C-2''), 125.5 (d, $J_{C,F}$ = 7.4 Hz, C-6''), 125.1 (C-8), 124.4 (d, $J_{C,F}$ = 2.7 Hz, C-6'), 119.8 (d, $J_{C,F}$ = 22.3 Hz, C-3a''), 115.6 (d, $J_{C,F}$ = 21.3 Hz, C-2'), 114.1 (d, $J_{C,F}$ = 21.3 Hz, C-4'), 109.7 (d, $J_{C,F}$ = 3.9 Hz, C-7''), 108.6 (d, $J_{C,F}$ = 18.5 Hz, C-5''), 104.6 (C-3''), 62.92 (NCH_2Ar), 54.8 (C-2, C-4), 54.4 (C-2, C-4), 36.9 (C-1, C-5), 36.8 (C-1, C-5); δ_F (376 MHz, $CDCl_3$): -113.55 (F-3'), -120.87 (F-4''); *m/z* (ES^+) 453.236 $[M+H]^+$; HRMS (ES^+) found $[M+H]^+$ 453.1445 $C_{25}H_{23}N_2O_2F_2S$ requires *M,* 453.1448.

7-(4''-fluoroindol-1''-ylsulfonyl)-3-{[4'-(trifluoromethyl)phenyl]methyl}-1,2,4,5-tetrahydro-3-benzazepine **66**

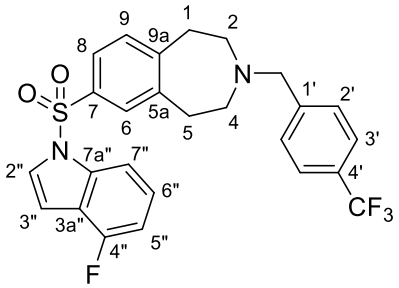

Following the general procedure for reductive amination, amine **33** (64.8 mg, 0.19 mmol) was combined with 4-(trifluoromethyl)benzaldehyde (32.9 mg, 0.19 mmol) to afford, after purification by silica column chromatography (0 – 30% Hexane/EtOAc), the title compound (26.4 mg, 0.053 mmol, 28%) as a yellow oil.

ν_{max} (ATR): 3149, 2949, 2820, 1490, 1433, 1377 (S=O), 1327, 1166 (S=O), 1123, 1069, 1032 cm^{1}; δ_H (600 MHz, $CDCl_3$): 7.77 (1H, d, *J* = 8.4, 0.9 Hz, 7"-*H*), 7.65 – 7.62 (1H, m, 8-*H*), 7.59 – 7.55 (3H, m, 6-*H*, 3'-*H*, 5'-*H*), 7.54 (1H, d, *J* = 3.7 Hz, 2"-*H*), 7.45 (2H, d, *J* = 7.9 Hz, 2'-*H*, 6'-*H*), 7.25 – 7.21 (1H, m, 6"-*H*), 7.15 (1H, d, *J* = 8.0 Hz, 9-*H*), 6.93 – 6.88 (1H, m, 5"-*H*), 6.75 (1H, d, *J* = 3.7 Hz, 3"-*H*), 3.62 (2H, s, NCH_2Ar), 2.91 (4H, m, 1-H_2, 5-H_2), 2.56 (4H, m, 2-H_2, 4-H_2); δ_C (151 MHz, $CDCl_3$): 156.0 (d, $J_{C,F}$ = 249.3 Hz, C-4"), 149.3 (C-5a), 143.8 (C-9a), 142.9 (C-1'), 137.0 (d, $J_{C,F}$ = 9.5 Hz, C-7a"), 135.8 (C-7), 130.0 (C-9), 129.6 (q, $J_{C,F}$ = 32.4 Hz, C-4'), 129.1 (C-2'), 127.0 (C-6), 126.4 (C-2"), 125.5 (d, $J_{C,F}$ = 7.5 Hz, 6"), 125.4 (q, $J_{C,F}$ = 3.8 Hz, C-3'), 125.2 (C-8), 124.6 (q, $J_{C,F}$ = 271.6 Hz, CF_3), 119.8 (d, $J_{C,F}$ = 22.4 Hz, C-3"), 109.7 (d, $J_{C,F}$ = 3.9 Hz, C-7"), 108.6 (d, $J_{C,F}$ = 18.5 Hz, C-5"), 104.6 (C-2"), 62.9 (NCH_2Ar), 54.8 (C-2, C-4), 54.5 (C-2, C-4), 36.8 (C-1, C-5), 36.7 (C-1, C-5); δ_F (376 MHz, $CDCl_3$): -62.4 (CF_3), -120.9 (4''-F); *m/z* (ES^+) 503.136 $[M+H]^+$; HRMS (ES^+) found $[M+H]^+$ 503.1425 $C_{26}H_{23}N_2O_2F_4S$ requires *M,* 503.1416.

7-(4''-fluoroindol-1''-ylsulfonyl)-3-(pyridin-4'-ylmethyl)-1,2,4,5-tetrahydro-3-benzazepine **67**

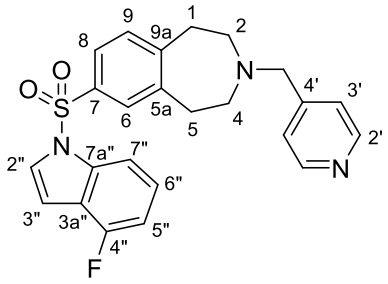

Following the general procedure for reductive amination, amine **33** (127.5 mg, 0.37 mmol) was combined with 4-pyridinecarboxaldehyde (42.4 mg, 0.40 mmol) to afford, after purification by silica column chromatography (0 – 80% [MeCN+10%MeOH]/EtOAc), the title compound (117.7 mg, 0.27 mmol, 73%) as a brown oil.

ν_{max} (ATR): 3150, 2944, 2818, 1489, 1375 (S=O), 1179 (S=O), 1166, 1128, 1032 cm^{1}; δ_H (700 MHz, $CDCl_3$): 8.54 (2H, d, *J* = 5.3 Hz, 2'-*H*, 6'-*H*), 7.77 (1H, d, *J* = 8.3 Hz, 7''-*H*), 7.64 (1H, dd, *J* = 7.9, 1.5 Hz, 8-*H*), 7.59 (1H, d, *J* = 1.5 Hz, 6-*H*), 7.54 (1H, d, *J* = 3.7 Hz, 2''-*H*), 7.27 (2H, d, *J* = 5.3 Hz, 3'-*H*, 5'-*H*), 7.27 – 7.21 (3H, m, 6''-*H*), 7.15 (1H, d, *J* = 7.9 Hz, 9-*H*), 6.94 – 6.87 (1H, m, 5''-*H*), 6.75 (1H, d, *J* = 3.7 Hz, 3''-*H*), 3.57 (2H, s, NCH_2Ar), 2.97 – 2.86 (4H, m, 1-H_2, 5-H_2), 2.57 (4H, m, 2-H_2, 4-H_2); δ_C (176 MHz, $CDCl_3$): 156.0 (d, $J_{C,F}$ = 249.4 Hz, C-4''), 150.0 (C-2', C-6'), 149.2 (C-5a), 148.0 (C-4'), 143.7 (C-9a), 137.0 (d, $J_{C,F}$ = 9.6 Hz, C-7a''), 135.8 (C-7), 130.0 (C-9), 127.0 (C-6), 126.4 (C-2''), 125.5 (d, $J_{C,F}$ = 7.5 Hz, C-6''), 125.2 (C-8), 123.8 (C-3', C-5'), 119.8 (d, $J_{C,F}$ = 22.3 Hz, C-3a''), 109.7 (d, $J_{C,F}$ = 3.8 Hz, C-7''), 108.6 (d, $J_{C,F}$ = 18.5 Hz, C-5''), 104.6 (C-3''), 62.3 (NCH_2Ar), 55.0 (C-2, C-4), 54.6 (C-2, C-4), 36.9 (C-1, C-5), 36.8 (C-1, C-5); δ_F (376 MHz, $CDCl_3$): -120.8; *m/z* (ES^+) 436.971 $[M+H]^+$; HRMS (ES^+) found $[M+H]^+$ 436.1508; $C_{24}H_{23}N_3O_2FS$ requires *M,* 436.1495.

7-(4''-fluoroindol-1''-ylsulfonyl)-3-[(4'-methylphenyl)methyl]-1,2,4,5-tetrahydro-3-benzazepine **68**

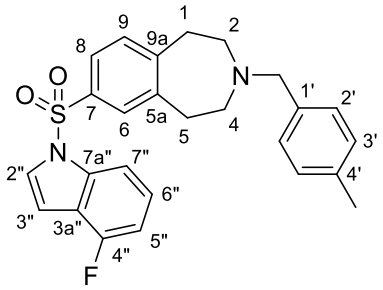

Following the general procedure for reductive amination, amine **33** (95.6 mg, 0.28 mmol) was combined with *p*-tolualdehyde (35.0 mg, 0.29 mmol) to afford, after purification by silica column chromatography (0 – 30% EtOAc/Hexane), the title compound (47.9 mg, 0.11 mmol, 39%) as a brown oil.

ν_{max} (ATR): 3154, 2947, 2915, 1489, 1433, 1375 (S=O), 1179 (S=O), 1166, 1126, 1031 cm^{1}; δ_H (600 MHz, $CDCl_3$): 7.91 (1H, d, *J* = 8.5 Hz, 7"-H_2), 7.76 (1H, d, *J* = 8.0 Hz, 8-*H*), 7.71 (1H, s, 6-*H*), 7.67 (1H, d, *J* = 3.7 Hz, 2"-*H*), 7.39 – 7.34 (1H, m, 6"-*H*), 7.32 (2H, d, *J* = 7.6 Hz, 2'-*H,* 6'-*H*), 7.28 – 7.23 (3H, m, 9-*H*, 3'-*H,* 5'-*H*), 7.03 (1H, dd, $J_{H,F}$ = 9.6 Hz, $J_{H,H}$ = 8.0 Hz, 5"-*H*), 6.88 (1H, d, *J* = 3.7 Hz, 3"-*H*), 3.68 (2H, s, NCH_2), 3.02 (4H, m, 1-H_2, 3-H_2), 2.68 (4H, m, 2-H_2, 4-H_2), 2.47 (3H, s, CH_3); δ_C (151 MHz, $CDCl_3$): 156.0 (d, $J_{C,F}$ = 249.2 Hz, C-4''), 149.5 (C-5a), 144.0 (C-9a), 137.0 (d, $J_{C,F}$ = 9.6 Hz, C-7a"), 136.9 (C-4'), 135.6 (C-7), 135.3 (C-1'), 129.9 (C-9), 129.1 (C-3'), 129.1 (C-2'), 126.9 (C-6), 126.4 (C-2"), 125.5 (d, $J_{C,F}$ = 7.4 Hz, C-6"), 125.0 (C-8), 119.8 (d, $J_{C,F}$ = 22.4 Hz, C-3a"), 109.7 (d, $J_{C,F}$ = 3.8 Hz, C-7"), 108.6 (d, $J_{C,F}$ = 18.6 Hz, C-5"), 104.5 (C-3"), 63.2 (NCH_2Ar), 54.6 (C-2, C-4), 54.3 (C-2, C-4), 36.9 (C-1, C-5), 36.8 (C-1, C-5), 21.2 (CH_3); δ_F (376 MHz, $CDCl_3$): -120.9; *m/z* (ES^+) 449.164 $[M+H]^+$; HRMS (ES^+) found $[M+H]^+$ 449.1690; $C_{26}H_{26}N_2O_2FS$ requires *M,* 449.1699.

3-benzyl-7-(4’-fluoroindol-1’-ylsulfonyl)-1,2,4,5-tetrahydro-3-benzazepine **69**

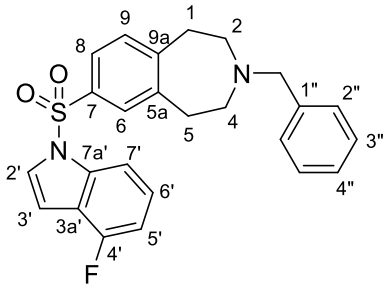

Following the general procedure for reductive amination, amine **33** (69.0 mg, 0.20 mmol) was combined with benzaldehyde (21.3 mg, 0.20 mmol) to afford, after purification by silica column chromatography (0 – 50% EtOAc/Hexane), the title compound (30.6 mg, 0.070 mmol, 35%) as a yellow oil.

ν_{max} (ATR): 3151, 2947, 2817, 1487, 1434, 1373 (S=O), 1362, 1177 (S=O), 1165, 1127, 1031 cm^{1}; δ_H (600 MHz, $CDCl_3$): 7.77 (1H, d, *J* = 8.4 Hz, 7’-*H*), 7.62 (1H, dd, *J* = 8.0, 2.0 Hz, 8-*H*), 7.57 (1H, d, *J* = 2.0 Hz, 6-*H*), 7.53 (1H, d, *J* = 3.7 Hz, 2’-*H*), 7.33 – 7.29 (4H, m, 2’’-H_2, 3’’-H_2), 7.26 – 7.21 (2H, m, 4’’-*H*, 6’-*H*), 7.13 (1H, d, *J* = 8.0 Hz, 9-*H*), 6.92 – 6.88 (1H, m, 5’-*H*), 6.74 (1H, dd, *J* = 3.7, 0.6 Hz, 3’-*H*), 3.58 (2H, s, NCH_2Ar), 2.89 (4H, m, 1-H_2, 5-H_2), 2.56 (4H, m, 2-H_2, 4-H_2); δ_C (151 MHz, $CDCl_3$): 155.8 (d, $J_{C,F}$ =249.2 Hz, C-4’), 149.4 (C-5a), 143.9 (C-9a), 138.3 (C-1’’), 136.9 (d, $J_{C,F}$ =9.5 Hz, C-7a’), 135.5 (C-7), 129.8 (C-9), 129.0 (C-2’’, C-6’’), 128.3 (C-3’’, C-5’’), 127.1 (C-4’’), 126.8 (C-6), 126.3 (C-2’), 125.3 (d, $J_{C,F}$ = 7.4 Hz, C-6’), 124.9 (C-8), 119.7 (d, $J_{C,F}$ = 22.3 Hz, C-3a’), 109.5 (d, $J_{C,F}$ = 3.8 Hz, C-7’), 108.4 (d, $J_{C,F}$ = 18.6 Hz, C-5’), 104.4 (C-3’), 63.3 (N*C*H_2Ar), 54.5 (C-2, C-4), 54.2 (C-2, C-4), 36.7 (C-1, C-5), 36.6 (C-1, C-5); δ_F (376 MHz, $CDCl_3$): -120.9; *m/z* (ES^+) 435.148 $[M+H]^+$; HRMS (ES^+) found $[M+H]^+$ 435.1544 ; $C_{25}H_{24}N_2O_2FS$ requires *M,* 435.1543.

3-[(4'-chlorophenyl)methyl]-7-[(4''-fluoroindol-1''-yl)sulfonyl]-1,2,4,5-tetrahydro-3-benzazepine **70**

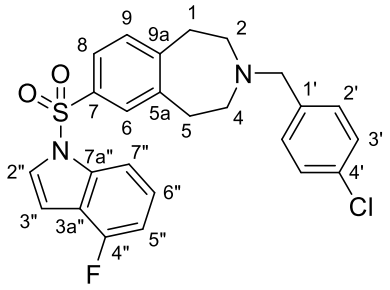

Following the general procedure for reductive amination, amine **33** (83.9 mg, 0.24 mmol) was combined with 4-clorobenzaldehyde (34.2 mg, 0.24 mmol) to afford, after purification by silica column chromatography (0 – 30% EtOAc/Hexane), the title compound (40.3 mg, 0.092 mmol, 38%) as a yellow oil.

ν_{max} (ATR): 3144, 2947, 2817, 1489, 1432, 1374 (S=O), 1179 (S=O), 1166, 1126, 1090, 1032 cm^{1}; δ_H (600 MHz, $CDCl_3$): 7.76 (1H, d, *J* = 8.4 Hz, 7''-*H*), 7.62 (1H, dd, *J* = 8.1, 2.0 Hz, 8-*H*), 7.57 (1H, d, *J* = 2.0 Hz, 6-*H*), 7.53 (1H, d, *J* = 3.7 Hz, 2''-*H*), 7.29 – 7.20 (5H, m, 2'-H_2, 3'-H_2, 6''-*H*), 7.13 (1H, d, *J* = 8.1 Hz, 9-*H*), 6.92 – 6.87 (1H, m, 5''-*H*), 6.74 (1H, d, *J* = 3.7 Hz, 3''-*H*), 3.52 (2H, s, NCH_2Ar), 2.88 (4H, m, 1-H_2, 5-H_2), 2.53 (4H, m, 2-H_2, 4-H_2); δ_C (151 MHz, $CDCl_3$): 156.0 (d, $J_{C,F}$ = 249.3 Hz, C-4''), 149.4 (C-5a), 143.9 (C-9a), 137.1 (C-1'), 137.0 (d, $J_{C,F}$ = 9.4 Hz, C-7a''), 135.7 (C-7), 132.9 (C-4'), 130.3 (C-2', C-6'), 129.9 (C-9), 128.6 (C-3', C-5'), 126.9 (C-6), 126.4 (C-2''), 125.5 (d, $J_{C,F}$ = 7.4 Hz, C-6''), 125.1 (C-8), 119.8 (d, $J_{C,F}$ = 22.3 Hz, C-3a''), 109.7 (d, $J_{C,F}$ = 3.8 Hz, C-7''), 108.6 (d, $J_{C,F}$ = 18.6 Hz, C-5''), 104.5 (C-3''), 62.7 (N*C*H_2Ar), 54.7 (C-2, C-4), 54.3 (C-2, C-4), 36.8 (C-1, C-5), 36.7 (C-1, C-5); δ_F (376 MHz, $CDCl_3$): -120.8; *m/z* (ES^+) 469.235 $[M(^{35}Cl)+H]^+$ (75%), 471.059 $[M(^{37}Cl)+H]^+$ (25%); HRMS (ES^+) found $[M+H]^+$ 469.1140; $C_{25}H_{23}N_2O_2FS^{35}Cl$ requires *M,* 469.1153.

7-(4''-fluoroindol-1''-ylsulfonyl)-3-[(4'-methoxyphenyl)methyl]-1,2,4,5-tetrahydro-3-benzazepine **71**

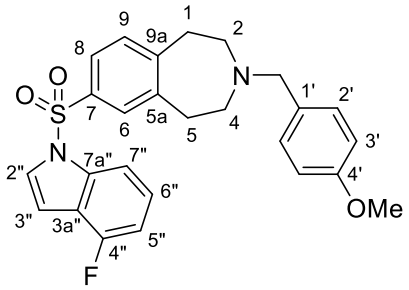

Following the general procedure for reductive amination, amine **33** (79.7 mg, 0.23 mmol) was combined with *p*-anisaldehyde (32.1 mg, 0.24 mmol) to afford, after purification by silica column chromatography (0 – 30% EtOAc/Hexane), the title compound (40.0 mg, 0.86 mmol, 37%) as a brown oil.

ν_{max} (ATR): 3152, 2948, 2912, 2828, 1515, 1489, 1433, 1375 (S=O), 1249, 1178 (S=O), 1127, 1033 cm^{1}; δ_H (600 MHz, $CDCl_3$): 7.77 (1H, d, *J* = 8.4 Hz, 7"-*H*), 7.63 (1H, dd, *J* = 8.0, 2.0 Hz, 8-*H*), 7.58 (1H, d, *J* = 2.0 Hz, 6-*H*), 7.54 (1H, d, *J* = 3.7 Hz, 2"-*H*), 7.25 – 7.23 (1H, m, 6"-*H*), 7.21 (2H, d, *J* = 8.5 Hz, 2'-H_2), 7.13 (1H, d, *J* = 8.0 Hz, 9-*H*), 6.91 (1H, dd, $J_{H,F}$ = 9.6 Hz, $J_{H,H}$ = 8.1 Hz, 5"-*H*), 6.85 (2H, d, *J* = 8.5 Hz, 3'-H_2), 6.75 (1H, d, *J* = 3.7 Hz, 3"-*H*), 3.80 (3H, s, CH_3), 3.53 (2H, s, NCH_2Ar), 2.89 (4H, m, 1-H_2, 5-H_2), 2.55 (4H, m, 2-H_2, 4-H_2); δ_C (151 MHz, $CDCl_3$): 158.9 (C-4'), 156.0 (d, $J_{C,F}$ = 249.2 Hz, C-4''), 149.5 (C-5a) , 144.0 (C-9a), 137.0 (d, $J_{C,F}$ = 9.6 Hz, 7a''), 135.6 (C-7), 130.4 (C-1'), 130.3 (C-2', C-6'), 129.9 (C-9), 126.9 (C-6), 126.4 (C-2"), 125.5 (d, $J_{C,F}$ = 7.4 Hz, C-6"), 125.0 (C-8), 119.8 (d, $J_{C,F}$ = 22.4 Hz, C-3a"), 113.8 (C-3', C-5'), 109.7 (d, $J_{C,F}$ = 3.9 Hz, C-7"), 108.6 (d, $J_{C,F}$ = 18.6 Hz, C-5"), 104.5 (C-3''), 62.9 (N*C*H_2Ar), 55.4 (CH_3), 54.5, 54.2 (C-2, C-4), 36.9, 36.7 (C-1, C-5); δ_F (376 MHz, $CDCl_3$): -120.9; *m/z* (ES^+) 465.158 $[M+H]^+$; HRMS (ES^+) found $[M+H]^+$ 465.1646; $C_{26}H_{26}N_2O_3FS$ requires *M,* 465.1648.

7-(4’-fluoroindol-1’-ylsulfonyl)-3-[2’’-(4’’’-fluorophenyl)ethyl]-1,2,4,5-tetrahydro-3-benzazepine **74**

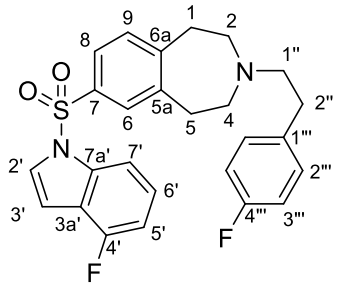

Following the general procedure for reductive amination, amine **33** (89.5 mg, 0.26 mmol) was combined with (4-fluorophenyl)acetaldehyde (36.9 mg, 0.27 mmol) to afford, after purification by silica column chromatography (0 – 30% Hexane/EtOAc), the title compound (62.6 mg, 0.13 mmol, 50%) as a yellow oil.

ν_{max} (ATR): 3147, 2950, 2818, 1489, 1433, 1376 (S=O), 1223, 1211, 1181 (S=O), 1165, 1127 cm^1; δ_H (600 MHz, $CDCl_3$): δ 7.78 (1H, d, *J* = 8.3 Hz, 7’- *H*), 7.64 (1H, dd, *J* = 8.0, 2.1 Hz, 8- *H*), 7.60 (1H, d, *J* = 2.1 Hz, 6- *H*), 7.55 (1H, d, *J* = 3.8 Hz, 2’- *H*), 7.26 – 7.21 (1H, m, 6’- *H*), 7.16 (1H, d, *J* = 8.0 Hz, 9- *H*), 7.14 – 7.09 (2H, m, 2’’’-*H,* 6’’’- *H*), 6.99 – 6.93 (2H, m, 3’’’-*H,* 5’’’- *H*), 6.91 (1H, dd, $J_{H,F}$ = 9.6 Hz, $J_{H,H}$ = 8.0 Hz, 5’- *H*), 6.76 (1H, d, *J* = 3.8, 0.9 Hz 3’-*H*), 2.93 (4H, m, 1- *H_2, 5- H_2*), 2.77 – 2.57 (8H, m, 1’’-*H_2, 2’’- H_2*, 2- *H_2,* 4- *H_2*); δ_C (151 MHz, $CDCl_3$): 161.5 (d, $J_{C,F}$ = 243.9 Hz, C-4’’’), 156.0 (d, $J_{C,F}$ = 249.3 Hz, C-4), 149.3 (C-5a), 143.9 (C-9a), 137.0 (d, $J_{C,F}$ = 9.5 Hz, C-7a’), 136.0 (d, $J_{C,F}$ = 2.4 Hz, C-1’’’), 135.8 (C-7), 130.1 (d, $J_{C,F}$ = 7.8 Hz, C-2’’’), 130.0 (C-9), 127.0 (C-6), 126.4 (C-2’), 125.5 (d, $J_{C,F}$ = 7.4 Hz, C-6’), 125.2 (C-8), 119.5 (d, $J_{C,F}$ = 22.3 Hz, C-3a’), 115.3 (d, $J_{C,F}$ = 21.2 Hz, C-3’’’), 109.7 (d, $J_{C,F}$ = 3.9 Hz, C-7’), 108.6 (d, $J_{C,F}$ = 18.7 Hz, C-5’), 104.6 (C-3’), 61.0 (C-1’’), 54.7 (C-2, C-4), 54.4 (C-2, C-4), 36.8 (C-1, C-5), 36.7 (C-1, C-5), 32.8 (C-2’’); δ_F (376 MHz, $CDCl_3$): -117.3 (F-4’’’), -120.8 (F-4’); *m/z* (ES^+) 467.297 $[M+H]^+$; HRMS (ES^+) found $[M+H]^+$ 467.1622 $C_{26}H_{25}N_2O_2F_2S$ requires *M,* 427.1605.

2-(4'-fluorophenyl)acetaldehyde[117] **76**

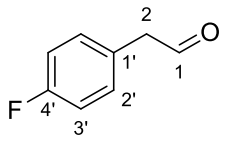

Following the general procedure for DMP oxidation, 4-fluorophenylethyl alcohol (1.08 g, 7.71 mmol) was converted to the title compound (1.04 g, 7.53 mmol, 98 %) and isolated as yellow oil.

ν_{max} (ATR): 3039, 2838, 1726 (C=O), 1516, 1251, 1067 cm^{-1}. δ_H (400 MHz, $CDCl_3$): 9.75 (1H, t, *J* = 2.2 Hz, 1-*H*), 7.22 – 7.13 (2H, m, 2'-*H*), 7.11 – 7.01 (2H, m, 3'-*H*), 3.68 (2H, t, *J* = 2.2 Hz, 2-CH_2). δ_C (101 MHz, $CDCl_3$): 199.1 (C=O), 162.4 (d, $J_{C,F}$ = 246.0 Hz, C-4'), 131.3 (d, $J_{C,F}$ = 8.1 Hz, C-2'), 127.7 (d, $J_{C,F}$ = 3.3 Hz, C-1'), 116.1 (d, $J_{C,F}$ = 21.6 Hz, C-3'), 49.8 (C-2). δ_F (376 MHz, $CDCl_3$): -115.13. Mass spectrometry data could not be obtained.

3'',4''-dimethyl-1-(2-phenylethyl)pyrrole-2'',5''-dione[158] **78**

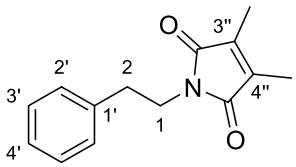

2,3-dimethylmaleic anhydride (1.62 g, 12.8 mmol) was added in one portion to a solution of 2-phenethylamine (1.72 g, 14.2 mmol) in water (5 mL·$mmol^{-1}$). The reaction was stirred at reflux 18 h until TLC analysis indicated complete consumption of the starting material. The maleimide, which precipitated out of the reaction mixture, was filtered off to give the title compound (2.70 g, 11.8 mmol, 92 %) as an off-white solid which was used without any further purification.

mp: 56 - 57 °C (lit.[158] mp: 54 – 56 °C) ; ν_{max} (ATR): 2942, 1702 (C=O), 1442, 1409, 1357 cm^1; δ_H (700 MHz, $CDCl_3$): 7.29 (2H, t, *J* = 7.4 Hz, 3'-*H,* 5'-*H*), 7.22 (2H, m, 4'-*H*, 2'-*H*, 6'-*H*), 3.72 (2H, t, *J* = 7.8 Hz, 1-H_2), 2.88 (2H, t, *J* = 7.8 Hz, 2-H_2), 1.94 (6H, s, CH_3); δ_C (176 MHz, $CDCl_3$): 172.2 (C=O), 138.3 (C-1'), 137.2 (C-3'', C-4''), 129.0 (C-3', C-5'), 128.6 (C-2', C-6'), 126.7 (C-

4), 39.3 (C-1), 34.9 (C-2), 8.8 (CH_3); *m/z* (ES^+) 230.241 $[M+H]^+$; HRMS ES^+ found $[M+H]^+$ 230.1190 $C_{14}H_{16}NO_2$ requires *M,* 230.1181.

4-[2'-(3'',4''-dimethyl-2'',5''-dioxopyrrol-1''-yl)ethyl]benzenesulfonyl chloride **79**

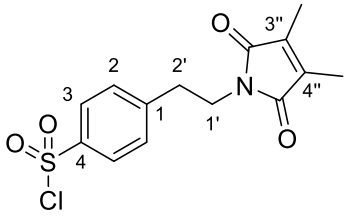

78 (1.11 g, 4.84 mmol) was added portionwise to chlorosulfonic acid (1.9 mL, 3.4 g, 29.2 mmol) in a 3-neck round bottom flask fit with a reflux condenser and a $CaCl_2$ drying tube, at 0 °C under an argon atmosphere. The mixture was allowed to stir at room temperature for 1 h then slowly warmed to 80°C and stirred at this temperature for a further 3 h. When TLC analysis indicated complete consumption of the starting material, the reaction was slowly poured over an ice-DCM mixture. The resultant mixture was separated and the aqueous layer extracted with cold DCM (3 × 20 mL). The combined organic extracts were dried with $MgSO_4$ and concentrated *in vacuo* to give the title compound (1.37 g, 4.18 mmol, 86%) as yellow oil which was used without any further purification.

ν_{max} (ATR): 2978, 1707 (C=O), 1443, 1386 (S=O), 1175 (S=O), 1010 cm^{-1}; δ_H (400 MHz, $CDCl_3$): 7.96 (2H, dd, *J* = 8.6, 1.9 Hz, 3-*H,* 5-*H*), 7.47 (2H, dd, *J* = 8.6, 1.9 Hz, 2-*H*, 6-*H*), 3.82 – 3.73 (2H, m, 1'-H_2), 3.03 – 2.99 (2H, m, 2'-H_2), 1.95 (6H, s, CH_3); δ_C (176 MHz, $CDCl_3$): 172.0 (C=O), 145.8 (C-1), 137.5 (C-3'', C-4''), 136.8 (C-4), 130.2 (C-2, C-6), 127.4 (C-3, C-5), 38.3 (C-1'), 34.8 (C-2'), 8.9 (CH_3); *m/z* (ES^+) 328.1 $[M(^{35}Cl)+H]^+$, 330.2 $[M(^{37}Cl)+H]^+$.

1’-[2’-(4-[(4’’-fluoroindol-1-yl)sulfonyl]phenyl)ethyl]-3’’’,4’’’-dimethylpyrrole-2’’’,5’’’-dione **80**

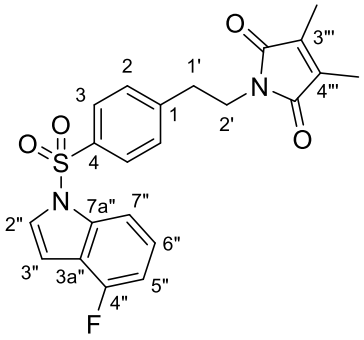

Following the general procedure for sulfamidation, sulfonylchloride **79** (2.16 g, 6.59 mmol) was combined with 4-fluoroindole (0.99 g, 7.33 mmol) to afford, after purification by silica column chromatography (0-40% Et_2O/Hexane), the title compound (0.78 g, 1.83 mmol, 28 %) as an off-white solid.

mp: 170-172 °C; ν_{max} (ATR): 3407, 3125, 1703 (C=O), 1486, 1372 (S=O), 1180 (S=O), 1112 cm^{-1}; δ_H (600 MHz, $CDCl_3$): 7.81 – 7.78 (2H, m, 4-*H*, 6-*H*), 7.76 (1H, dd, *J* = 8.4, 0.9 Hz, 7’’-*H*), 7.53 (1H, d, *J* = 3.8 Hz, 2’’-*H*), 7.31 – 7.28 (2H, m, 2-*H*, 6-*H*), 7.26 – 7.22 (1H, td, $J_{H,H}$ = 8.4 Hz, $J_{H,F}$ = 5.3 Hz, 6’’-*H*), 6.91 (1H, ddd, $J_{H,F}$ = 9.7 Hz, $J_{H,H}$ = 8.4, 0.9 Hz, 5’’-*H*), 6.75 (1H, dd, *J* = 3.8, 0.9 Hz, 3’’-*H*), 3.69 – 3.63 (2H, m, 1’-H_2), 2.89 (2H, dd, *J* = 8.6, 6.7 Hz, 2’-H_2), 1.89 (6H, s, CH_3); δ_C (151 MHz, $CDCl_3$): 171.7 (C=O), 155.8 (d, $J_{C,F}$ = 249.5 Hz, C-4’’), 145.1 (C-1), 137.2 (C-3’’’, C-4’’’), 136.8 (d, $J_{C,F}$ = 9.6 Hz, C-7a’’), 136.2 (C-4), 129.8 (C-2, C-6), 127.1 (C-3, C-5), 126.2 (C-2’), 125.5 (d, $J_{C,F}$ = 7.5 Hz, C-6’’), 119.7 (d, $J_{C,F}$ = 22.2 Hz, C-3a’’), 109.5 (d, $J_{C,F}$ = 4.0 Hz, C-7’’), 108.6 (d, $J_{C,F}$ = 18.6 Hz, C-5’’), 104.7 (C-3’’), 38.1 (C-2’), 34.4 (C-1’), 8.6 (CH_3); δ_F (376 MHz, $CDCl_3$): -120.82; *m/z* (ES^+) 427.205 $[M+H]^+$; HRMS ES^+ found $[M+H]^+$ 427.1134 $C_{25}H_{20}N_2O_2FS$ requires *M,* 427.1128.

N-(2'-phenylethyl)acetamide[159] **83**

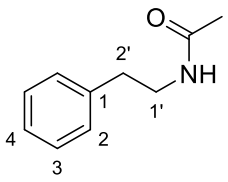

Acetic anhydride (6.85 mL, 7.41 g, 72.6 mmol) was added portionwise to a cooled (0 ˚C) solution of 2-phenethylamine (8.30 mL, 8.00 g, 66.0 mmol) and pyridine (5.85 mL, 5.74 g, 72.6 mmol). After the addition was complete, the reaction was stirred at 90°C for 24 h until TLC analysis indicated complete consumption of the starting material. The reaction mixture poured onto crushed ice and stirred with a glass rod for 5 minutes. Concentraded HCl (10 mL) was then added and the organic layer extracted with EtOAc (3 x 50 mL), washed with $NaCO_3$ (2 x 20 mL), dried with $MgSO_4$, and concentrated *en vaccuo*. The crude residue purified by recrystallization from petroleum ether to give the title compound (10.52 g, 64.5 mmol, 98%) as a yellow solid.

mp: 51-53 °C (lit.[159] mp: 52 °C); ν_{max} (ATR): 3286 (NH), 2938, 1659 (C=O), 1564, 1298 cm^{-1}; δ_H (700 MHz, $CDCl_3$): 7.31 (2H, t, *J* = 7.5 Hz, 3-*H*, 5-*H*), 7.23 (1H,t, *J* = 7.5 Hz, 4-*H*), 7.19 (2H, d, *J* = 7.5 Hz, 2-*H*, 6-*H*), 5.48 (1H, br, N*H*), 3.52 (2H, q, *J* = 6.8 Hz, 1'-H_2), 2.82 (2H, t, *J* = 6.8 Hz, 2'-H_2), 1.94 (3H, s, CH_3); δ_C (176 MHz, $CDCl_3$): 70.1 (C=O), 139.0 (C-1), 128.9 (C-2, C-6), 128.8 (C-3, C-5), 126.7 (C-4), 40.8 (C-1'), 35.8 (C-2'), 23.5 (CH_3); *m/z* (ES^+) 164.199 $[M+H]^+$; HRMS ES^+ found $[M+H]^+$ 164.1078 $C_{10}H_{14}NO$ requires *M,* 164.1075.

4-(2'-acetamidoethyl)benzenesulfonyl chloride[160] **84**

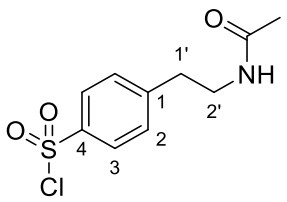

83 (1.23 g, 7.54 mmol) was added portionwise to chlorosulfonic acid (2.51 mL, 4.39 g, 37.7 mmol) in a 3-neck round bottom flask fit with a reflux condenser and a $CaCl_2$ drying tube, at 0 °C under an argon atmosphere. The mixture was allowed to stir at room temperature

for 1 h then slowly warmed to 80°C and stirred at this temperature for a further 3 h. When TLC analysis indicated complete consumption of the starting material, the reaction was slowly poured over an ice-DCM mixture. The resultant mixture was separated and the aqueous layer extracted with cold DCM (3 × 20 mL). The combined organic extracts were dried with $MgSO_4$ and concentrated *in vacuo.* The crude residue purified by recrystallization from hexane-DCM to give the title compound (1.51 g, 5.78 mmol, 77%) as long white needles.

mp: 144 - 145 °C (lit.[161] 142.5 – 144 °C); ν_{max} (ATR): 3287, 2931, 1601 (C=O), 1384 (S=O), 1156 (S=O) cm^{-1}; δ_H (700 MHz, $CDCl_3$): 7.98 (2H, d, *J* = 8.3 Hz, 3-*H*, 5-*H*), 7.45 (2H, d, *J* = 8.3 Hz, 2-*H*, 6-*H*), 5.56 (1H, br, N*H*), 3.54 (2H, q, *J* = 7.0 Hz, 2'-H_2), 2.97 (3H, t, *J* = 7.0 Hz, 1'-H_2), 1.97 (3H, s, CH_3); δ_C (176 MHz, $CDCl_3$): 170.3 (C=O), 147.7 (C-1), 142.8 (C-4), 130.2 (C-2, C-6), 127.5 (C-3, C-5), 40.4 (C-2'), 36.0 (C-1'), 23.4 (CH_3); *m/z* (ASAP) 262.0 $[M(^{35}Cl)+H]^+$; 264.0 $[M(^{37}Cl)+H]^+$.

N-{2-[4'-(4''-fluoroindol-1''-ylsulfonyl)phenyl]ethyl}acetamide **85**

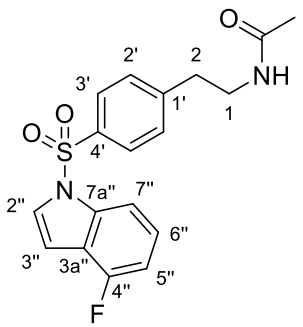

Following the general procedure for sulfamidation, sulfonylchloride **84** (0.38 g, 1.45 mmol) was combined with 4-fluoroindole (0.22 g, 1.60 mmol) to afford, after purification by silica column chromatography (0-10% MeOH/DCM), the title compound (0.13 g, 0.36 mmol, 25 %) as a pink semi-solid.

ν_{max} (ATR): 2968, 1631 (C=O), 1487, 1375 (S=O), 1183 (S=O), 1092, 1024 cm^{-1}; δ_H (600 MHz, $CDCl_3$): 7.82 (2H, d, *J* = 8.5 Hz, 3'-*H,* 5'-*H*), 7.78 (1H, dd, $J_{H,H}$ = 8.4 Hz, $J_{H,F}$ = 0.8 Hz, 7''-*H*), 7.54 (2H, d, *J* = 3.7 Hz, 2''-*H*), 7.28 (2H, d, *J* = 8.5 Hz, 2'-*H, 6*'-*H*), 7.25 – 7.19 (1H, m, 6''-*H*), 6.92 (1H, ddd, $J_{H,F}$ = 9.7 Hz, $J_{H,H}$ = 8.1, 0.8 Hz, 5''-*H*), 6.76 (1H, dt, *J* = 3.7, 0.8 Hz, 3''-*H*), 5.42

(1H, br, N*H*), 3.44 (2H, q, *J* = 7.0 Hz, 1-H_2), 2.83 (2H, t, *J* = 7.0 Hz, 2-H_2), 1.91 (3H, s, CH_3); δ_C (151 MHz, $CDCl_3$): 170.2 (C=O), 156.0 (d, $J_{C,F}$ = 249.3 Hz, C-4''), 146.2 (C-1'), 137.0 (d, $J_{C,F}$ = 9.4 Hz, C-7a''), 136.3 (C-4'), 129.9 (C-2', C-6'), 127.3 (C-3', C-5'), 126.4 (C-2''), 125.7 (d, $J_{C,F}$ = 7.6 Hz, C-6''), 119.9 (d, $J_{C,F}$ = 22.5 Hz, C-3a''), 109.7 (d, $J_{C,F}$ = 3.9 Hz, C-7''), 108.8 (d, $J_{C,F}$ = 18.7 Hz, C-5''), 104.8 (C-3''), 40.3 (C-1), 35.8 (C-2), 23.4 (CH_3); δ_F (376 MHz, $CDCl_3$, 2:1 mixture of rotamers A, B): -120.71 (A), -121.24 (B); *m/z* (ES^+) 361.5 $[M+H]^+$.

N-methyl-N-(2-phenylethyl)acetamide[162] **88**

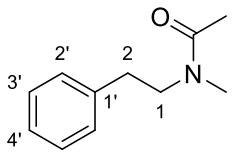

Following the general procedure for acetamide protection, *N*-Methyl-*N*-phenethylamine (1.00 g, 7.40 mmol) was converted to the title compound (1.18 g, 6.65 mmol, 90%) and isolated as a yellow oil.

ν_{max} (ATR): 3498, 3034, 2939, 2166, 2034, 1635 (C=O), 1495, 1405, 1036, 1006 cm^{-1}; δ_H (700 MHz, $CDCl_3$, 1:1 mixture of rotamers A, B): 7.33 – 7.27 (2H, m, 3'-*H*, 5'-*H*), 7.26 – 7.23 (1H, m, 4'-*H*), 7.23 – 7.19 (2H, m, 2'-*H,* 4'-*H*), 7.17 – 7.14 (1H, m, 2'-*H*), 3.60 – 3.56 (2H, m, 1-H_2, A), 3.53 – 3.48 (2H, m, 1-H_2, B), 2.95 (3H, s, NCH_3, A), 2.87 (3H, s, NCH_3, B), 2.86-2.82 (2H, m, 2-H_2), 2.06 (3H, s, CCH_3, B), 1.86 (3H, s, CCH_3, A); δ_C (176 MHz, $CDCl_3$, 1:1 mixture of rotamers A, B): 170.7 (C=O), 170.5 (C=O), 139.4 (C-1', B), 138.4 (C-1', A), 129.0 (C-2', C-6'), 128.9 (C-3', C-5'), 128.9 (C-2', C-6'), 128.6 (C-3', C-5'), 126.9 (C-4'), 126.4 (C-4'), 52.7 (C-1, A), 49.9 (C-1, B), 37.0(N*C*H_3), 35.0 (C-2), 33.9 (C-2), 33.5(N*C*H_3), 22.1 (C*C*H_3, B), 21.1 (C*C*H_3, A); *m/z* (ES^+) 178.274 $[M+H]^+$; HRMS ES^+ found $[M+H]^+$ 178.1230 $C_{11}H_{16}NO$ requires *M,* 178.1232.

N-(2-{4'-[(4''-fluoroindol-1''-ylsulfonyl]phenyl}ethyl)-N-methylacetamide **90**

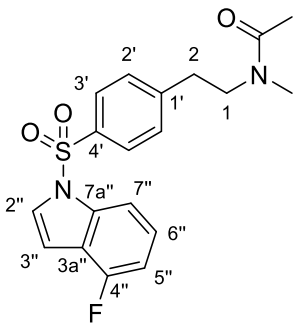

88 (1.20 g, 6.77 mmol) was added portionwise to chlorosulfonic acid (2.64 mL, 4.73 g, 40.6 mmol) in a 3-neck round bottom flask fit with a reflux condenser and a $CaCl_2$ drying tube, at 0 °C under an argon atmosphere. The mixture was allowed to stir at room temperature for 1 h then slowly warmed to 80°C and stirred at this temperature for a further 3 h. When TLC analysis indicated complete consumption of the starting material, the reaction was slowly poured over an ice-DCM mixture. The resultant mixture was separated and the aqueous layer extracted with cold DCM (3 × 20 mL). The combined organic extracts were dried with $MgSO_4$ and concentrated *in vacuo* to give sulfonyl choloride **89** (1.50 g, 5.42 mmol, 80%) as a brown oil which could not be characterized and was taken immediately forward to the next step.

Following the general procedure for sulfamidation, sulfonylchloride **89** (1.50 g, 5.44 mmol) was then combined with 4-fluoroindole (73.5 g, 5.44 mmol) to afford, after purification by silica column chromatography (0-10% MeOH/DCM), the title compound (452.0 mg, 1.21 mmol, 22%) as a light brown oil.

ν_{max} (ATR): 2937, 1631 (C=O), 1489, 1415, 1374 (S=O), 1182 (S=O), 1126, 1034 cm^{-1}; δ_H (600 MHz, $CDCl_3$, 2:1 mixture of rotamers A, B): 7.84 – 7.78 (2H, m, 3'-*H*, 5'-*H*), 7.77 – 7.72 (1H, m, 7"-*H*), 7.53 (1H, m, 2"-*H*), 7.32 – 7.28 (2H, m, 2'-*H,* 6'-*H*), 7.26 – 7.20 (1H, m, 6"-*H*), 6.94 – 6.88 (1H, m, 5"-*H*), 6.75 (1H, m, 3"-*H*), 3.51 (2H, t, *J* = 7.5 Hz, 1-H_2, *B*), 3.44 (2H, t, *J* = 7.2 Hz, 1-H_2, A), 2.87 (3H, s, NCH_3, B), 2.86 – 2.82 (2H, m, 2-H_2), 2.81 (3H, s, NCH_3, A), 2.01 3H, (s, CCH_3, A), 1.72 (3H, s, CCH_3, B); δ_C (176 MHz, $CDCl_3$, 2:1 mixture of rotamers A, B): 170.7 (C=O, A), 170.3 (C=O, B), 156.0 (d, $J_{C,F}$ = 249.4 Hz, C-4"), 146.4 (C-1', A), 145.3 (C-1', B), 137.0 (d, $J_{C,F}$ = 9.4, 3.8 Hz, 7a", A), 137.0 (d, $J_{C,F}$ = 9.3 Hz, 7a", B), 136.6 (C-4', B), 136.1 (C-4', A), 129.9 (C-2', A), 129.9 (C-2', B), 127.5 (C-3', B), 127.2 (C-3', A), 126.4 (C-2", A),

126.4 (C-2”, B), 125.7 (d, $J_{C,F}$ = 7.5 Hz, C-6”, B), 125.6 (d, $J_{C,F}$ = 7.4 Hz, C-6”, A), 119.9 (d, $J_{C,F}$ = 22.0 Hz, C-3a”, B), 119.8 (d, $J_{C,F}$ = 22.3 Hz, C-3a”, A), 109.7 (d, $J_{C,F}$ = 4.0 Hz, C-7”, A), 109.7 (d, $J_{C,F}$ = 4.2 Hz, C-7”, B), 108.9 (d, $J_{C,F}$ = 19.0 Hz, C-5”, B), 108.7 (d, $J_{C,F}$ = 18.6 Hz, C-5”, A), 105.1 (C-3”, B), 104.8 (C-3”, A), 51.9 (C-1, B), 49.0 (C-1, A), 36.9 (NCH_3, A), 34.8 (C-2, B), 33.7 (C-2, A), 33.5 (NCH_3, B), 22.0 (CH_3, A), 20.9 (CH_3, B); δ_F (376 MHz, $CDCl_3$, 2:1 mixture of rotamers A, B): -120.64 (B), -120.81 (A); *m/z* (ES^+) 375.327 $[M+H]^+$; HRMS ES^+ found $[M+H]^+$ 375.1187 $C_{19}H_{20}N_2O_3FS$ requires *M,* 375.1179.

(2-(4’-(4’’-fluoroindol-1’’-ylsulfonyl)phenyl)ethyl)(methyl)amine **91**

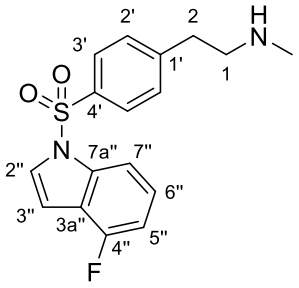

Following the general procedure for acetamide deprotection, **90** (452.0 mg, 1.21 mmol) was hydrolyzed to afford the title compound (258.0 mg, 0.776 mmol, 64%) as a brown oil.

ν_{max} (ATR): 2945, 2181, 2032, 1488, 1434, 1376 (S=O), 1181 (S=O), 1126, 1032 cm^{-1}; δ_H (700 MHz, $CDCl_3$): 7.81 (2H, d, *J* = 8.4 Hz, 3’-*H*, 5’-*H*), 7.78 (1H, d, *J* = 8.3 Hz, 7”-*H*), 7.54 (1H, d, *J* = 3.7 Hz, 2”-*H*), 7.29 (2H, d, *J* = 8.4 Hz, 2’-*H*, 6’-*H*), 7.24 (1H, dt, $J_{H,H}$ = 8.4 Hz, $J_{H,F}$ = 5.1 Hz, 6”-*H*), 6.91 (1H, dd, $J_{H,F}$ = 9.0, $J_{H,H}$ = 8.4 Hz, 5”-*H*), 6.75 (1H, dd, *J* = 3.7, 0.9 Hz, 3”-*H*), 2.80 – 2.79 (4H, m, 1-H_2, 2-H_2), 2.40 (3H, s, CH_3), 1.44 (1H, br, N*H*); δ_C (176 MHz, $CDCl_3$): 156.0 (d, $J_{C,F}$ = 249.5 Hz, C-4”), 147.5 (C-1’), 137.0 (d, $J_{C,F}$ = 9.7 Hz, C-7a”), 136.0 (C-4’), 129.8 (C-2’), 127.2 (C-3’), 126.4 (C-2”), 125.6 (d, $J_{C,F}$ = 7.4 Hz, C-6”), 119.9 (d, $J_{C,F}$ = 22.3 Hz, C-5”), 109.7 (d, $J_{C,F}$ = 4.0 Hz, C-7”), 108.7 (d, $J_{C,F}$ = 18.6 Hz, C-5”), 104.7 (C-3”), 52.5 (C-1), 36.4 (CH_3), 36.3 (C-2); δ_F (376 MHz, $CDCl_3$): -120.82; *m/z* (ES^+) 333.205 $[M+H]^+$; HRMS ES^+ found $[M+H]^+$ 333.1082 $C_{17}H_{18}N_2O_2FS$ requires *M,* 333.1073.

(2-(4'-((4''-fluoroindol-1''-ylsulfonyl)phenyl)ethyl)(methyl)((pyridin-3'''-yl)methyl)amine **92**

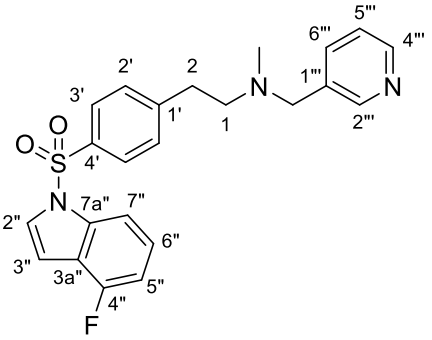

Following the general procedure for N-alkylation, amine **91** (122.0 mg, 0.367 mmol) was combined with 3-(bromomethyl)pyridine hydrobromide (115.0 mg, 0.667 mmol) to give, after purification by silica column chromatography (0-40% MeOH/Et_2O), the title compound (24.0 mg, 0.57 mmol, 16%) as a brown oil.

ν_{max} (ATR): 2950, 2799, 1488, 1433, 1376 (S=O), 1182 (S=O), 1126, 1031 cm^{-1}; δ_H (600 MHz, $CDCl_3$): 8.45 – 8.43 (2H, m, 4'''-*H*, 2'''-*H*), 7.78 (3H, m, 3'-*H*, 5'-*H*, 7''-*H*), 7.54 (1H, d, *J* = 3.7 Hz, 2''-*H*), 7.41 (1H, d, *J* = 7.8 Hz, 6'''-*H*), 7.26 – 7.21 (3H, m, 2'-*H*, 6'-*H*, 6''-*H*), 7.07 (1H, ddd, *J* = 7.8, 4.7, 0.9 Hz, 5'''-*H*), 6.91 (1H, ddd, $J_{H,F}$ = 9.6 Hz, $J_{H,H}$ = 8.1, 0.8 Hz, 5''-*H*), 6.75 (1H, dd, *J* = 3.7, 0.8 Hz, 3''-*H*), 3.48 (2H, s, NCH_2Ar), 2.78 (2H, t, *J* = 7.4 Hz, 2-H_2), 2.58 (2H, t, *J* = 7.4 Hz, 1-H_2), 2.24 (3H, s, CH_3); δ_C (176 MHz, $CDCl_3$): 156.0 (d, $J_{C,F}$ = 249.4 Hz, C-4''), 150.3 (C-2'''), 148.8 (C-4'''), 147.7 (C-1'), 137.0 (d, $J_{C,F}$ = 9.5 Hz, C-7a''), 136.5 (C-6'''), 135.8 (C-4'), 134.2 (C-1'''), 129.8 (C-2'), 127.0 (C-3'), 126.4 (C-2''), 125.6 (d, $J_{C,F}$ = 7.5 Hz, C-6''), 123.4 (C-5'''), 119.9 (d, $J_{C,F}$ = 22.4 Hz, C-3a''), 109.7 (d, $J_{C,F}$ = 3.9 Hz, C-7''), 108.7 (d, $J_{C,F}$ = 18.7 Hz, C-5''), 104.7 (C-3''), 59.5 (CH_2- 1'''), 57.9 (C-1), 42.1 (CH_3), 33.9 (C-2); δ_C (376 MHz, $CDCl_3$): -120.79; *m/z* (ES^+) 424.303$[M+H]^+$; HRMS ES^+ found $[M+H]^+$ 424.1513; $C_{23}H_{23}FN_3O_2S$ requires *M*, 424.1495.

2-(4’-(4’’-fluoroindol-1’’-ylsulfonyl)phenyl)ethyl)((4’’’-fluorophenyl)methyl)methylamine **93**

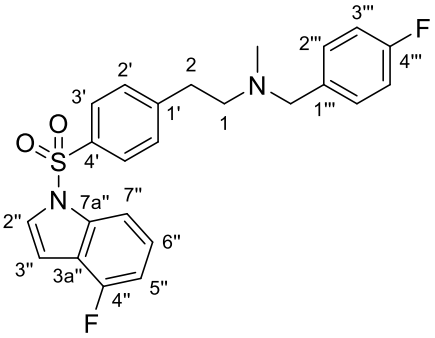

Following the general procedure for reductive amination, amine **91** (91.0 mg, 0.27 mmol) was combined with 4-fluorobenzaldehyde (40 mg, 0.32 mmol) to afford, after purification by silica column chromatography (0-100% EtOAc/Hexane), the title compound (37 mg, 0.084 mmol, 31%) as a light brown oil.

ν_{max} (ATR): 2951, 2799, 1434, 1377 (S=O), 1182 (S=O), 1126, 1032 cm^{-1}; δ_H (700 MHz, $CDCl_3$): 7.79 – 7.76 (3H, m, 3’-*H*, 5’-*H*, 7’’-*H*), 7.54 (1H, d, *J* = 3.7 Hz, 2’’-*H*), 7.26 – 7.20 (3H, m, 2’-*H*, 6’-*H*, 6’’-*H*), 7.10 – 7.05 (2H, m, 2’’’-*H*, 6’’’-*H*), 6.90 (1H, ddd, $J_{H,F}$ = 9.6 Hz, $J_{H,H}$ = 8.1, 0.8 Hz, 5’’-*H*), 6.89 – 6.84 (2H, m, 3’’’-*H*, 5’’’-*H*), 6.75 (1H, dd, *J* = 3.7, 0.8 Hz, 3’’-*H*), 3.42 (2H, s, NCH_2Ar), 2.77 (2H, t, *J* = 7.4 Hz, 2-H_2), 2.54 (2H, t, *J* = 7.4 Hz, 1-H_2), 2.21 (3H, s, CH_3); δ_C (176 MHz, $CDCl_3$): 162.0 (d, $J_{C,F}$ = 244.9 Hz, C-4’’’), 156.0 (d, $J_{C,F}$ = 249.4 Hz, C-4’’), 148.0 (C-1’), 137.0 (d, $J_{C,F}$ = 9.5 Hz, C-7a’’), 135.7 (C-4’), 134.5 (d, $J_{C,F}$ = 3.1 Hz, C-1’’), 130.3 (d, $J_{C,F}$ = 7.9 Hz, C-2’’’), 129.9 (C-2’), 127.0 (C-3’), 126.4 (C-2’’), 125.6 (d, $J_{C,F}$ = 7.5 Hz, C-6’’), 119.9 (d, $J_{C,F}$ = 22.3 Hz, C-3a’’), 115.1 (d, $J_{C,F}$ = 21.3 Hz, C-3’’’), 109.7 (d, $J_{C,F}$ = 3.8 Hz, C-7’’), 108.7 (d, $J_{C,F}$ = 18.7 Hz, C-5’’), 104.7 (C-3’’), 61.5 (C- 1’’’), 57.8 (C-1), 42.1 (CH_3), 33.9 (C-2); δ_F (376 MHz, $CDCl_3$): -120.78 (C-4’’), -115.78 (C-4’’’); *m/z* (ES^+) 441.266 $[M+H]^+$; HRMS ES^+ found $[M+H]^+$ 441.1458 $C_{24}H_{23}N_2O_2F_2S$ requires *M,* 441.1448.

(2-(4'-(4''-fluoroindol-1''-ylsulfonyl)phenyl)ethyl)(2'''-(4^{IV}-fluorophenyl)ethyl)methylamine **94**

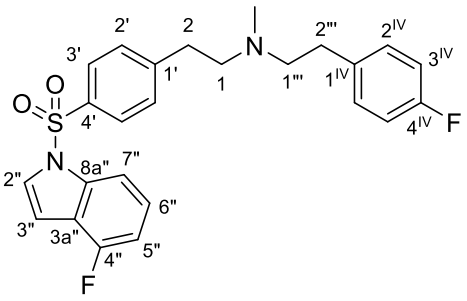

Following the general procedure for reductive amination, amine **91** (107.0 mg, 0.322 mmol) was combined with aldehyde **76** (65 mg, 0.47 mmol) to afford, after purification by silica column chromatography (0-100% EtOAc/Hexane), the title compound (29 mg, 0.064 mmol, 20%) as a light brown oil.

ν_{max} (ATR): 2947, 2856, 2799, 1489, 1434, 1377 (S=O), 1183 (S=O), 1126, 1032 cm^{-1}; δ_H (600 MHz, $CDCl_3$): 7.80 – 7.75 (3H, m, 3'-*H*, 5'-*H*, 7''-*H*), 7.54 (1H, d, *J* = 3.7 Hz, 2''-*H*), 7.27 – 7.21 (3H, m, 2'-*H*, 6'-*H*, 6''-*H*,), 7.10 – 7.05 (2H, m, 2^{IV}-*H*, 6^{IV}-*H*), 6.96 – 6.88 (3H, m, 5''-H_2, 3^{IV}-*H*, 5^{IV}-*H*), 6.75 (1H, dd, *J* = 3.7, 0.8 Hz, 3''-*H*), 2.74 (2H, t, *J* = 7.7 Hz, 2-H_2), 2.70 – 2.65 (2H, t, *J* = 7.8 Hz, 2'''-H_2), 2.62 – 2.56 (4H, m, 1-H_2, 1'''-H_2), 2.31 (3H, s, CH_3); δ_C (176 MHz, $CDCl_3$): 161.5 (d, J = 243.8 Hz, C-4^{IV}), 156.0 (d, J = 249.4 Hz, C-4''), 147.9 (C-1'), 137.0 (d, J = 9.6 Hz, C-7a''), 136.0 (d, J = 3.2 Hz, C-1^{IV}), 135.7 (C-4'), 130.1 (d, J = 7.7 Hz, C-2^{IV}), 129.8 (C-2'), 127.0 (C-3'), 126.4 (C-4''), 125.5 (d, J = 7.5 Hz, C-6''), 119.9 (d, J = 22.3 Hz, C-3a''), 115.24 (d, J = 21.1 Hz, C-3^{IV}), 109.70 (d, J = 3.9 Hz, C-7''), 108.7 (d, J = 18.6 Hz, C-5''), 104.7 (C-3''), 59.5 (C-1'''), 58.6 (C-1), 42.1 (CH_3), 33.8 (C-2), 33.1 (C-2'''); δ_F (376 MHz, $CDCl_3$): -117.31 (C-4^{IV}), -120.82 (C-4''); *m/z* (ES$^+$) 455.326 $[M+H]^+$; HRMS ES$^+$ found $[M+H]^+$ 455.1598; $C_{25}H_{25}F_2N_2O_2S$ requires *M*, 455.1605.

3-(4'-fluorophenyl)propan-1-ol[163] **99**

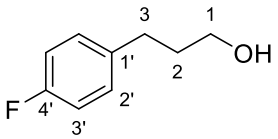

Following the general procedure for $LiAlH_4$ Reduction, 3,4-fluorophenylpropionic acid (1.05 g, 6.28 mmol) was reduced to afford, after purification by silica column chromatography (45% Et_2O / 55% Petroleum Ether), the title compound (0.956 g, 6.20 mmol, 99 %) as a colorless oil.

ν_{max} (ATR): 3332 (br, OH), 2940, 2868, 1509, 1222, 1044 cm^{-1}; δ_H (700 MHz, $CDCl_3$): 7.17 – 7.13 (2H, m, 2'-*H*), 6.99 – 6.94 (2H, m, 3'-*H*), 3.67 (2H, q, *J* = 6.2 Hz, 1-CH_2), 2.69 (2H, t, *J* = 7.7 Hz, 3-CH_2), 1.87 – 1.84 (2H, m, 2-CH_2), 2.69 (2H, t, *J* = 5.0 Hz, O*H*); δ_C (176 MHz, $CDCl_3$): 161.2 (d, $J_{C,F}$ = 243.4 Hz, C-4'), 137.6 (d, $J_{C,F}$ = 3.3 Hz, C-1'), 129.7 (d, $J_{C,F}$ = 7.8 Hz, C-2'), 115.1 (d, $J_{C,F}$ = 21.1 Hz, C-3'), 62.1 (C-1), 34.3 (C-2), 31.2 (C-3); δ_F (376 MHz, $CDCl_3$): -117.74. Mass spectrometry data could not be obtained.

3-(4'-fluorophenyl)propanal[164] **100**

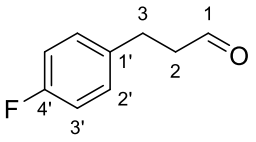

Following the general procedure for DMP oxidation, 4-fluorophenylethyl alcohol (0.96 g, 6.2 mmol) was converted to afford, after successive washes with $Na_2S_2O_5$, ether, and $NaHCO_3$, to give the title compound (62 mg, 0.41 mmol, 6 %) as yellow oil. (10% dec.)

ν_{max} (ATR): 3074, 2931, 2652, 1708 (C=O), 1510, 1219 cm^{-1}; δ_H (700 MHz, $CDCl_3$): 9.81 (t, $J_{H,H}$ = 1.3 Hz, 1H, 1-*H*), 7.17 – 7.13 (m, 2H, 2'-*H*, 6'-*H*), 7.00 – 6.95 (m, 2H, 3'-*H*, 5'-*H*), 2.93 (t, $J_{H,H}$ = 7.5 Hz, 2H, 3-H_2), 2.78 – 2.75 (m, 2H, 2-H_2); δ_C (176 MHz, $CDCl_3$): 201.4 (C=O), 161.6 (d, $J_{C,F}$ = 244.2 Hz, C-4'), 136.1 (d, $J_{C,F}$ = 3.2 Hz, C-1'), 129.9 (d, $J_{C,F}$ = 7.9 Hz, C-2'), 115.5 (d, $J_{C,F}$ = 21.3 Hz, C-3'), 45.5 (C-2), 27.4 (C-3); δ_F (376 MHz, $CDCl_3$): -116.94. Mass spectrometry data could not be obtained.

(2''-[4'''-(4^{IV}-fluoroindol-1^{IV}-ylsulfonyl)phenyl)ethyl)(3-(4'-fluorophenyl)propyl)methylamine **95**

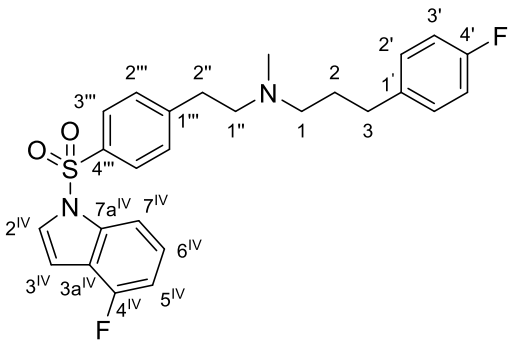

Following the general procedure for reductive amination, amine **91** (107.0 mg, 0.322 mmol) was combined with aldehyde **100** (54 mg, 0.35 mmol) to afford, after purification by silica column chromatography (0-100% EtOAc/Hexane), the title compound (32 mg, 0.068 mmol, 21%) as a light brown oil.

ν_{max} (ATR): 2944, 2859, 2795, 1490, 1434, 1373 (S=O), 1183 (S=O), 1128, 1033 cm^{-1}; δ_H (700 MHz, $CDCl_3$): 7.79 (2H, d, *J* = 8.5 Hz, 3'''-*H*, 5'''-*H*), 7.77 (1H, d, *J* = 8.3 Hz, 7^{IV}-*H*), 7.53 (1H, d, *J* = 3.7 Hz, 2^{IV}-*H*), 7.27 (2H, d, *J* = 8.5 Hz, 2'''-*H*, 6'''-*H*), 7.23 (1H, td, $J_{H,H}$ = 8.3 Hz, $J_{H,F}$ = 5.2 Hz, 6^{IV}-*H*), 7.06 – 7.02 (2H, m, 2'-*H*, 6'-*H*), 6.95 – 6.91 (2H, m, 3'-*H*, 5'-*H*), 6.89 (1H, dd, $J_{H,F}$ = 9.7 Hz, $J_{H,H}$ = 8.3 Hz, 5^{IV}-*H*), 6.73 (1H, dd, *J* = 3.7, 0.9 Hz, 3^{IV}-*H*), 2.75 (2H, t, *J* = 7.6 Hz, 2''-H_2), 2.54 (2H, t, *J* = 7.6 Hz, 1''-H_2), 2.49 (2H, t, *J* = 7.6 Hz, 3-H_2), 2.34 (2H, t, *J* = 7.6 Hz, 1-H_2), 2.24 (3H, s, CH_3), 1.70 (2H, p, *J* = 7.6 Hz, 2-H_2); δ_C (176 MHz, $CDCl_3$): 161.4 (d, $J_{C,F}$ = 243.3 Hz, C-4'), 156.0 (d, $J_{C,F}$ = 249.4 Hz, C-4^{IV}), 147.9 (C-1'''), 137.7 (d, $J_{C,F}$ = 3.1 Hz, C-1'), 137.0 (d, $J_{C,F}$ = 9.4 Hz, C-7a^{IV}), 134.7 (C-4'''), 129.8 (C-2'''), 129.8 (d, $J_{C,F}$ = 7.7 Hz, C-2'), 127.1 (C-3'''), 126.4 (C-2^{IV}), 125.5 (d, $J_{C,F}$ = 7.4 Hz, C-6^{IV}), 119.9 (d, $J_{C,F}$ = 22.4 Hz, C-3^{IV}), 115.2 (d, $J_{C,F}$ = 21.0 Hz, C-3'), 109.7 (d, $J_{C,F}$ = 3.9 Hz, C-7^{IV}), 108.7 (d, $J_{C,F}$ = 18.6 Hz, C-5^{IV}), 104.7 (C-3^{IV}), 58.6 (C-1''), 56.81 (C-1), 42.0 (CH_3), 33.8 (C-2''), 32.6 (C-3), 29.1 (C-2); δ_F (376 MHz, $CDCl_3$): -117.70 (4'-F), -120.79 (4^{IV}-F); *m/z* (ES+) 469.267 $[M+H]^+$; HRMS ES$^+$ found $[M+H]^+$ 469.1758; $C_{26}H_{27}N_2O_2SF_2$ requires *M*, 469.1761.

(2''-(4'''-(4^{IV}-fluoroindol-1^{IV}-ylsulfonyl)phenyl)ethyl)(methyl)(2-(pyridin-3'-yl)ethyl])amine **96**

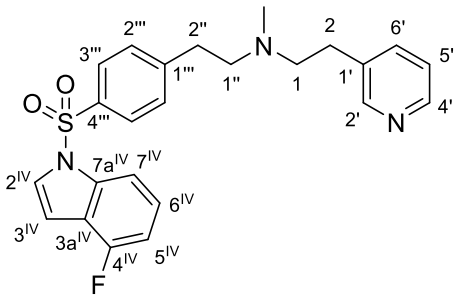

Following the general procedure for catalytic reductive amination, amine **91** (134.0 mg, 0.403 mmol) was combined with pyridine-3-yl-acetic acid hydrochloride (34 mg, 0.25 mmol) to afford, after purification by silica column chromatography (0-40% MeOH/Et_2O), the title compound (10 mg, 0.023 mmol, 6%) as a yellow oil.

ν_{max} (ATR): 2944, 2857, 2798, 1488, 1433, 1371 (S=O), 1183 (S=O), 1128, 1035 cm^{-1}; δ_H (700 MHz, $CDCl_3$): 8.44 – 8.40 (2H, m, 2'-*H*, 4'-*H*), 7.78 – 7.75 (3H, m, 7^{IV}-*H*, 3'''-*H*, 5'''-*H*), 7.54 (1H, d, *J* = 3.7 Hz, 2^{IV}-*H*), 7.41 (1H, dt, *J* = 7.8, 2.0 Hz, 6'-*H*), 7.26 – 7.21 (3H, m, 6^{IV}-*H*, 2'''-*H*, 6'''-*H*), 7.12 (1H, dd, *J* = 7.8, 4.8 Hz, 5'-*H*), 6.90 (1H, dd, $J_{H,F}$ = 9.6 Hz, $J_{H,H}$ = 8.1 Hz, 5^{IV}-*H*), 6.75 (1H, d, *J* = 3.7 Hz, 3^{IV}-*H*), 2.74 (2H, t, *J* = 7.6 Hz, 2''-H_2), 2.70 (2H, t, *J* = 7.6 Hz, 2-H_2), 2.61 (4H, m, 1''-H_2, 1-H_2), 2.31 (3H, s, CH_3); δ_C (176 MHz, $CDCl_3$): 156.0 (d, $J_{C,F}$ = 249.5 Hz, C-4^{IV}), 150.2 (C-2'), 147.75 (C-1'''), 147.72 (C-4'), 137.0 (d, $J_{C,F}$ = 9.5 Hz, C-7a^{IV}), 136.2 (C-6'), 135.8 (C-1'), 135.7 (C-4'''), 129.8 (C-2'''), 127.1 (C-1'''), 126.4 (C-2^{IV}), 125.5 (d, $J_{C,F}$ = 7.4 Hz, 6), 123.4 (C-5'), 119.9 (d, $J_{C,F}$ = 22.3 Hz, C-3^{IV}), 109.7 (d, $J_{C,F}$ = 3.9 Hz, C-7^{IV}), 108.7 (d, $J_{C,F}$ = 18.5 Hz, C-5^{IV}), 104.7 (C-3^{IV}), 58.9 (C-1), 58.5 (C-1''), 41.9 (CH_3), 33.8 (C-2''), 31.0 (C-2); δ_F (376 MHz, $CDCl_3$): -120.80; *m/z* (ES+) 438.299 $[M+H]^+$; HRMS ES$^+$ found $[M+H]^+$ 438.1661 $C_{24}H_{25}N_3O_2SF$ requires *M*, 438.1652.

3-(pyridin-3'-yl)propanal[165] **104**

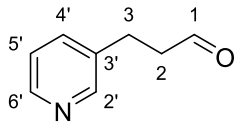

Following the general procedure for DMP oxidation, 3-pyridinepropanol (1.01 g, 7.39 mmol) was converted to afford the title compound (0.969 g, 7.17 mmol, 97 %) as a brown oil.

ν_{max} (ATR): 3039, 2931, 1724 (C=O), 1428, 1135 cm^{-1}; δ_H (600 MHz, $CDCl_3$): 9.83 (1H, t, *J* = 1.0 Hz, 1-*H*), 8.48 (1H, d, *J* = 2.4 Hz, 2'-*H*), 8.46 (1H, dd, *J* = 4.8, 1.6 Hz, 6'-*H*), 7.53 (1H, ddd, *J* = 7.9, 2.4, 1.6 Hz, 4'-*H*), 7.22 (1H, ddd, *J* = 7.9, 4.8, 0.9 Hz, 5'-*H*), 2.96 (2H, t, *J* = 7.4 Hz, 3-CH_2), 2.84 – 2.80 (2H, m, 2-CH_2); δ_C (151 MHz, $CDCl_3$): 200.6 (C=O), 149.9 (2'-C), 147.9 (4'-C), 136.1 (C-6'), 136.0 (3'-C), 123.60 (C-5'), 44.9 (C-2), 25.3 (C-3); *m/z* (ES^+) 136.058 $[M+H]^+$; HRMS ES^+ found $[M+H]^+$ 136.0768 $C_8H_{10}NO$ requires *M,* 136.0762.

(2''-[4'''-(4^{IV}-fluoroindol-1^{IV}-ylsulfonyl)phenyl]ethyl)(methyl)(3-(pyridin-3'-yl)propyl)amine **97**

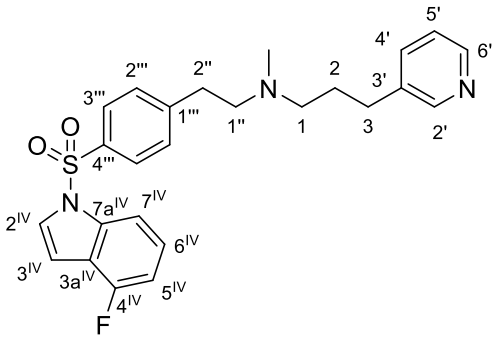

Following the general procedure for reductive amination, amine **91** (77.0 mg, 0.23 mmol) was combined with aldehyde **104** (34 mg, 0.25 mmol) to afford, after purification by silica column chromatography (0-40% MeOH/Et_2O), the title compound (17 mg, 0.038 mmol, 16%) as a yellow oil.

ν_{max} (ATR): 2944, 2860, 2796, 1488, 1433, 1376 (S=O), 1183 (S=O), 1166, 1127, 1031 cm^{-1}; δ_H (600 MHz, $CDCl_3$): 8.42 (1H, dd, *J* = 4.8, 1.9 Hz, 6'-*H*), 8.36 (1H, dd, *J* = 1.9, 0.9 Hz, 2'-*H*),

7.79 (2H, d, *J* = 8.5 Hz, 3'''-*H*, 5'''-*H*), 7.76 (1H, dd, *J* = 8.3, 0.8 Hz, 7^{IV}-*H*), 7.52 (1H, d, *J* = 3.8 Hz, 2^{IV}-*H*), 7.39 (1H, dt, *J* = 7.8, 1.9 Hz, 4'-*H*), 7.27 (2H, d, *J* = 8.5 Hz, 2'''-*H*, 6'''-*H*), 7.21 (1H, td, $J_{H,H}$ = 8.3 Hz, $J_{H,F}$ = 5.2 Hz, 6^{IV}-*H*), 7.16 (1H, ddd, *J* = 7.8, 4.8, 0.9 Hz, 5'-*H*), 6.88 (1H, ddd, $J_{H,F}$ = 9.6 Hz, $J_{H,H}$ = 8.3, 0.8 Hz, 5^{IV}-*H*), 6.72 (1H, dd, *J* = 3.8, 0.8 Hz, 3^{IV}-*H*), 2.74 (2H, t, *J* = 7.5 Hz, 2''-H_2), 2.53 (2H, t, *J* = 7.5 Hz, 1''-H_2), 2.49 (2H, t, *J* = 7.5 Hz, 3-H_2), 2.33 (2H, t, *J* = 7.5 Hz, 1-H_2), 2.23 (3H, s, CH_3), 1.71 (2H, p, *J* = 7.5 Hz, 2-H_2); δ_C (151 MHz, $CDCl_3$): 155.9 (d, $J_{C,F}$ = 249.3 Hz, C-4^{IV}), 150.0 (C-2'), 148.0 (C-1), 147.5 (C-6'), 137.3 (C-3'), 137.0 (d, $J_{C,F}$ = 9.5 Hz, C-$7a^{IV}$), 135.9 (C-4'), 135.7 (C-4''), 129.8 (C-2'''), 127.0 (C-3'''), 126.4 (C-2^{IV}), 125.52 (d, $J_{C,F}$ = 7.5 Hz, C-6^{IV}), 123.4 (C-5'), 119.8 (d, $J_{C,F}$ = 22.3 Hz, C-$3a^{IV}$), 109.7 (d, $J_{C,F}$ = 3.9 Hz, C-7^{IV}), 108.6 (d, $J_{C,F}$ = 18.5 Hz, C-5^{IV}), 104.7 (C-3^{IV}), 58.6 (C-1''), 56.6 (C-1), 41.9 (CH_3), 33.8 (C-2''), 30.5 (C-2'), 30.5 (C-3), 28.7 (C-2); δ_F (376 MHz, $CDCl_3$): -120.77; *m/z* (ES^+) 452.437 $[M+H]^+$; HRMS ES^+ found $[M+H]^+$ 452.1820 $C_{25}H_{26}N_3O_2SF$ requires *M*, 452.1808.

N-[2-(3'-bromophenyl)ethyl]acetamide[166] **110**

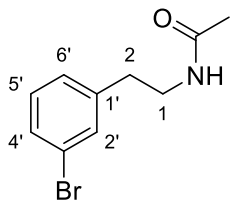

Following the general procedure for acetyl protection, 2-(3'-bromophenyl)ethanamine (2.32 g, 11.6 mmol) was converted to afford the title compound (2.84 g, 11.6 mmol, 100 %) and isolated as a yellow oil.

ν_{max} (ATR): 3289 (NH), 3086, 2941, 2174, 2006, 1652 (C=O), 1559 cm^{-1}; δ_H (400 MHz, $CDCl_3$): 7.40 – 7.33 (2H, m, 2'-*H*, 4'-*H*), 7.18 (1H, t, *J* = 7.6 Hz, 5'-*H*), 7.12 (1H, d, *J* = 7.6 Hz, 6'-*H*), 5.79 (1H, s, N*H*), 3.50 (2H, q, *J* = 6.6 Hz, 1-CH_2), 2.80 (2H, t, *J* = 7.0 Hz, 2-CH_3), 1.98 (3H, s, CH_3); δ_C (151 MHz, $CDCl_3$): 170.5 (C=O), 141.2 (C-1'), 131.8 (C-2'), 130.2 (C-5'), 129.7 (C-4'), 127.4 (C-6'), 122.7 (C-3'), 40.6 (C-1), 35.3 (C-2), 23.2 (C H_3); *m/z* (ES^+) 242.131 $[M(^{79}Br)H]^+$; 244.118 $[M(^{81}Br)H]^+$; HRMS ES^+ found $[M+H]^+$ 242.0199 $C_{10}H_{13}{}^{79}BrNO$ requires *M,* 242.0181.

N-[2-(3'-bromophenyl)ethyl]-N-methylacetamide **111**

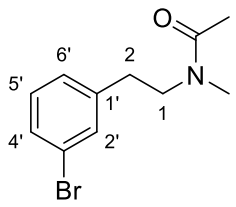

A solution of **110** (2.64 g, 10.9 mmol) in anhydrous THF (15.0 mL) was added to a suspension of NaH (60% in mineral oil) (0.79 g, 19.6 mmol) in anhydrous THF under an argon atmosphere. The resulting solution was allowed to stir at 0 °C for 1 h and at room temperature for 45 min. Next, after cooling the mixture to 0 °C, methyl iodide (1.7 g, 0.75 mL, 12.0 mmol) was added dropwise and the mixture was stirred at this temperature for 10 min. The reaction mixture was then warmed to room temperature and allowed to stir for 16 h until the reaction was judged complete by TLC. The reaction was carefully quenched by the dropwise addition of NH_4Cl followed by removal of the solvent under reduced pressure. The resultant mixture extracted with Et_2O and the combined organic layers dried with $MgSO_4$ and concentrated to give the crude product. Purification by column chromatography (0% - 100% EtOAc/Pet. Ether) gave the title compound (2.11 g, 8.23 mmol, 76%) as a yellow oil.

ν_{max} (ATR): 2939, 2170, 2034, 1641 (C=O), 1480, 1405 cm^{-1}; δ_H (400 MHz, $CDCl_3$): 7.42 – 7.30 (2H, m, 2'-*H*, 4'-*H*), 7.22 – 7.05 (2H, m, 5'-*H*, 6'-*H*), 3.56 (2H, t, *J* = 7.6 Hz, 1-CH_2), 3.50 (2H, t, *J* = 7.3 Hz, 1-CH_2), 2.91 (3H, s, NCH_3), 2.90 (3H, s, NCH_3), 2.81 (2H, m, 2-CH_2), 2.08 (3H, s, NCH_3), 1.93 (3H, s, CCH_3); δ_C (101 MHz, $CDCl_3$): 170.8 (C=O), 170.7 (C=O), 141.6 (C-1'), 141.5 (C-1'), 132.0(C-2'), 131.9 (C-2'), 130.5 (C-5'), 130.2 (C-4'), 131.1 (C-5'), 129.6 (C-4'), 127.6 (C-6'), 127.6 (C-6'), 122.9 (C-3'), 122.6 (C-3'), 52.4 (C-1), 49.7 (C-1), 37.1 (NCH_3), 34.6 (C-2), 33.6 (C-2), 33.5 (NCH_3), 22.0 (C$\underline{C}H_3$), 21.1 (C$\underline{C}H_3$); *m/z* (ES^+) 256.180 $[M(^{79}Br)H]^+$; 258.171 $[M(^{81}Br)H]^+$; HRMS ES^+ found $[M(^{79}Br)H]^+$ 256.0345; $C_{11}H_{15}{}^{79}BrNO$ requires *M,* 256.0337.

[2-(3'-bromophenyl)ethyl](methyl)amine[167] **108**

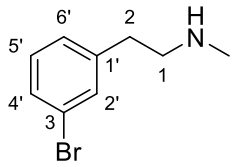

Following the general procedure for acetamide deprotection, **111** (1.38 g, 5.39 mmol) was hydrolyzed to afford the title compound (1.14 g, 5.32 mmol, 99%) as a yellow oil.

ν_{max} (ATR): 3280 (br, NH), 2938, 2796, 1604, 1473, 1115 cm^{-1}; δ_H (600 MHz, $CDCl_3$): 7.39 – 7.33 (2H, m, 2'-*H*, 4'-*H*), 7.18 – 7.12 (2H, m, 5'-*H*, 6'-*H*), 4.05 (1H, s, N*H*), 2.96 – 2.87 (4H, m, 1-H_2, 2-H_2), 2.51 (3H, s, CH_3); δ_C (151 MHz, $CDCl_3$): 141.3 (C-1'), 131.9 (C-2'), 130.3 (C-5'), 129.8 (C-4'), 127.5 (C-6'), 122.8 (C-3'), 52.0 (C-2), 35.2 (NCH_3), 34.6 (C-1); *m/z* (ES^+) 214.071 $[M(^{79}Br)H]^+$; 216.047 $[M(^{81}Br)H]^+$; HRMS ES^+ found $[M(^{79}Br)H]^+$ 214.0248; $C_9H_{13}{}^{79}BrNO$ requires *M,* 214.0231.

[2-(3'-bromophenyl)ethyl][(4''-fluorophenyl)methyl]methylamine **114**

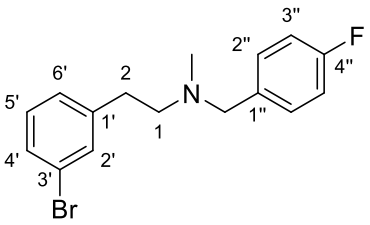

Following the general procedure for reductive amination, amine **108** (1.12 g, 5.25 mmol) was combined with 4-fluorobenzaldehyde (0.64 g, 5.16 mmol) to afford, after purification by silica column chromatography (0 – 35% EtOAc/Hexane), the title compound (1.05 g, 3.25 mmol, 63%) as a yellow oil.

ν_{max} (ATR): 2925, 1630, 1487, 1430, 1376, 1182, 1128 cm^{-1}; δ_H (600 MHz, $CDCl_3$): 7.33 (2H, m, 2'-*H*, 4'-*H*), 7.22 (2H, m, 2''-*H*, 6''-*H*), 7.14 (1H, m, 5'-*H*), 7.09 (1H, m, 6'-*H*), 7.0 – 6.98 (2H, m, 3''-*H*, 5''-*H*), 3.49 (2H, s, NCH_2), 2.77 (2H, dd, *J* = 8.9, 6.4 Hz, 2-H_2), 2.6 – 2.6 (2H, m, 1-H_2), 2.25 (3H, s, CH_3); δ_C (151 MHz, $CDCl_3$): 162.1 (d, $J_{C,F}$ = 244.7 Hz, C-4''), 143.0 (C-1'), 134.8 (d, $J_{C,F}$ = 3.2 Hz, C-1''), 131.9 (C-2'), 130.5 (d, $J_{C,F}$ = 7.9 Hz, C-2'', C-6''), 130.0 (C-3'),

129.2 (C-4'), 127.6 (C-6'), 122.5 (C-3'), 115.2 (d, $J_{C,F}$ = 21.1 Hz, C-3'', C-5''), 61.6 (NCH_2), 58.6 (C-1), 42.2 (CH_3), 33.7 (C-2); δ_F (376 MHz, $CDCl_3$): -116.05; *m/z* (ES^+) 322.284 $[M(^{79}Br)H]^+$; 324.260 $[M(^{81}Br)H]^+$; HRMS ES^+ found $[M(^{79}Br)H]^+$ 322.0609; $C_{16}H_{18}{}^{79}BrNO$ requires *M,* 322.0607.

5.2 Biological Experimental Details

5.2.1 General experimental details

MATERIALS: Biological grade materials, solvents, reagents and media components were purchased from commercial suppliers and were used without further purification unless otherwise stated. Amphotericin B and cycloheximide were purchased from Sigma-Aldrich. Reactions and media were prepared using ultrapure distilled, deionized water from Milli-Q® water purification system. Solutions of test compounds were made up in DMSO. 10 mM stock solutions of the synthesized analogues were prepared in dimethyl sulfoxide (DMSO) and stored at 0 – 4 °C. Subsequent dilutions were completed in growth media so that all final drug concentrations contained 1% DMSO.

INSTRUMENTS AND EQUIPMENT: 1.5 mL Eppendorfs were used during the preparation of serial dilutions. Media was sterilized by filtration using a vacuum filter equipped with a 0.22 µm pore CA membrane. A Neubauer hemocytometer was used to count cells. 96-well plates used were Nest Biotechnology Co., Ltd cell culture plates (clear); Corning® Costar® cell culture plates (clear); Corning® V-bottom (clear). Fluorescence quantification was carried out using Synergy H4 and FLx800 microplate readers with Gen5® 1.08 data analysis software from Biotek.

5.2.2 Growth media and fluorescent indicator

Details of the growth media composition, which must be sterilized by filtration, are indicated in Table 5.1. The composition of resazurin solution, the fluorescent indicator, is also given below.

Growth Media/Solution	Volume/Mass	Stock Solution
Schneider's Insect Medium (stock) (1 L, pH 7.0)	24.5 g 0.4 g 0.6 g 1 L	Schneider's Insect Medium $NaHCO_3$ $CaCl_2$ 1 M HCl (for pH adjustment) 1 M NaOH (for pH adjustment) Water
Schneider's Insect Medium (50 ml, pH 7.0, 15% FBS)	42.5 ml 7.5 ml 0.5 mL	Schneider's Insect Medium (stock) Heat-inactivated fetal bovine serum (FBS) Penicillin/Steptomycin (Pen Strep)
Resazurin Solution	5 mg 40 ml	Resazurin sodium salt Phosphate Buffered Saline (PBS)

Table 5.1: Media and resazurin compositions

5.2.3. Protocols

The following biological procedures were carried out under sterile conditions.

5.2.3.1 *Leishmania* Promastigote Culture

Frozen samples of *Leishmania major* (MHOM/IL/81/Friedlin; FV1 strain; WT and *ΔLCB2*), *Leishmania amazonensis* (MHOM/Br/75/JOSEFA), and *Leishmania mexicana (MNYC/BZ/M379)* were rapidly defrosted and added to Schneider's Insect Medium (pH 7.0, 15% FBS, 5 mL). The promastigotes were maintained at 26 °C in Schneider's Insect Medium (pH 7.0, 15% FBS). *Leishmania major* (MHOM/IL/81/Friedlin; FV1 strain; *pX*)

promastigotes were maintained at 26 °C in Schneider's insect medium (pH 7.0, 15% FBS, 5 mL), supplemented with 40 μg·mL^{-1} G418 (Gibco BRL). Frozen stocks were prepared by adding the culture (900 μL) to DMSO (100 μL) and cooling to −150 °C.

5.2.3.2 Promastigote dose-response assay

The following protocol was adapted from a literature procedure.[13] The test compounds and controls (50 μL) were dispensed in triplicate into a sterile 96-well plate. *Leishmania* promastigotes in Schneider's insect medium (50 μL at 1 × 10^{6} parasites·μL^{-1}) were added to a final concentration of 5.0 × 10^{5} parasites·μL^{-1}. Amphotericin B and cycloheximide were used as positive controls while untreated parasites with 1% DMSO were used as a negative control. The plate was then incubated at 26 °C for 48 hours. Resazurin solution (10 μL) was added and the plate incubated at 26 °C for an additional 4 h prior to measurement using a fluorescence plate reader Ex570/Em685. EC_{50} values were calculated using sigmoidal regression analysis (GraphPad Prism).

References

(1) Hotez, P.; Ottesen, E.; Fenwick, A.; Molyneux, D. In *Hot Topics in Infection and Immunity in Children III. Advances in Experimental Medicine and Biology*; Pollard, A. J., Finn, A., Eds.; Springer: New York, 2006; Vol. 582, pp 23–33.

(2) Cox, F. E. G. *Clin. Microbiol. Rev.* **2002**, *15* (4), 595.

(3) Alvar, J.; Yactayo, S.; Bern, C. *Trends Parasitol.* **2006**, *22* (12), 552.

(4) Manderson, L.; Aagaard-Hansen, J.; Allotey, P.; Gyapong, M.; Sommerfeld, J. *PLoS Negl. Trop. Dis.* **2009**, *3* (2), e332.

(5) Hotez, P. J.; Aksoy, S.; Brindley, P. J.; Kamhawi, S. *PLoS Negl. Trop. Dis.* **2020**, *14* (1), e0008001.

(6) World Health Organization. *Control of the leishmaniases: report of a meeting of the WHO Expert Committee on the Control of Leishmaniases*; Geneva.

(7) Hotez, P. J.; Dumonteil, E.; Heffernan, M. J.; Bottazzi, M. E. In *Hot Topics in Infection and Immunity in Children IX. Advances in Experimental Medicine and Biology, vol 746*; N. Curtis, Finn, A., Pollard, A., Eds.; Springer: New York, NY, 2013; pp 1–12.

(8) Jannin, J.; Gabrielli, A. F. In *Handbook of Clinical Neurology*; H.H. Garcia, Tanowitz, H. B., Brutto, O. H. Del, Eds.; Elsevier B.V., 2013; Vol. 114, pp 3–8.

(9) Hotez, P. J.; Molyneux, D. H.; Fenwick, A.; Ottesen, E.; Sachs, S. E.; Sachs, J. D. *PLoS Med.* **2006**, *3* (5), 576.

(10) Pace, D. *J. Infect.* **2014**, *69* (S1), S10.

(11) Desjeux, P. *Comp. Immunol. Microbiol. Infect. Dis.* **2004**, *27* (5), 305.

(12) Croft, S. L.; Barrett, M. P.; Urbina, J. A. *Trends Parasitol.* **2005**, *21* (11), 508.

(13) Mina, J. G.; Mosely, J. A.; Ali, H. Z.; Shams-Eldin, H.; Schwarz, R. T.; Steel, P. G.; Denny, P. W. *Int. J. Biochem. Cell Biol.* **2010**, *42* (9), 1553.

(14) Cunningham, A. C. *Exp. Mol. Pathol.* **2002**, *72*, 132.

(15) McGwire, B. S.; Satoskar, A. R. *Q J Med* **2014**, *107* (1), 7.

(16) Zambrano-Villa, S.; Rosales-Borjas, D.; Carrero, J. C.; Ortiz-Ortiz, L. *Trends Parasitol.* **2002**, *18* (6), 272.

(17) Chawla, B.; Madhubala, R. *J. Parasit. Dis.* **2010**, *34* (1), 1.

(18) Iqbal, H.; Ishfaq, M.; Wahab, A.; Abbas, M. N.; Ahmad, I.; Rehman, A.; Zakir, M. *Asian Pacific J. Trop. Dis.* **2016**, *6* (1), 1.

(19) Mansueto, P.; Seidita, A.; Vitale, G.; Cascio, A. *Travel Med. Infect. Dis.* **2014**, *12* (6), 563.

(20) Gramiccia, M.; Gradoni, L. *Int. J. Parasitol.* **2005**, *35* (11–12), 1169.

(21) Okwor, I.; Uzonna, J. *Am. J. Trop. Med. Hyg.* **2016**, *94* (3), 489.

(22) Herwaldt, B. L. *Lancet* **1999**, *354* (9185), 1191.

(23) Rogers, M. E.; Chance, M. L.; Bates, P. A. *Parasitology* **2002**, *124* (5), 495.

(24) Pillai, A. B.; Xu, W.; Zhang, O.; Zhang, K. *PLoS Negl. Trop. Dis.* **2012**, *6* (12), e1944.

(25) Bates, P. A. *Int. J. Parasitol.* **2007**, *37* (10), 1097.

(26) Singh, N.; Kumar, M.; Singh, R. K. *Asian Pac. J. Trop. Med.* **2012**, *5* (6), 485.

(27) Murray, H. W.; Berman, J. D.; Davies, C. R.; Saravia, N. G. *Lancet* **2005**, *366* (9496), 1561.

(28) Singh, O. P.; Singh, B.; Chakravarty, J.; Sundar, S. *Infect. Dis. Poverty* **2016**, *5* (1), 19.

(29) Sakthianandeswaren, A.; Foote, S. J.; Handman, E. *Trends Parasitol.* **2009**, *25* (8), 383.

(30) Kevric, I.; Cappel, M. A.; Keeling, J. H. *Dermatol. Clin.* **2015**, *33* (3), 579.

(31) WHO Leishmaniasis control programme. Annual country reports. *Status of endemicity of cutaneous leishmaniasis, 2015*; Geneva, 2017.

(32) Berman, J. D. *Clin. Infect. Dis.* **1997**, *24* (4), 684.

(33) Sundar, S.; Chakravarty, J. *Expert Opin. Pharmacother.* **2013**, *14* (1), 53.

(34) Kevric, I.; Cappel, M. A.; Keeling, J. H. *Dermatol. Clin.* **2015**, *33* (3), 579.

(35) Handler, M. Z.; Patel, P. A.; Kapila, R.; Al-Qubati, Y.; Schwartz, R. A. *J. Am. Acad. Dermatol.* **2015**, *73* (6), 897.

(36) Killick-Kendrick, R. *Clin. Dermatol.* **1999**, *17*, 279.

(37) Lynn, M. a; McMaster, W. R. *Trends Parasitol.* **2008**, *24* (3), 103.

(38) de Vries, H. J. C.; Reedijk, S. H.; Schallig, H. D. F. H. *Am. J. Clin. Dermatol.* **2015**, *16* (2), 99.

(39) WHO Leishmaniasis control programme. Annual country reports. *Status of endemicity of visceral leishmaniasis, 2015*; Geneva, 2017.

(40) Freitas-Junior, L. H.; Chatelain, E.; Kim, H. A.; Siqueira-Neto, J. L. *Int. J. Parasitol. Drugs Drug Resist.* **2012**, *2*, 11.

(41) Wamai, R. G.; Kahn, J.; Mcgloin, J.; Ziaggi, G. *J. Glob. Heal. Sci.* **2020**, *2* (1), e3.

(42) Savoia, D. *J. Infect. Dev. Ctries.* **2015**, *9* (6), 588.

(43) Saporito, L.; Giammanco, G. M.; De Grazia, S.; Colomba, C. *Int. J. Infect. Dis.* **2013**, *17* (8), e572.

(44) Stockdale, L.; Newton, R. *PLoS Negl. Trop. Dis.* **2013**, *7* (6), e2278.

(45) Croft, S. L.; Olliaro, P. *Clin. Microbiol. Infect.* **2011**, *17*, 1478.

(46) Ali, H. Z.; Harding, C. R.; Denny, P. W. *Biochem. Res. Int.* **2012**, *2012*, 691363.

(47) Ilg, T. *Parasitol. Today* **2000**, *16* (11), 489.

(48) Ilg, T.; Handman, E.; Stierhof, Y.-D. *Biochem. Soc.* **1999**, *27* (I 999), 518.

(49) Descoteaux, A.; Turco, S. J. *Biochim. Biophys. Acta - Mol. Basis Dis.* **1999**, *1455* (2–3), 341.

(50) Eggimann, G. A.; Sweeney, K.; Bolt, H. L.; Rozatian, N.; Cobb, S. L.; Denny, P. W. *Molecules* **2015**, *20* (2), 2775.

(51) Tiuman, T. S.; Santos, A. O.; Ueda-Nakamura, T.; Filho, B. P. D.; Nakamura, C. V. *Int. J. Infect. Dis.* **2011**, *15* (8), e525.

(52) Santos, D. O.; Coutinho, C. E. R.; Madeira, M. F.; Bottino, C. G.; Vieira, R. T.; Nascimento, S. B.; Bernardino, A.; Bourguignon, S. C.; Corte-Real, S.; Pinho, R. T.; Rodrigues, C. R.; Castro, H. C. *Parasitol. Res.* **2008**, *103* (1), 1.

(53) de Menezes, J. P. B.; Guedes, C. E. S.; Petersen, A. L. de O. A.; Fraga, D. B. M.; Veras, P. S. T. *Biomed Res. Int.* **2015**, *2015*, 1.

(54) Kaur, G.; Rajput, B. *J. Parasitol. Res.* **2014**, *2014*, 726328.

(55) Stunkard, A. J.; Sundar, S.; Chakravarty, J.; Zeidan, Y. H.; Hannun, Y. A. *Psychiatry Interpers. Biol. Process.* **2009**, *162* (3), 214.

(56) Coler, R. N.; Reed, S. G. *Trends Parasitol.* **2005**, *21* (5), 244.

(57) Denny, P. W.; Smith, D. F. *Mol. Microbiol.* **2004**, *53* (3), 725.

(58) Denny, P. W.; Shams-Eldin, H.; Price, H. P.; Smith, D. F.; Schwarz, R. T.; Bates, P. A. *J. Biol. Chem.* **2006**, *281* (38), 28200.

(59) Hirabayashi, Y.; Igarashi, Y.; Merrill, A. H. *Sphingolipids Synthesis, Transport and*

Cellular Signaling; Hirabayashi, Y., Igarashi, Y., Merrill, A. H., Eds.; Springer Japan: Tokyo, 2006.

(60) Zeidan, Y. H.; Hannun, Y. A. *Trends Mol. Med.* **2007**, *13* (8), 327.

(61) Futerman, A. H.; Hannun, Y. A. *EMBO Rep.* **2004**, *5* (8), 777.

(62) Karlsson, K.-A. *Lipids* **1970**, *5* (11), 878.

(63) Ramstedt, B.; Slotte, J. P. *FEBS Lett.* **2002**, *531*, 33.

(64) Merrill, A. H. *J. Biol. Chem.* **2002**, *277* (29), 25843.

(65) Young, S. A.; Mina, J. G.; Denny, P. W.; Smith, T. K. *Biochem. Res. Int.* **2012**, *2012*, 248135.

(66) Futerman, A. H.; Riezman, H. *Trends Cell Biol.* **2005**, *15* (6), 312.

(67) Mina, J. G.; Mosely, J. a; Ali, H. Z.; Denny, P. W.; Steel, P. G. *Org. Biomol. Chem.* **2011**, *9* (6), 1823.

(68) Hannun, Y. A.; Obeid, L. M. *Nat. Rev. Mol. Cell Biol.* **2008**, *9*, 139.

(69) Zhang, K.; Bangs, J. D.; Beverley, S. M. *Adv. Exp. Med. Biol.* **2010**, *688*, 238.

(70) Xu, W.; Xin, L.; Soong, L.; Zhang, K. *Infect. Immun.* **2011**, *79* (8), 3377.

(71) Zhang, O.; Xu, W.; Pillai, A. B.; Zhang, K. *PLoS One* **2012**, *7* (1), e351059.

(72) Zhang, K.; Beverley, S. M. *Mol. Biochem. Parasitol.* **2010**, *170* (2), 55.

(73) Zhang, O.; Wilson, M. C.; Xu, W.; Hsu, F.-F.; Turk, J.; Kuhlmann, F. M.; Wang, Y.; Soong, L.; Key, P.; Beverley, S. M.; Zhang, K. *PLoS Pathog.* **2009**, *5* (12), e1000692.

(74) Zhang, K.; Hsu, F.; Scott, D. A.; Docampo, R.; Turk, J.; Beverley, S. M. *Mol. Microbiol.* **2005**, *55* (5), 1566.

(75) Heidler, S. A.; Radding, J. A. *Antimicrob. Agents Chemother.* **1995**, *39* (12), 2765.

(76) Nagiec, M. M.; Nagiec, E. E.; Baltisberger, J. A.; Wells, G. B.; Lester, R. L.; Dickson, R. C. *J. Biol. Chem.* **1997**, *272* (15), 9809.

(77) Tanaka, A. K.; Valero, V. B.; Takahashi, H. K.; Straus, A. H. *J. Antimicrob. Chemother.* **2007**, *59* (3), 487.

(78) Koeller, C. M.; Heise, N. *Enzyme Res.* **2011**, *2011*, 648159.

(79) Nagiec, M. M.; Nagiec, E. E.; Baltisberger, J. A.; Wells, G. B.; Lester, R. L.; Dickson, R. C. *J. Biol. Chem.* **1997**, *272* (15), 9809.

(80) Goren, M. A.; Fox, B. G.; Bangs, J. D. *Biochemistry* **2012**, *50* (41), 8853.

(81) Sevova, E. S.; Goren, M. A.; Schwartz, K. J.; Hsu, F. F.; Turk, J.; Fox, B. G.; Bangs, J. D. *J. Biol. Chem.* **2010**, *285* (27), 20580.

(82) Sutterwala, S. S.; Hsu, F.-F.; Sevova, E. S.; Schwartz, K. J.; Zhang, K.; Key, P.; Turk, J.; Beverley, S. M.; Bangs, J. D. *Mol. Microbiol.* **2008**, *70* (2), 281.

(83) Huitema, K.; van den Dikkenberg, J.; Brouwers, J. F.; Holthuis, J. C. M. *EMBO J.* **2004**, *23* (1), 33.

(84) UniProtKB - E9AFX2 (SLS_LEIMA) http://www.uniprot.org/uniprot/E9AFX2 (accessed Oct 5, 2017).

(85) Norcliffe, J. L. High Throughput Screening to Identify, Develop, and Analyse Inositol Phosphorylceramide Inhibitors as Novel Antileishmanials, Durham University, 2015.

(86) Norcliffe, J. L.; Mina, J. G.; Alvarez, E.; Cantizani, J.; Dios-, F. De; Colmenarejo, G.; Valle, S. G.; Marco, M.; Fiandor, J. M.; Martin, J. J.; Steel, P. G.; Denny, P. W. *Sci entific Reports* **2018**, *8*, 3938.

(87) Scott, P.; Novais, F. O. *Nat. Rev. Immunol.* **2016**, *16* (9), 581.

(88) McConville, M. J.; Handman, E. *Int. J. Parasitol.* **2007**, *37*, 1047.

(89) McConville, M. J.; Naderer, T. *Annu. Rev. Microbiol.* **2011**, *65*, 543.

(90) White, R. E.; Miller, J. P.; Favreau, L. V; Bhattacharyya, A. *J. Am. Chem. Soc.* **1986**, *108* (6), 6024.

(91) Hjelmeland, L. M.; Aronow, L.; Trudell, J. R. *Biochem. Biophys. Res. Commun.* **1977**, *76* (2), 541.

(92) Miwa, G. T.; Lu, A. Y. H. *BioEssays* **1987**, *7* (5), 215.

(93) Mihalak, K. B.; Carroll, F. I.; Luetje, C. W. *Mol. Pharmacol.* **2006**, *70* (3), 801.

(94) Smith, B. M.; Smith, J. M.; Tsai, J. H.; Schultz, J. A.; Gilson, C. A.; Estrada, S. A.; Chen, R. R.; Park, D. M.; Prieto, E. B.; Gallardo, C. S.; Sengupta, D.; Dosa, P. I.; Covel, J. A.; Ren, A.; Webb, R. R.; Beeley, N. R. A.; Martin, M.; Morgan, M.; Espitia, S.; Saldana, H. R.; Bjenning, C.; Whelan, K. T.; Grottick, A. J.; Menzaghi, F.; Thomsen, W. J. *J. Med. Chem.* **2008**, *51*, 305.

(95) Fish, P. V.; Brown, A. D.; Evrard, E.; Roberts, L. R. *Bioorganic Med. Chem. Lett.* **2009**, *19* (7), 1871.

(96) Vandana, A.; Yadav, Y.; Kishore, D. *Orient. J. Chem.* **2013**, *29* (4), 1643.

(97) Liang, J. T.; Liu, J.; Shireman, B. T.; Tran, V.; Deng, X.; Mani, N. S. *Org. Process Res. Dev.* **2010**, *14* (2), 380.

(98) Liang, H.; Zhang, D.; Yue, Y.; Shi, Z.; Zhao, S. *Arch. der Pharm. Chem. Life Sci.* **2010**, *343*, 114.

(99) Chen, S. jun; Xu, Y.; Liang, Y. mei; Cao, Y.; Lv, J. yan; Pang, J. xin; Zhou, P. zheng. *Acta Pharmacol. Sin.* **2019**, *40*, 746.

(100) Kargbo, R. B.; Sajjadi-hashemi, Z.; Roy, S.; Jin, X.; Herr, R. J. *Tetrahedron Lett.* **2018**, *54* (15), 2018.

(101) Hesek, D.; Lee, M.; Noll, B. C.; Fisher, J. F.; Mobashery, S. *J. Org. Chem.* **2012**, *74* (6), 2567.

(102) Chang, M.; Chan, C.; Lin, S.; Hsu, R. *Tetrahedron* **2012**, *68* (50), 10272.

(103) Flaih, N.; Chuong, P.; Galons, H. *Tetrahedron Lett.* **1999**, *40*, 3697.

(104) Harvey, R. G.; Pataki, J.; Cortez, C.; Raddo, P. Di; Yang, C. *J. Org. Chem.* **1991**, *56* (3), 1210.

(105) Zhang, J.; Xiang, Y.; Xu, W.; Jian, S. WO2015/143692 A1, 2015.

(106) Braje, W. M.; Haupt, A.; Lubisch, W.; Grandel, R.; Drescher, K.; Geneste, H.; Unger, L.; Sauer, D. US2005/137186 A1, 2005.

(107) Dutton, W. M. Development and application of the vinylepoxide - dihydrofuran rearrangement, Durham University, 2000.

(108) Laguzza, B.; Ganem, B. *Tetrahedron Lett.* **1981**, *22* (16), 1483.

(109) Ziegler, F.; Brown, E.; Sobolov, S. *J. Org. Chem.* **1990**, *55* (11), 3691.

(110) Sundberg, R. J.; Hamilton, G. S.; Laurino, J. P. *J. Org. Chem.* **1988**, *53* (5), 976.

(111) Kumar, P.; Cherian, S. K.; Jain, R.; Show, K. *Tetrahedron Lett.* **2014**, *55* (52), 7172.

(112) Liu, F.; Majo, V. J.; Prabhakaran, J.; Milak, M. S.; Mann, J. J.; Parsey, R. V; Kumar, J. S. D. *Bioorg. Med. Chem.* **2011**, *19* (17), 5255.

(113) Murphy, K. Validation Inositol Phosphoryl Ceramide Synthase (IPCS) as an Anti-Protocoal Target, Durham University, 2016.

(114) Boudreault, N.; Leblanc, Y. *Org. Synth.* **1997**, *74*, 241.

(115) Macdonald, G. J.; Branch, C. L.; Hadley, M. S.; Johnson, C. N.; Nash, D. J.; Smith, A. B.; Stemp, G.; Thewlis, K. M.; Vong, A. K. K.; Austin, N. E.; Jeffrey, P.;

Winborn, K. Y.; Boyfield, I.; Hagan, J. J.; Middlemiss, D. N.; Reavill, C.; Riley, G. J.; Watson, J. M.; Wood, M.; Parker, S. G.; Ashby, C. R. *J. Med. Chem.* **2003**, *46* (23), 4952.

(116) Xu, H.; Wang, Y. *Chinese J. Chem.* **2010**, *28* (1), 125.

(117) Szcześniak, P.; Buda, S.; Lefevre, L.; Staszewska-Krajewska, O.; Mlynarski, J. *European J. Org. Chem.* **2019**, *2019* (41), 6973.

(118) Correa, R.; Filho, V. C.; Schlemper, V.; Nunes, R. *Pharm. Sci.* **1997**, *3*, 67.

(119) Cremlyn, R.; Nunes, R. *Phosphorus and Sulfur* **1987**, *31*, 245.

(120) Andrews, K. G.; Summers, D. M.; Donnelly, L. J.; Denton, R. M. *Chem. Commun.* **2016**, *52* (9), 1855.

(121) Hamada, T.; Yonemitsu, O. *Synthesis (Stuttg).* **1986**, *10*, 852.

(122) Hale, M. R.; Baker, C. T.; Stammers, T. A.; Sherrill, T. G.; Spaltenstein, A.; Furfine, E. S.; Maltais, F.; Andrews, C. W. I.; Miller, J. F.; Samano, V. US6319946 (B1), 2001.

(123) Papageorgiou, G.; Corrie, J. E. T. *Tetrahedron* **1999**, *55* (1), 237.

(124) Loevezijn, A.; Iwena Bakker, W. I.; Stoit, A.; Resnick, A. A. M.; Venhorst, J.; De Haan, M.; Kruse, C. G. WO 2009/115515 Al, 2009.

(125) Ziegler, D. S.; Wei, B.; Knochel, P. *Chem. A Eur. J.* **2018**, *25* (11), 2695.

(126) Krasovskiy, A.; Knochel, P. *Angew. Chemie Int. Ed.* **2004**, *43*, 3333.

(127) Du, R.; Hotez, P. J.; Al-salem, W. S.; Acosta-serrano, A. *PLoS Negl. Trop. Dis.* **2016**, *10* (5), 1.

(128) Monge-Maillo, B.; López-Vélez, R. *Drugs* **2013**, *73* (17), 1889.

(129) Adolfo, G.; Romero, S.; Vinitius, M.; Guerra, D. E. F.; Paes, M. G.; Mace, V. D. E.

O. *Am. J. Trop. Med. Hyg.* **2001**, *65* (5), 456.

(130) Lindoso, J. A. L.; Costa, J. M. L.; Queiroz, I. T.; Goto, H. *Res. Rep. Trop. Med.* **2012**, No. 3, 69.

(131) Arevalo, J.; Ramirez, L.; Adaui, V.; Zimic, M.; Tulliano, G.; Lazo, M.; Doncker, S. De; Maurer, A.; Chappuis, F.; Dujardin, J.; Llanos-cuentas, A. *J. Infect. Dis.* **2007**, *195* (12), 1846.

(132) Rogers, M. B.; Hilley, J. D.; Dickens, N. J.; Wilkes, J.; Bates, P. A.; Depledge, D. P.; Harris, D.; Her, Y.; Herzyk, P.; Imamura, H.; Otto, T. D.; Sanders, M.; Seeger, K.; Dujardin, J.; Berriman, M.; Smith, D. F.; Hertz-fowler, C.; Mottram, J. C. *Genome Res.* **2011**, *21*, 2129.

(133) Burger, A. *Prog. Drug Res.* **1991**, *37*, 287.

(134) Meanwell, N. A. *J. Med. Chem.* **2018**, *61* (14), 5822.

(135) Fleming, F. F.; Yao, L.; Ravikumar, P. C.; Funk, L.; Shook, B. C. *J. Med. Chem.* **2010**, *53* (22), 7902.

(136) Nassar, A. E. F.; Kamel, A. M.; Clarimont, C. *Drug Discov. Today* **2004**, *9* (23), 1020.

(137) Thompson, T. N. *Med. Res. Rev.* **2001**, *21* (5), 412.

(138) Bellec, G.; Goasduff, T.; Dreano, Y.; Menez, J. F.; Berthou, F. *Cancer Lett.* **1996**, *100* (1–2), 115.

(139) Bellec, G.; Dréano, Y.; Lozach, P.; Ménez, J. F.; Berthou, F. *Carcinogenesis* **1996**, *17* (9), 2029.

(140) Denny, P. W.; Goulding, D.; Ferguson, M. A. J.; Smith, D. F. *Mol. Microbiol.* **2004**, *52* (2), 313.

(141) Zhang, K.; Hsu, F.-F.; Scott, D. A.; Docampo, R.; Turk, J.; Beverley, S. M. *Mol. Microbiol.* **2005**, *55* (5), 1566.

(142) Zhang, K.; Showalter, M.; Revollo, J.; Hsu, F. F.; Turk, J.; Beverley, S. M. *EMBO J.* **2003**, *22* (22), 6016.

(143) Moraes, I.; Evans, G.; Sanchez-Weatherby, J.; Newstead, S.; Shaw, P. D. *Biochim. Biophys. Acta* **2014**, *1838* (1), 78.

(144) Finkelstein, J. M. *Nature* **2014**, *21* (511).

(145) Caffrey, M.; Cherezov, V. *Nat. Protoc.* **2010**, *4* (5), 706.

(146) Landau, E. M.; Rosenbusch, J. P. *Proc. Natl. Acad. Sci. U. S. A.* **1996**, *93* (25), 14532.

(147) Smith, E.; Collins, I. *Future Med. Chem.* **2015**, *7* (2), 159.

(148) Murale, D. P.; Hong, S. C.; Haque, M. M.; Lee, J. S. *Proteome Sci.* **2016**, *15*, 14.

(149) Robinette, D.; Neamati, N.; Tomer, K. B.; Borchers, C. H. *Expert Rev. Proteomics* **2006**, *3* (4), 399.

(150) Li, G.; Dong, H.; Ma, Y.; Shao, K.; Li, Y.; Wu, X.; Wang, S.; Shao, Y.; Zhao, W. *Bioorganic Med. Chem. Lett.* **2019**, *29* (16), 2327.

(151) Hall, A. W.; Taylor, R. J. K.; Simmonds, S. H.; Strange, P. G. *J. Med. Chem.* **1987**, *30* (10), 1879.

(152) Shen, Y.; Feng, X.; Li, Y.; Zhang, G.; Jiang, Y. *Synlett* **2002**, *2002* (5), 793.

(153) Burns, J. A.; Whitesides, G. M. *J. Am. Chem. Soc.* **1990**, *112* (17), 6296.

(154) Muth, C. W.; Steiniger, D. O.; Papanastassiou, Z. B. *J. Am. Chem. Soc.* **1952**, *77* (7), 1006.

(155) Das, S.; Möller, K.; Junge, K.; Beller, M. *Chem. - A Eur. J.* **2011**, *17* (27), 7414.

(156) Lowen, G. T.; Almond, M. R.; Rideout, J. L. . *J. Heterocycl. Chem.* **1992**, *29* (6), 1663.

(157) Hawes, E. M.; Davis, H. L. *J. Heterocycl. Chem.* **1973**, *10*, 39.

(158) Sortino, M.; Zacchino, S. A. *Tetrahedron Asymmetry* **2010**, *21* (5), 535.

(159) Perecim, G. P.; Rodrigues, A.; Raminelli, C. *Tetrahedron Lett.* **2015**, *56* (49), 6848.

(160) Ha-Duong, N.-T.; Dijols, S.; Marques-Soares, C.; Minoletti, C.; Dansette, P. M.; Mansuy, D. *J. Med. Chem.* **2001**, *44* (22), 3622.

(161) Miller, B. Y. E.; Sprague, J. M.; Mcburney, F.; Sprague, J. M. *J. Am. Chem. Soc.* **1940**, *62* (8), 209.

(162) Wu;, G.-S.; Martinelli;, L. C.; Blanton, C. D. J. .; H., C. R. *J. Heterocycl. Chem.* **1977**, *14*, 11.

(163) Szostak, M.; Spain, M.; Procter, D. J. *Org. Lett.* **2012**, *14* (3), 840.

(164) Donslund, A. S.; Neumann, K. T.; Corneliussen, N. P.; Grove, E. K.; Herbstritt, D.; Daasbjerg, K.; Skrydstrup, T. *Chem. - A Eur. J.* **2019**, *25* (42), 9856.

(165) Goulet, M.; Wyvratt, M. J.; Lin, P.; Chu, L.; Girotra, N. N. US6156767A, 2000.

(166) Akhter, S.; Lund, B. A.; Ismael, A.; Langer, M.; Isaksson, J.; Christopeit, T.; Leiros, H. K. S.; Bayer, A. *Eur. J. Med. Chem.* **2018**, *145*, 634.

(167) Herth, M. M.; Hansen, H. D.; Ettrup, A.; Dyssegaard, A.; Lehel, S.; Kristensen, J.; Knudsen, G. M. *Bioorganic Med. Chem.* **2012**, *20* (14), 4574.

Appendix

NMR Spectra

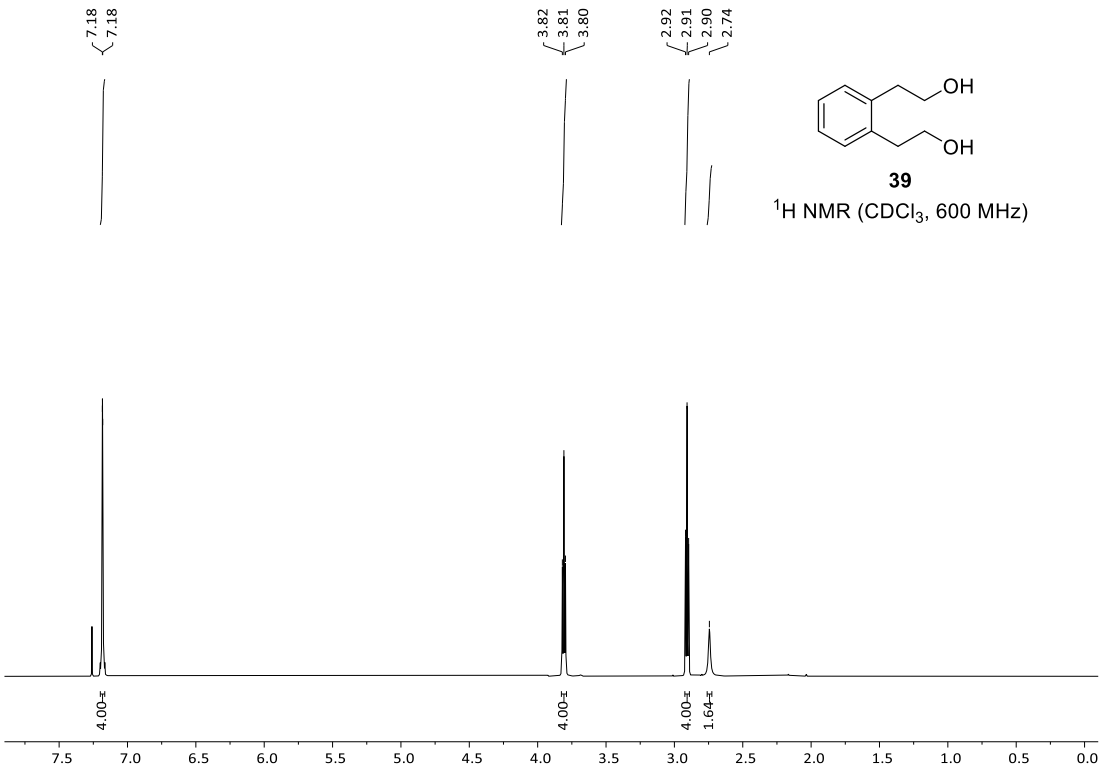

39

^{1}H NMR ($CDCl_3$, 600 MHz)

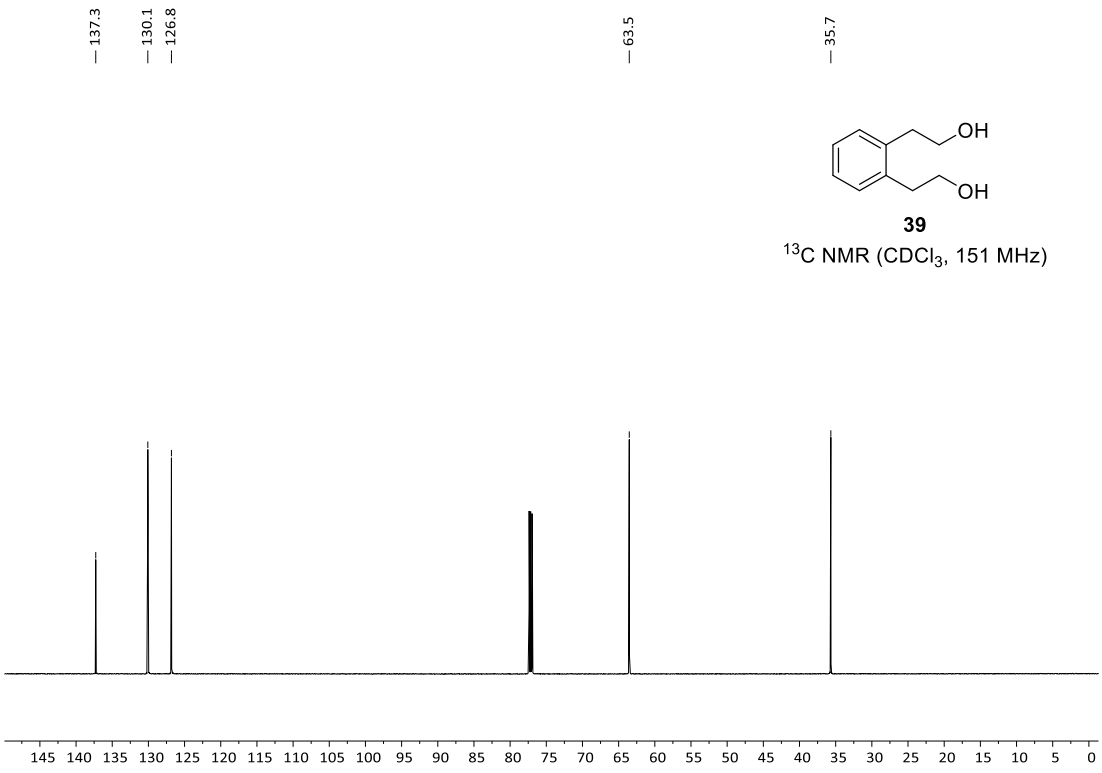

39

^{13}C NMR ($CDCl_3$, 151 MHz)

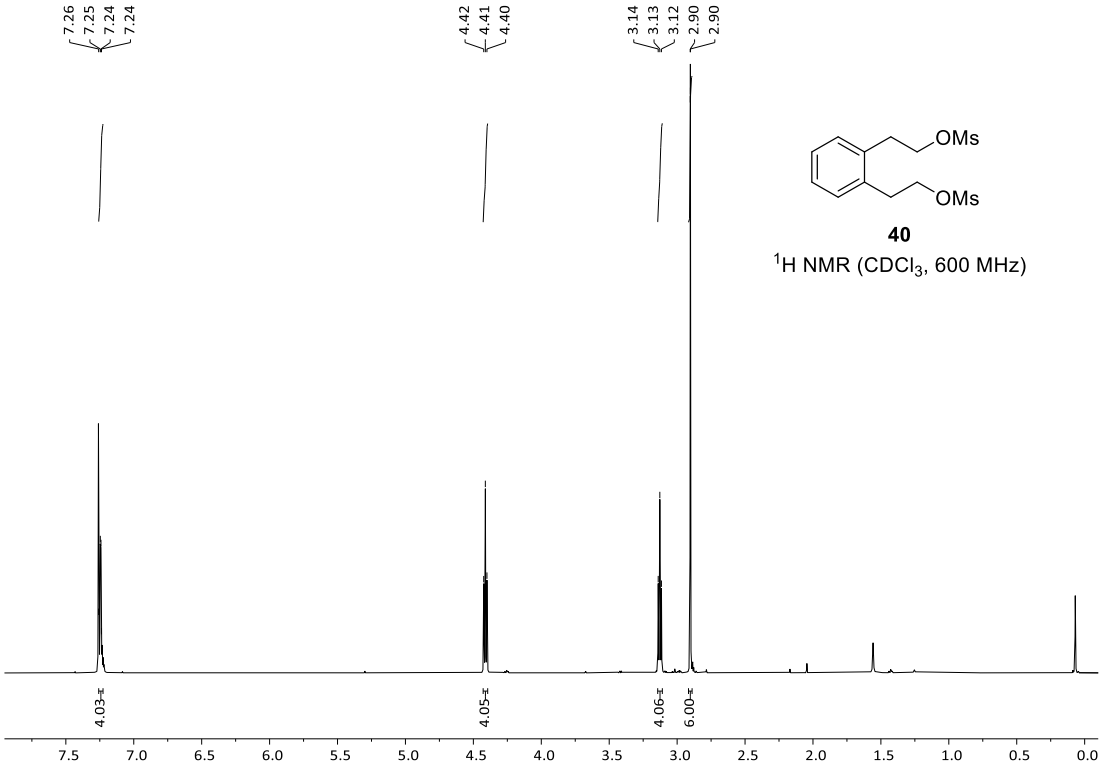

40

^{1}H NMR ($CDCl_3$, 600 MHz)

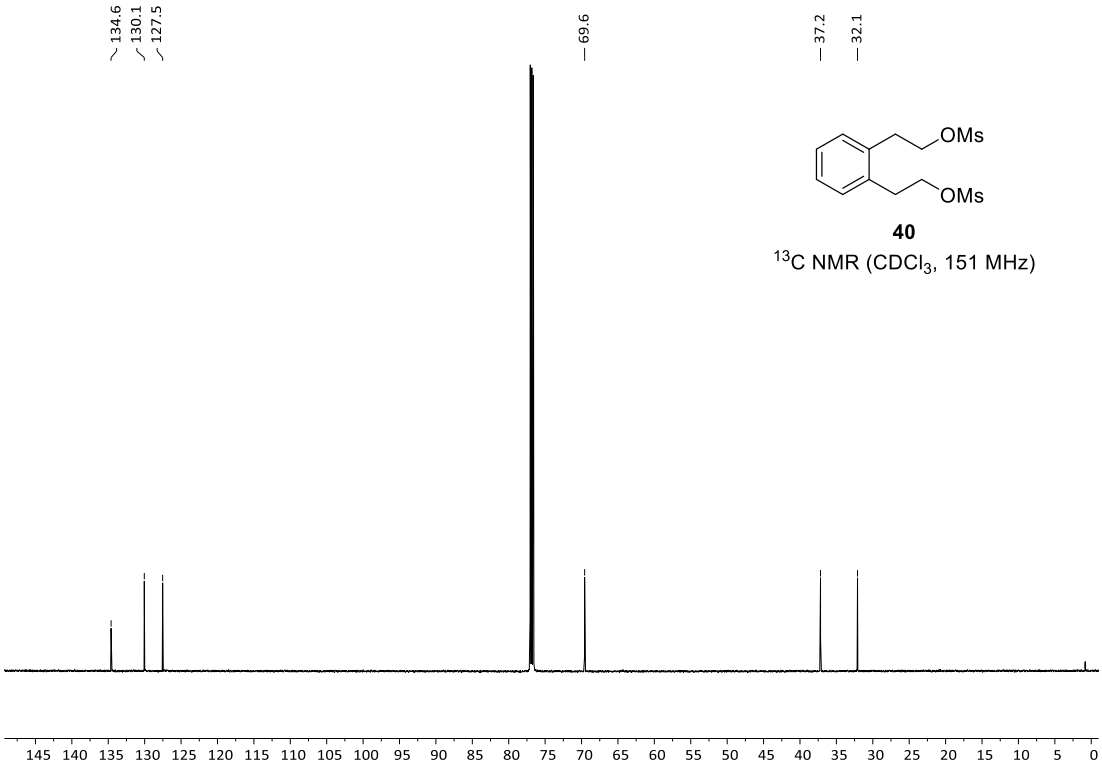

40

^{13}C NMR ($CDCl_3$, 151 MHz)

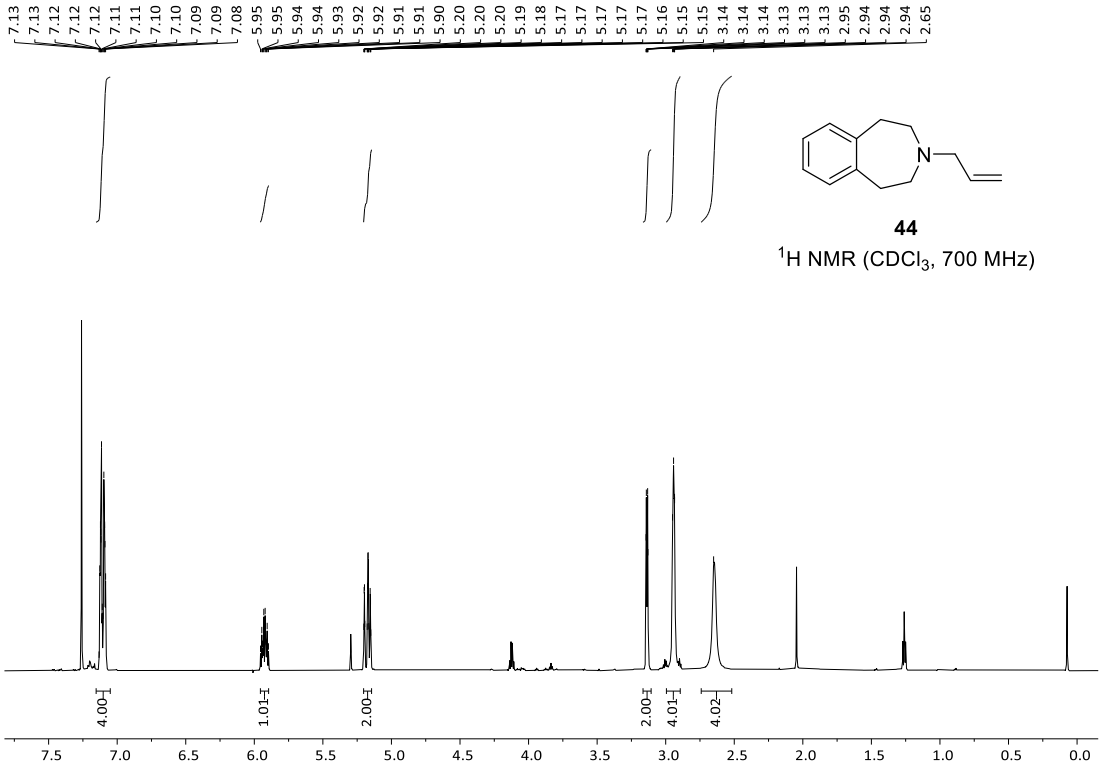

44

^{1}H NMR ($CDCl_3$, 700 MHz)

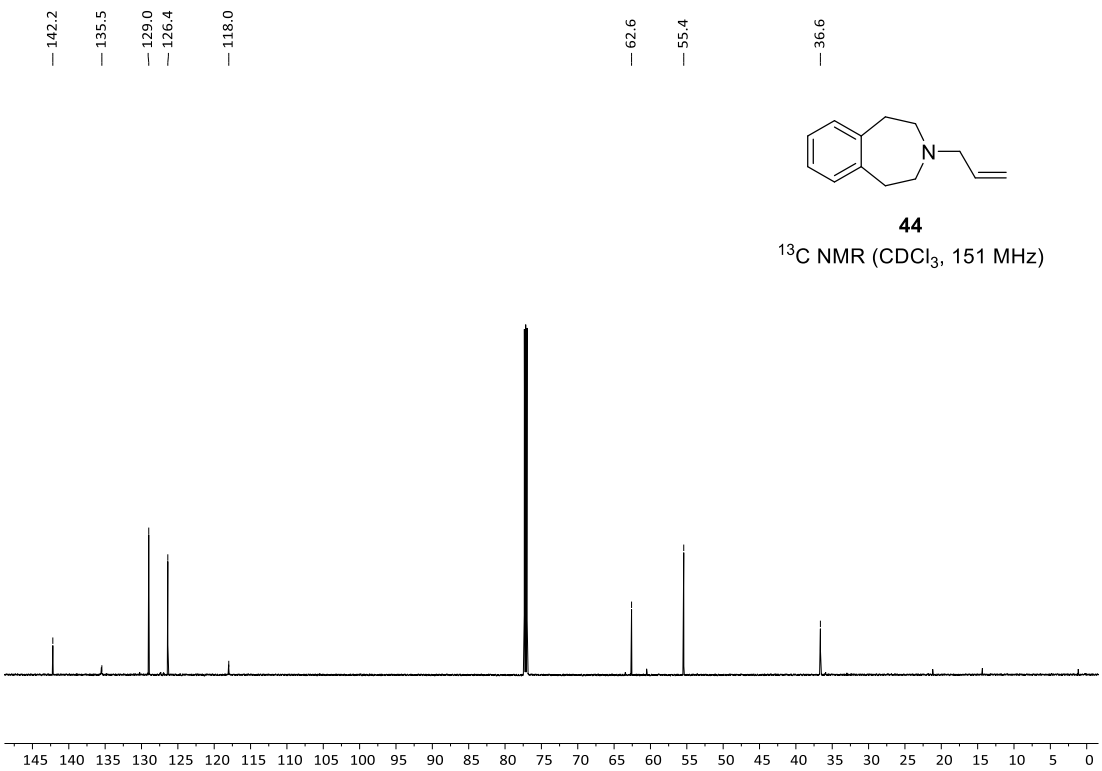

44

^{13}C NMR ($CDCl_3$, 151 MHz)

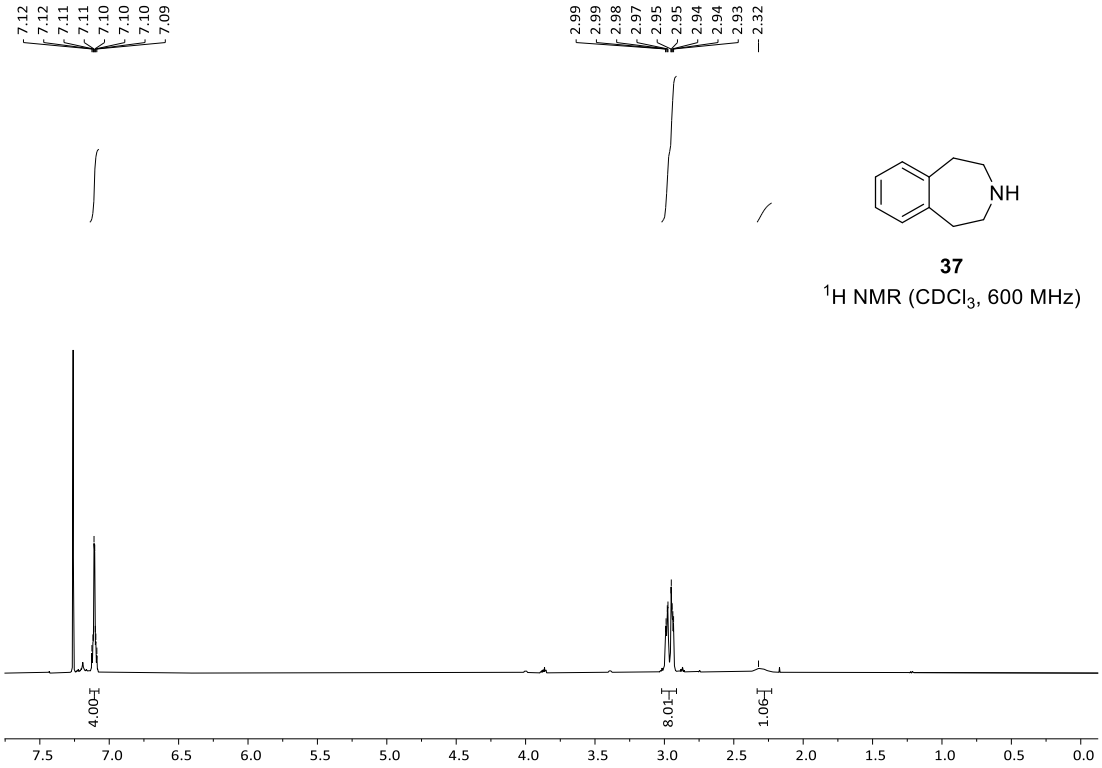

37

^{1}H NMR ($CDCl_3$, 600 MHz)

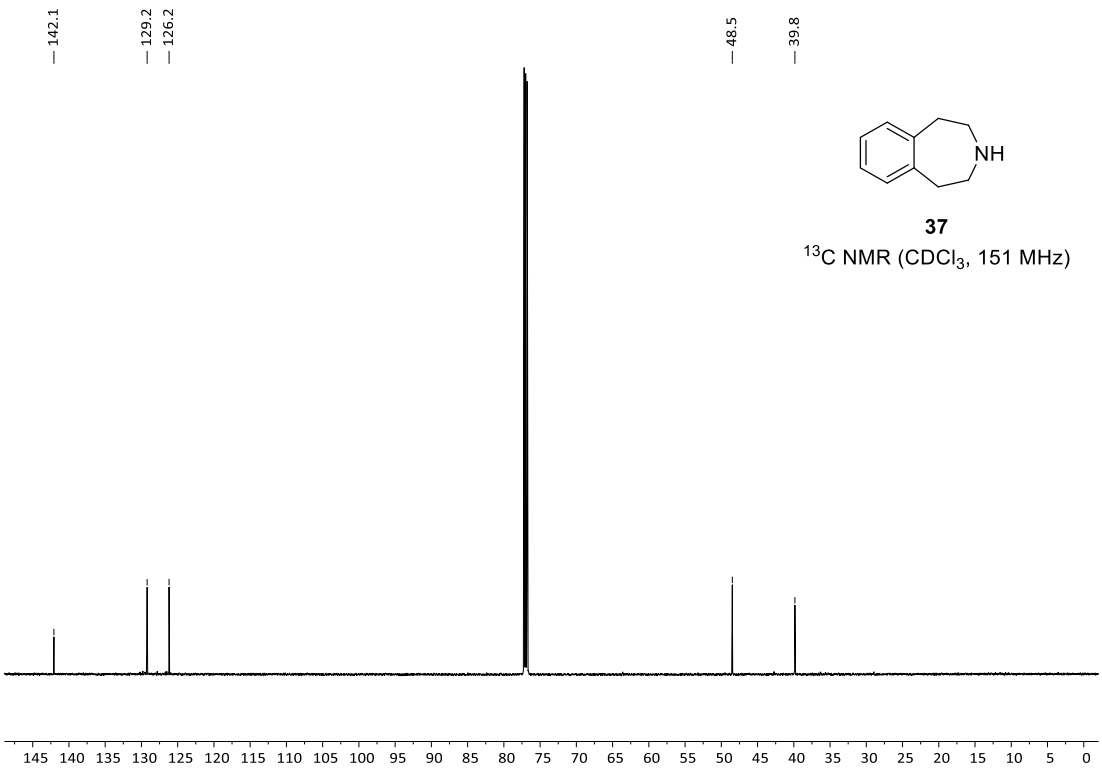

37

^{13}C NMR ($CDCl_3$, 151 MHz)

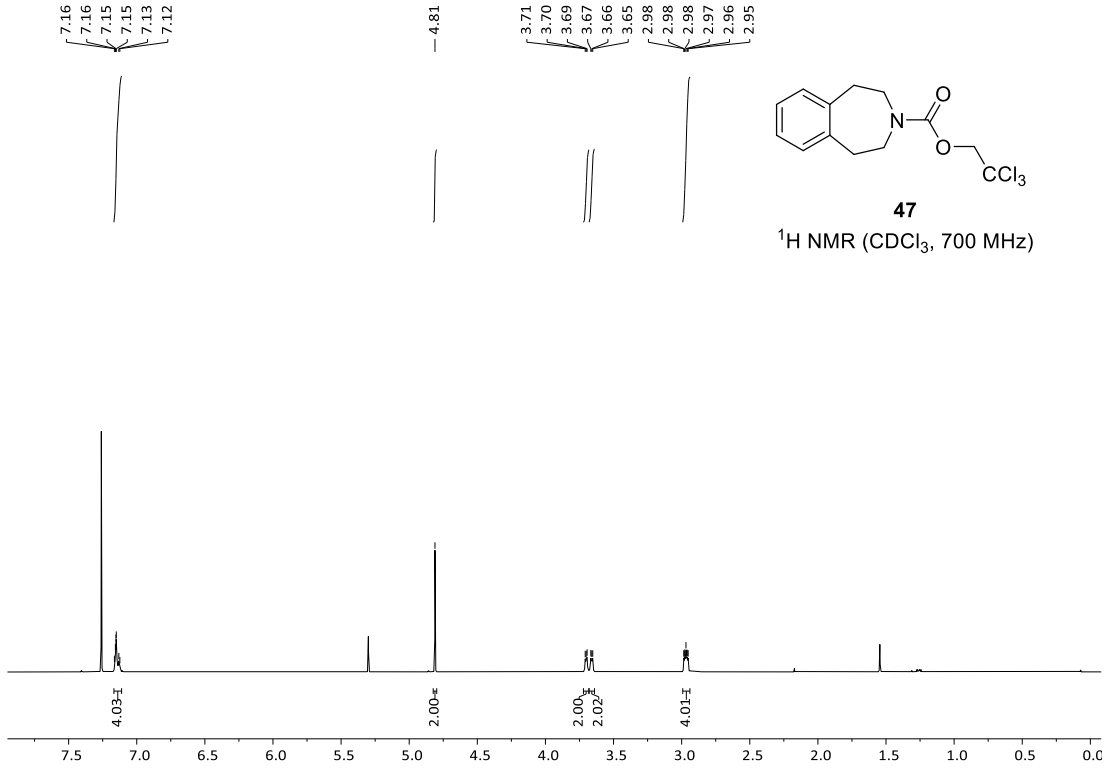

47

^{1}H NMR ($CDCl_3$, 700 MHz)

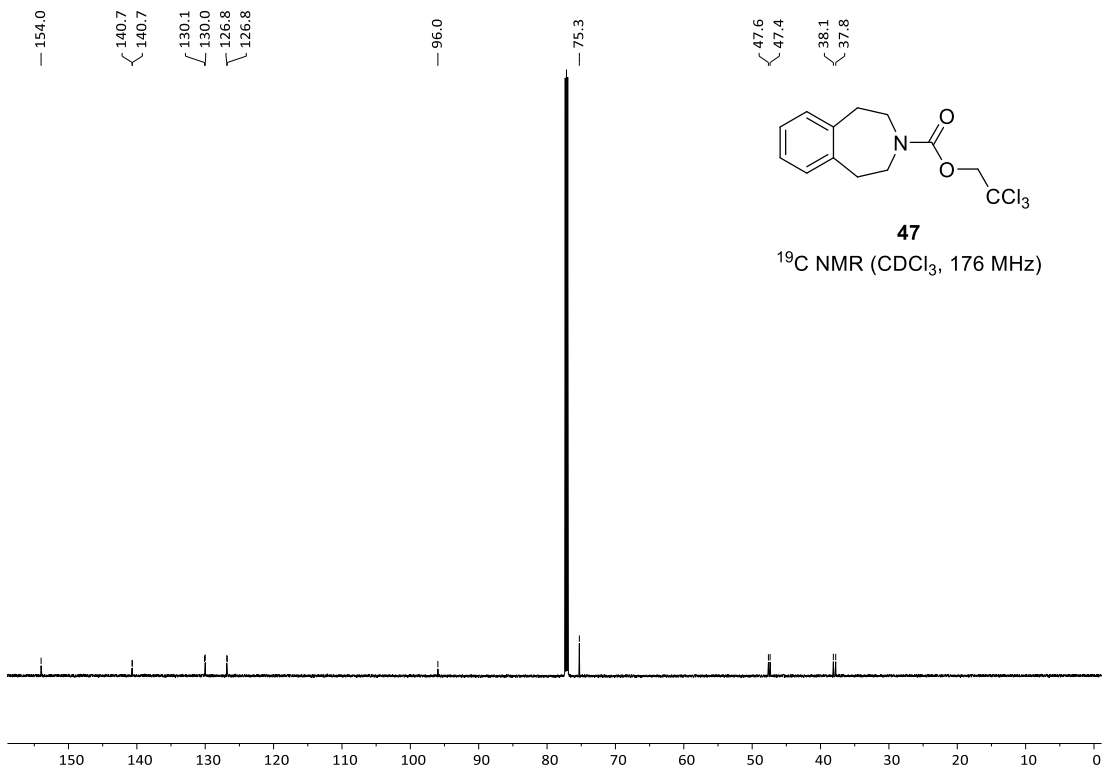

47

^{19}C NMR ($CDCl_3$, 176 MHz)

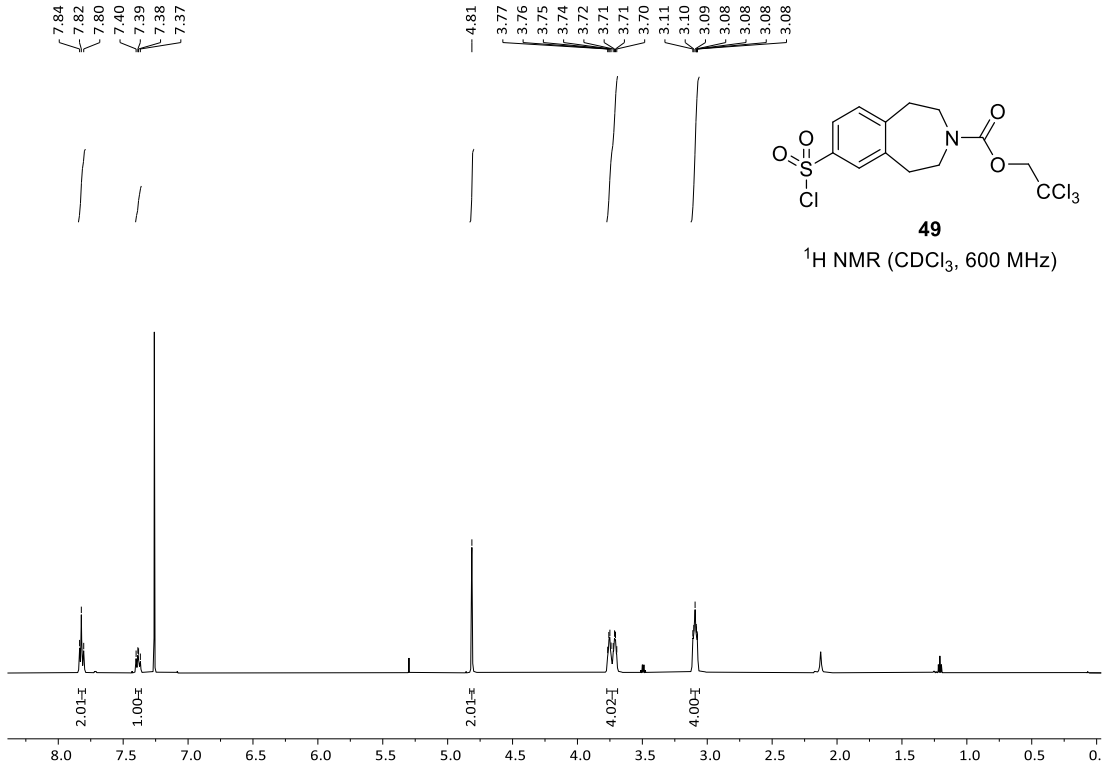

49

^{1}H NMR ($CDCl_3$, 600 MHz)

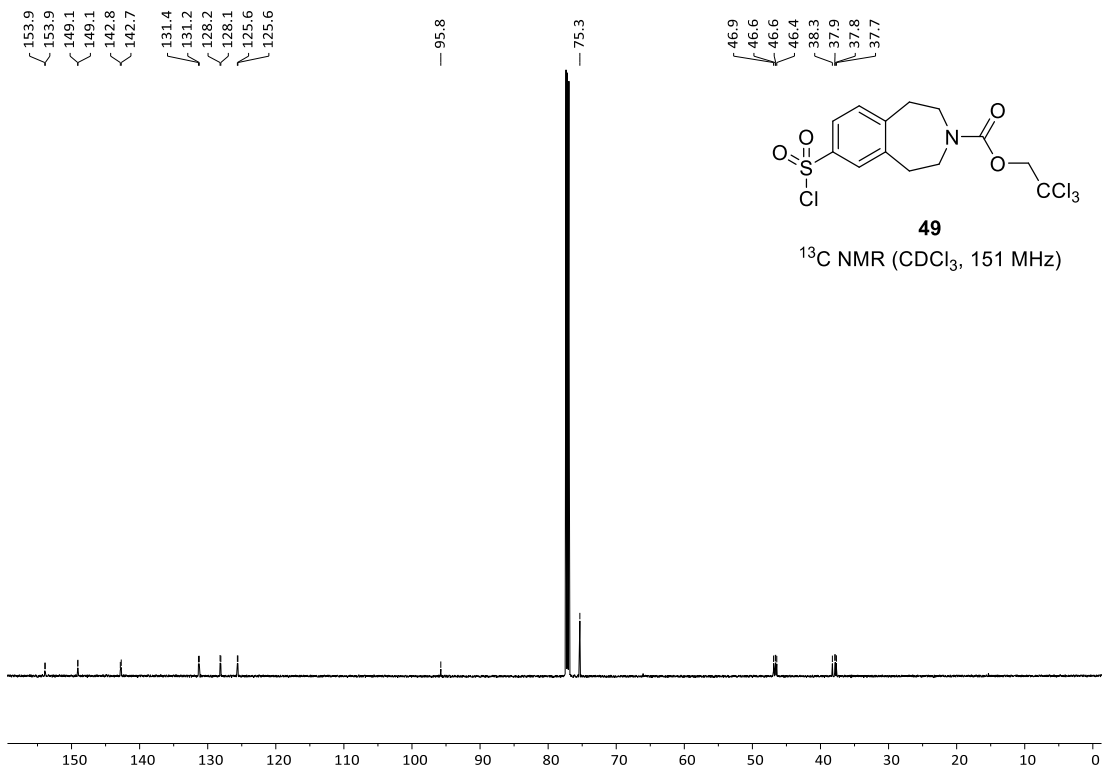

49

^{13}C NMR ($CDCl_3$, 151 MHz)

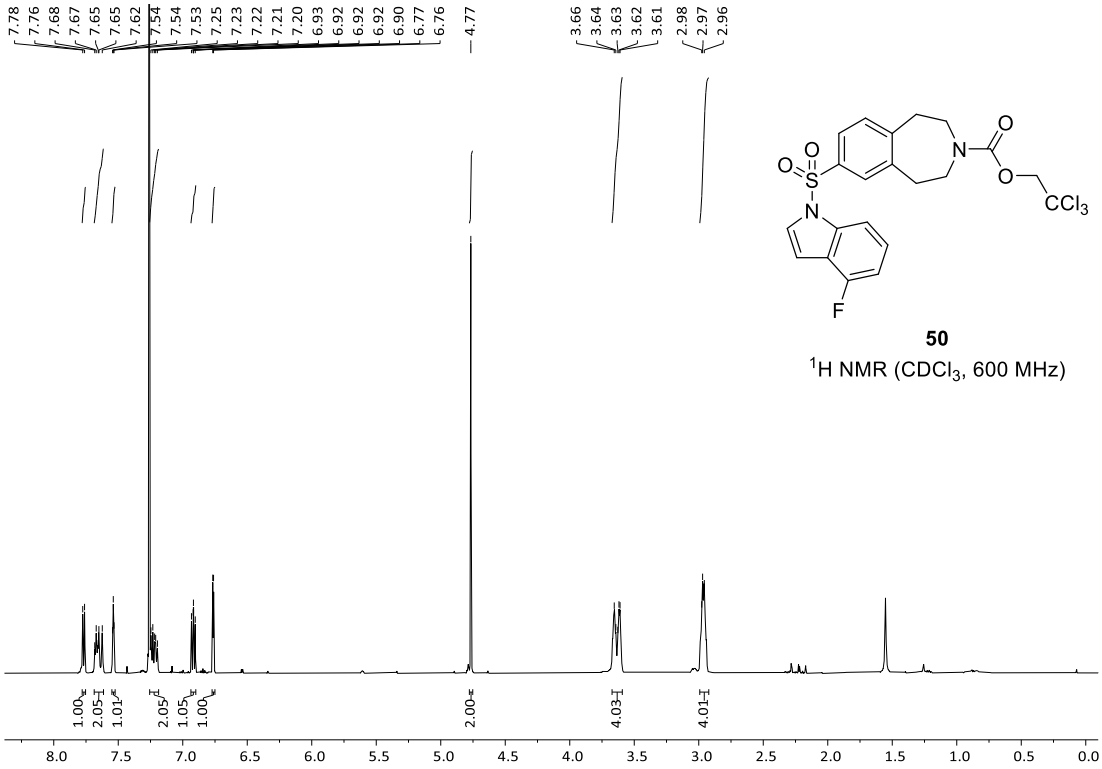

50

^{1}H NMR ($CDCl_3$, 600 MHz)

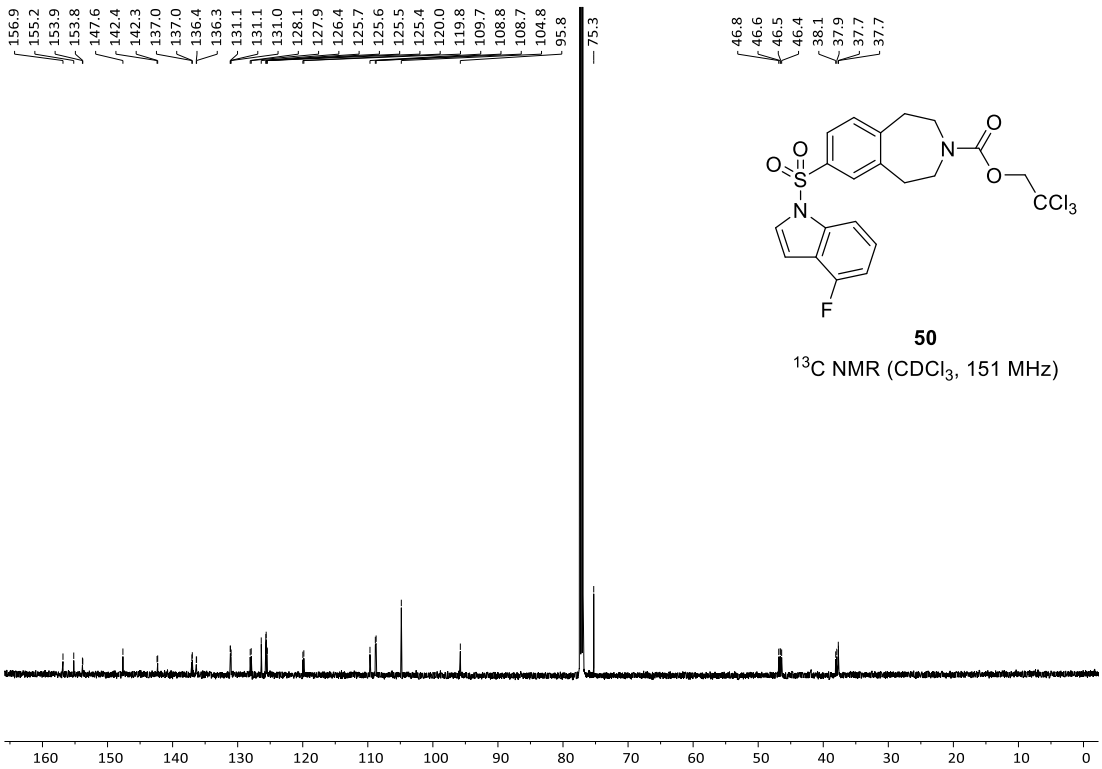

50

^{13}C NMR ($CDCl_3$, 151 MHz)

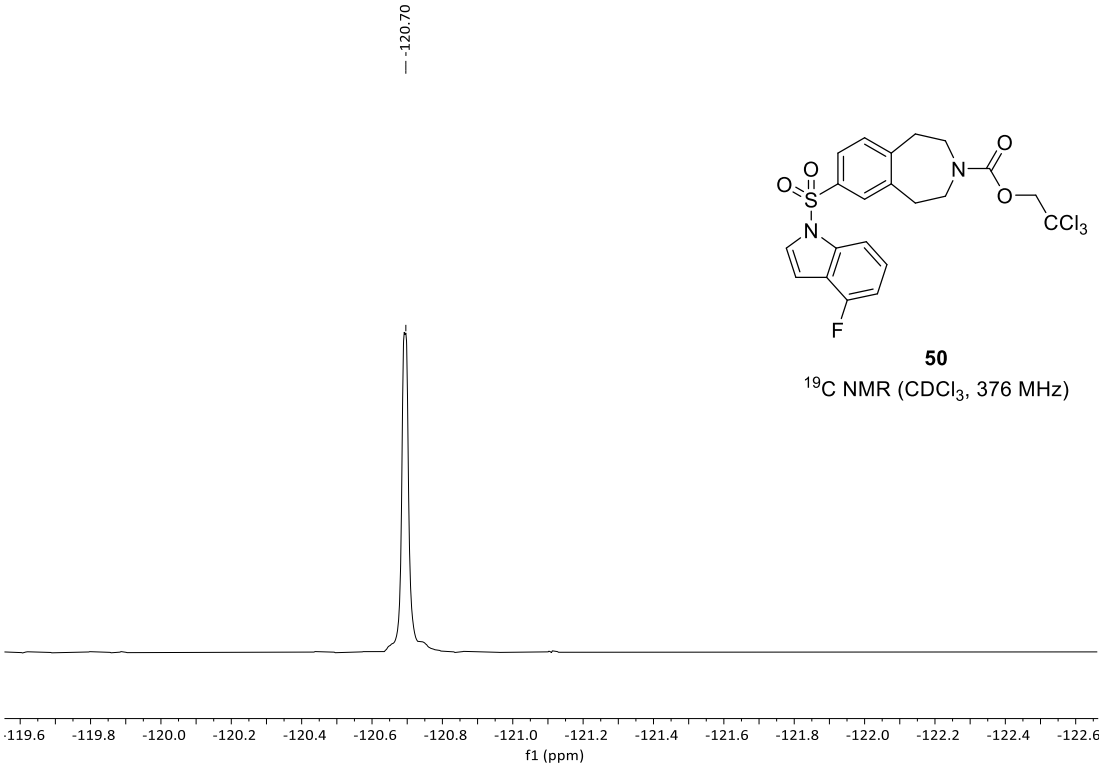

50

^{19}C NMR ($CDCl_3$, 376 MHz)

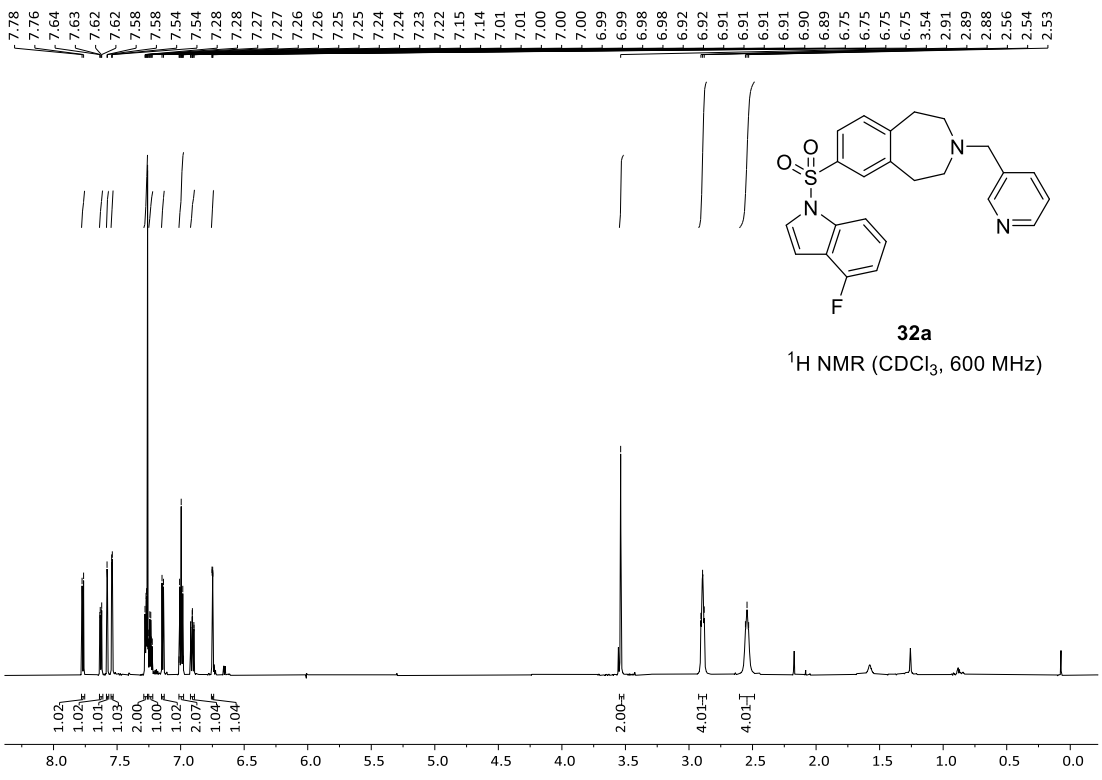

32a

^{1}H NMR ($CDCl_3$, 600 MHz)

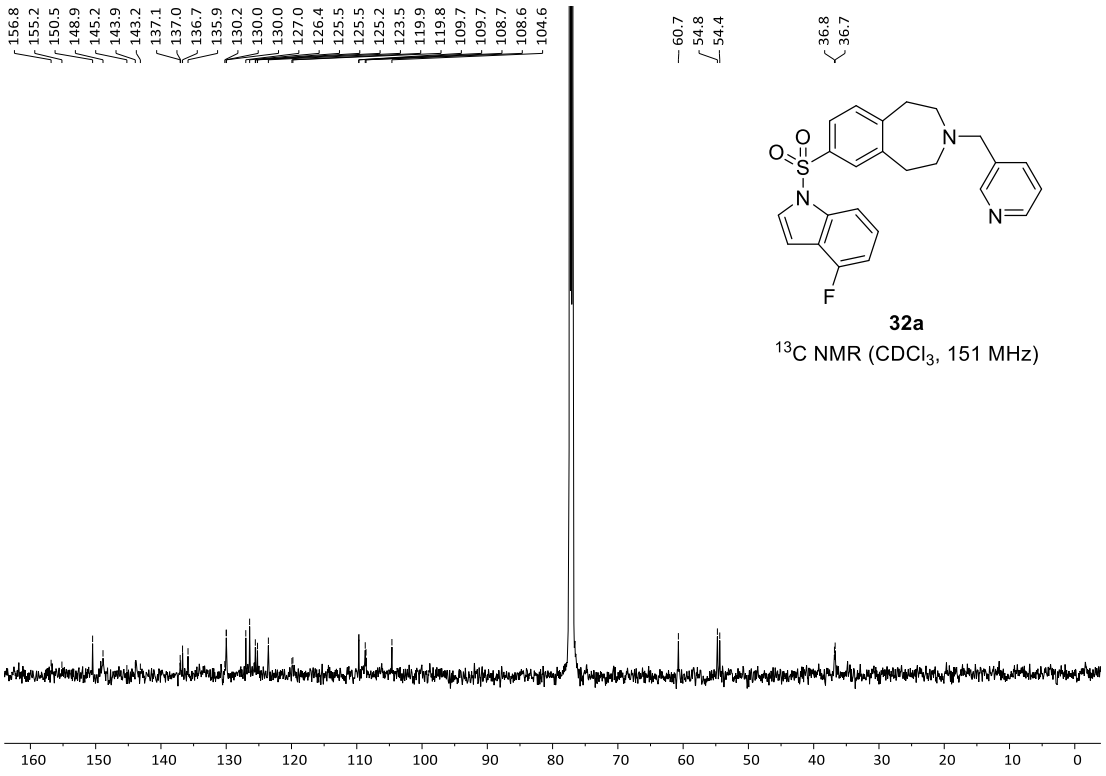

32a

^{13}C NMR ($CDCl_3$, 151 MHz)

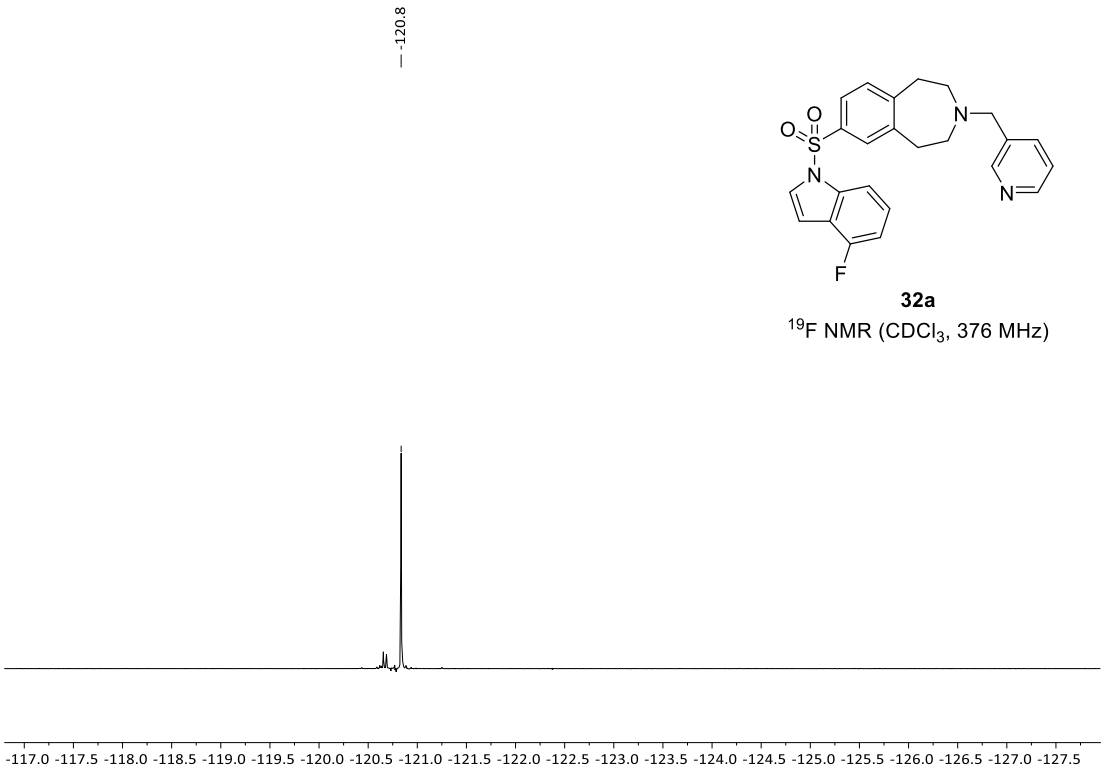

32a

^{19}F NMR ($CDCl_3$, 376 MHz)

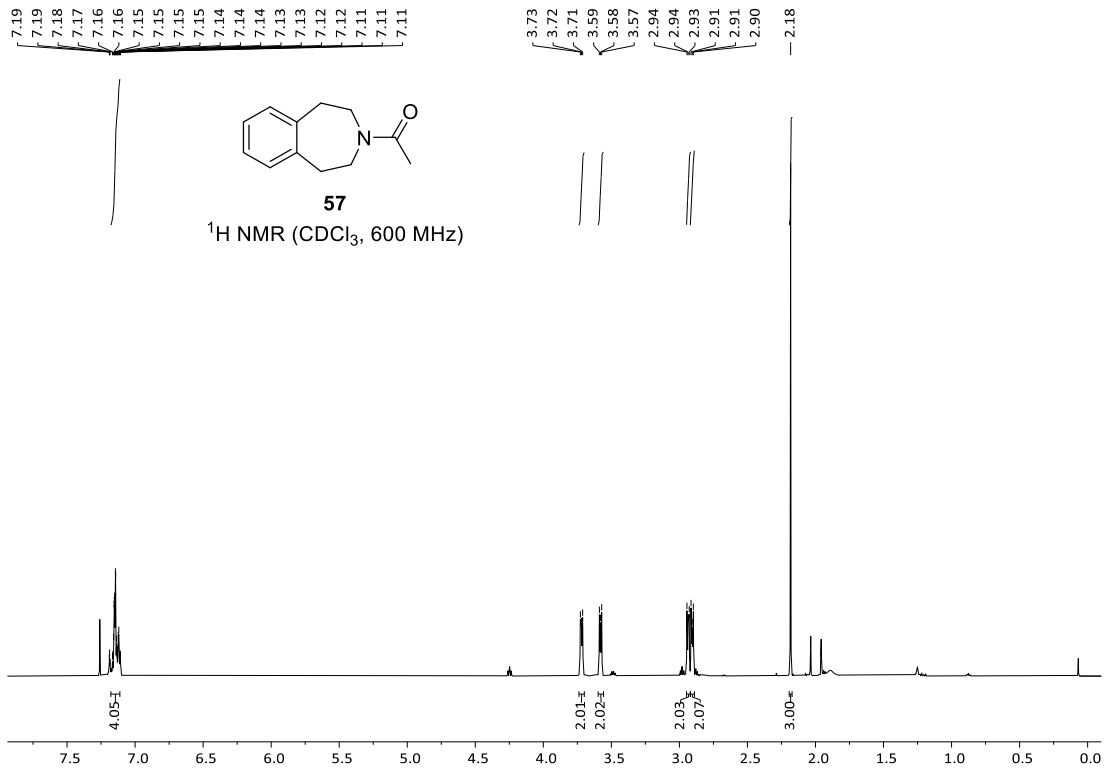

57

^{1}H NMR ($CDCl_3$, 600 MHz)

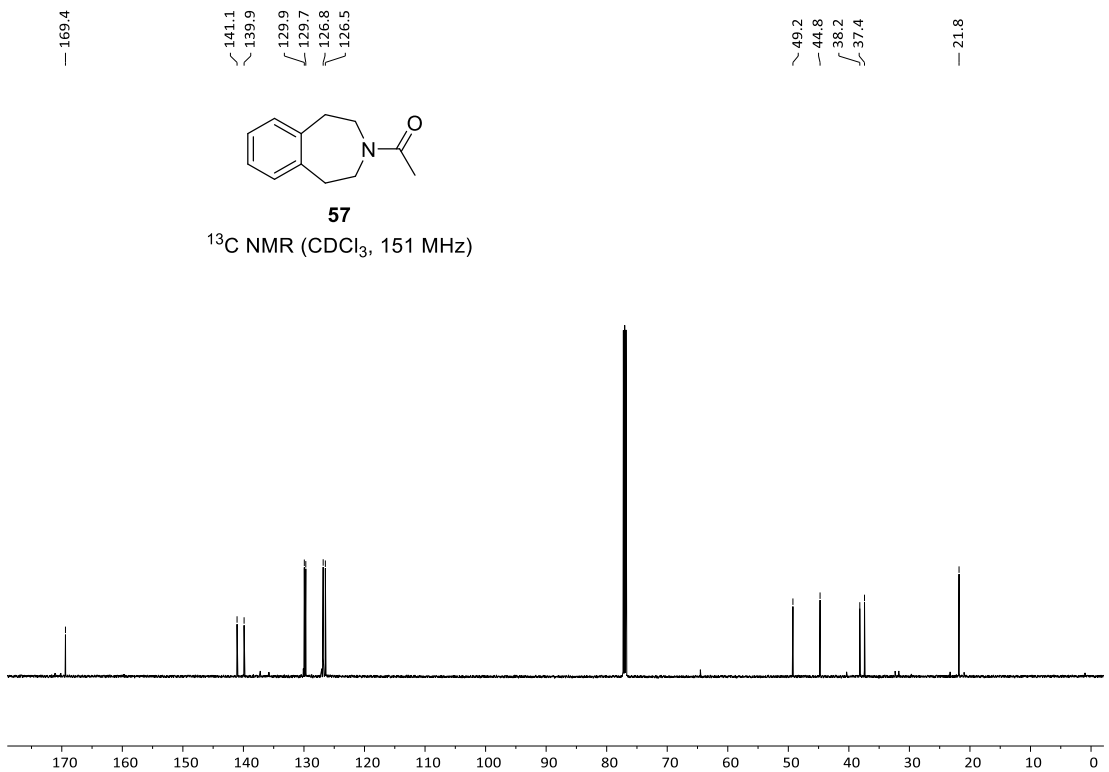

57

^{13}C NMR ($CDCl_3$, 151 MHz)

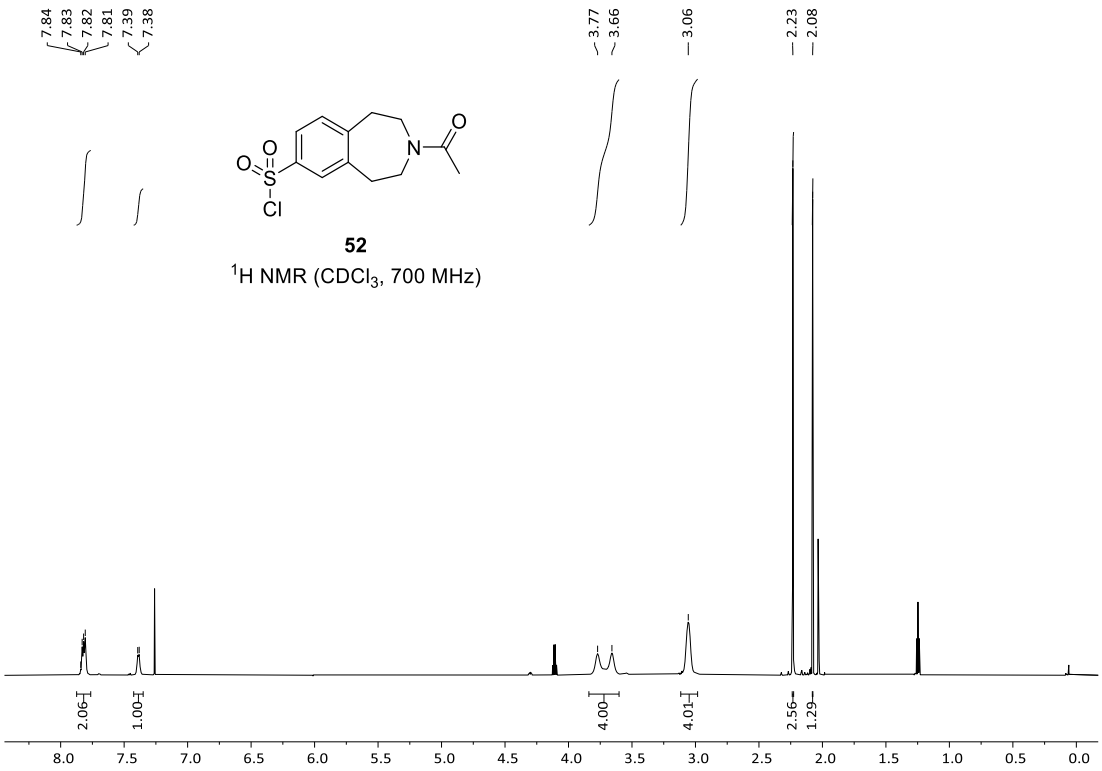

52

^{1}H NMR ($CDCl_3$, 700 MHz)

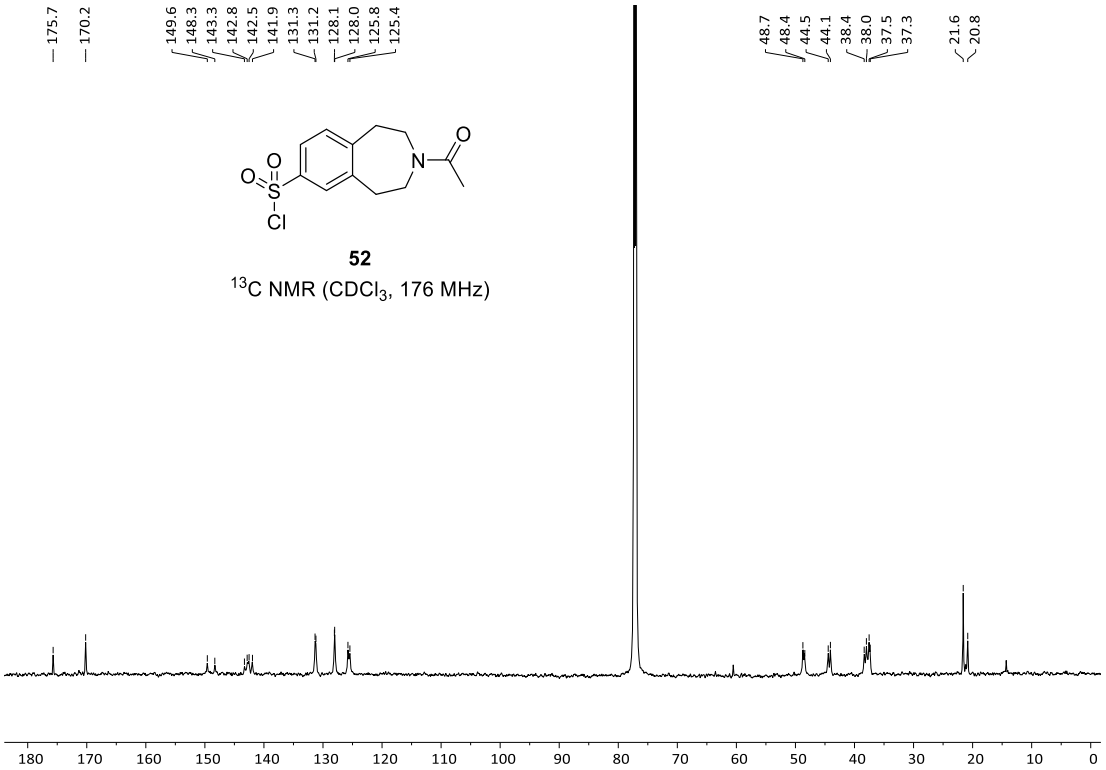

52

^{13}C NMR ($CDCl_3$, 176 MHz)

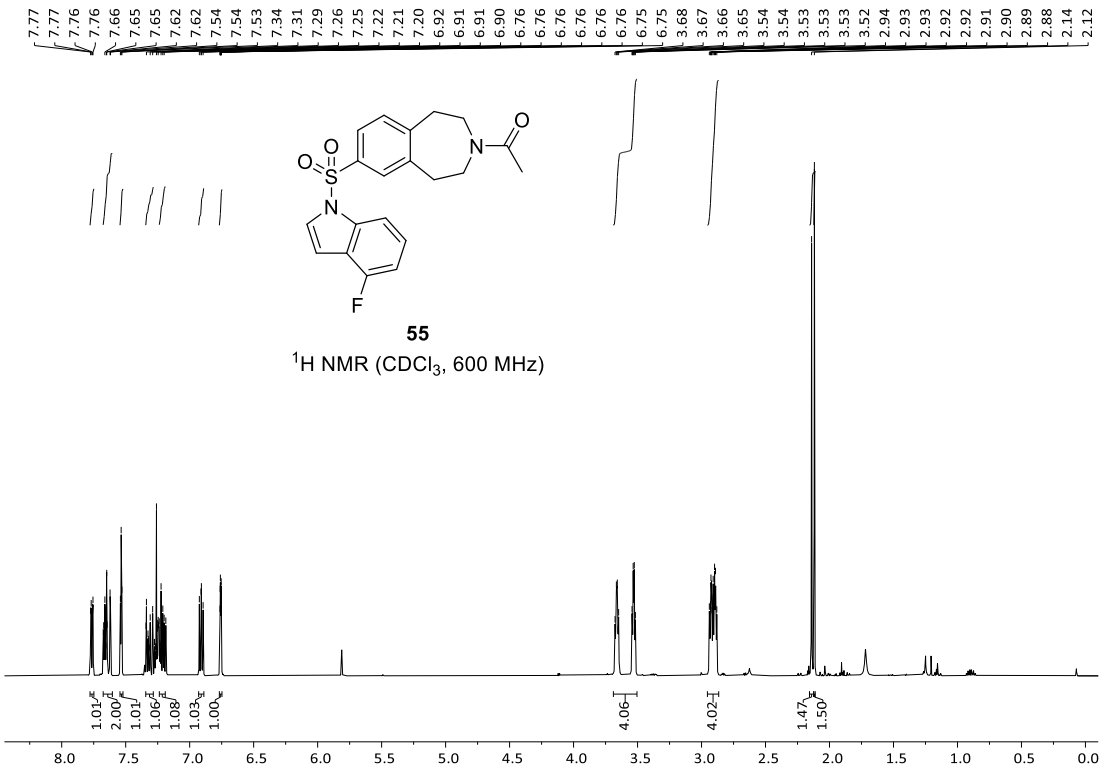

55

^{1}H NMR ($CDCl_3$, 600 MHz)

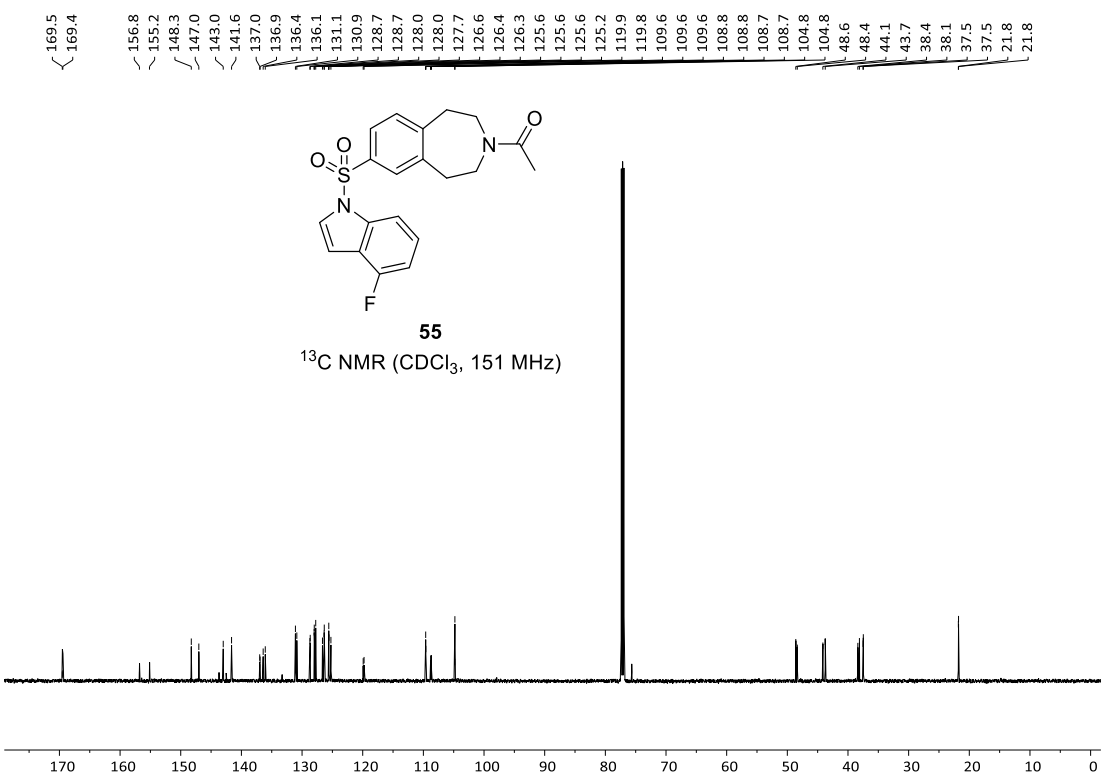

55

^{13}C NMR ($CDCl_3$, 151 MHz)

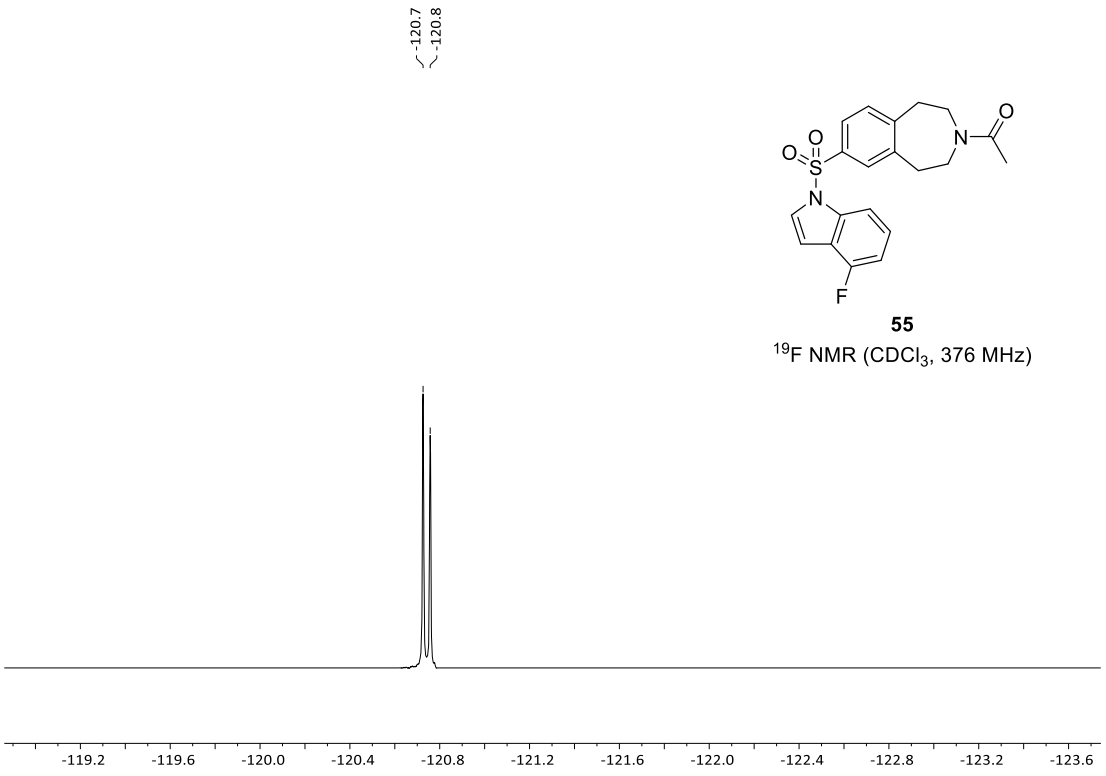

55

^{19}F NMR ($CDCl_3$, 376 MHz)

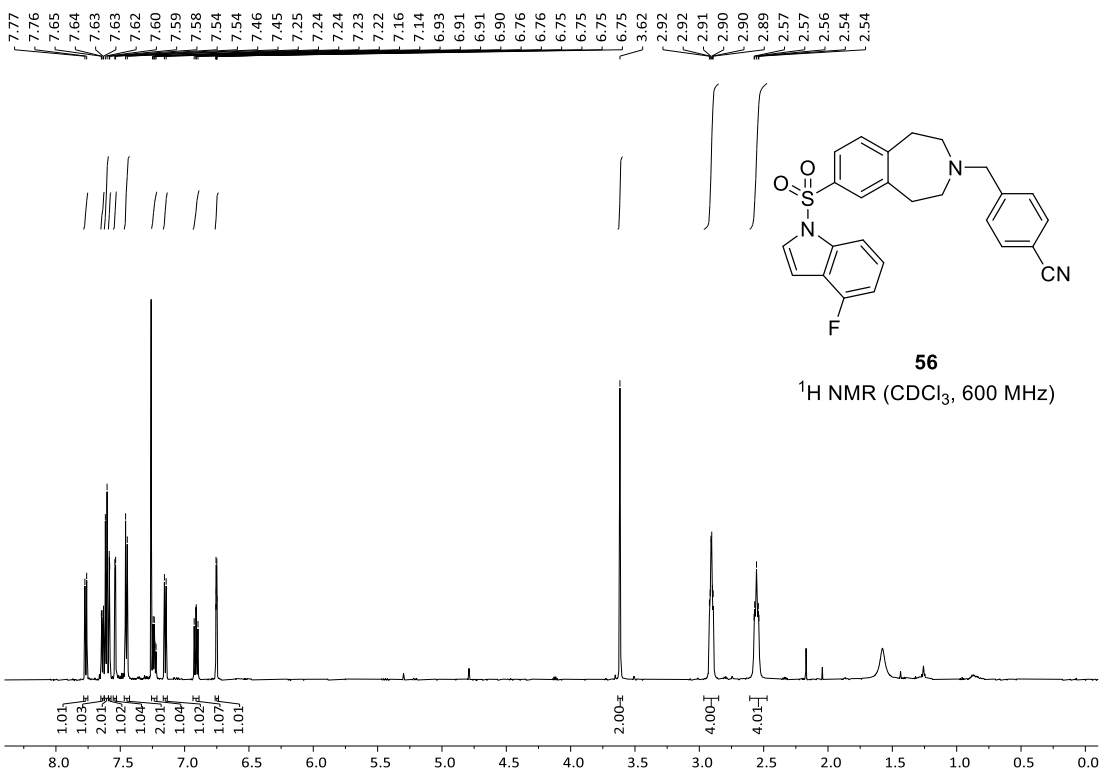

56

^{1}H NMR ($CDCl_3$, 600 MHz)

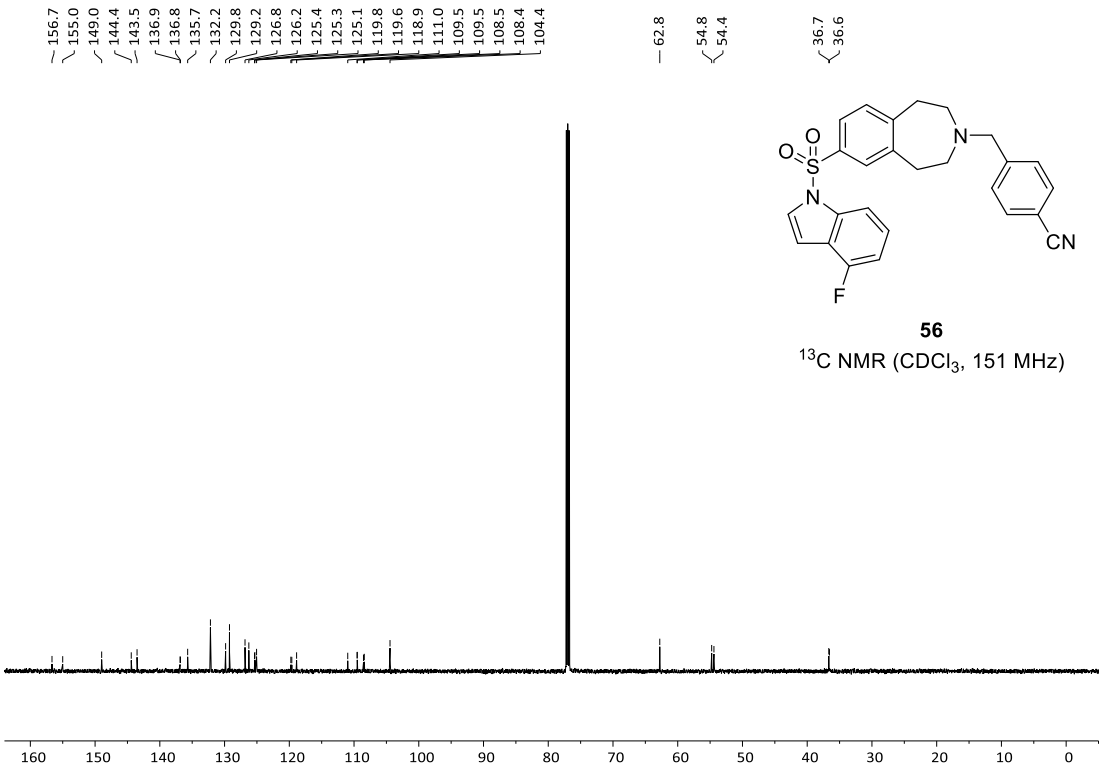

56

^{13}C NMR ($CDCl_3$, 151 MHz)

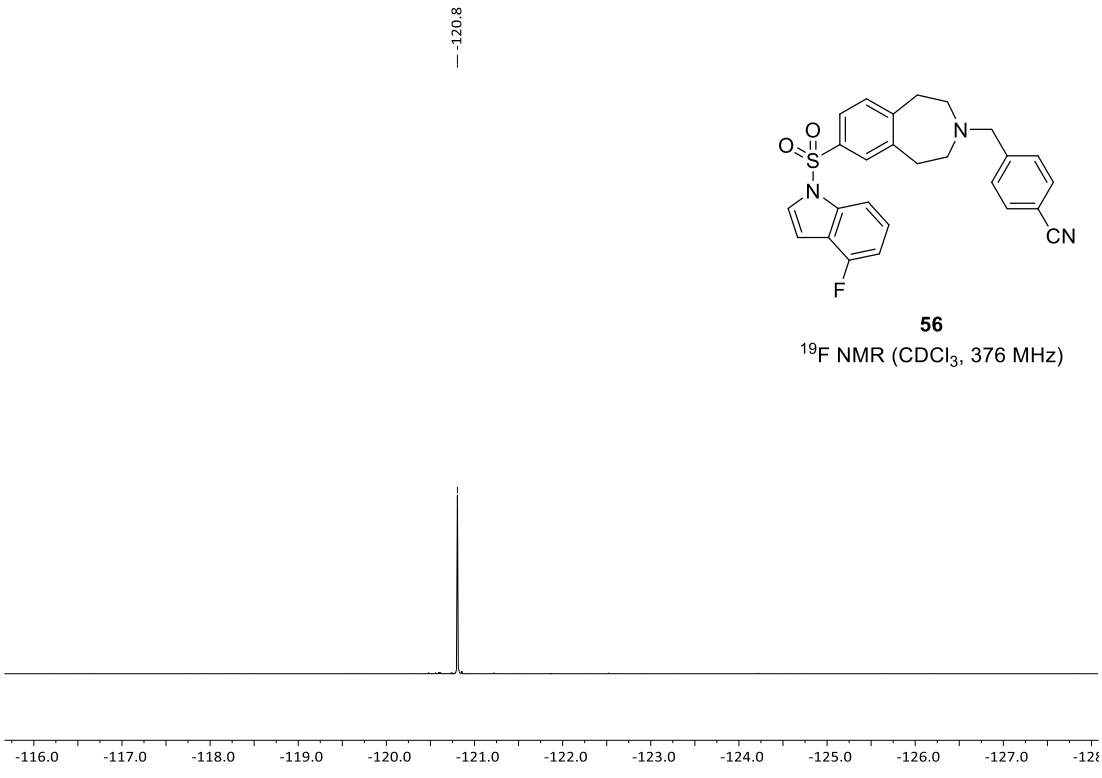

56

^{19}F NMR ($CDCl_3$, 376 MHz)

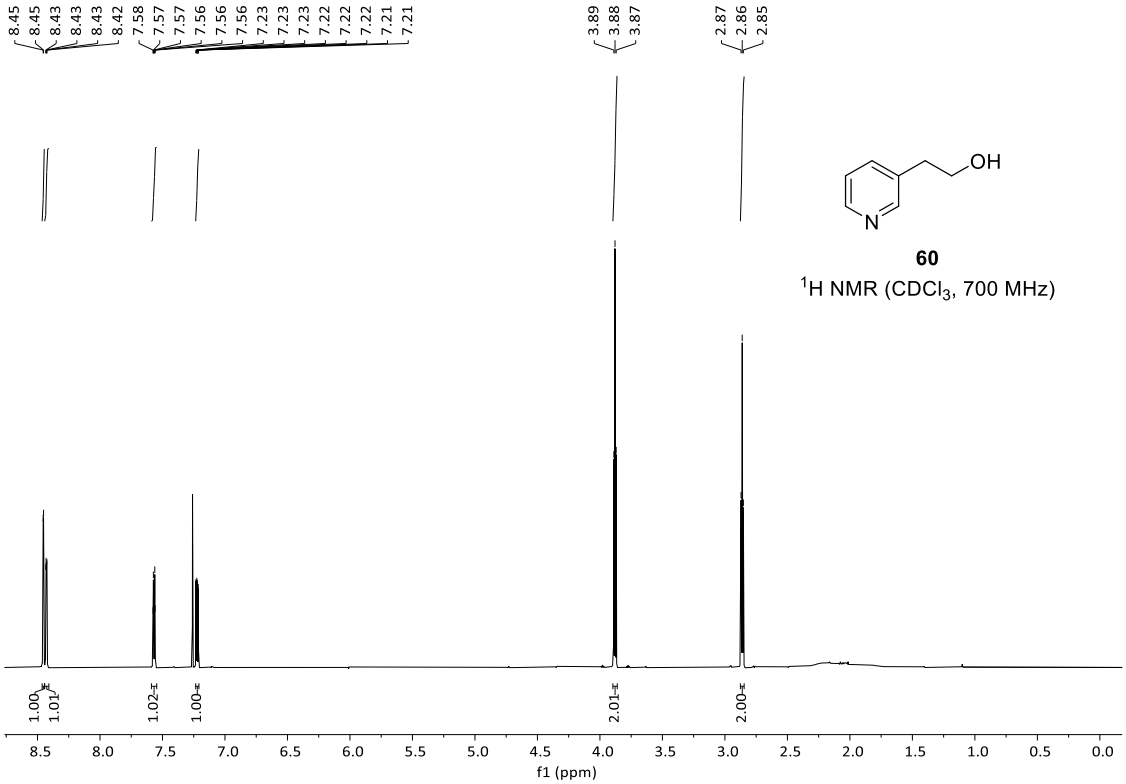

60

^{1}H NMR ($CDCl_3$, 700 MHz)

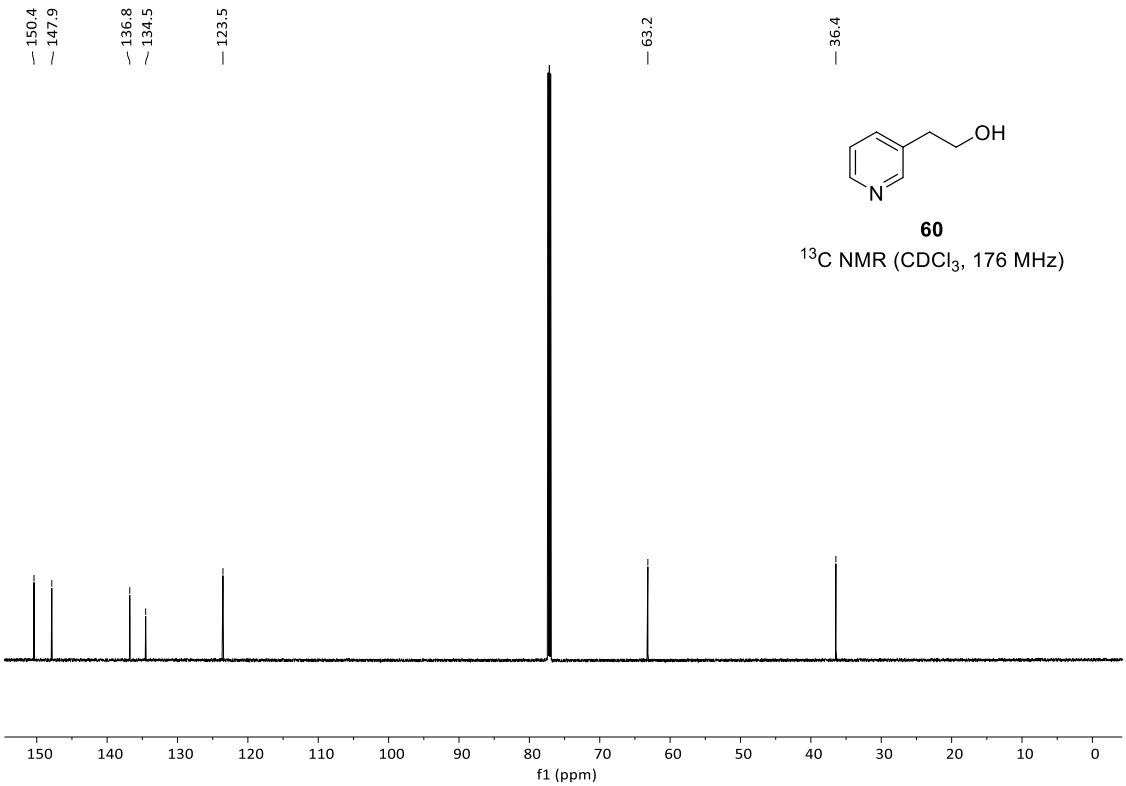

60

^{13}C NMR ($CDCl_3$, 176 MHz)

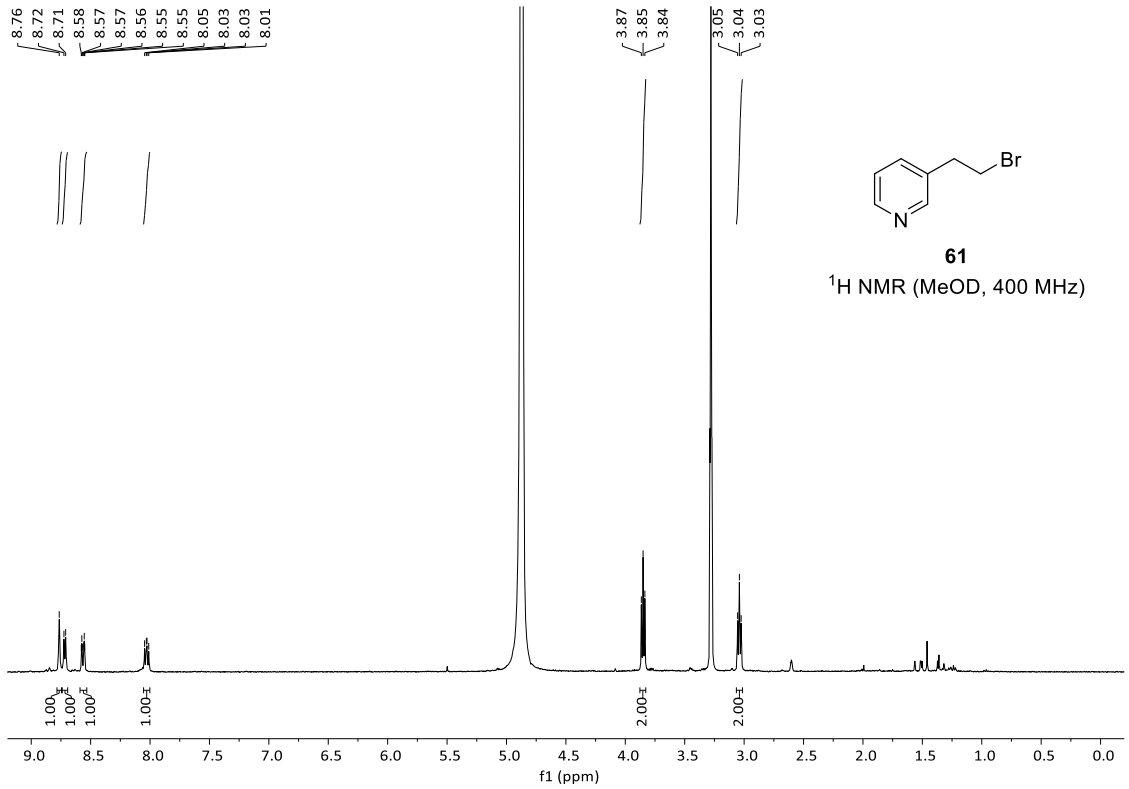

61

^{1}H NMR (MeOD, 400 MHz)

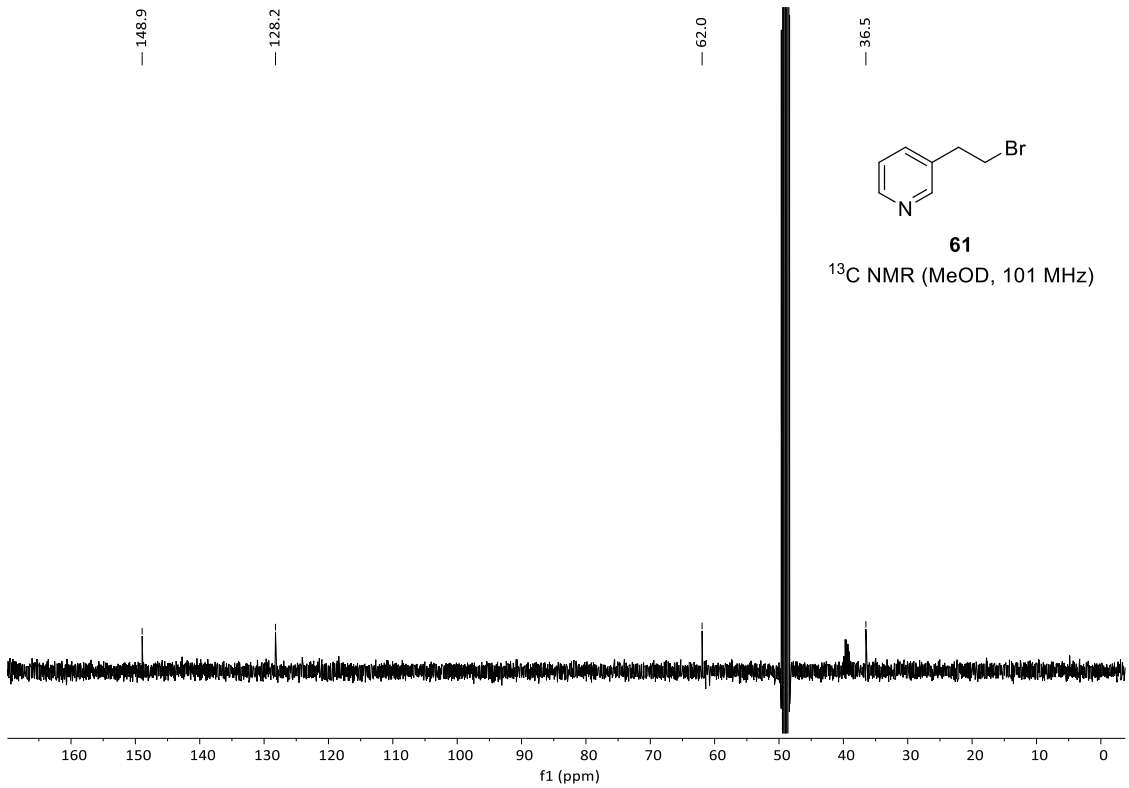

61

^{13}C NMR (MeOD, 101 MHz)

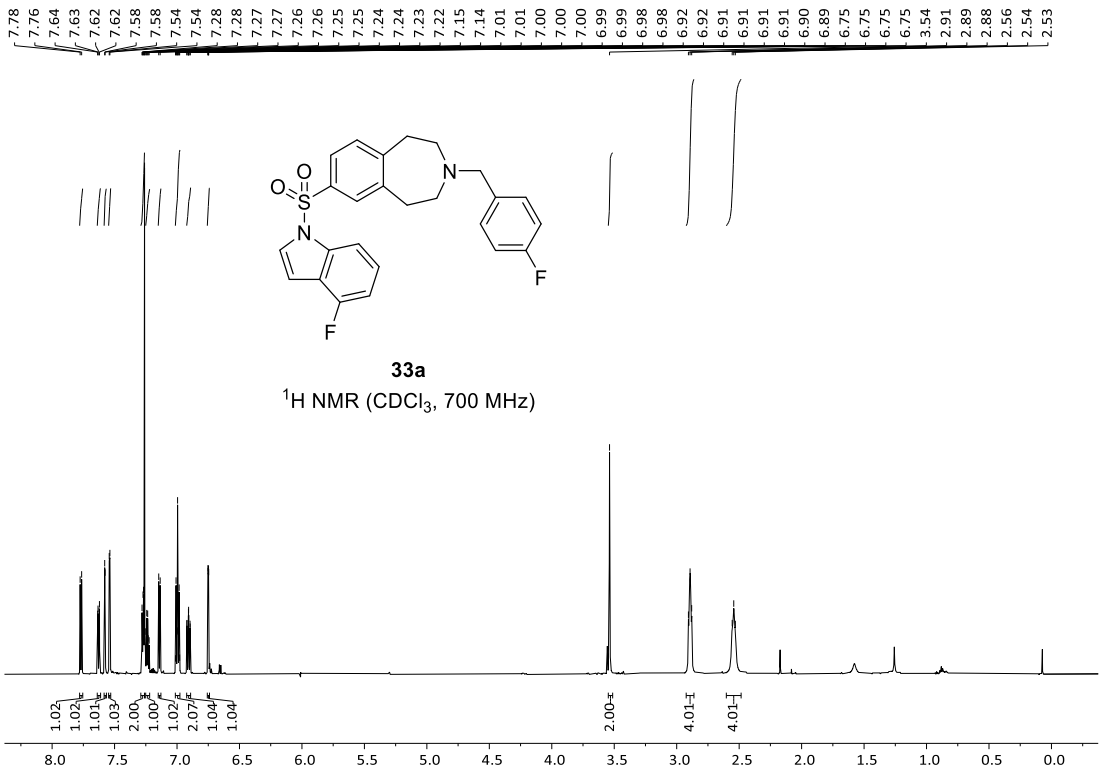

33a

^{1}H NMR ($CDCl_3$, 700 MHz)

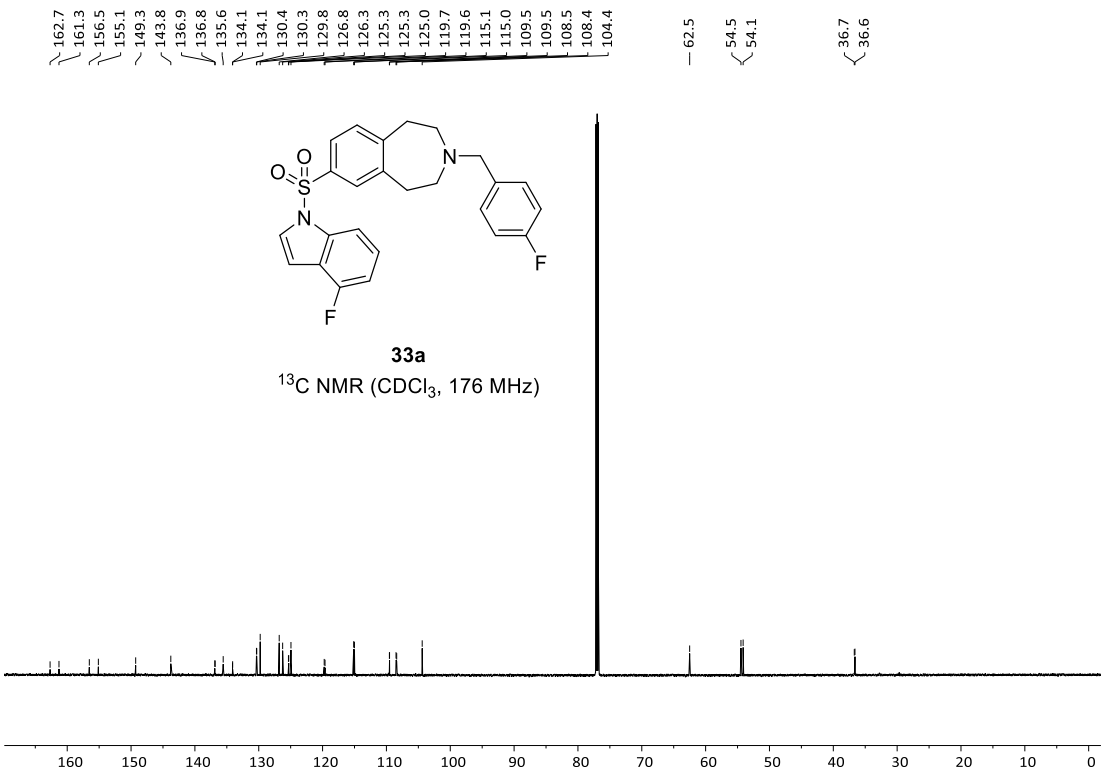

33a

^{13}C NMR ($CDCl_3$, 176 MHz)

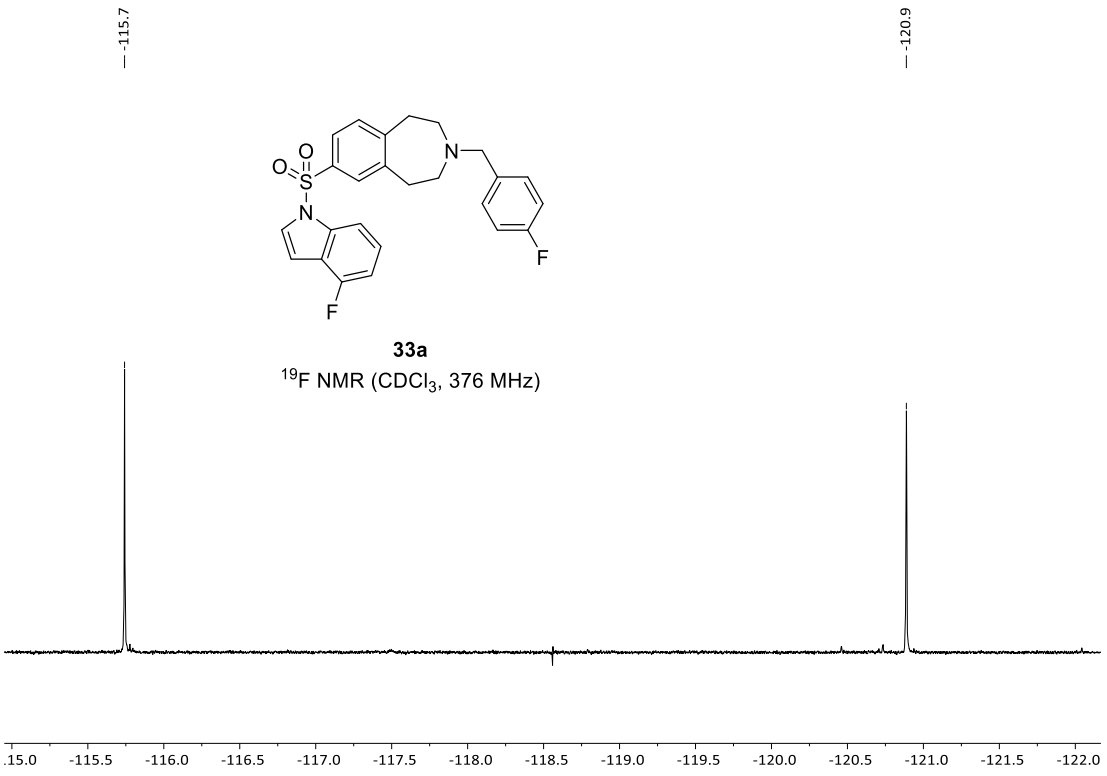

33a

^{19}F NMR ($CDCl_3$, 376 MHz)

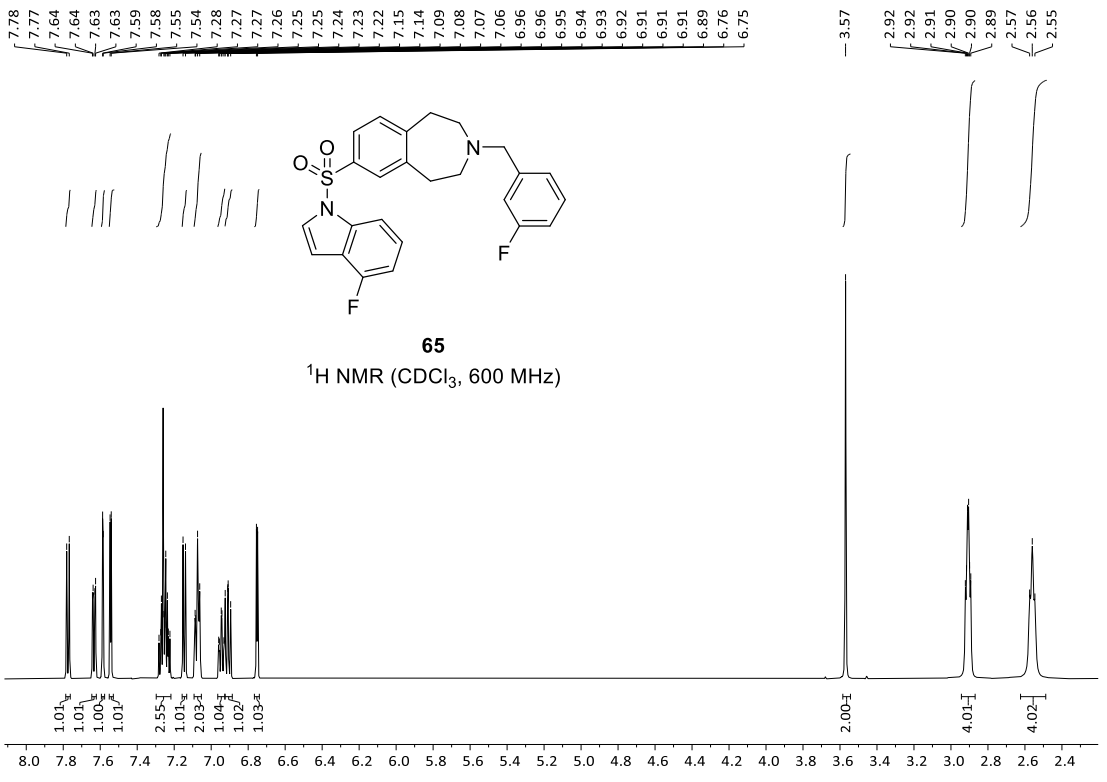

65

^{1}H NMR ($CDCl_3$, 600 MHz)

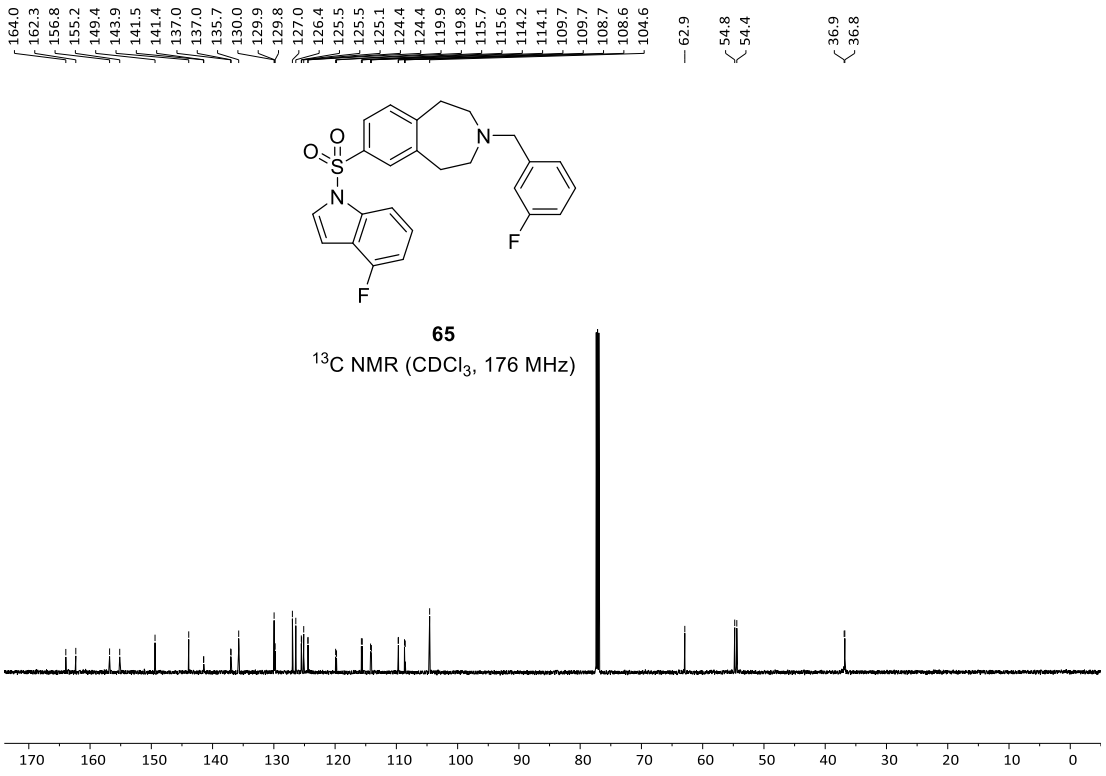

65

^{13}C NMR ($CDCl_3$, 176 MHz)

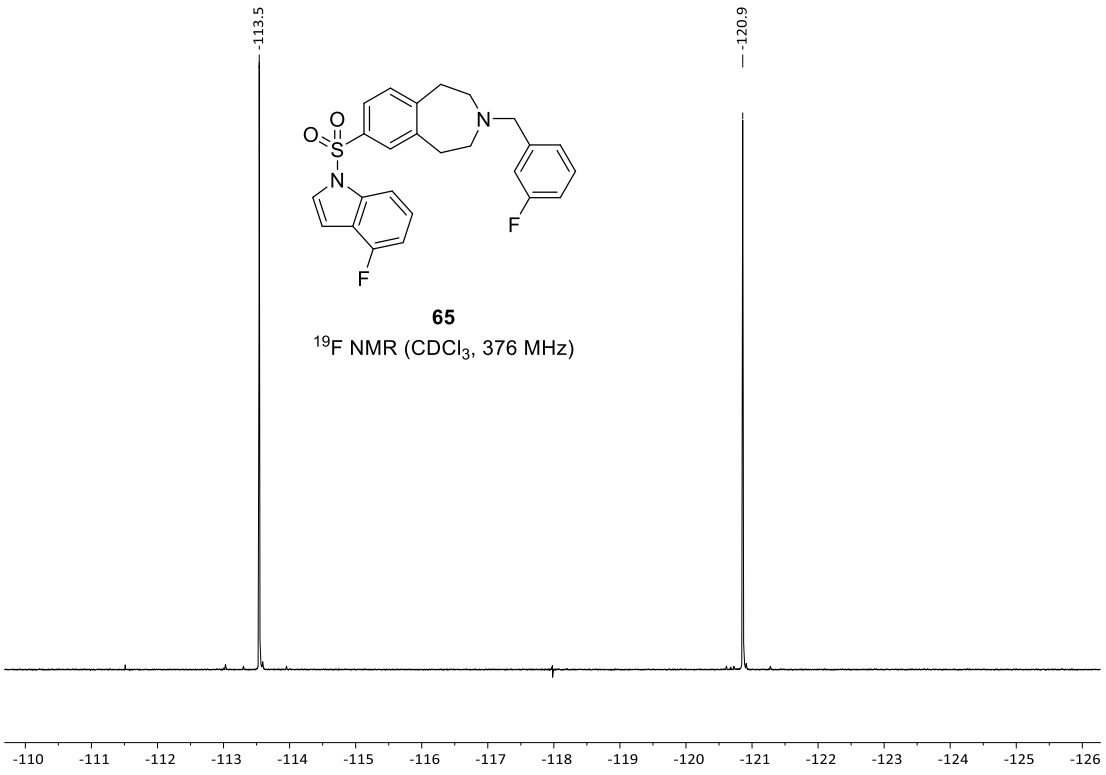

65

^{19}F NMR ($CDCl_3$, 376 MHz)

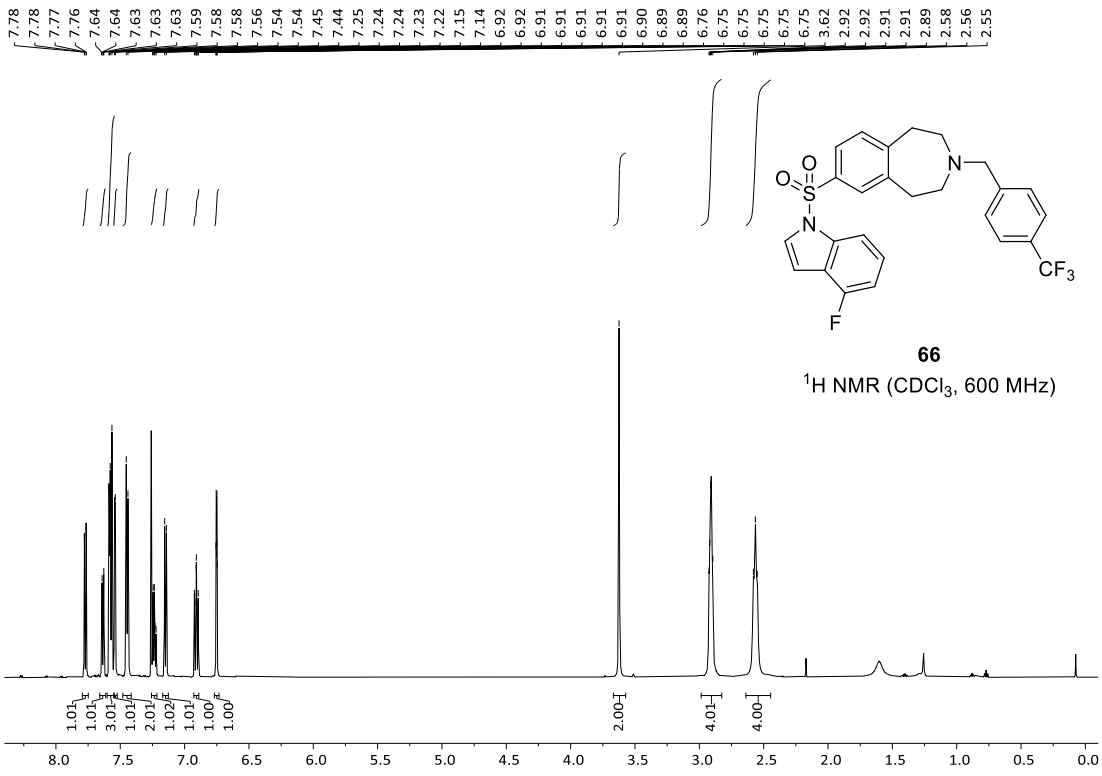

66

^{1}H NMR ($CDCl_3$, 600 MHz)

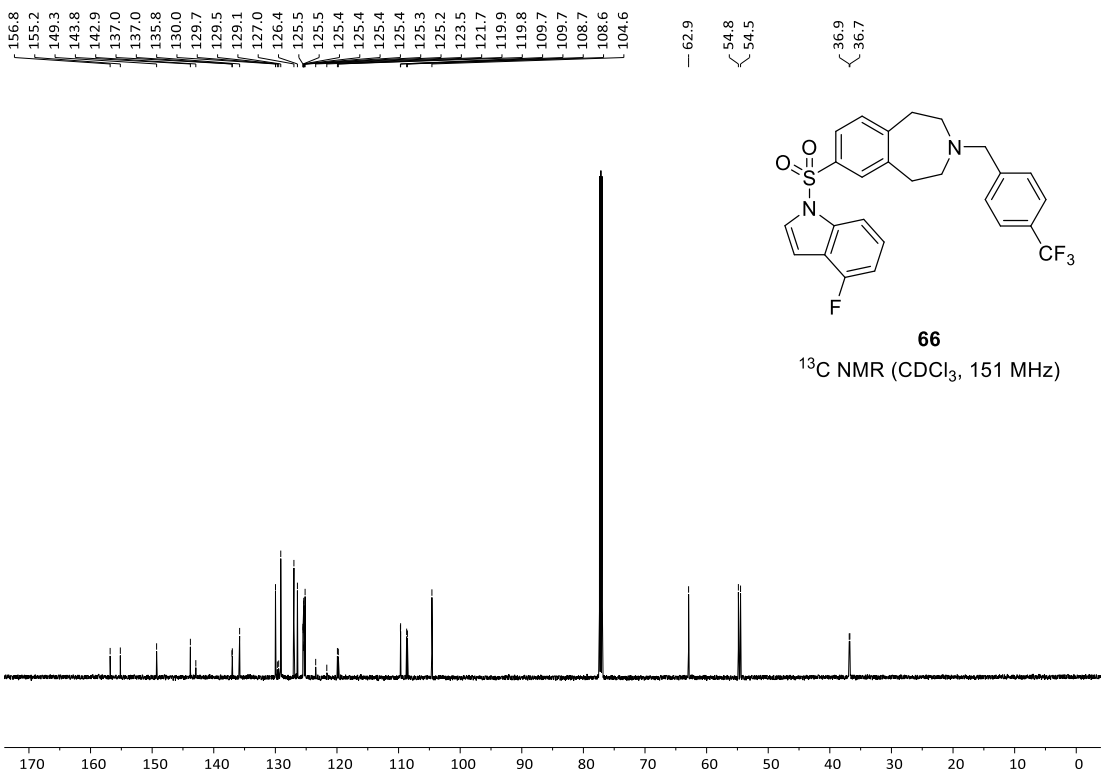

66

^{13}C NMR ($CDCl_3$, 151 MHz)

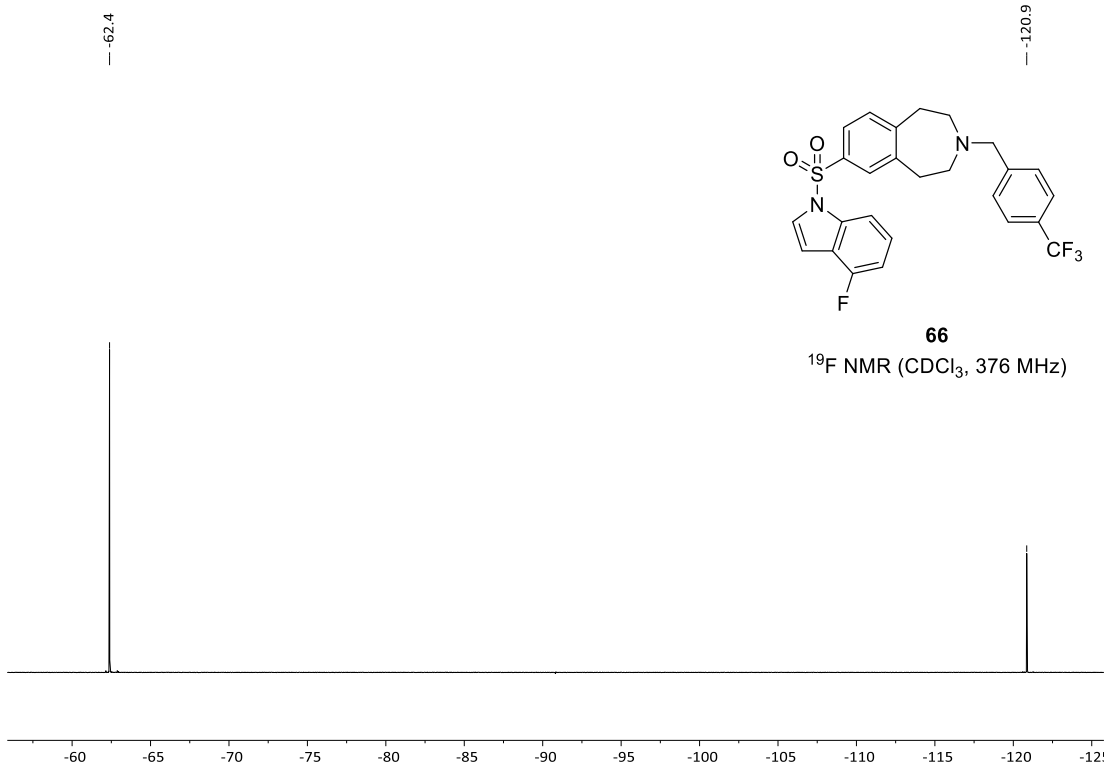

66

^{19}F NMR ($CDCl_3$, 376 MHz)

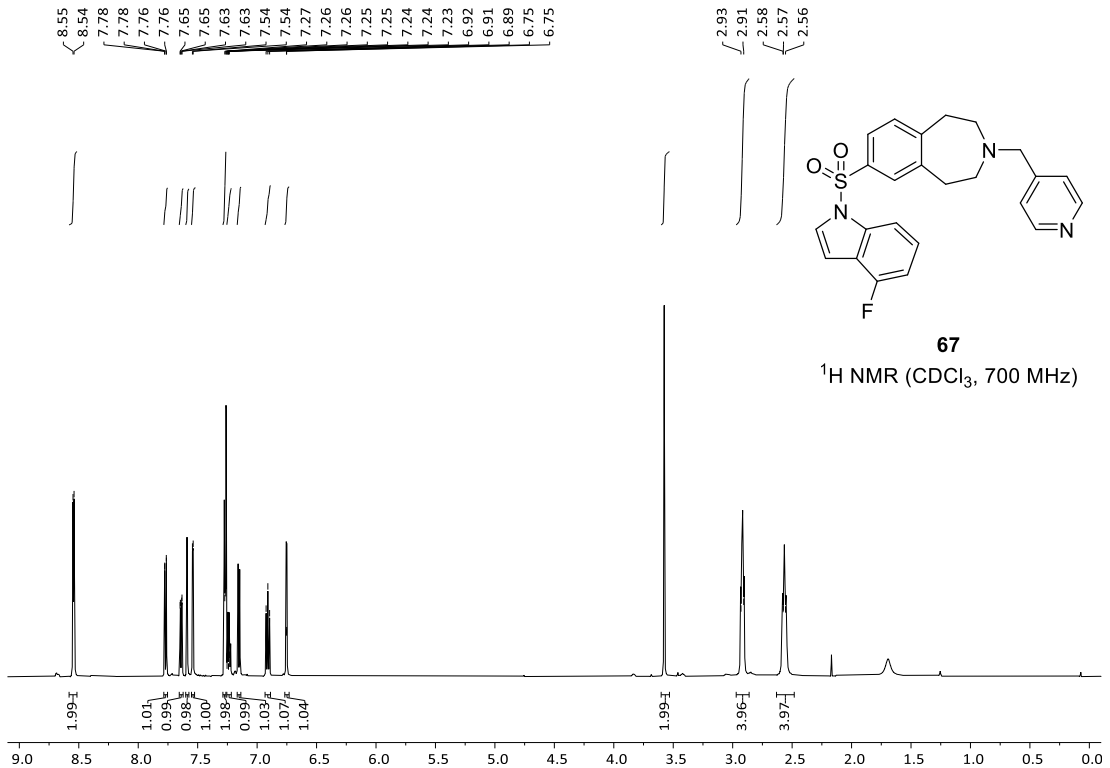

67

^{1}H NMR ($CDCl_3$, 700 MHz)

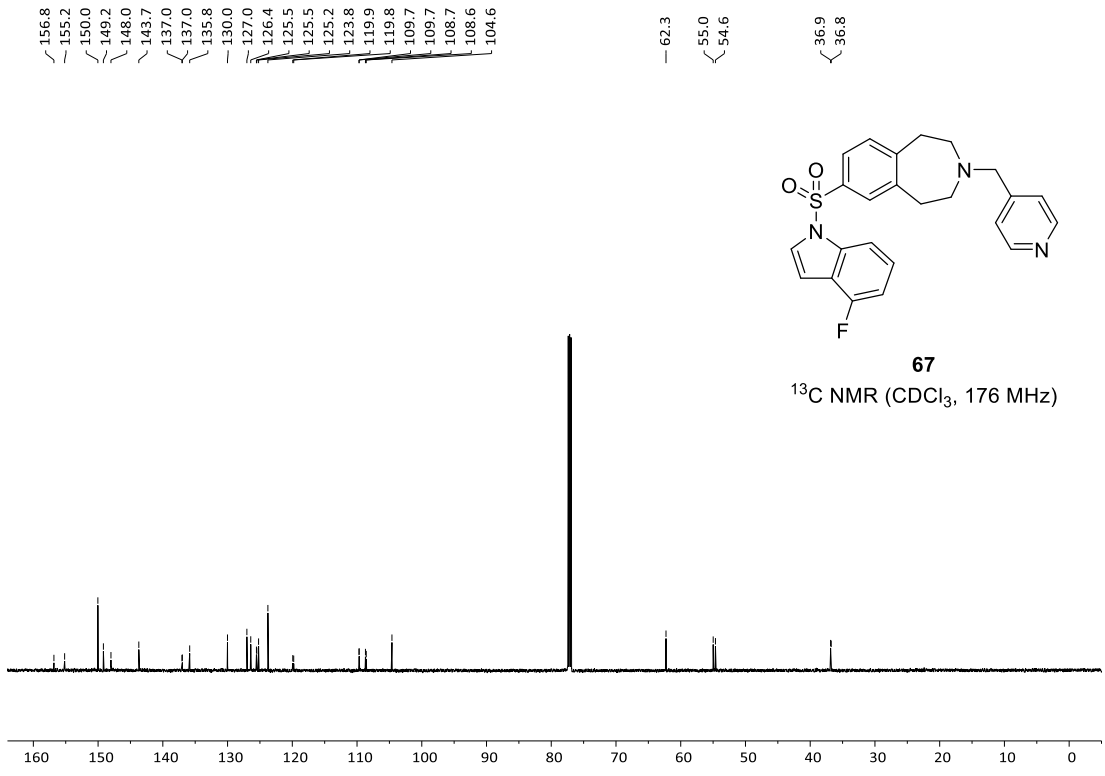

67

^{13}C NMR ($CDCl_3$, 176 MHz)

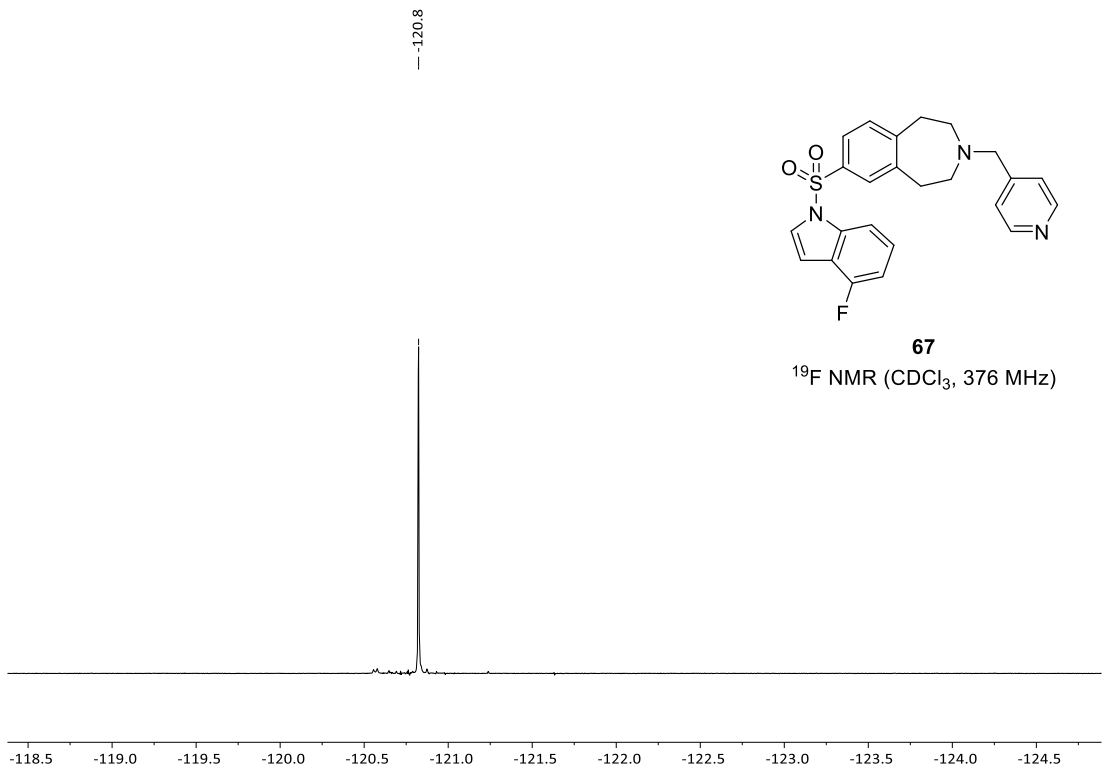

67

^{19}F NMR ($CDCl_3$, 376 MHz)

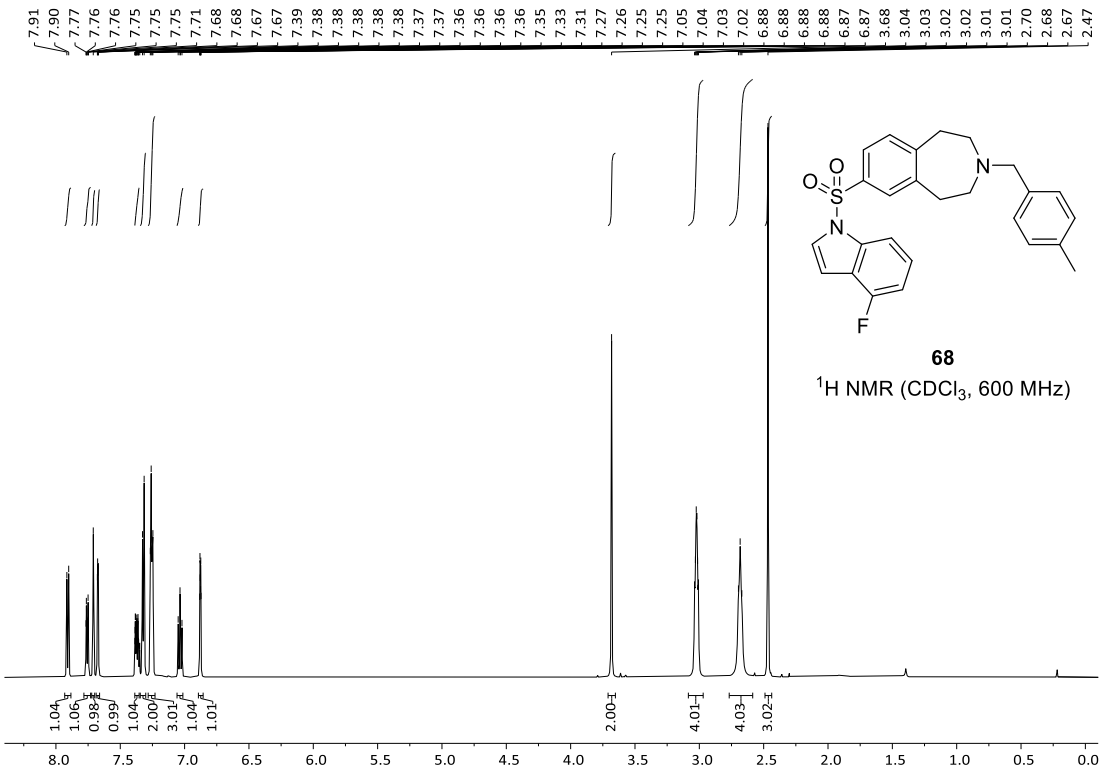

68

^{1}H NMR ($CDCl_3$, 600 MHz)

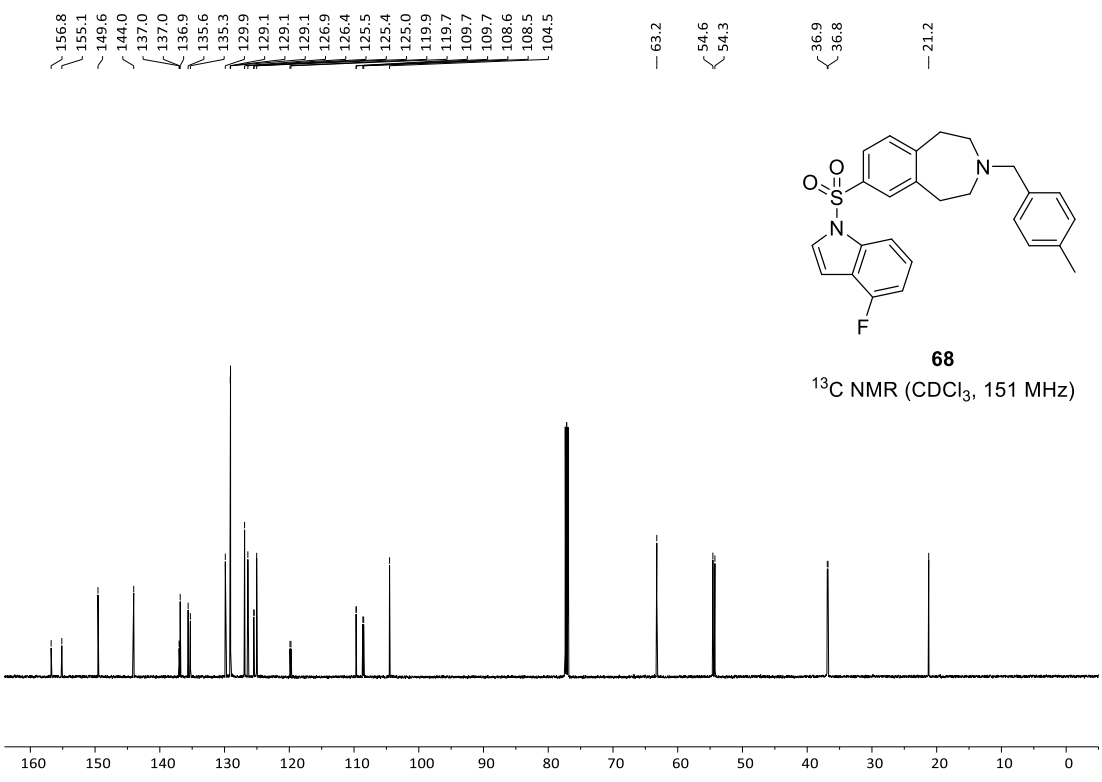

68

^{13}C NMR ($CDCl_3$, 151 MHz)

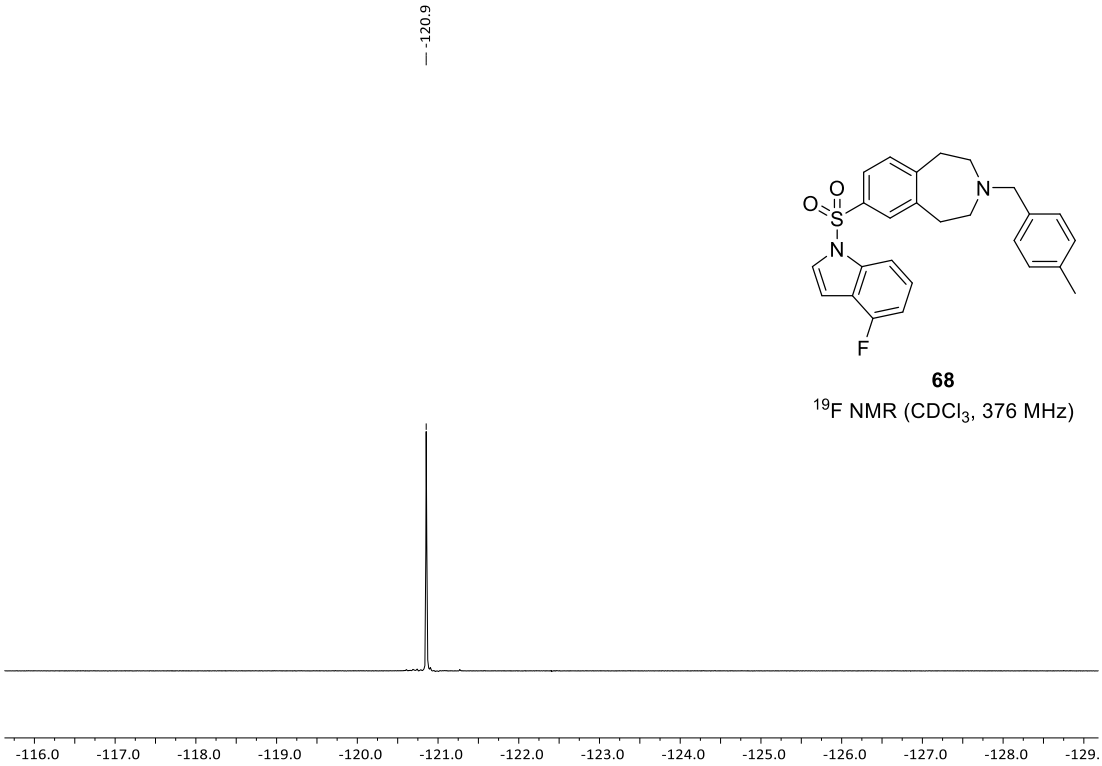

68

^{19}F NMR ($CDCl_3$, 376 MHz)

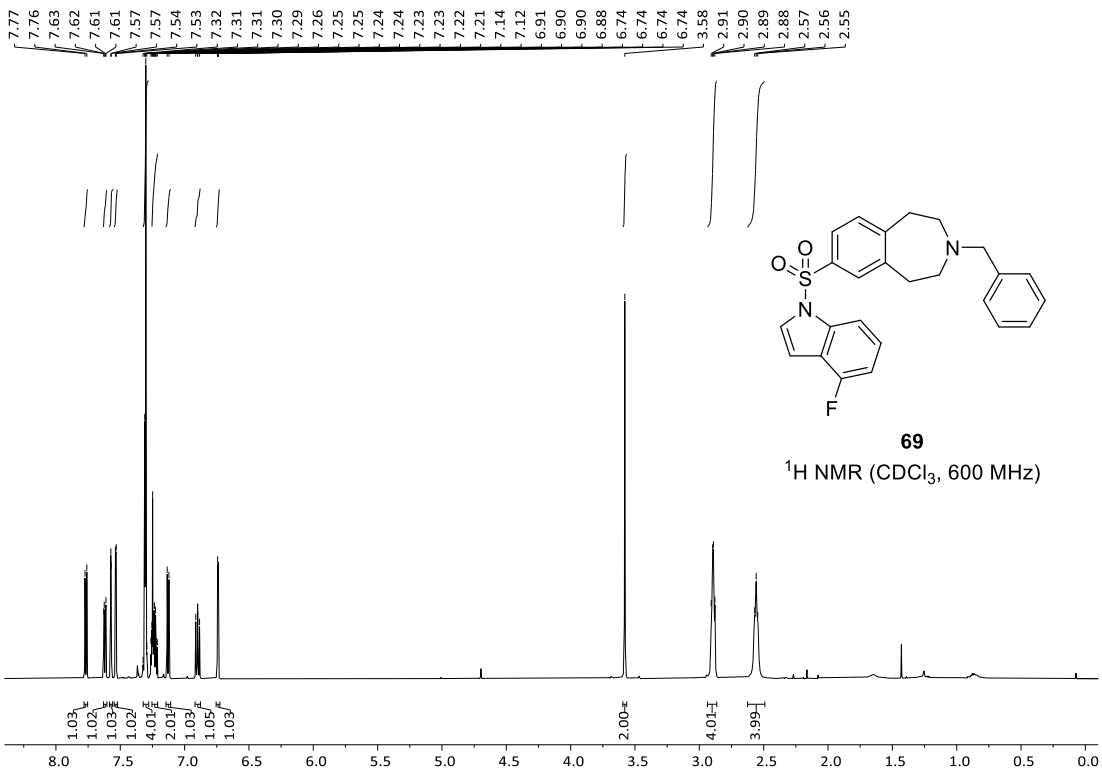

69

^{1}H NMR ($CDCl_3$, 600 MHz)

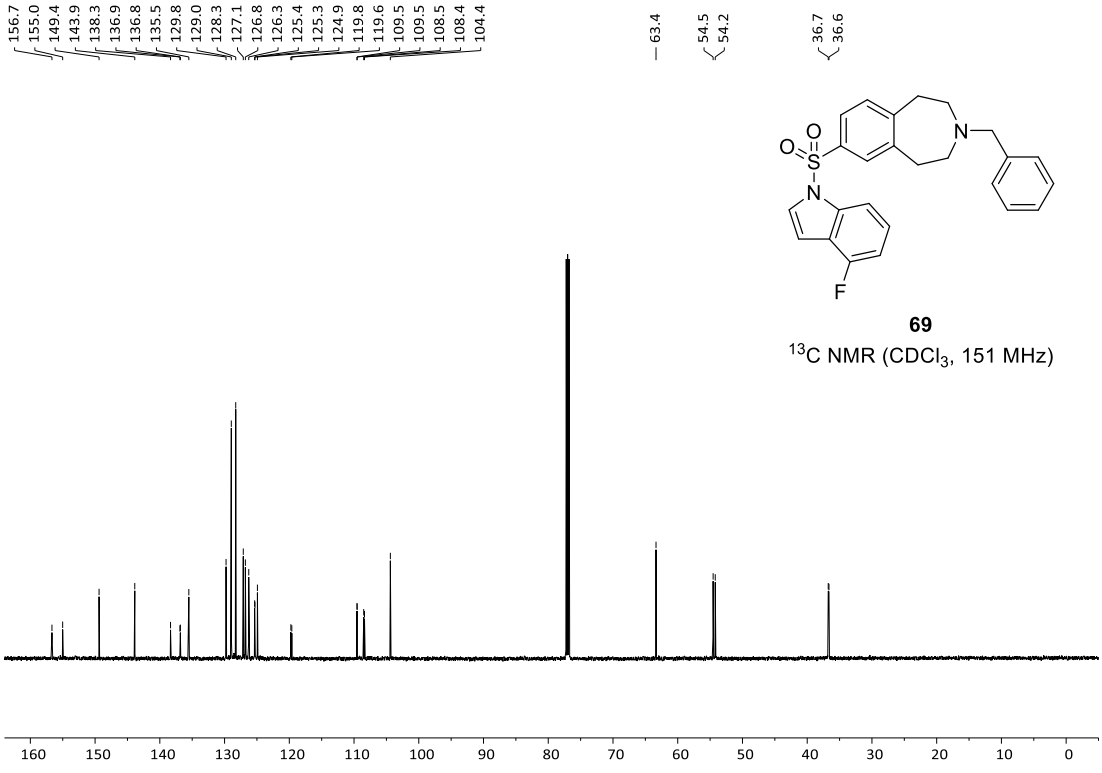

69

^{13}C NMR ($CDCl_3$, 151 MHz)

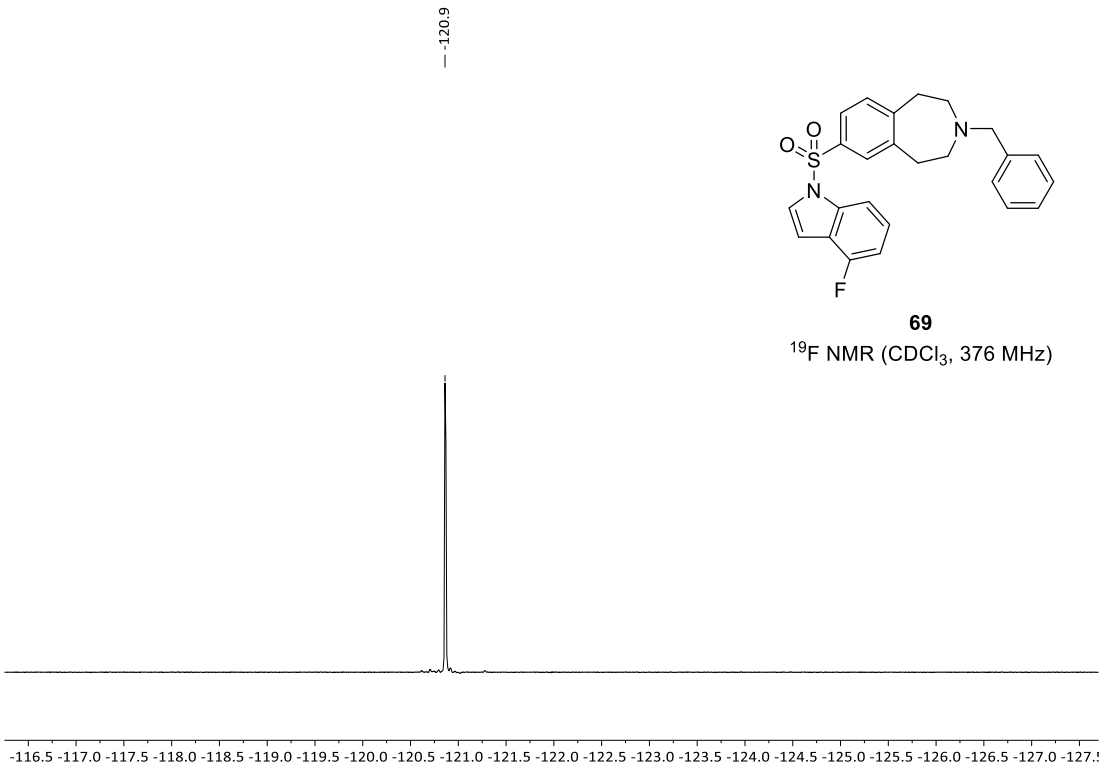

69

^{19}F NMR ($CDCl_3$, 376 MHz)

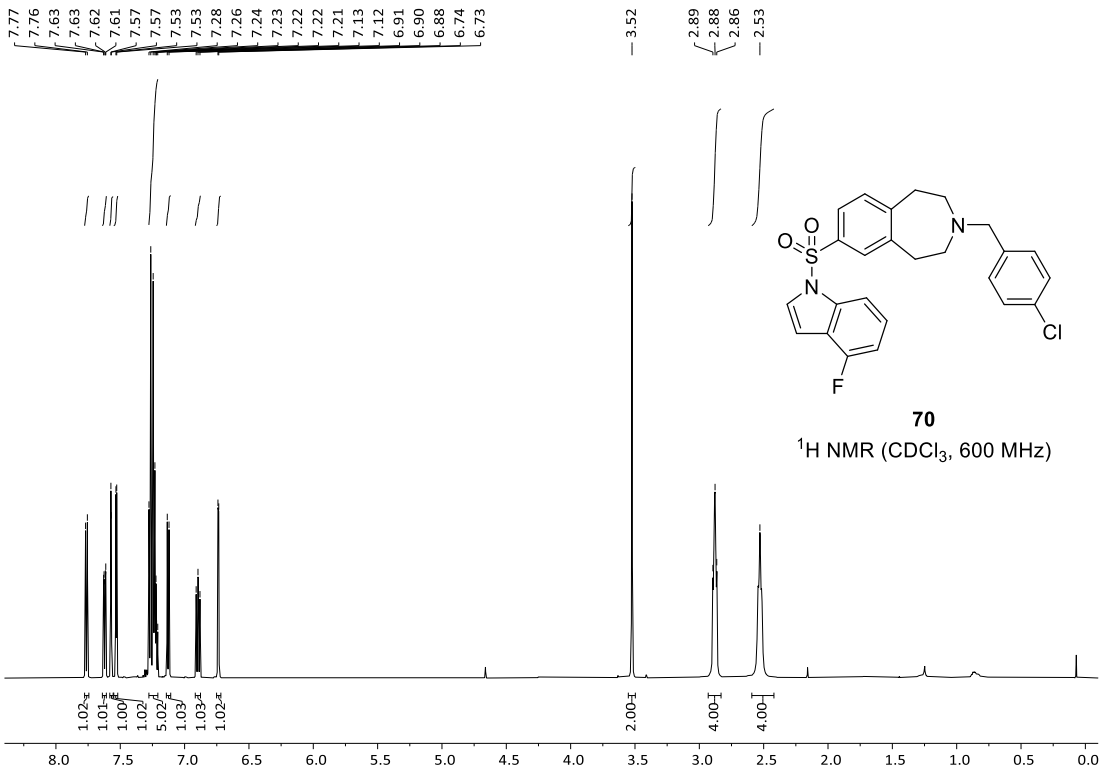

70

^{1}H NMR ($CDCl_3$, 600 MHz)

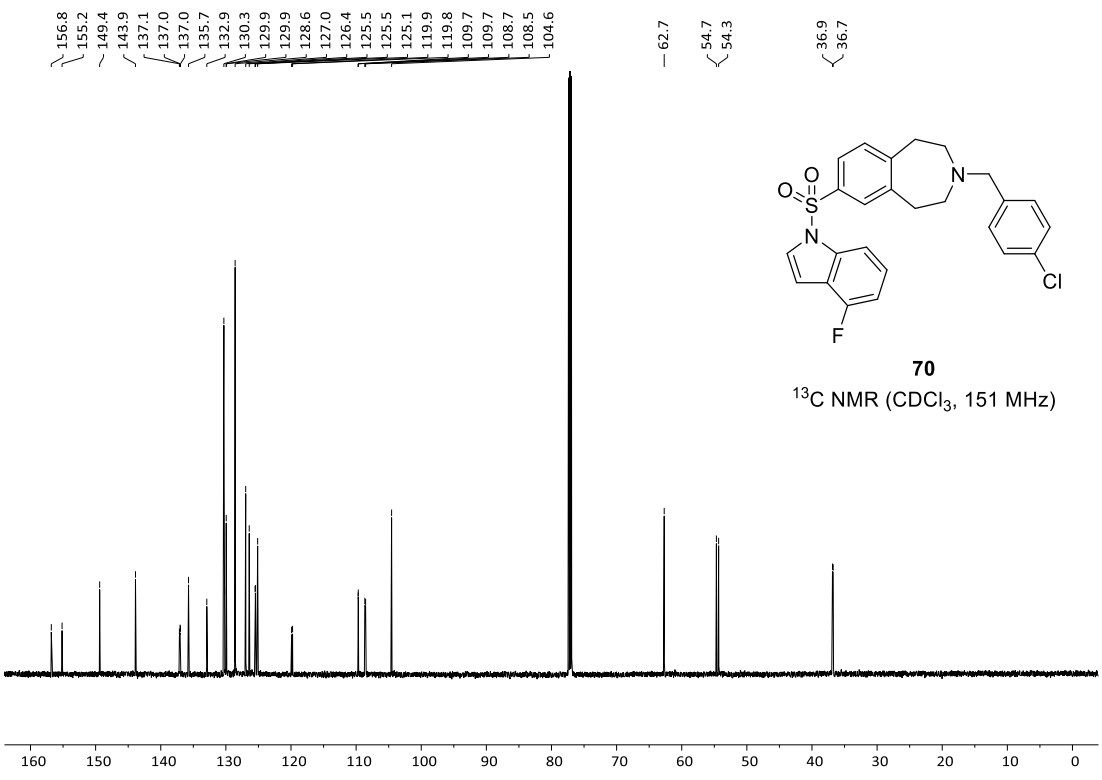

70

^{13}C NMR ($CDCl_3$, 151 MHz)

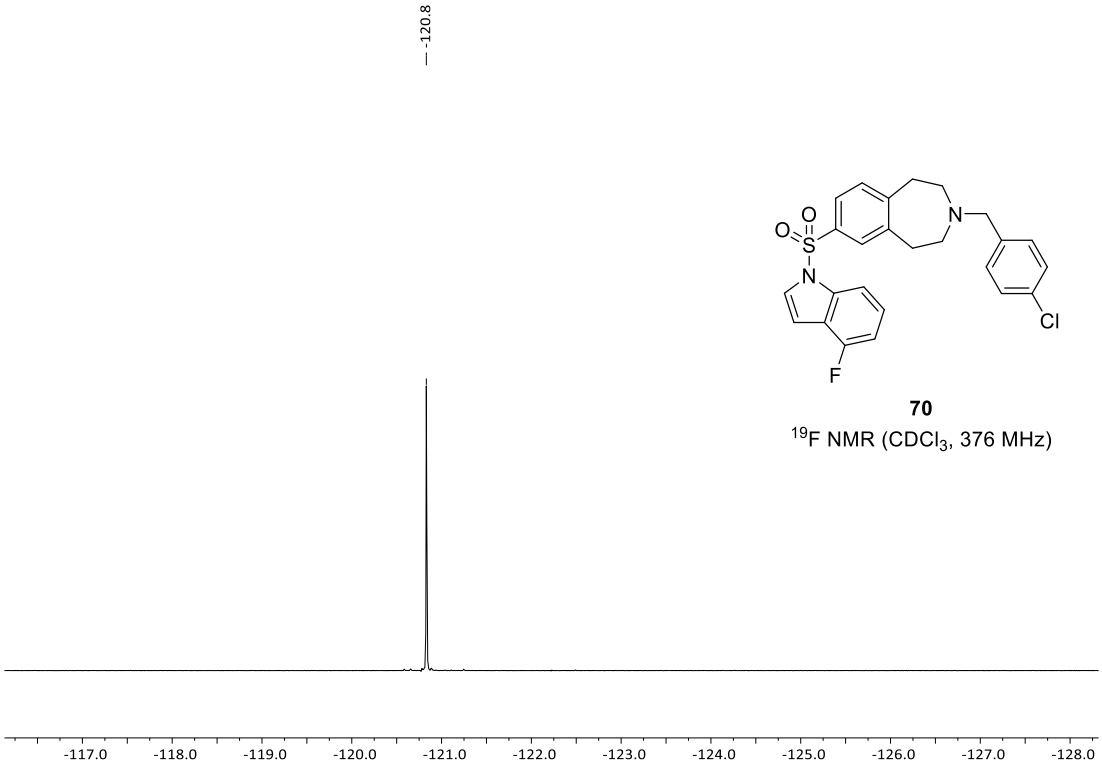

70

^{19}F NMR ($CDCl_3$, 376 MHz)

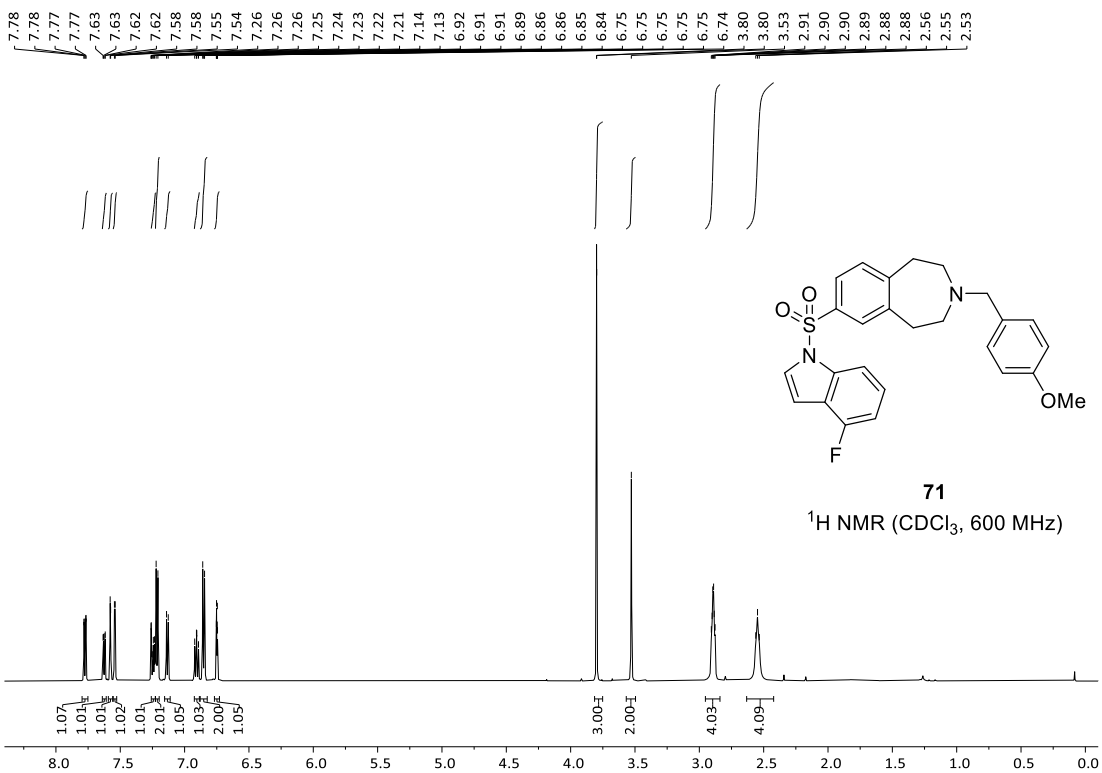

71

^{1}H NMR ($CDCl_3$, 600 MHz)

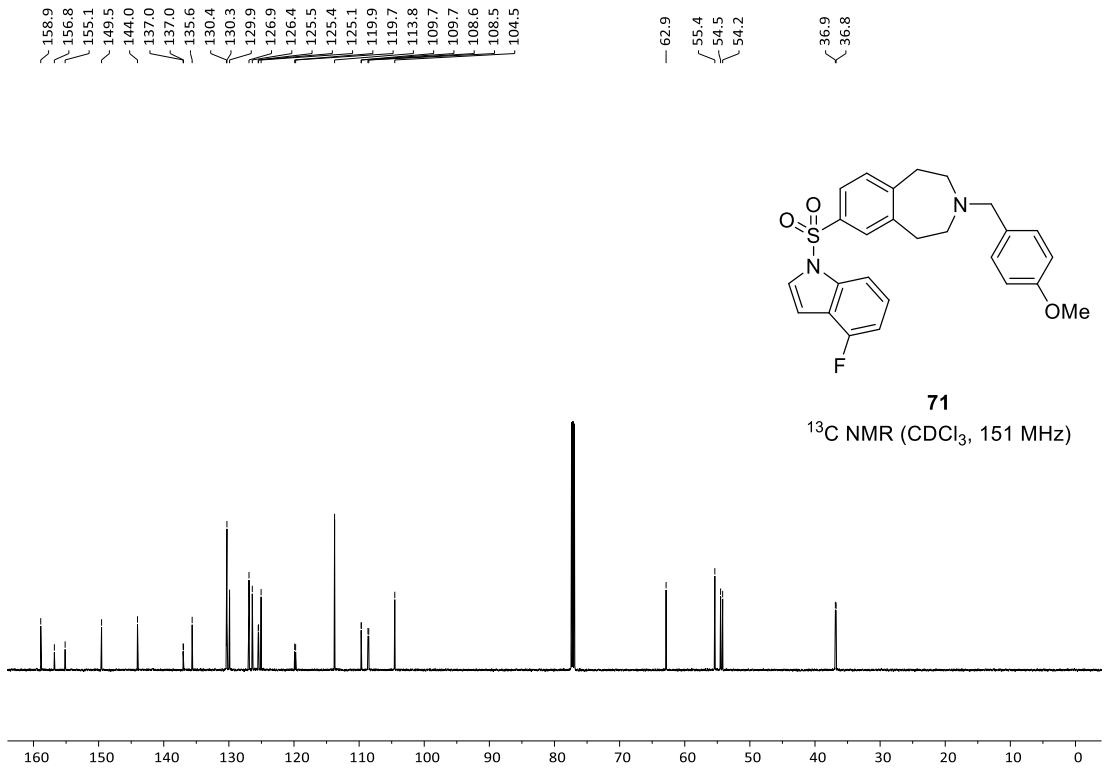

71

^{13}C NMR ($CDCl_3$, 151 MHz)

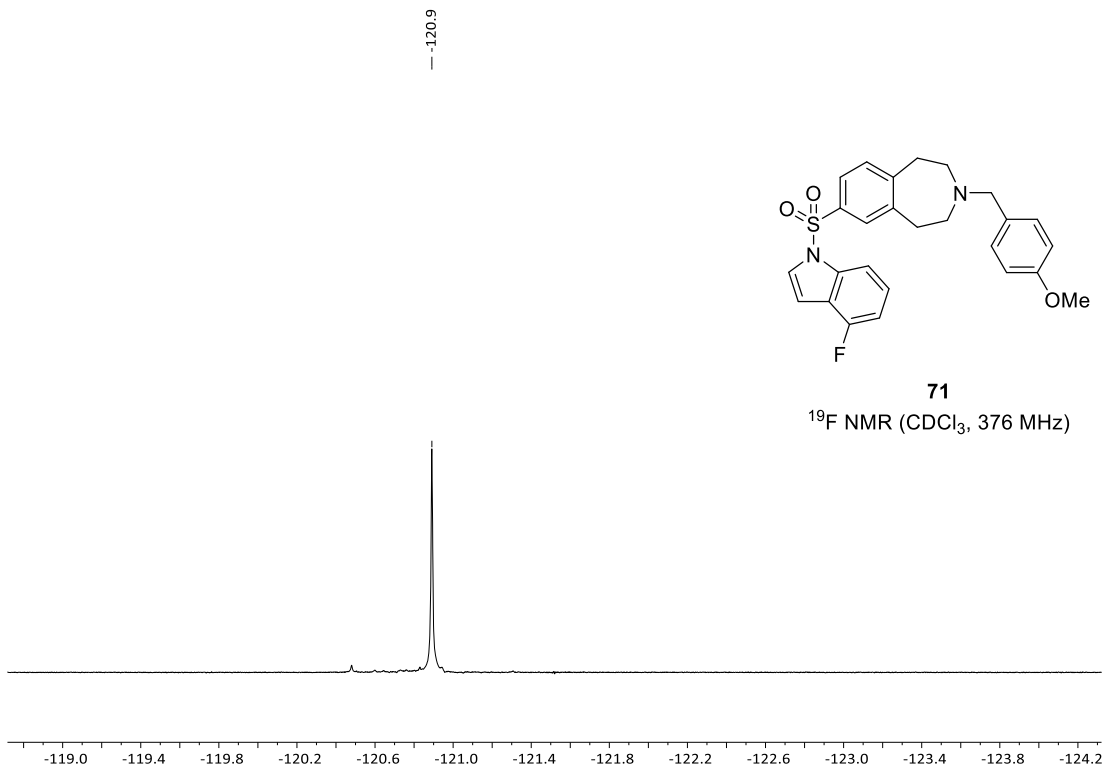

71

^{19}F NMR ($CDCl_3$, 376 MHz)

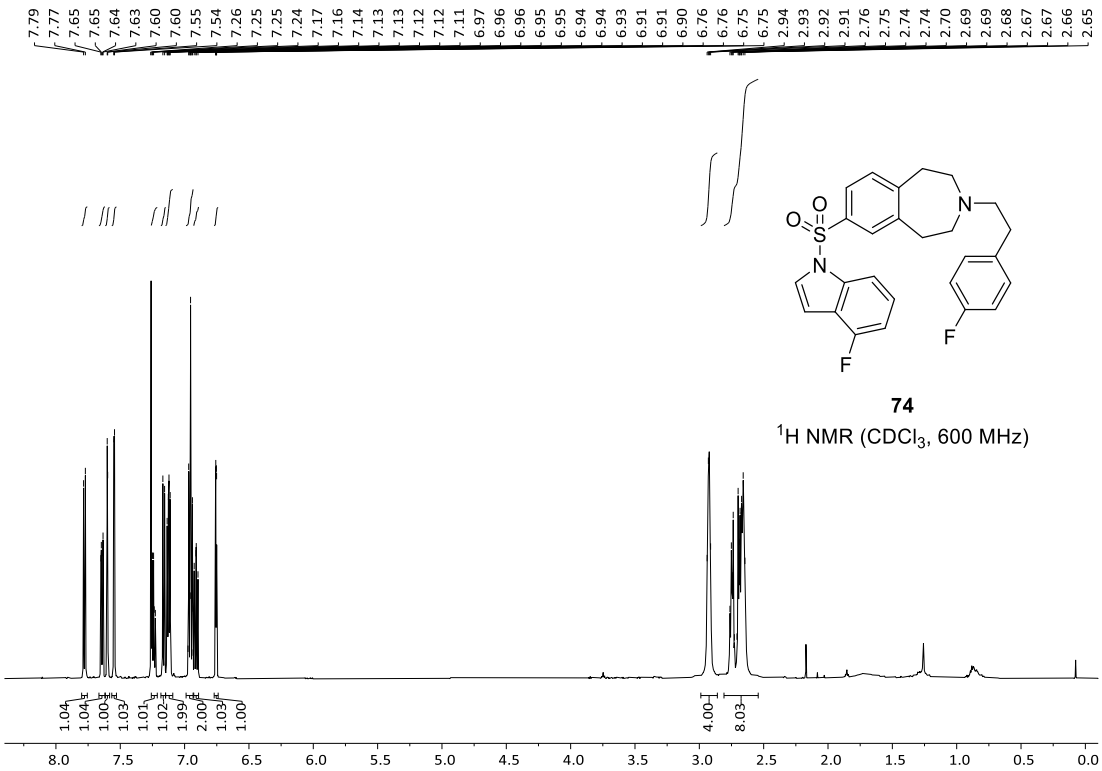

74

^{1}H NMR ($CDCl_3$, 600 MHz)

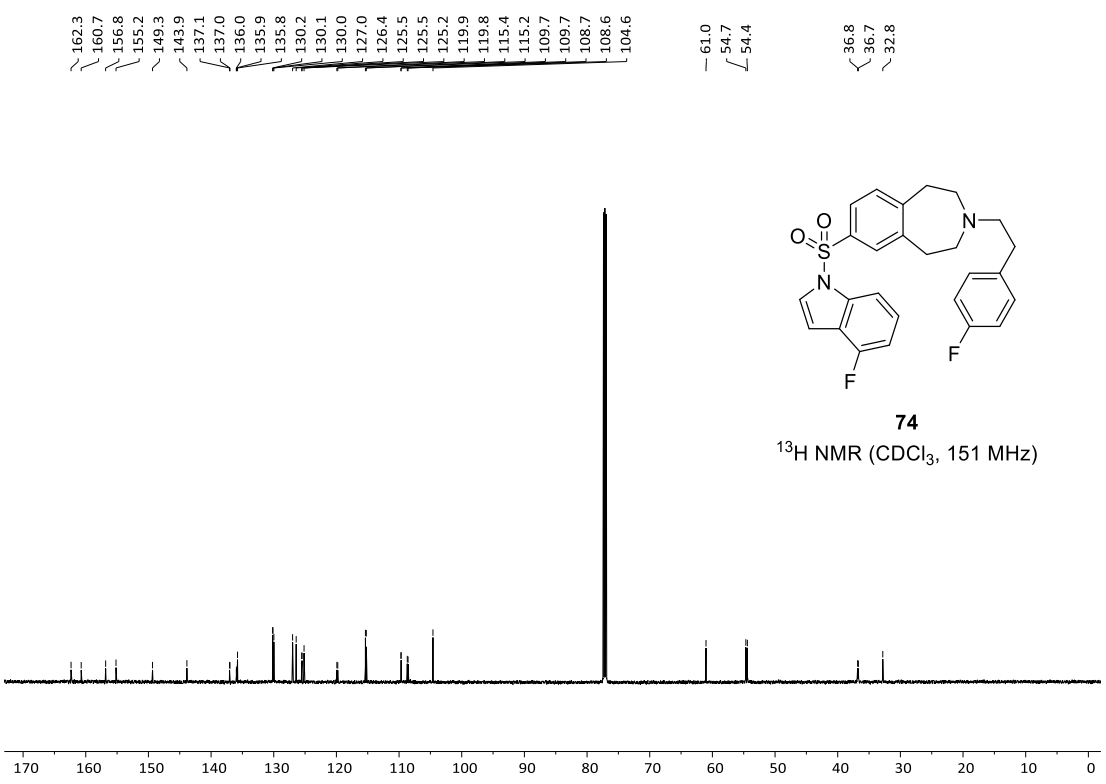

74

^{13}H NMR ($CDCl_3$, 151 MHz)

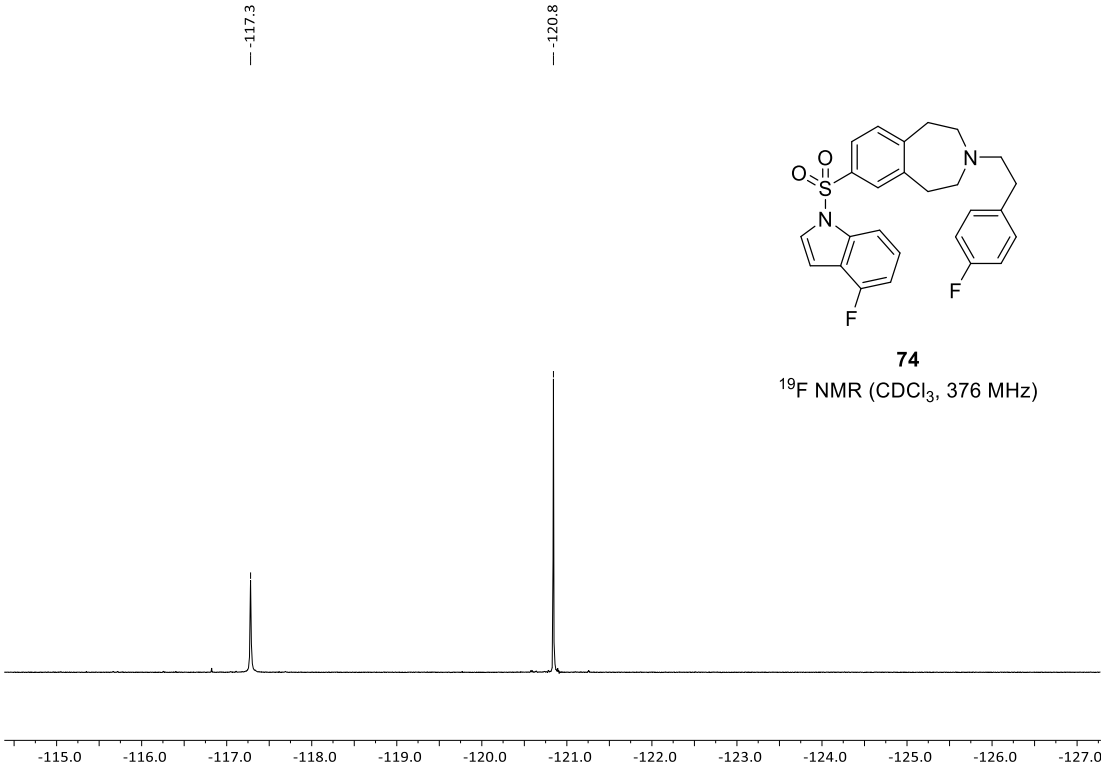

74

^{19}F NMR ($CDCl_3$, 376 MHz)

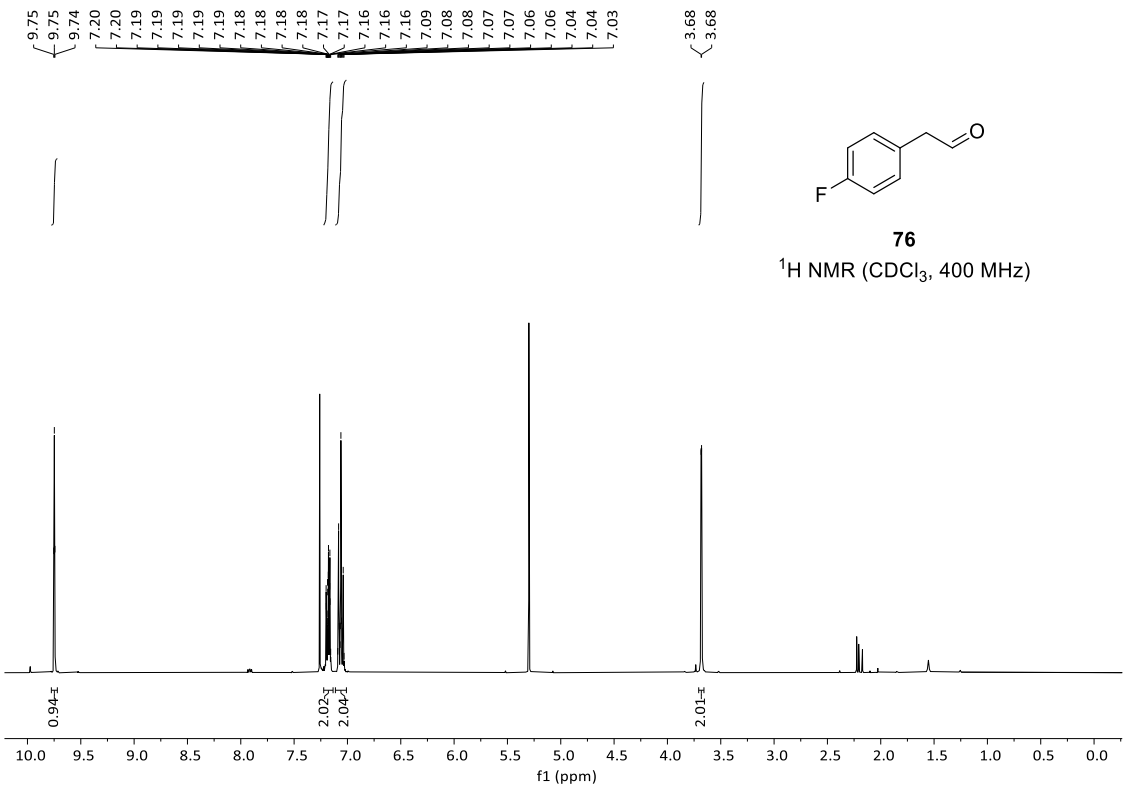

76

^{1}H NMR ($CDCl_3$, 400 MHz)

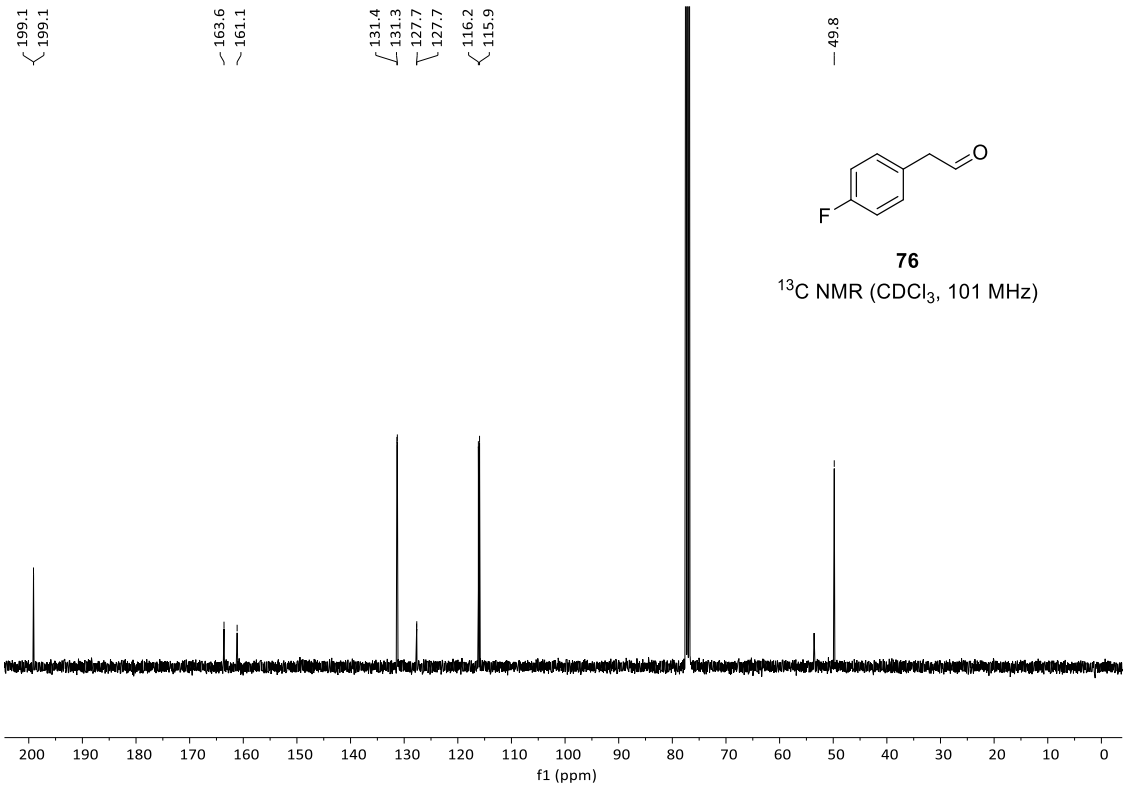

76

^{13}C NMR ($CDCl_3$, 101 MHz)

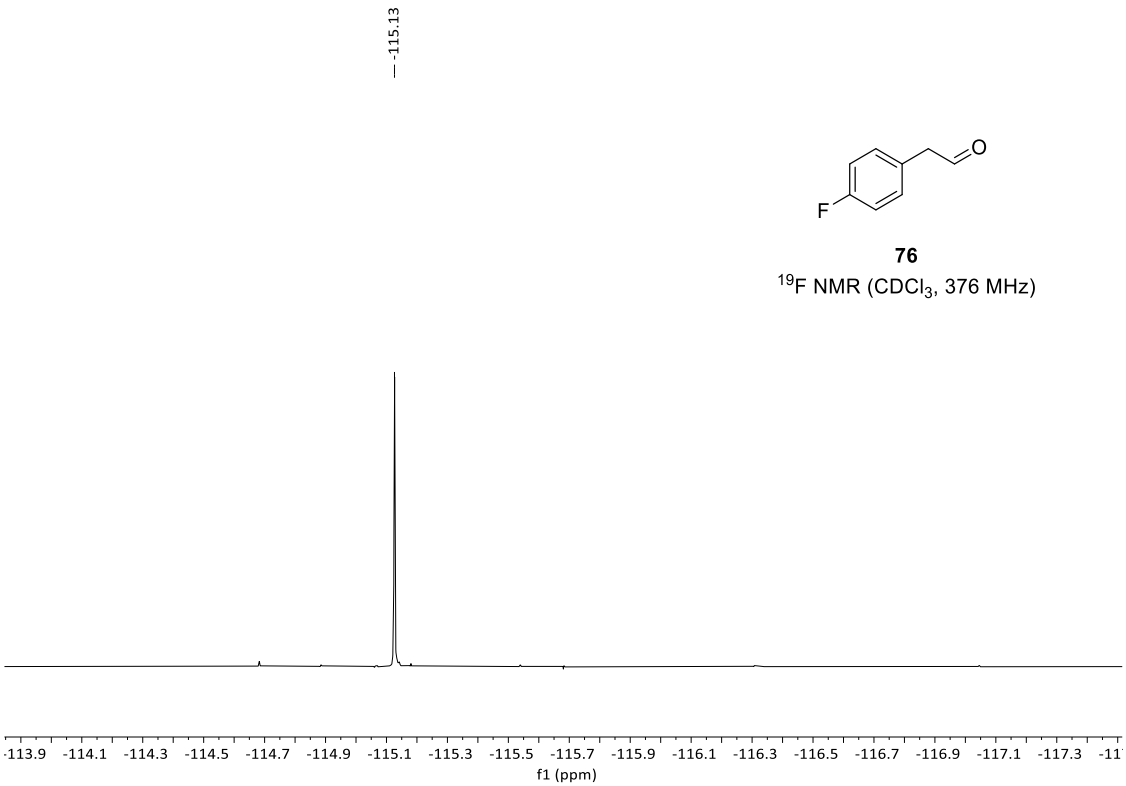

76

^{19}F NMR ($CDCl_3$, 376 MHz)

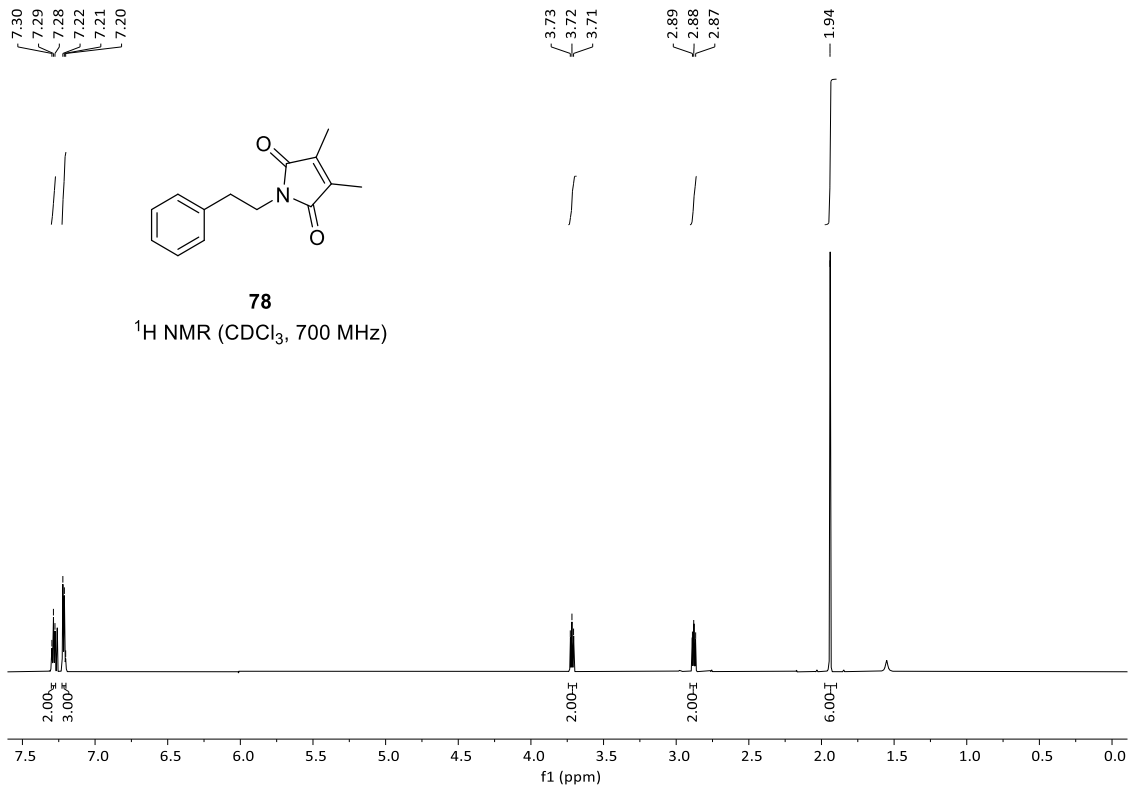

78

^{1}H NMR ($CDCl_3$, 700 MHz)

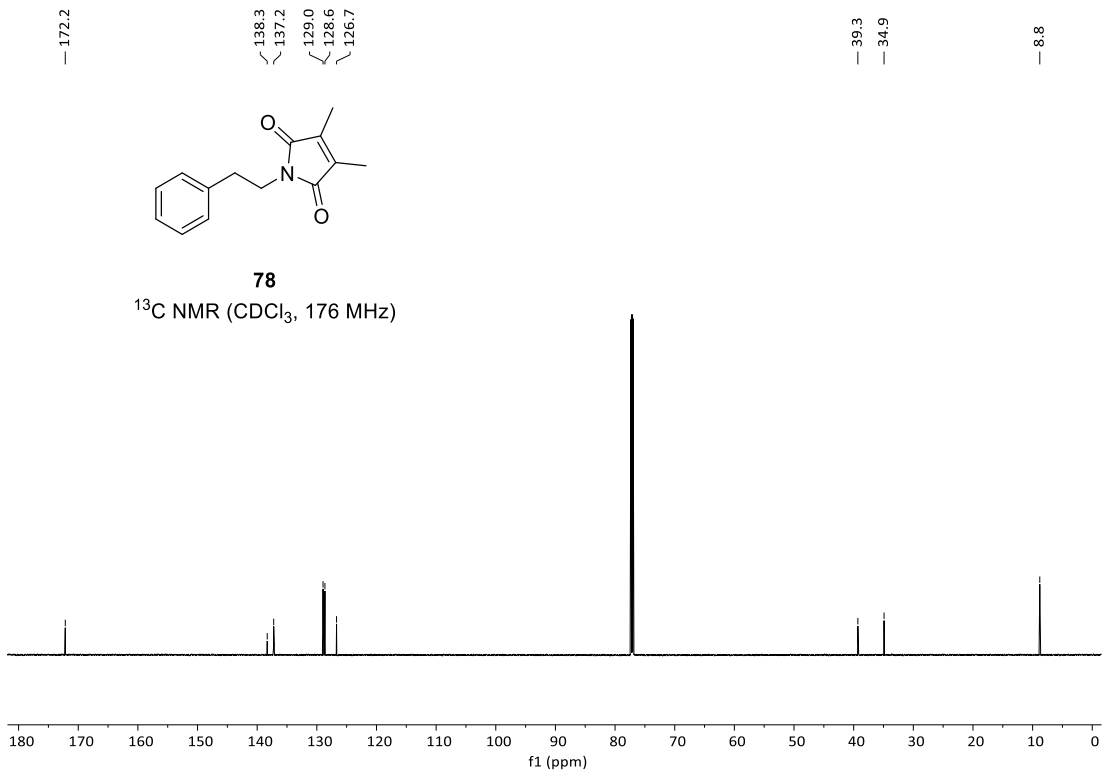

78

^{13}C NMR ($CDCl_3$, 176 MHz)

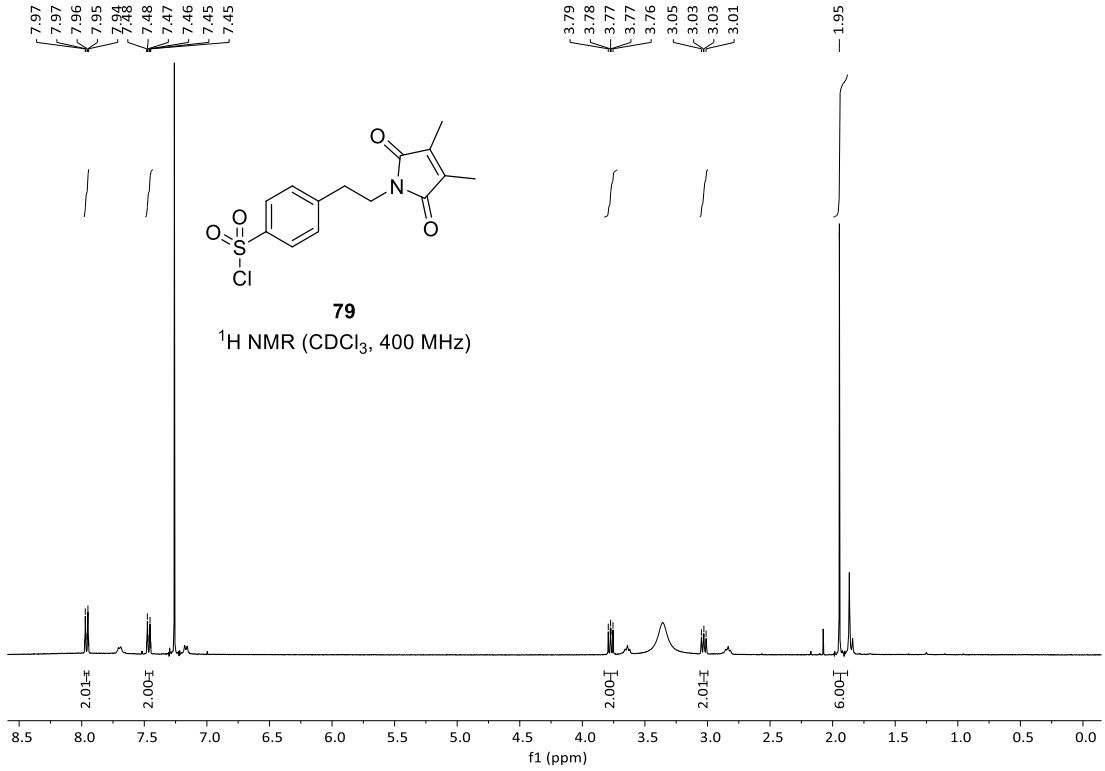

79

^{1}H NMR ($CDCl_3$, 400 MHz)

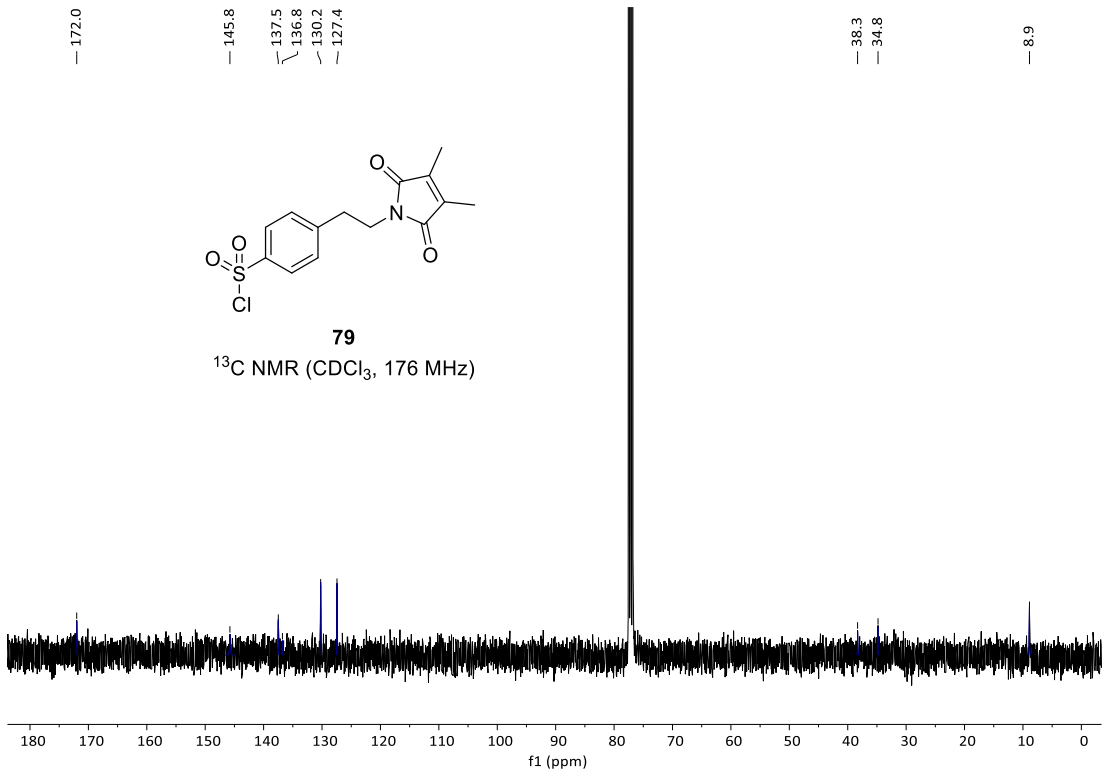

79

^{13}C NMR ($CDCl_3$, 176 MHz)

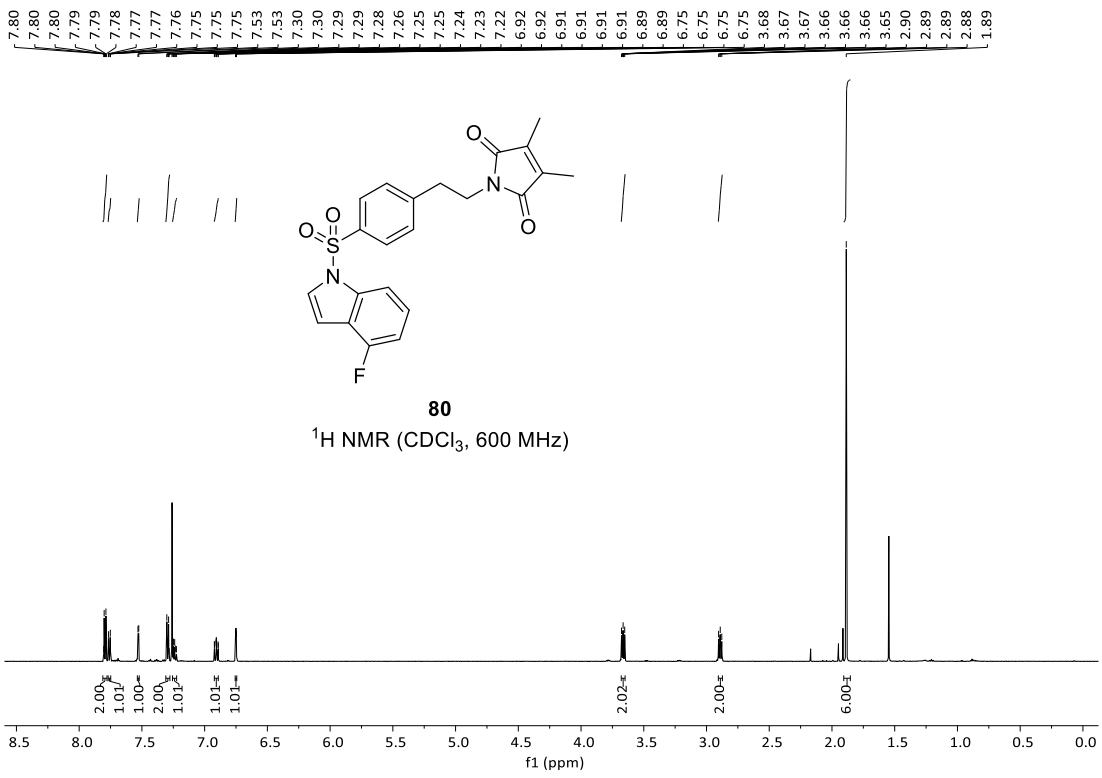

80

^{1}H NMR ($CDCl_3$, 600 MHz)

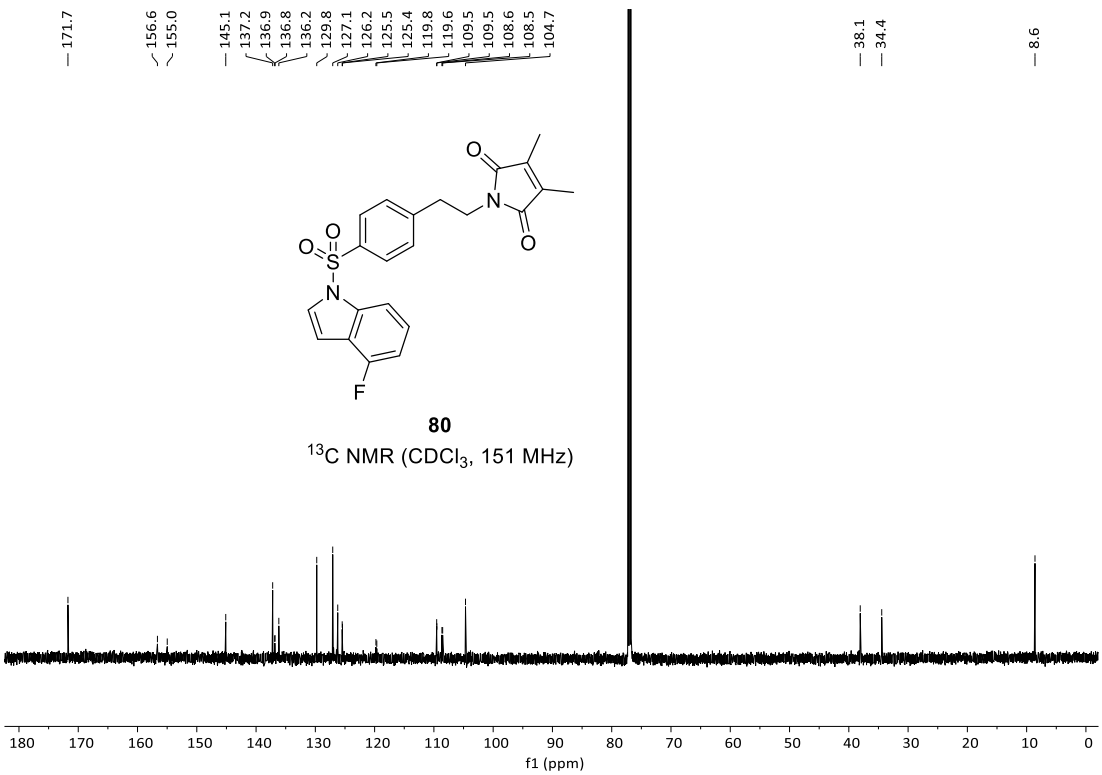

80

^{13}C NMR ($CDCl_3$, 151 MHz)

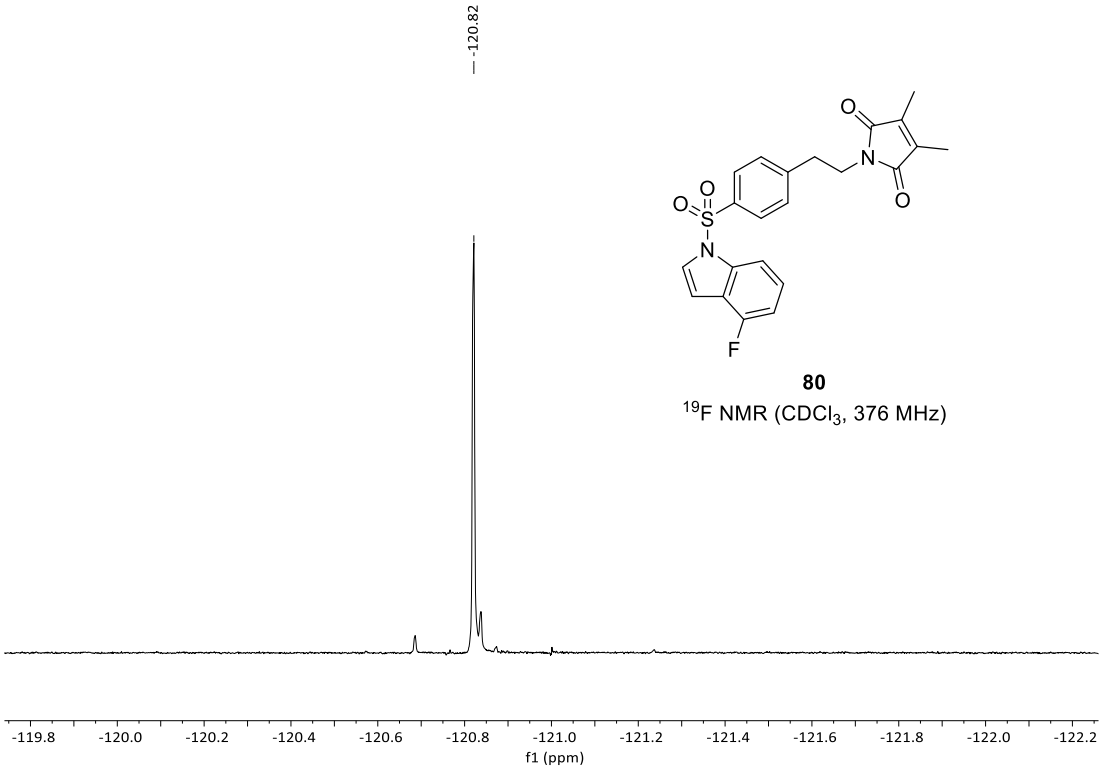

80

^{19}F NMR ($CDCl_3$, 376 MHz)

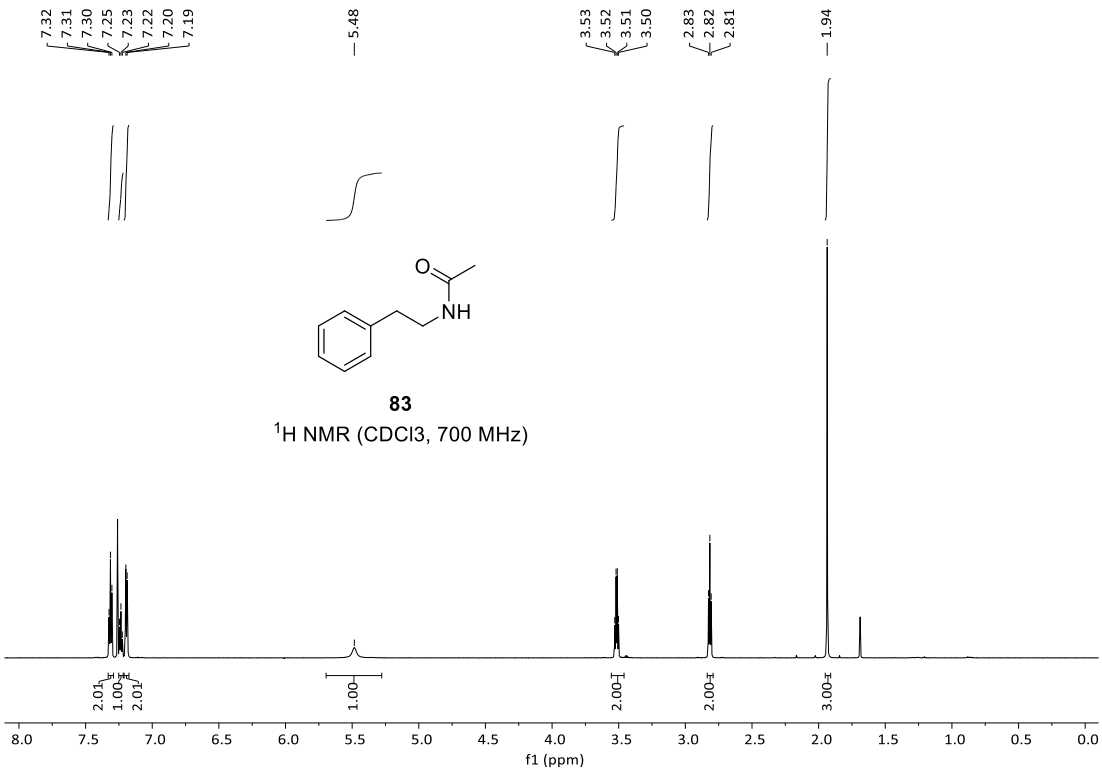

83

^{1}H NMR (CDCl3, 700 MHz)

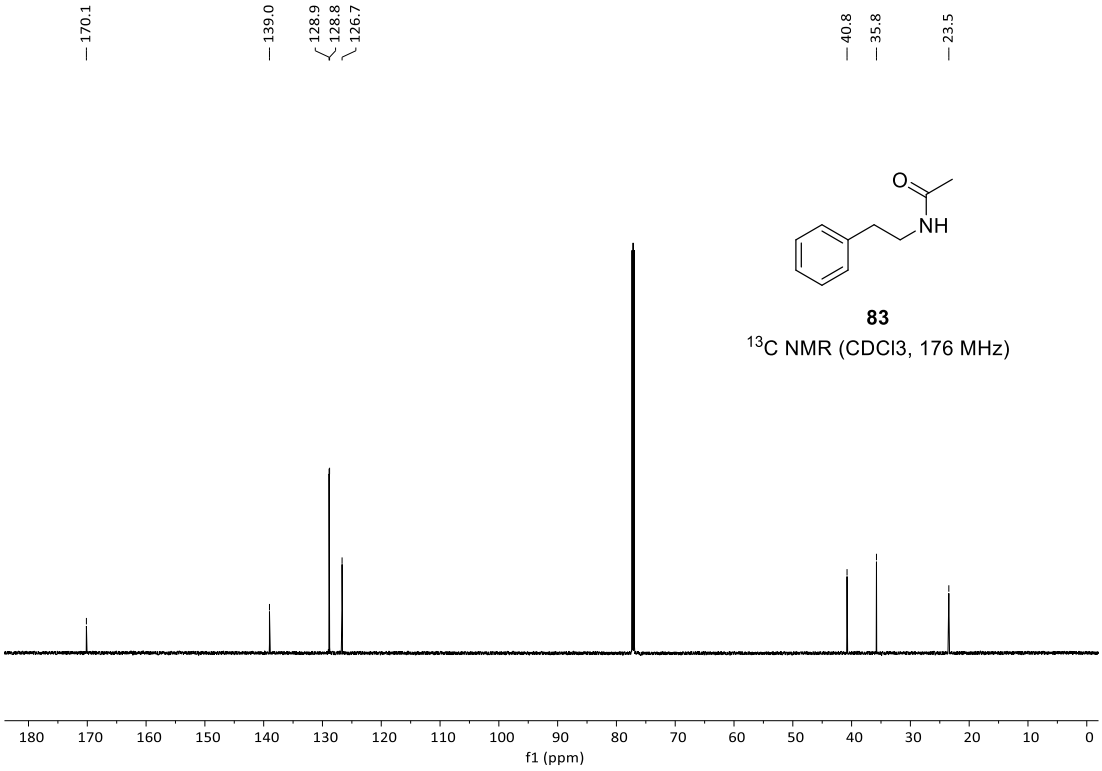

83

^{13}C NMR (CDCl3, 176 MHz)

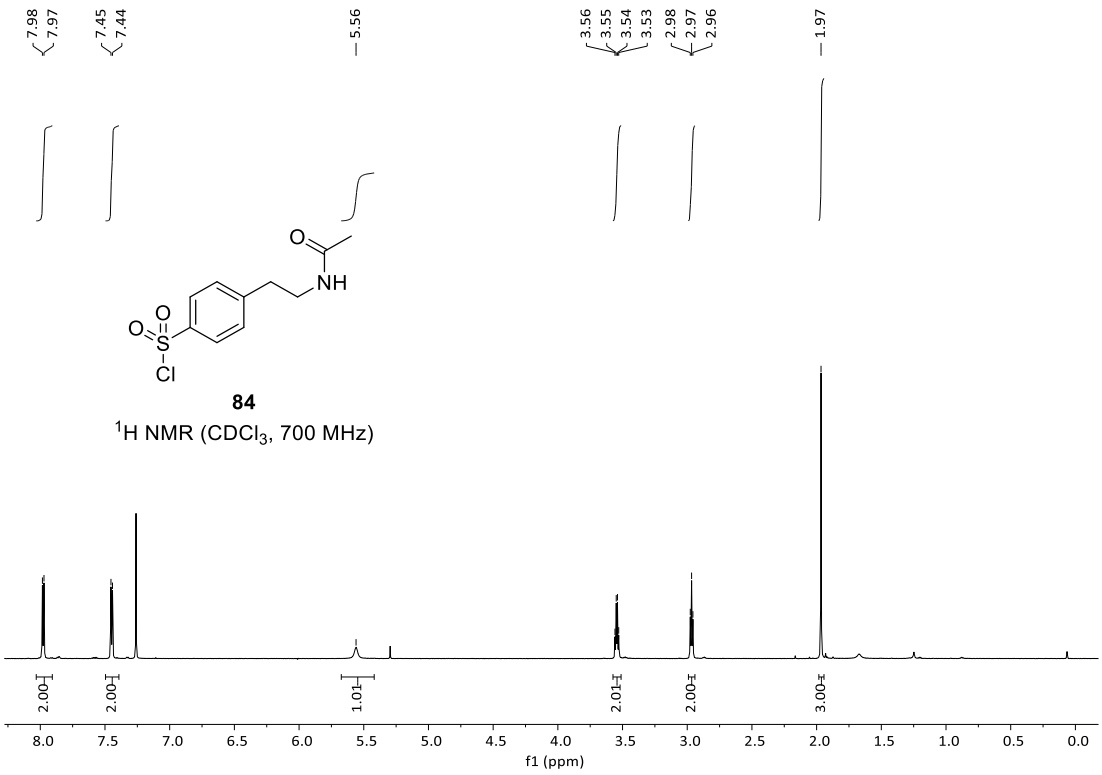

84

^{1}H NMR ($CDCl_3$, 700 MHz)

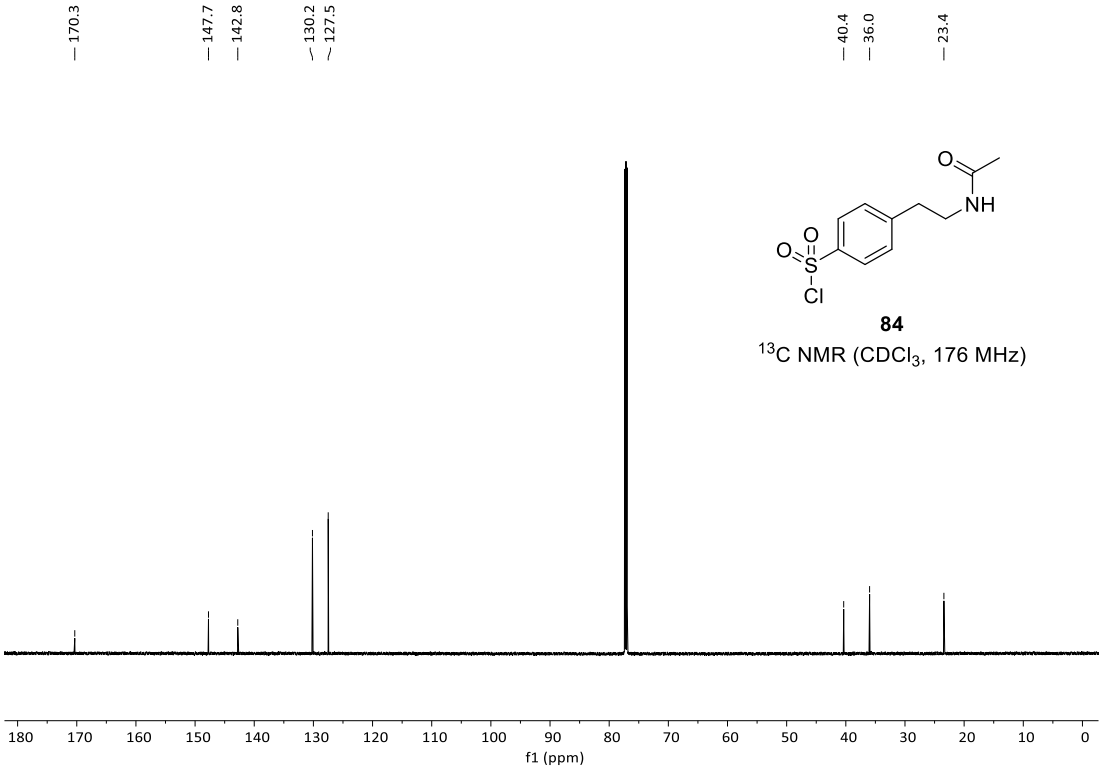

84

^{13}C NMR ($CDCl_3$, 176 MHz)

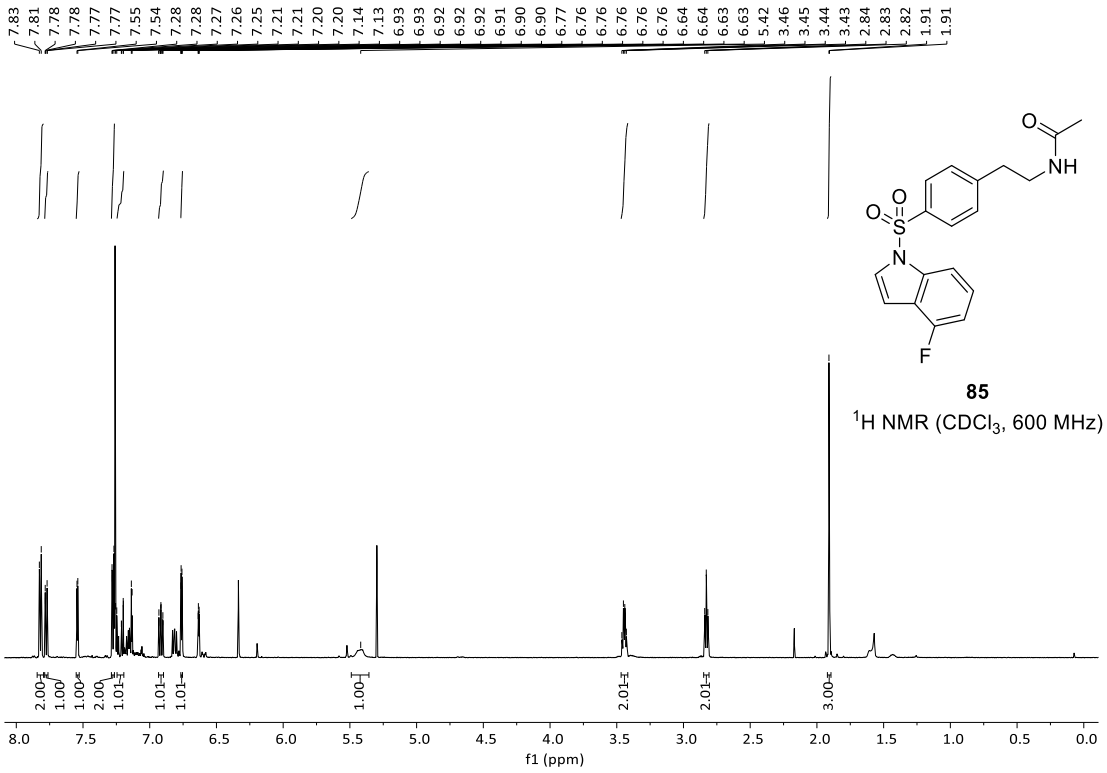

85

^{1}H NMR ($CDCl_3$, 600 MHz)

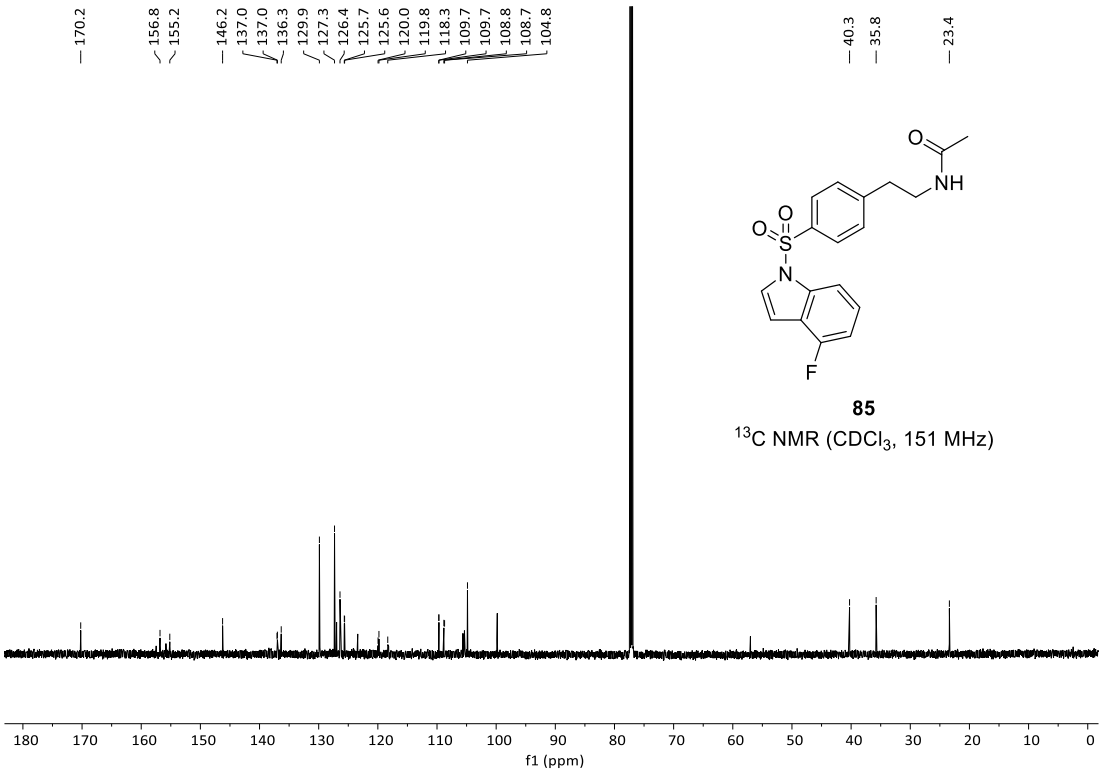

85

^{13}C NMR ($CDCl_3$, 151 MHz)

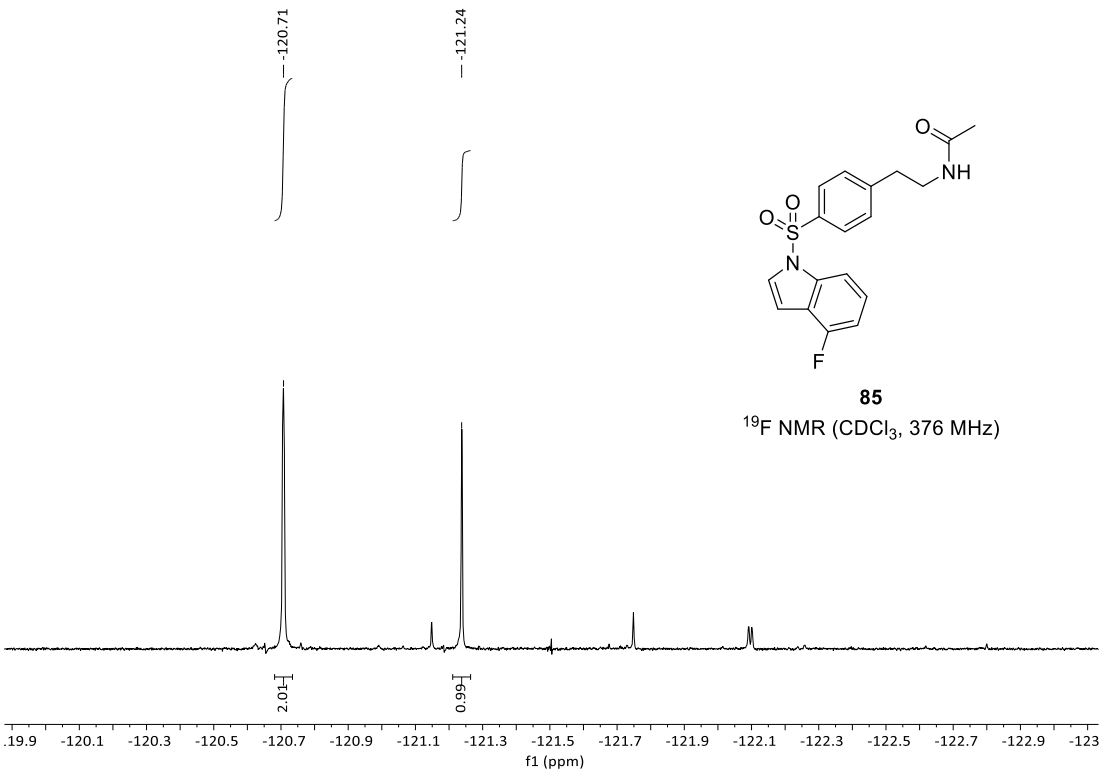

85

^{19}F NMR ($CDCl_3$, 376 MHz)

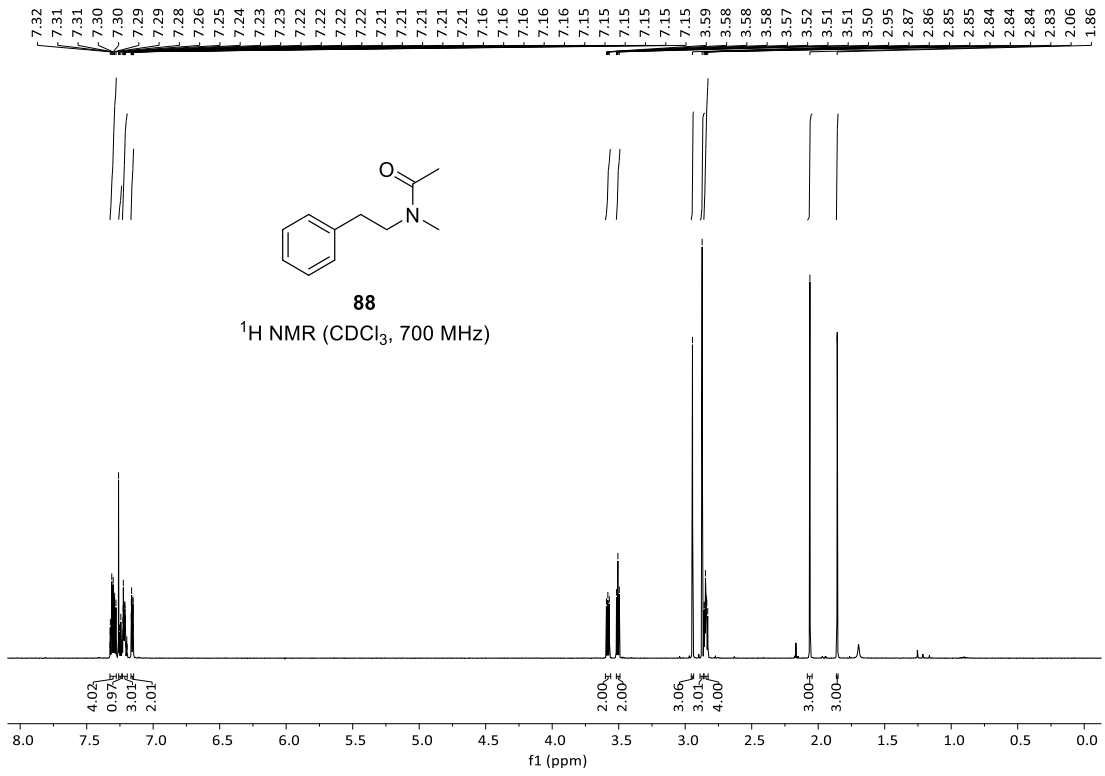

88

^{1}H NMR ($CDCl_3$, 700 MHz)

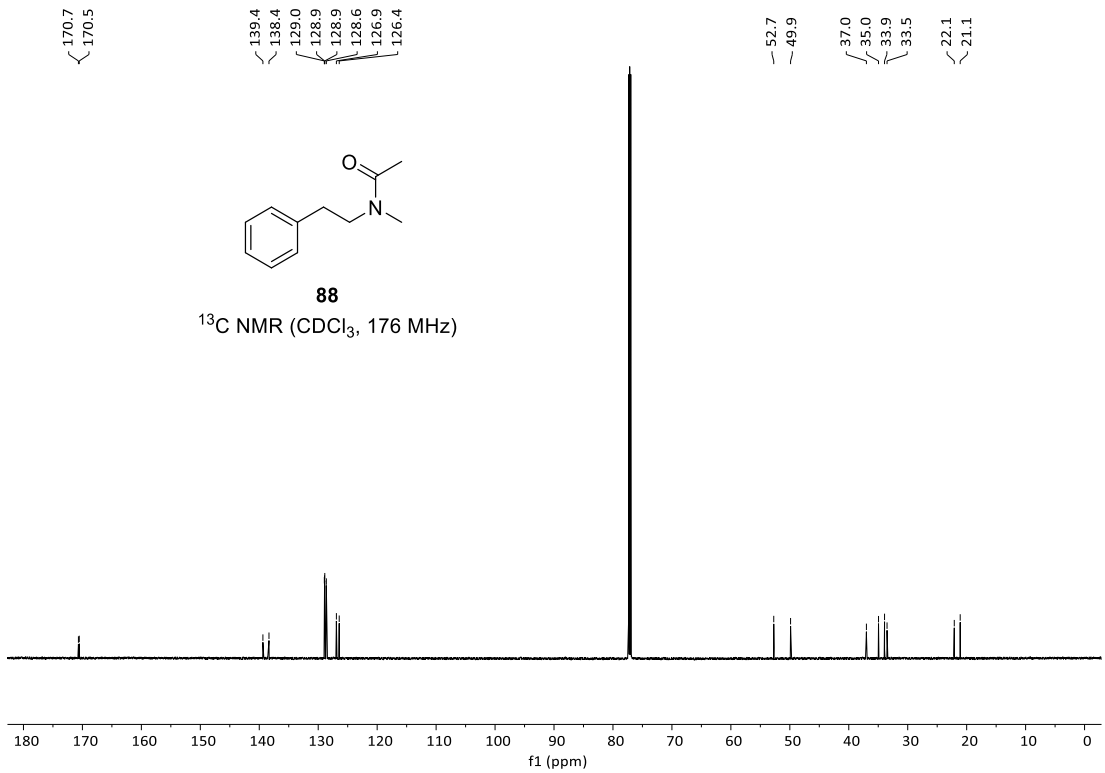

88

^{13}C NMR ($CDCl_3$, 176 MHz)

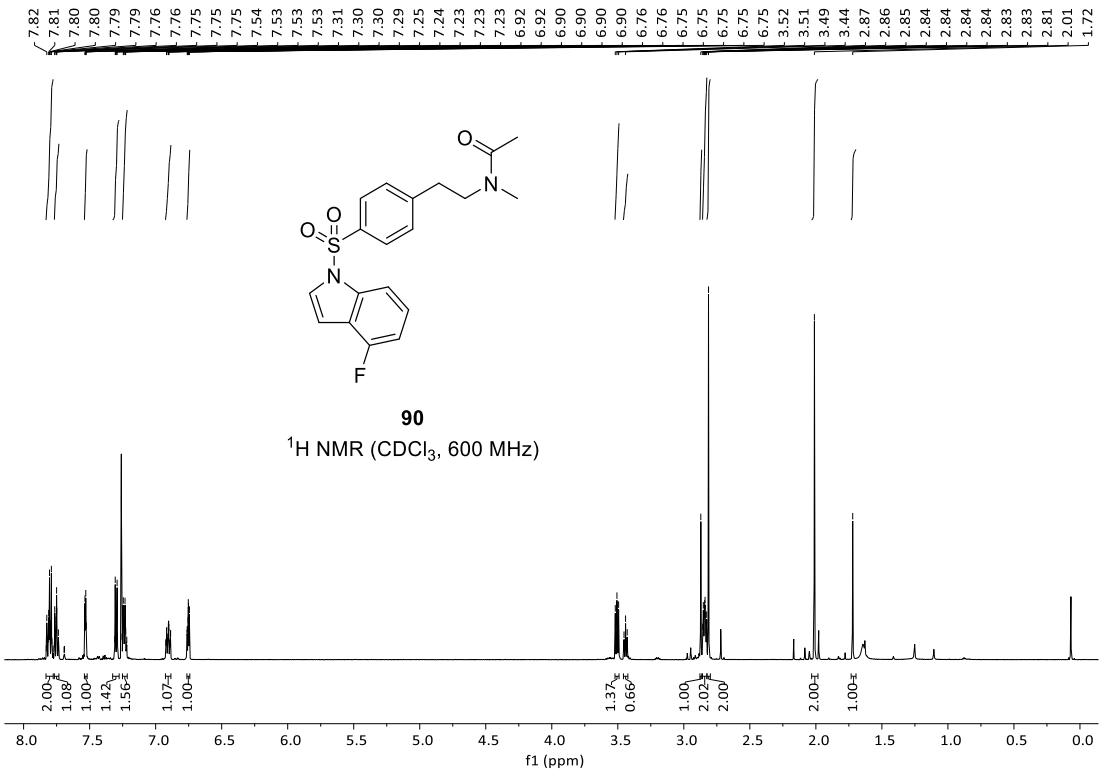

90

^{1}H NMR ($CDCl_3$, 600 MHz)

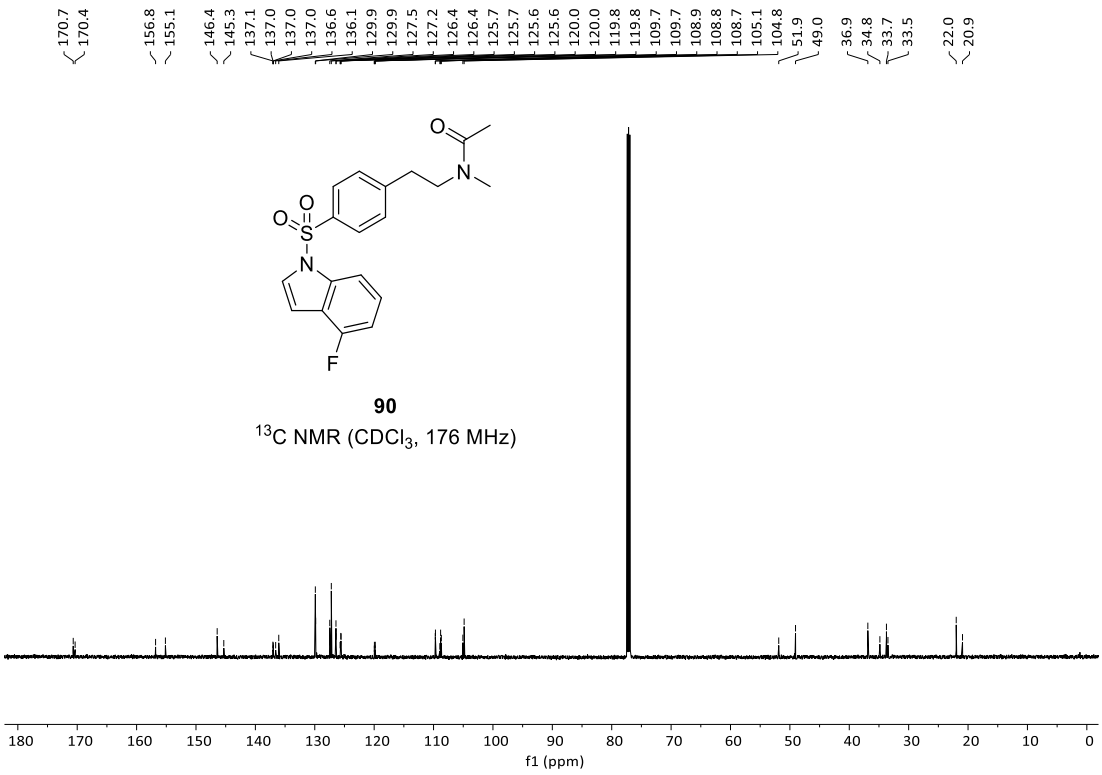

90

^{13}C NMR ($CDCl_3$, 176 MHz)

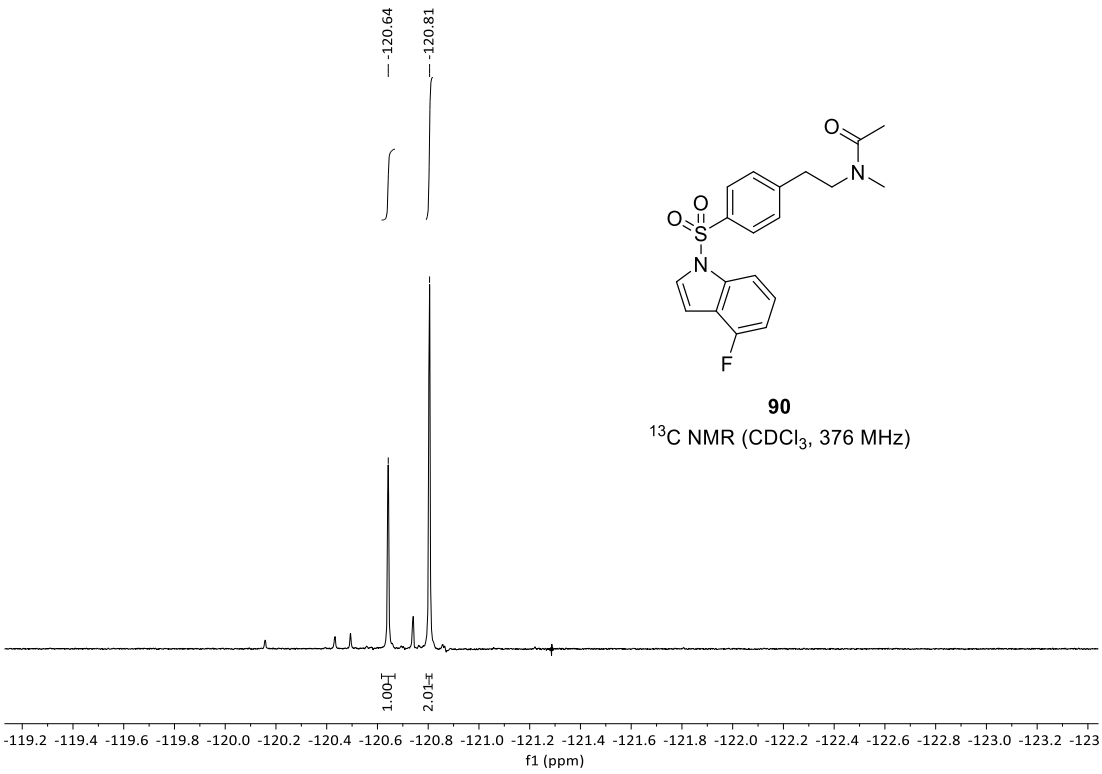

90

^{13}C NMR ($CDCl_3$, 376 MHz)

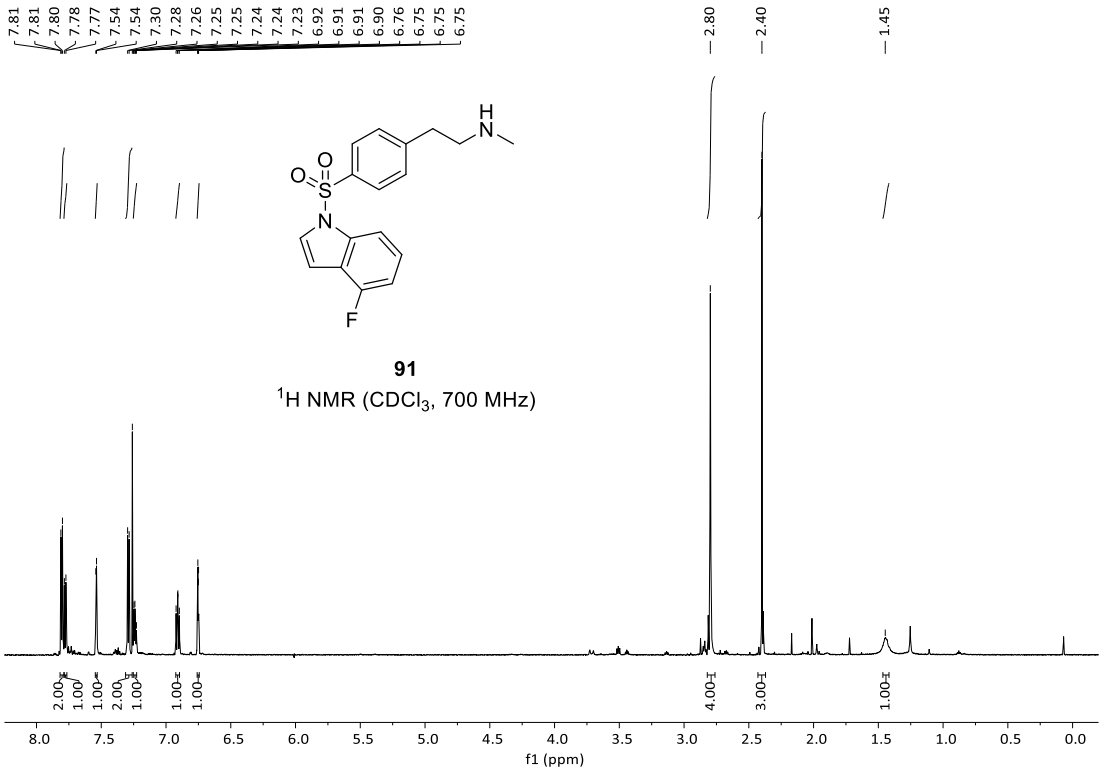

91

^{1}H NMR ($CDCl_3$, 700 MHz)

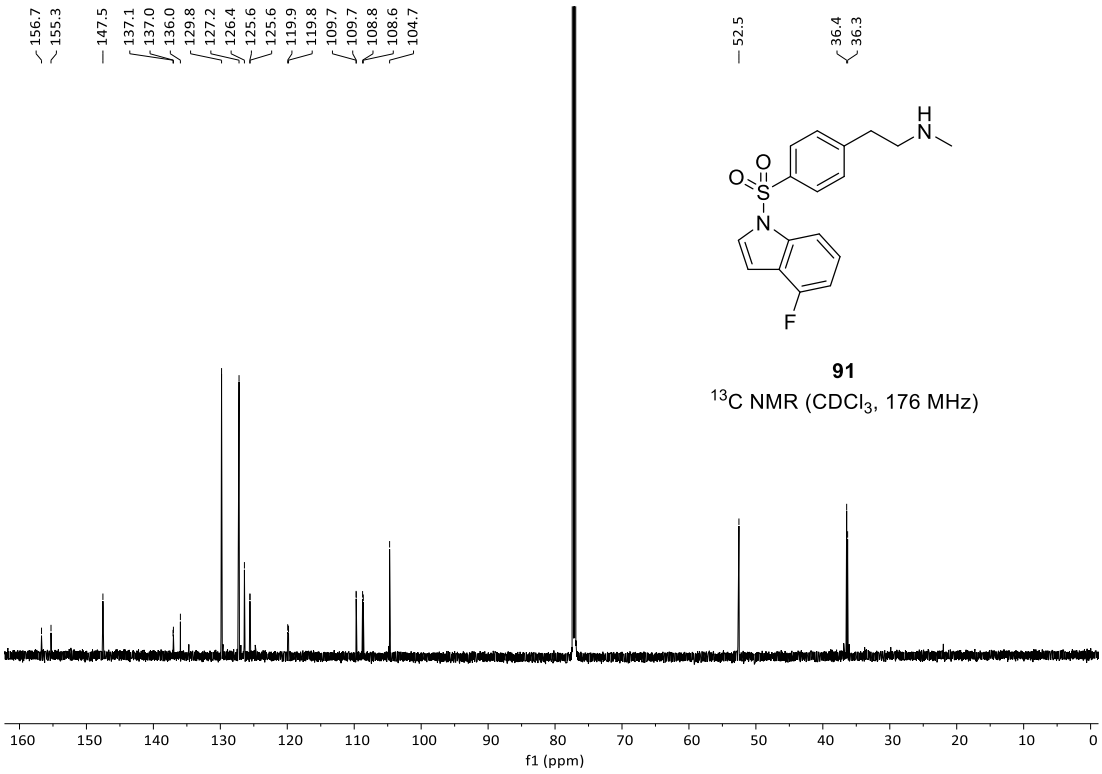

91

^{13}C NMR ($CDCl_3$, 176 MHz)

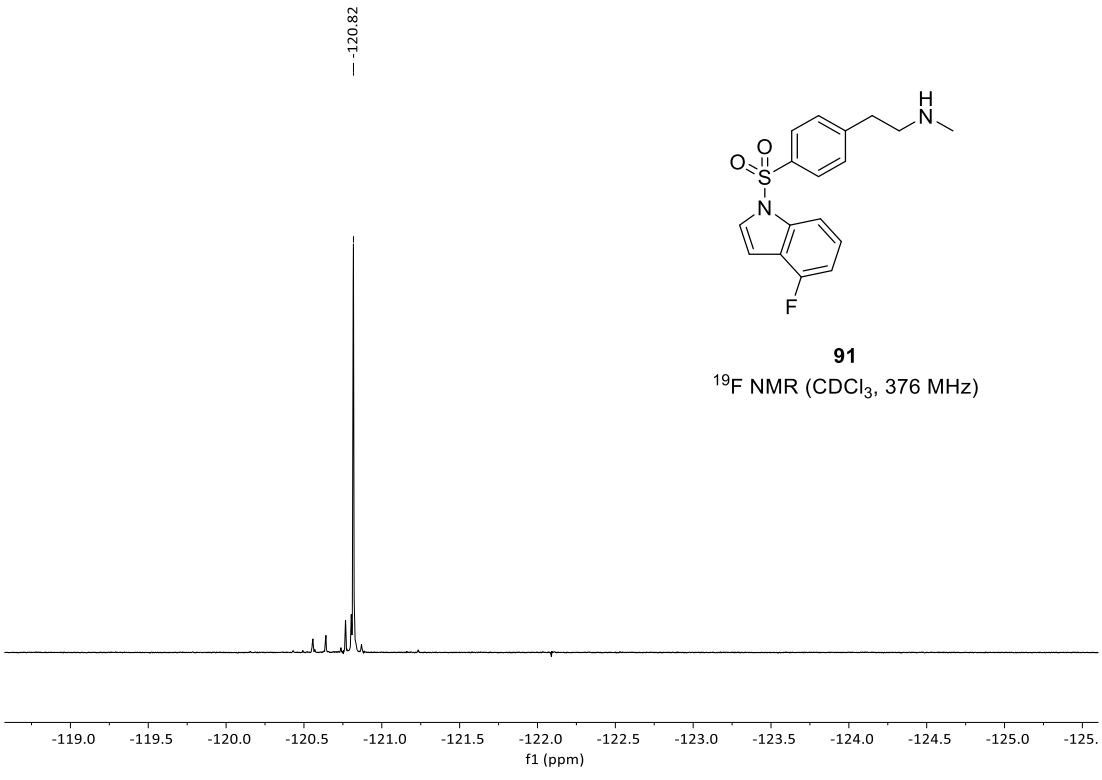

91

^{19}F NMR ($CDCl_3$, 376 MHz)

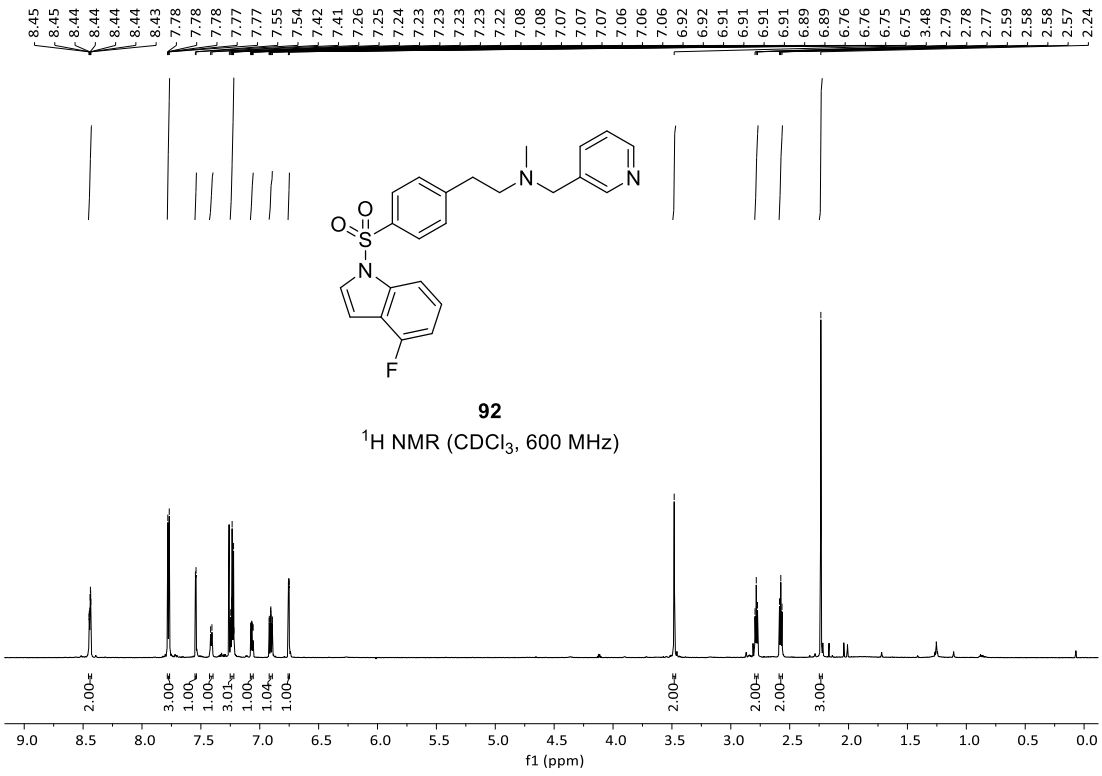

92

^{1}H NMR ($CDCl_3$, 600 MHz)

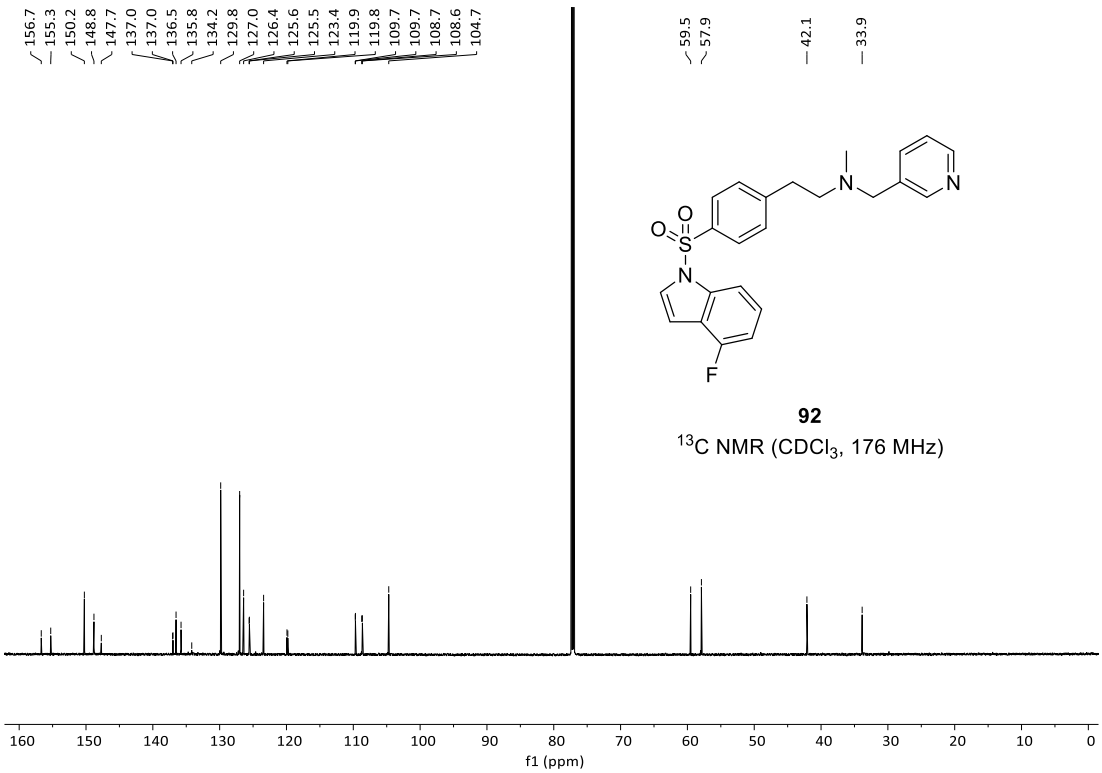

92

^{13}C NMR ($CDCl_3$, 176 MHz)

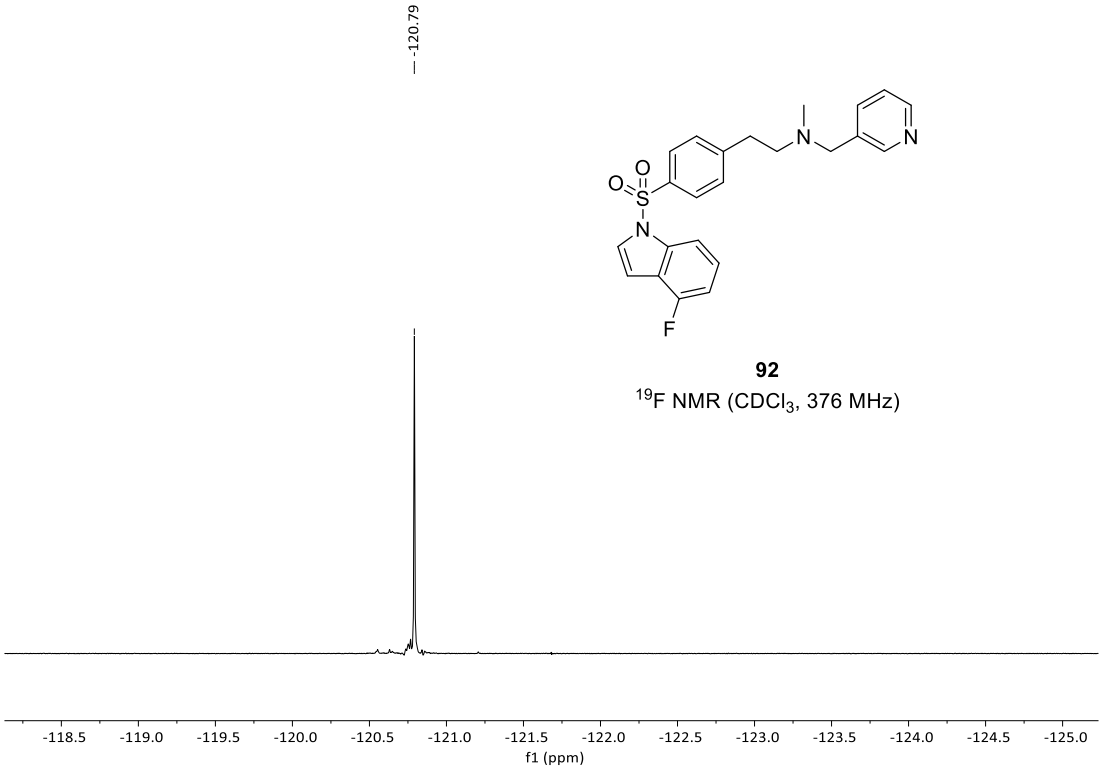

92

^{19}F NMR ($CDCl_3$, 376 MHz)

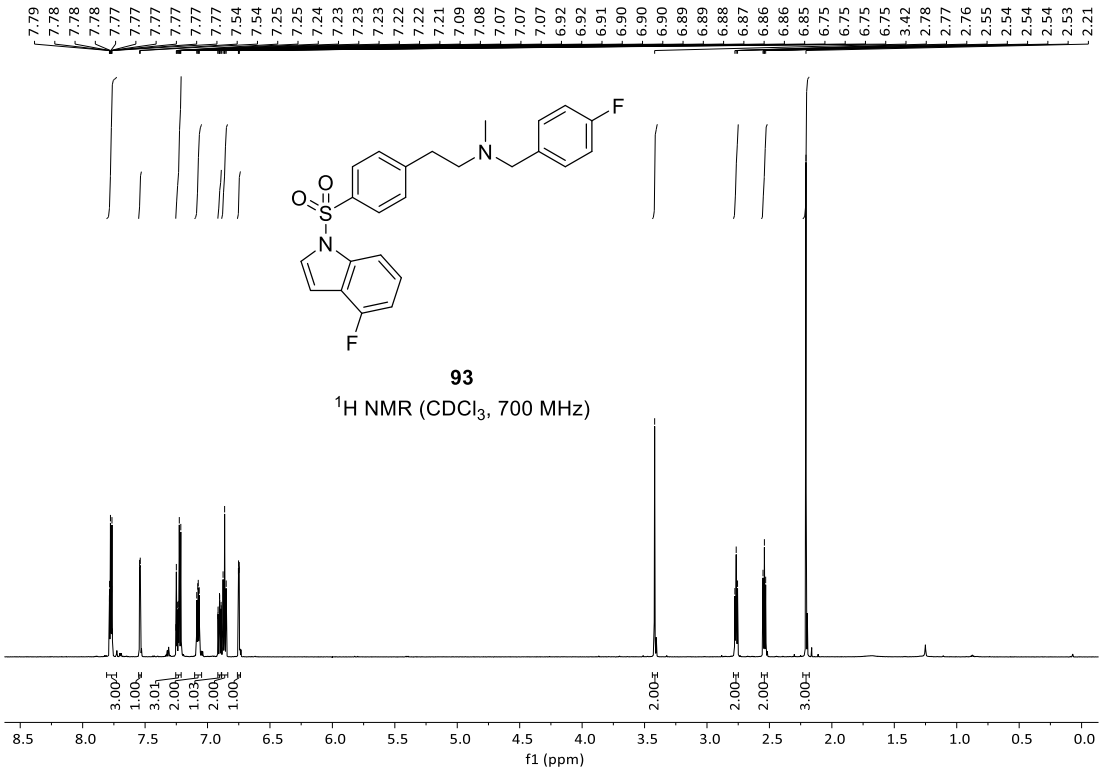

93

^{1}H NMR ($CDCl_3$, 700 MHz)

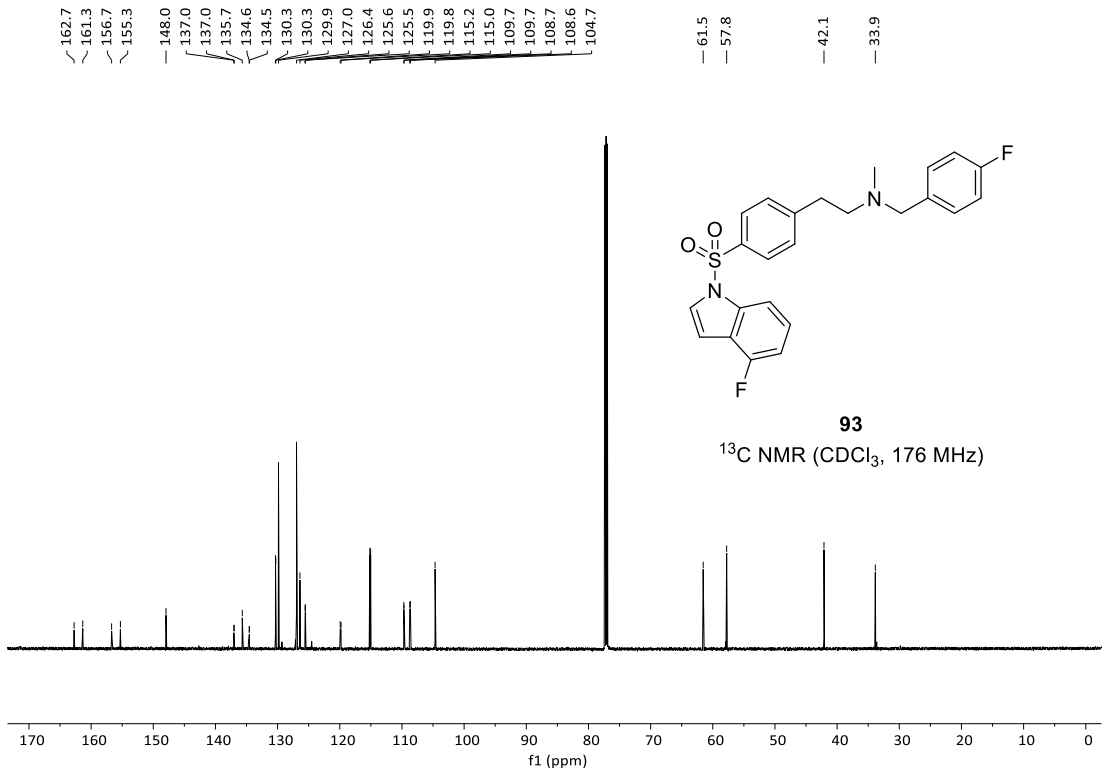

93

^{13}C NMR ($CDCl_3$, 176 MHz)

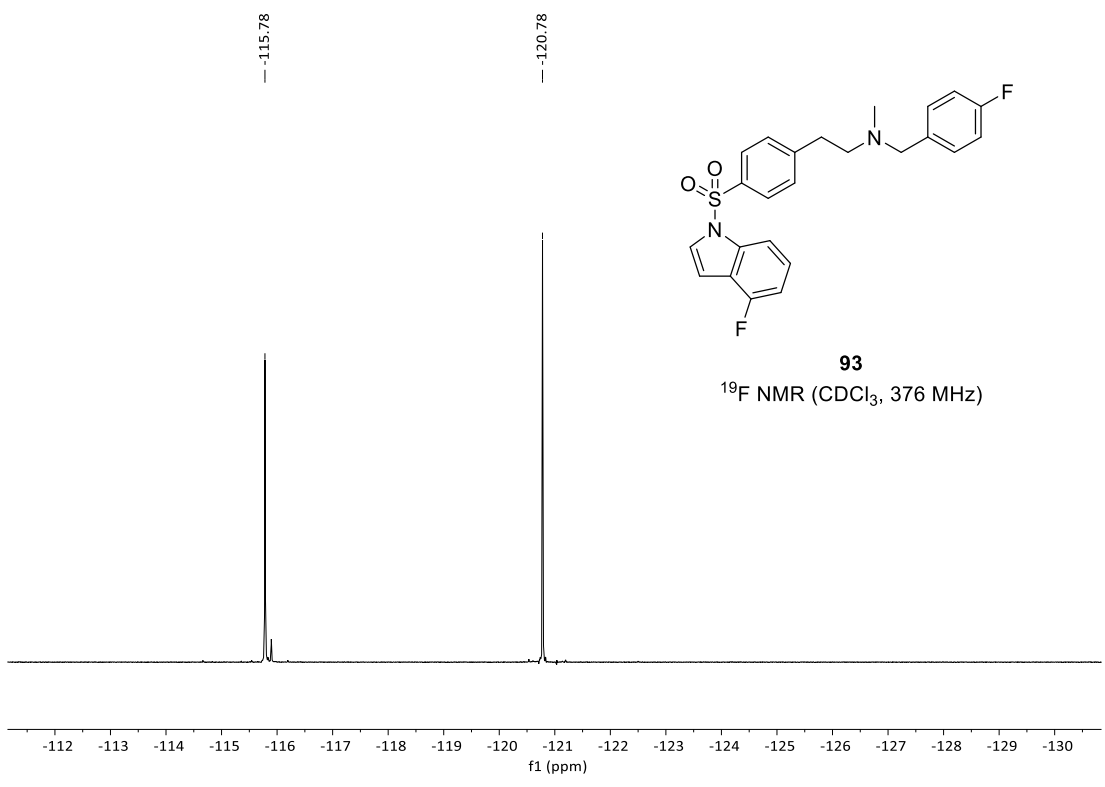

93

^{19}F NMR ($CDCl_3$, 376 MHz)

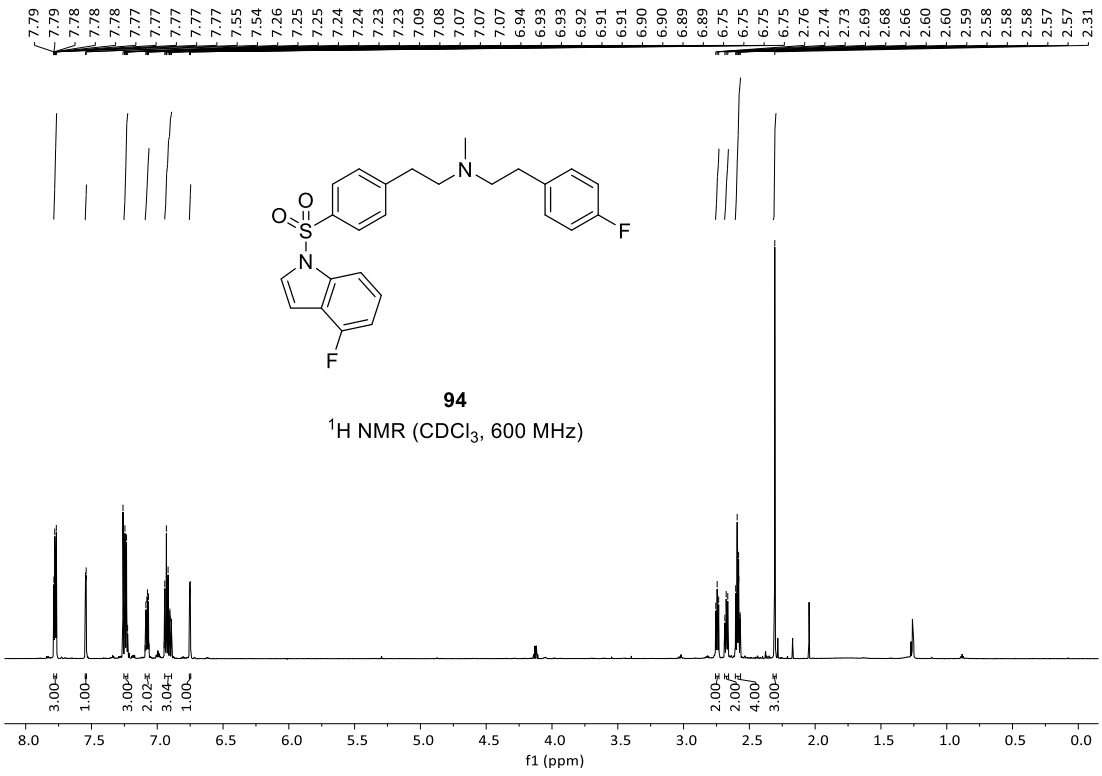

94

^{1}H NMR ($CDCl_3$, 600 MHz)

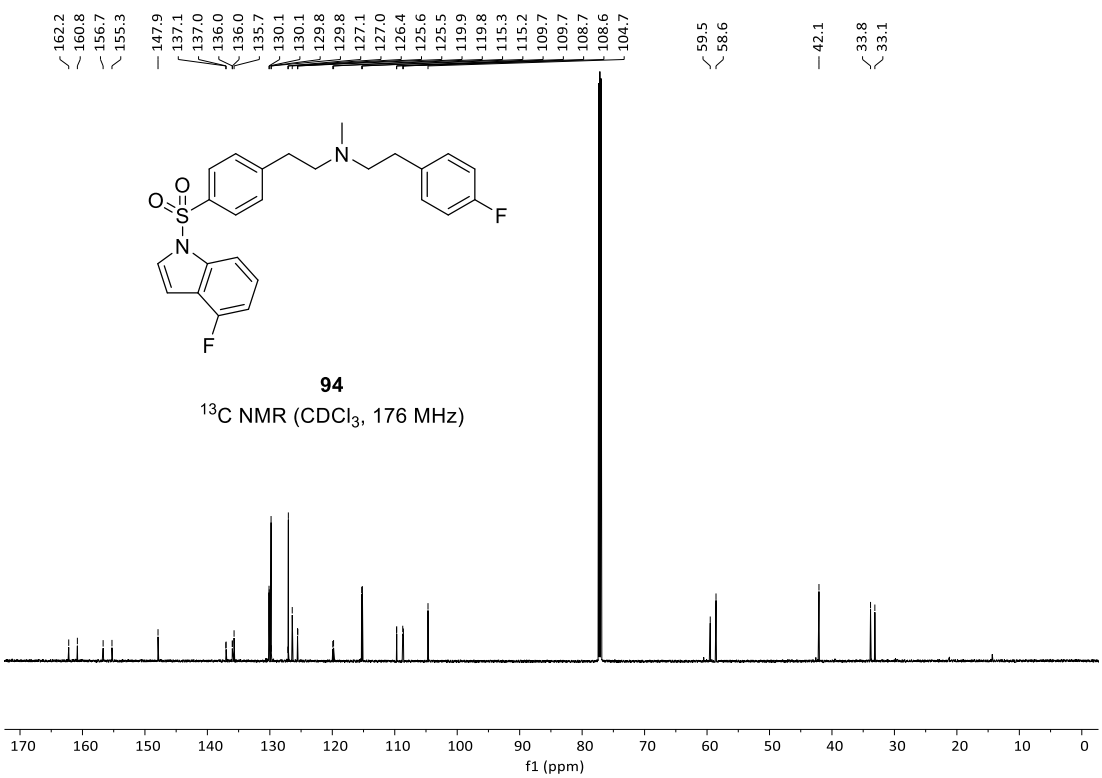

94

^{13}C NMR ($CDCl_3$, 176 MHz)

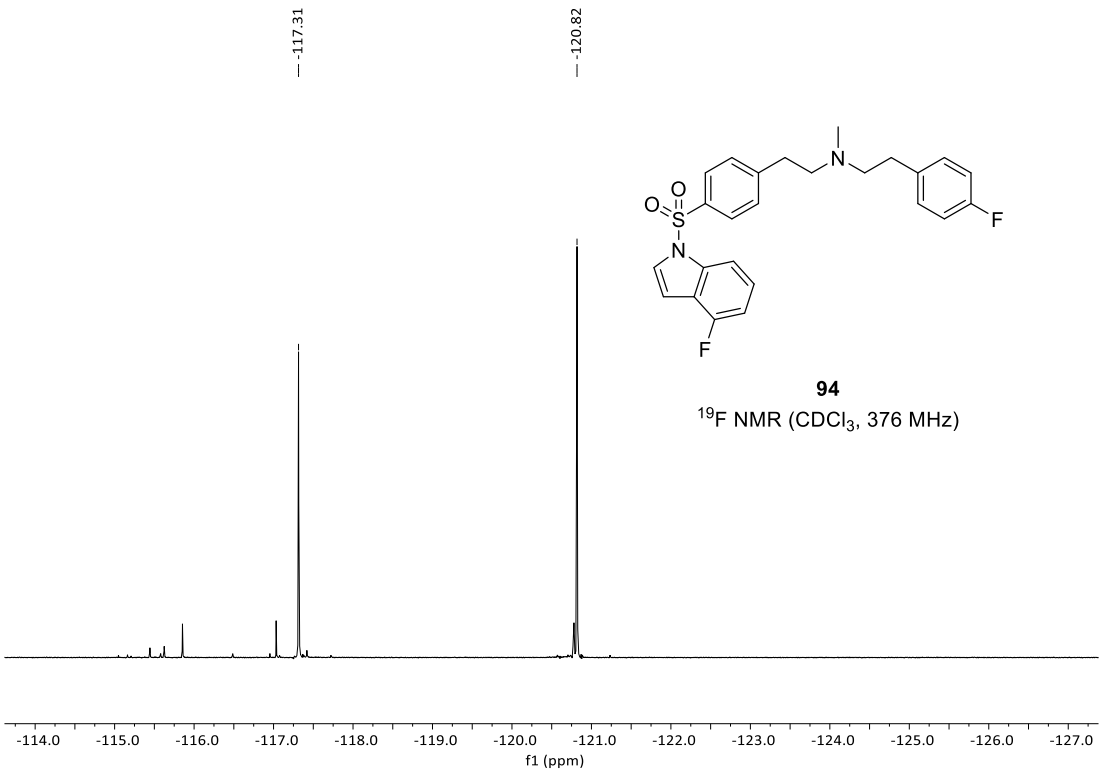

94

^{19}F NMR ($CDCl_3$, 376 MHz)

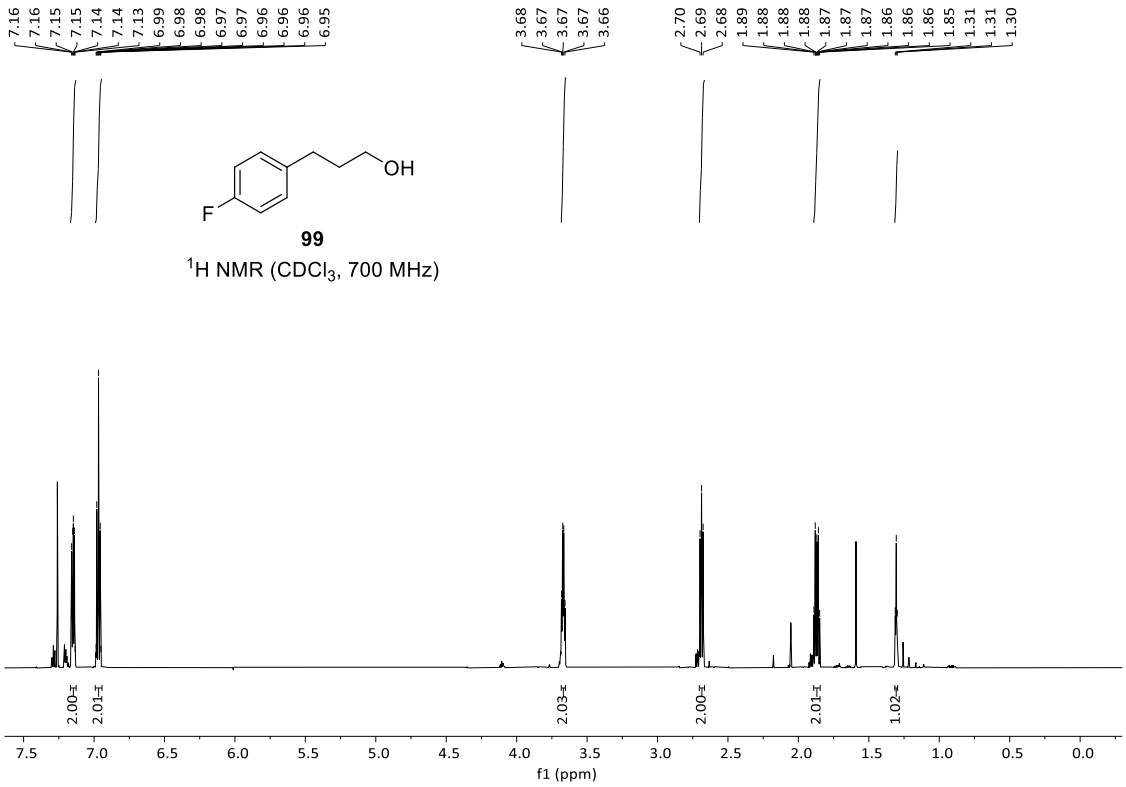

99

^{1}H NMR ($CDCl_3$, 700 MHz)

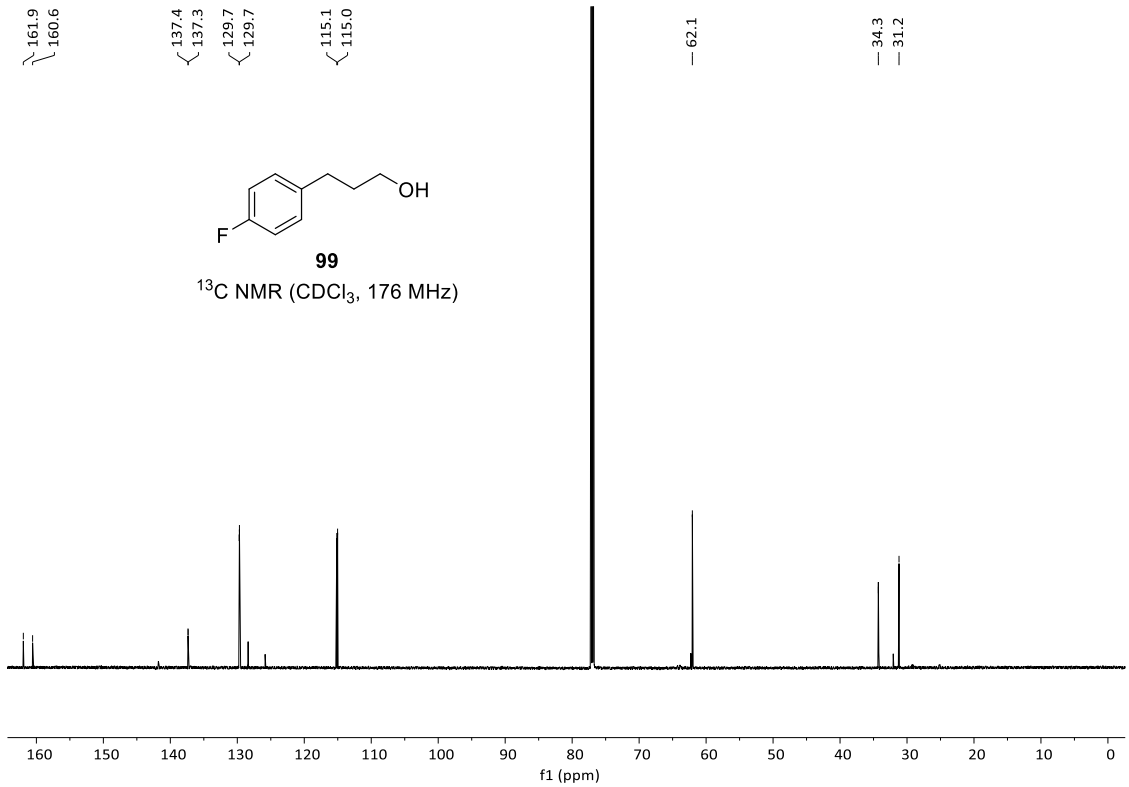

99

^{13}C NMR ($CDCl_3$, 176 MHz)

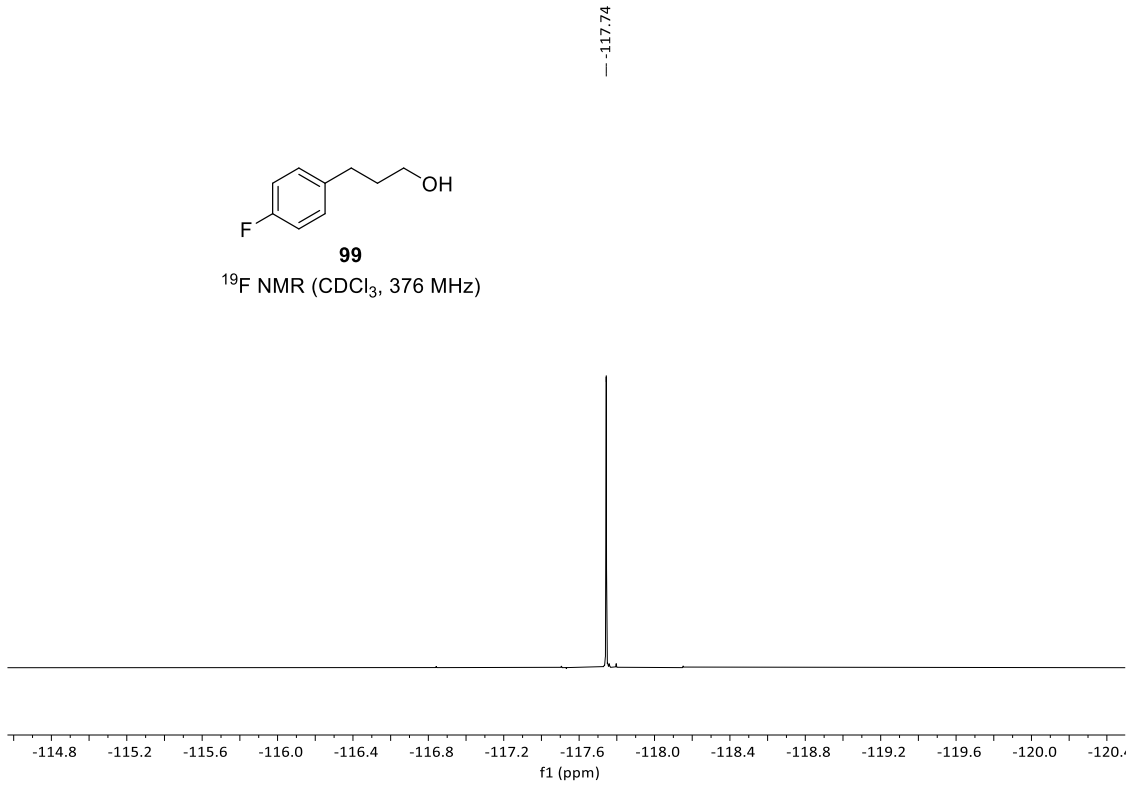

99

^{19}F NMR ($CDCl_3$, 376 MHz)

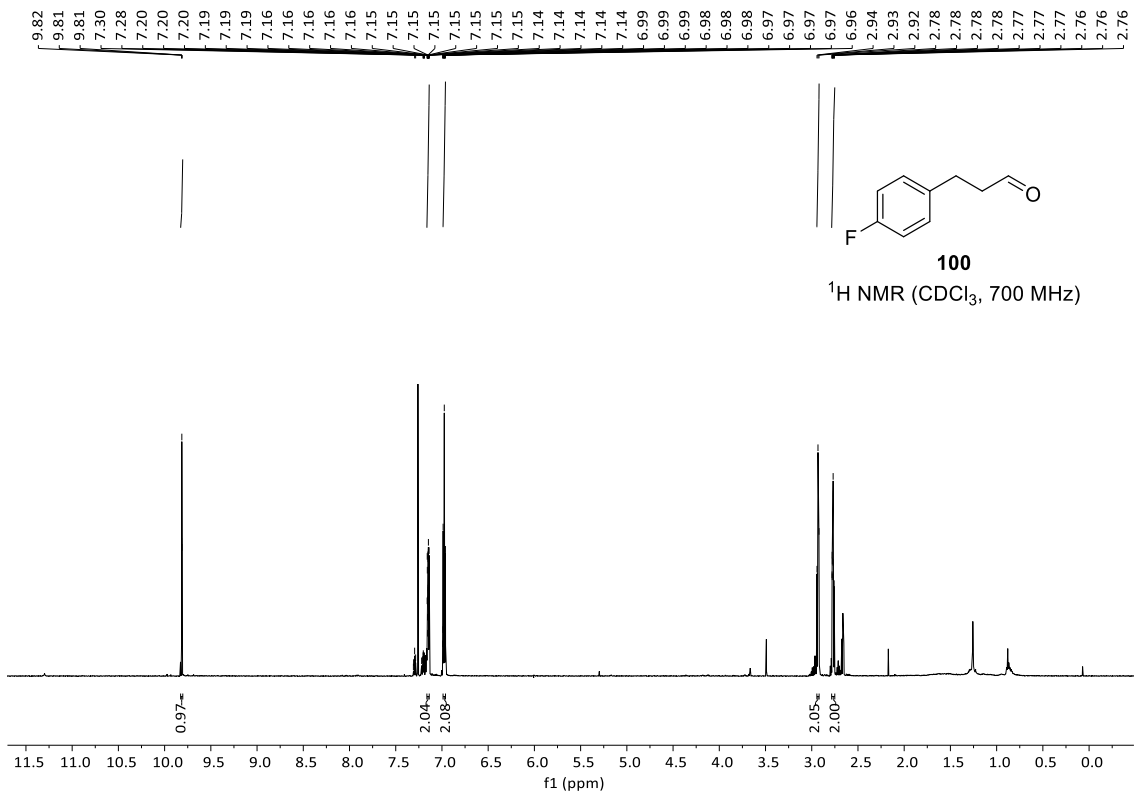
9.82 9.81 9.81 7.30 7.28 7.20 7.20 7.20 7.19 7.19 7.19 7.16 7.16 7.16 7.16 7.15 7.15 7.15 7.15 7.15 7.15 7.15 7.14 7.14 7.14 7.14 7.14 6.99 6.99 6.99 6.98 6.98 6.98 6.97 6.97 6.97 6.97 6.96 2.94 2.93 2.92 2.78 2.78 2.78 2.78 2.77 2.77 2.77 2.76 2.76 2.76
O
F
100
^{1}H NMR ($CDCl_3$, 700 MHz)
0.97
2.04
2.08
2.05
2.00
11.5 11.0 10.5 10.0 9.5 9.0 8.5 8.0 7.5 7.0 6.5 6.0 5.5 5.0 4.5 4.0 3.5 3.0 2.5 2.0 1.5 1.0 0.5 0.0
f1 (ppm)

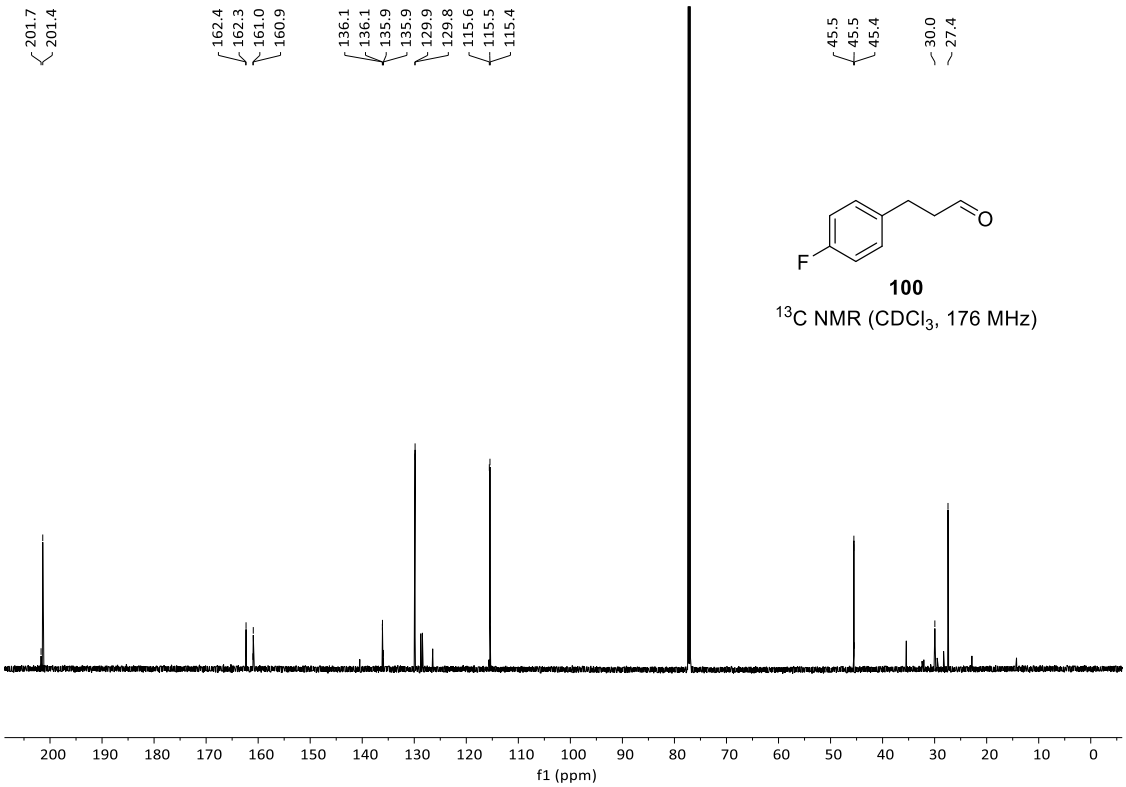

100

^{13}C NMR ($CDCl_3$, 176 MHz)

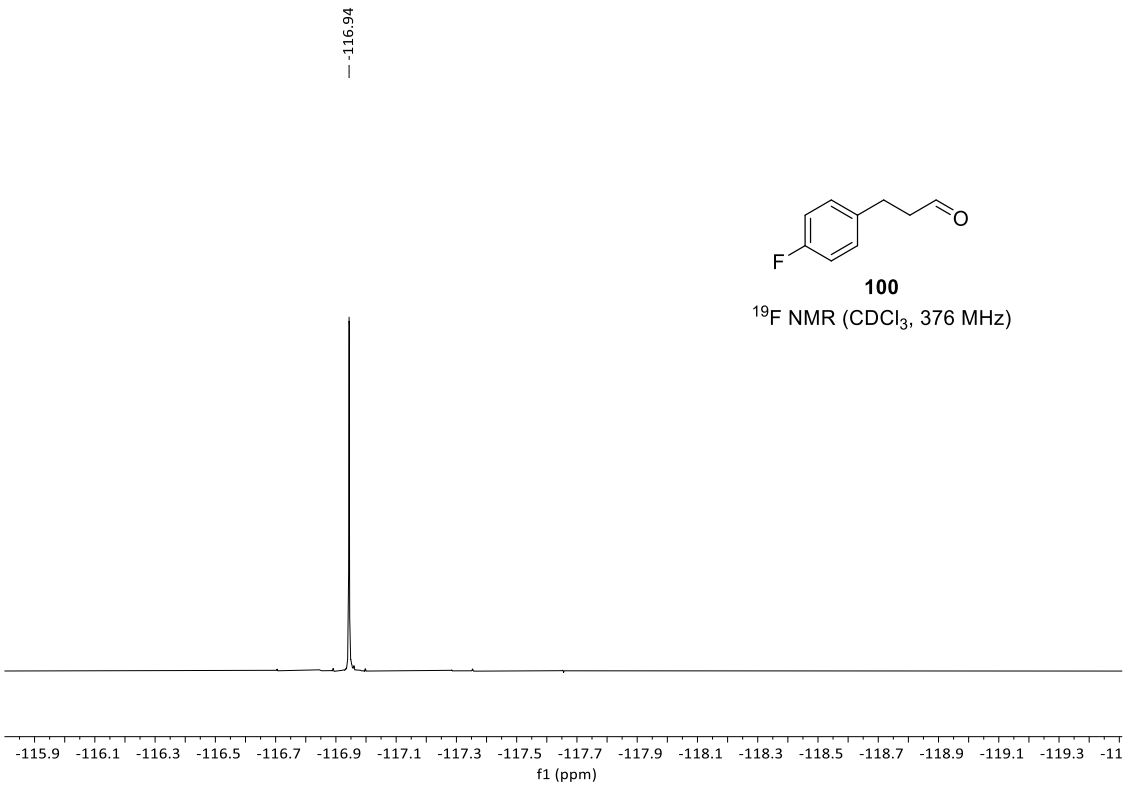

100

^{19}F NMR ($CDCl_3$, 376 MHz)

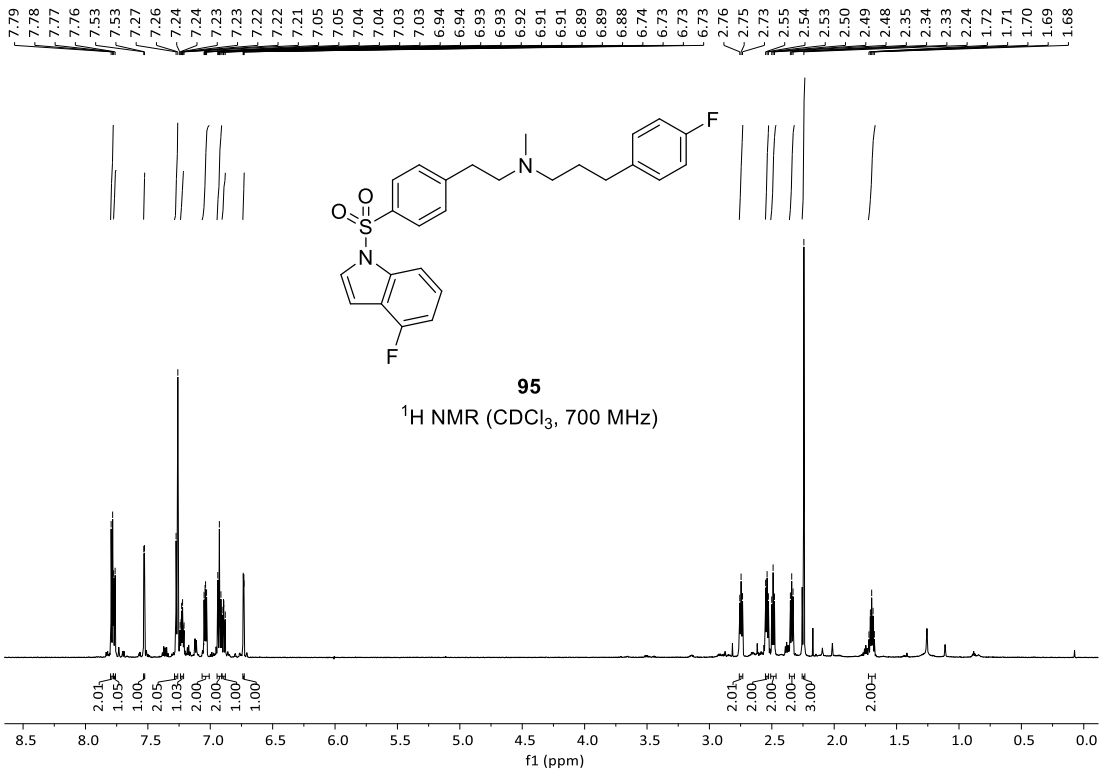

95

^{1}H NMR ($CDCl_3$, 700 MHz)

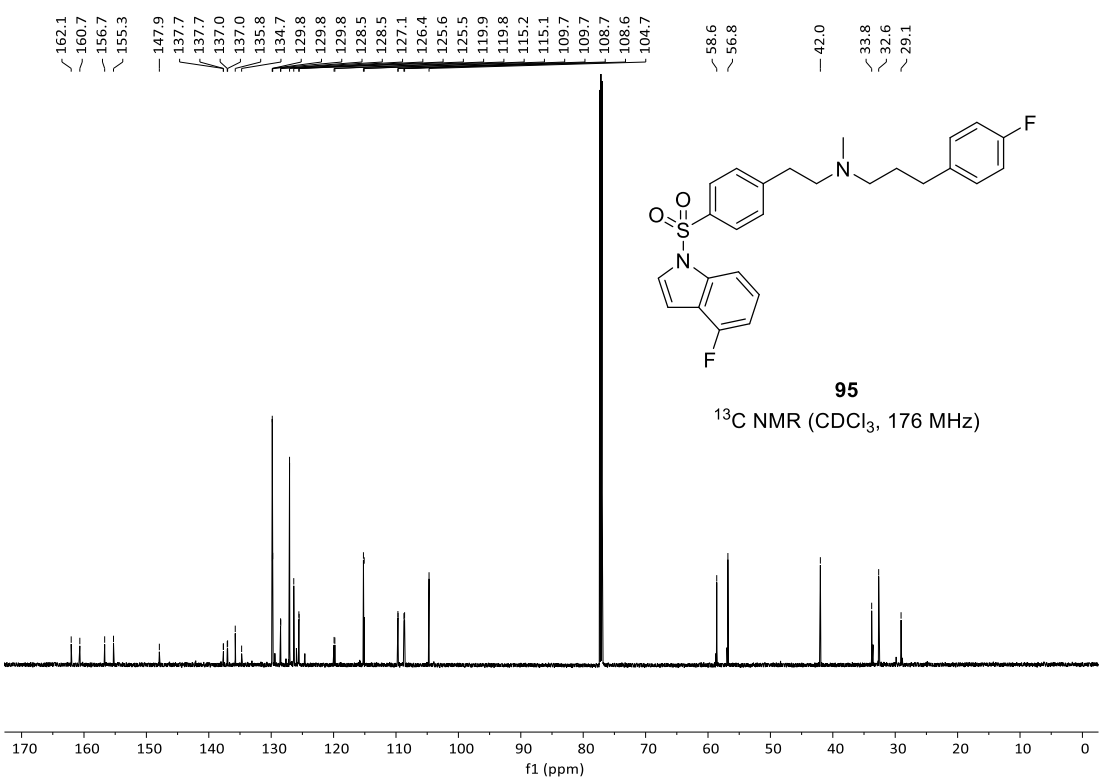

95

^{13}C NMR ($CDCl_3$, 176 MHz)

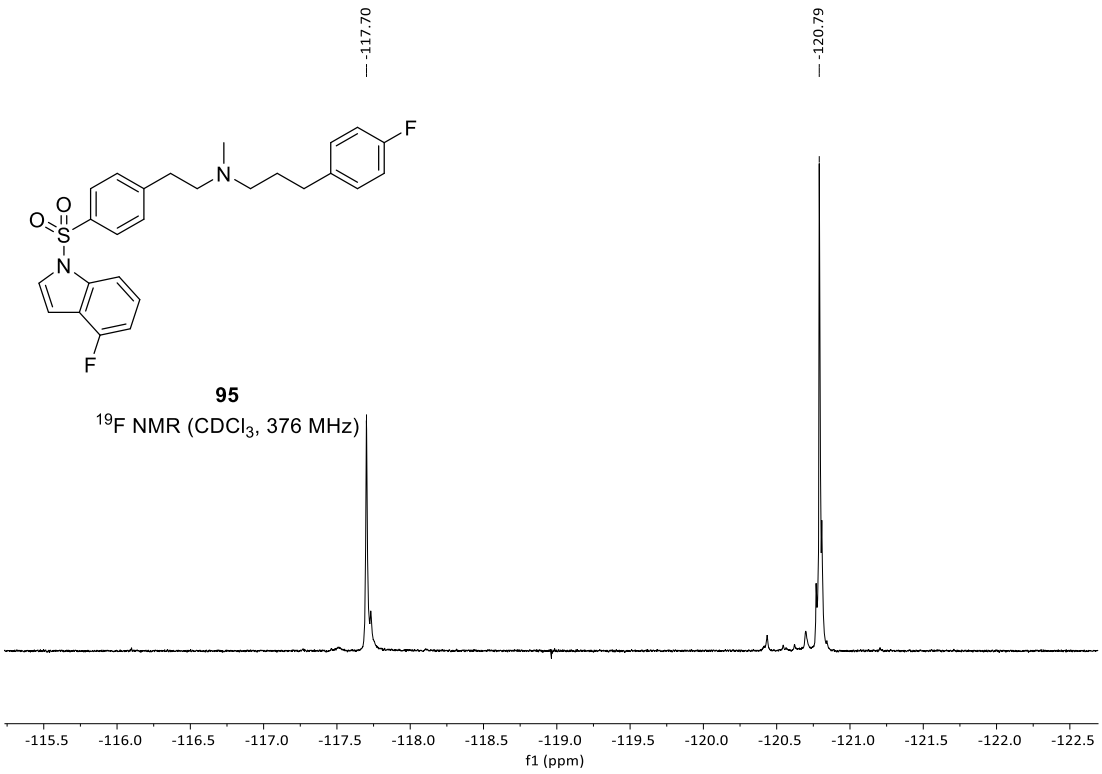

95

^{19}F NMR ($CDCl_3$, 376 MHz)

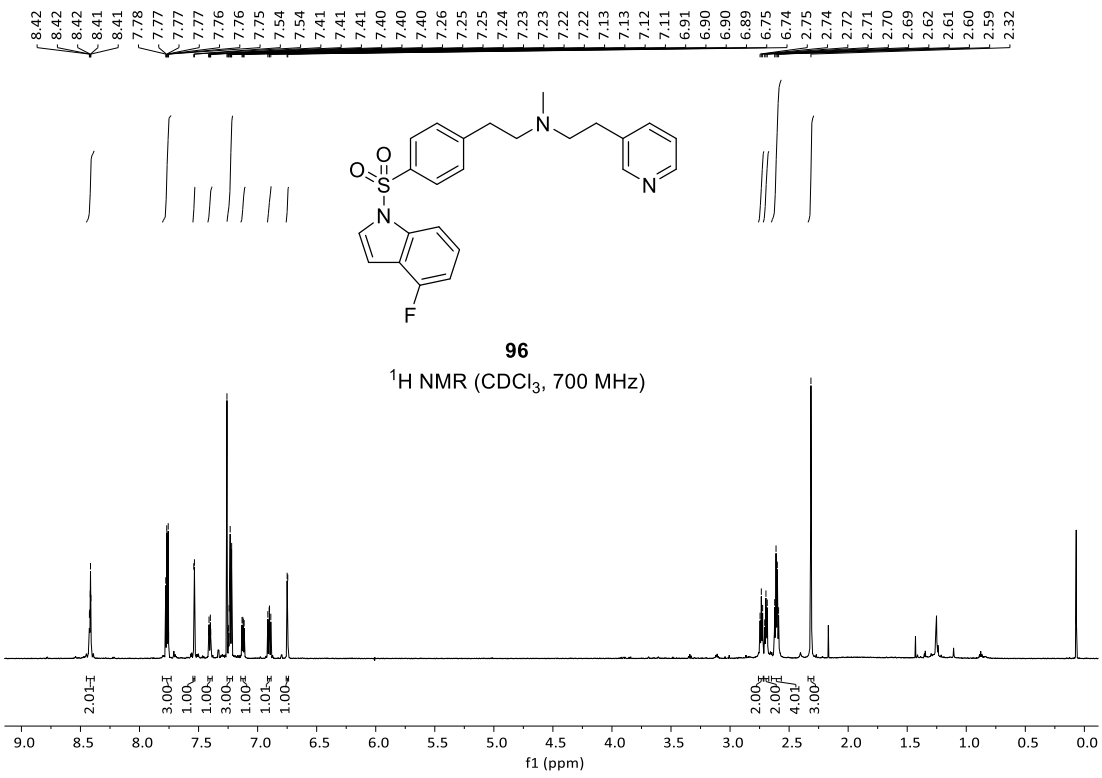

96

^{1}H NMR ($CDCl_3$, 700 MHz)

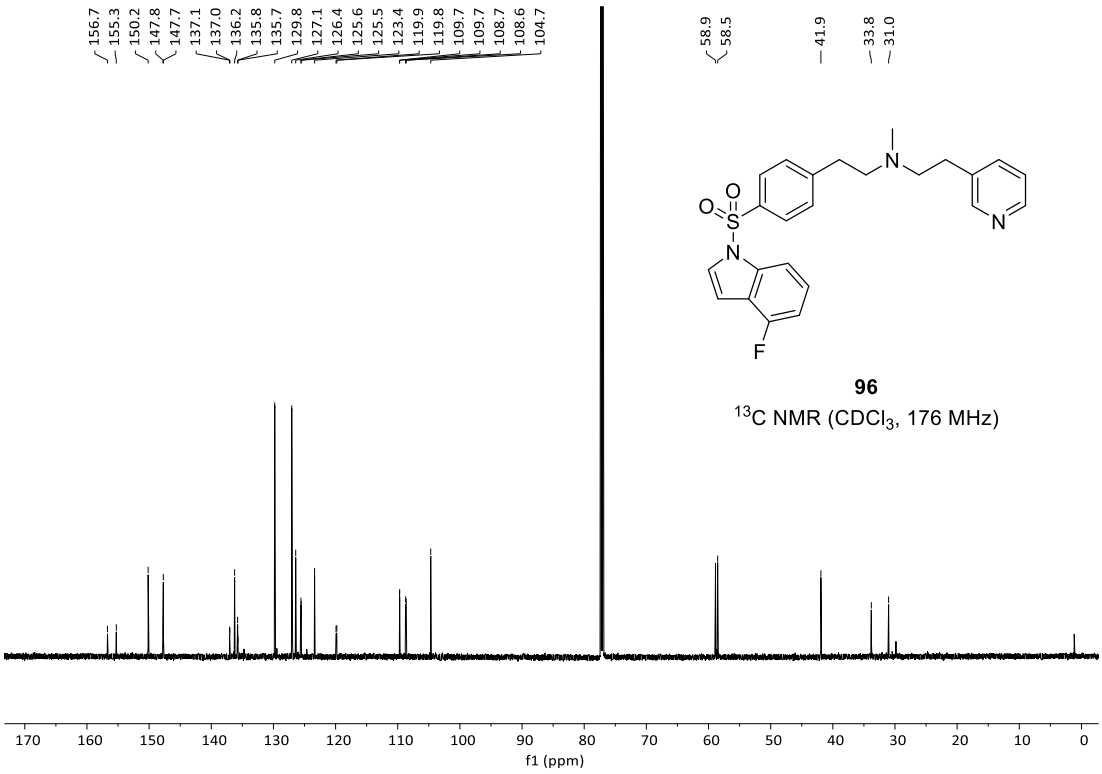

96

^{13}C NMR ($CDCl_3$, 176 MHz)

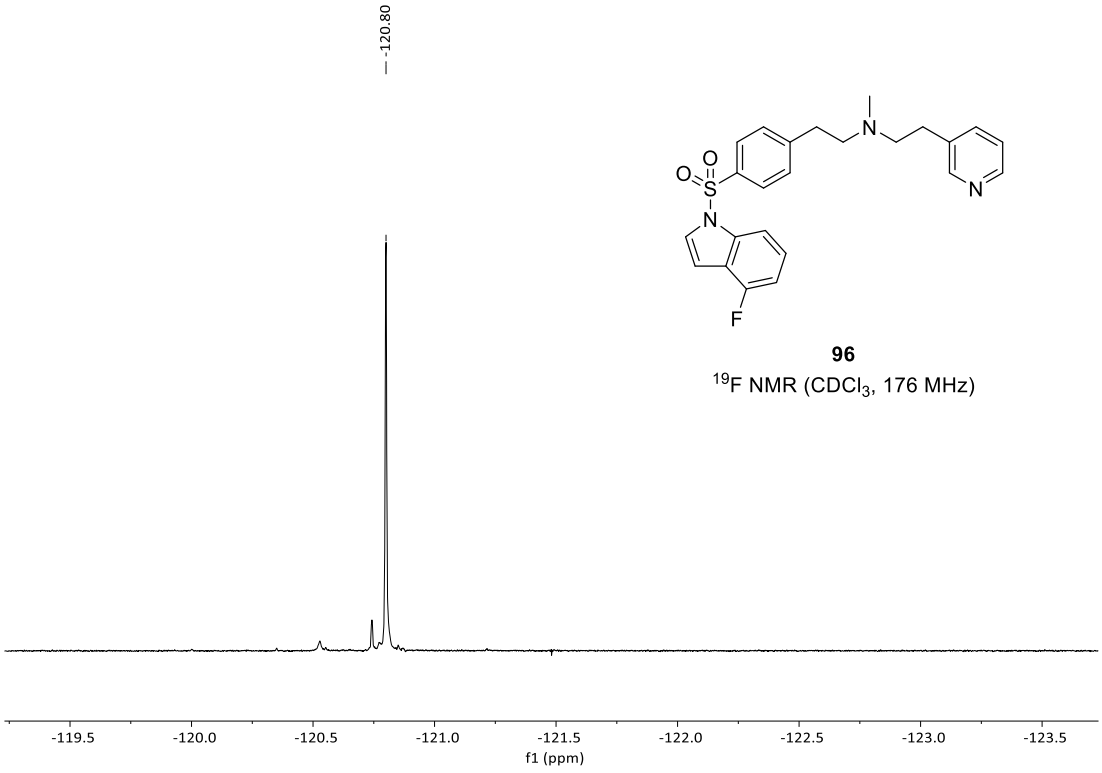

96

^{19}F NMR ($CDCl_3$, 176 MHz)

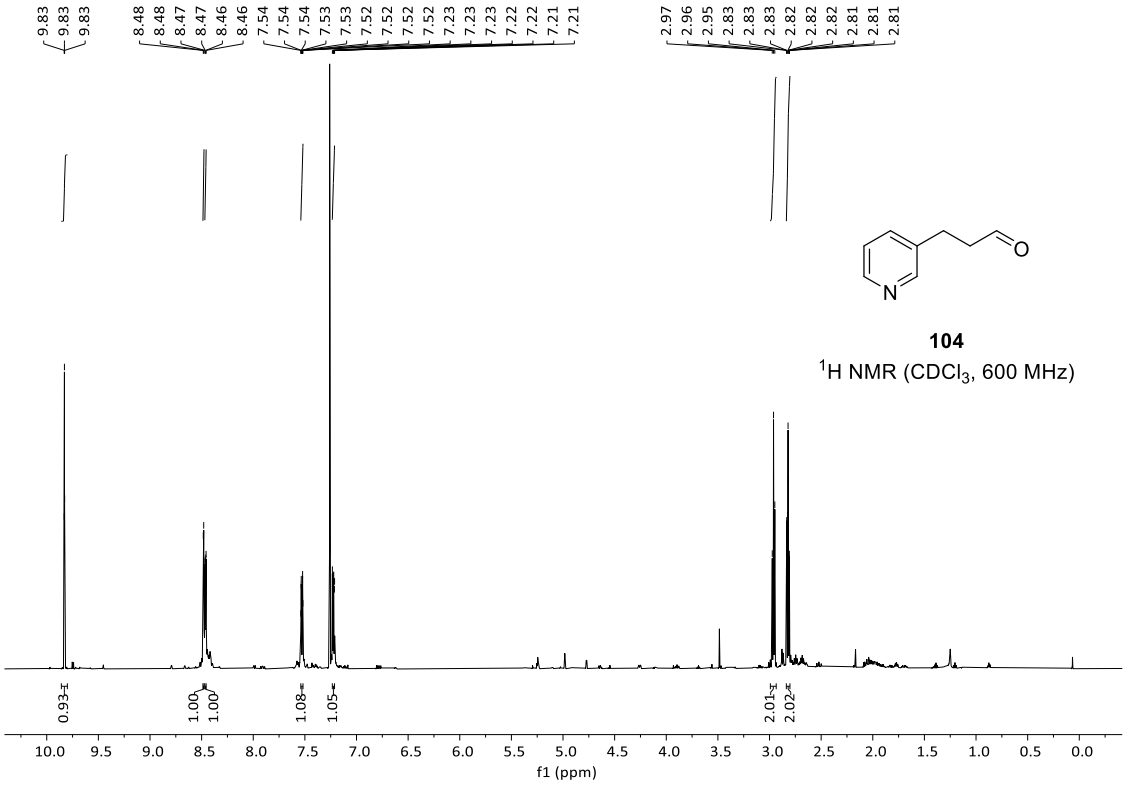

104

^{1}H NMR ($CDCl_3$, 600 MHz)

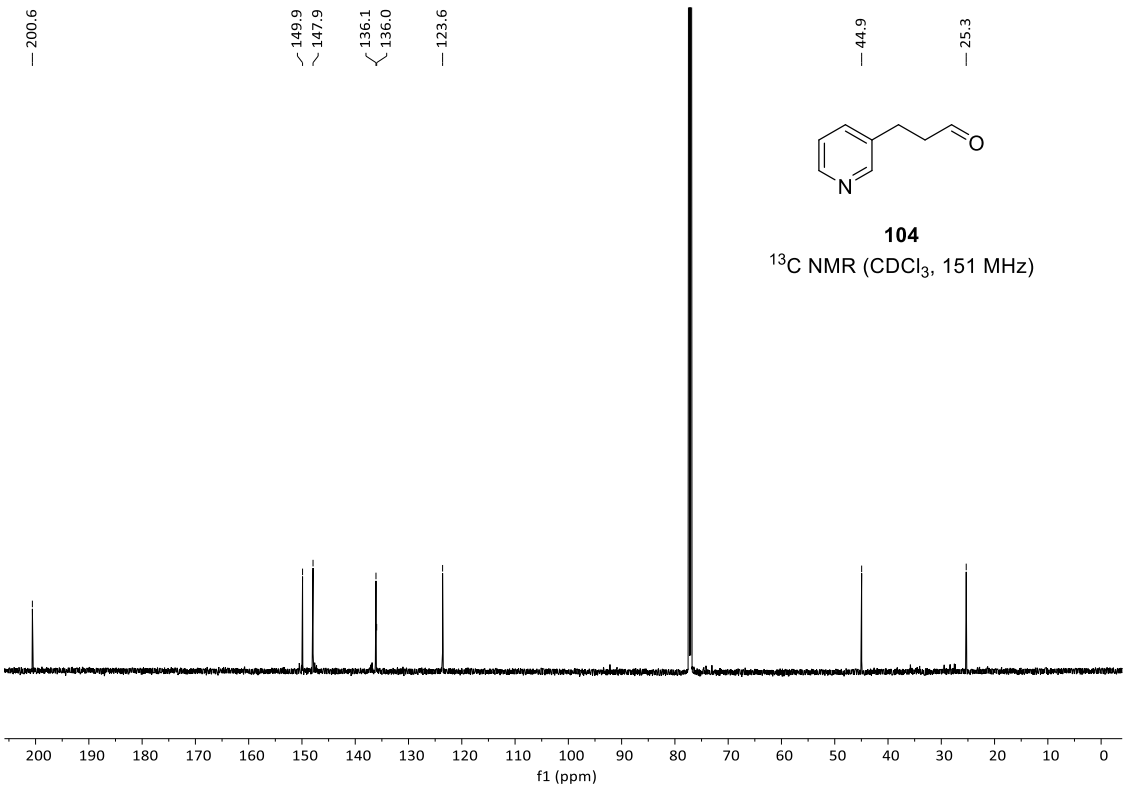

104

^{13}C NMR ($CDCl_3$, 151 MHz)

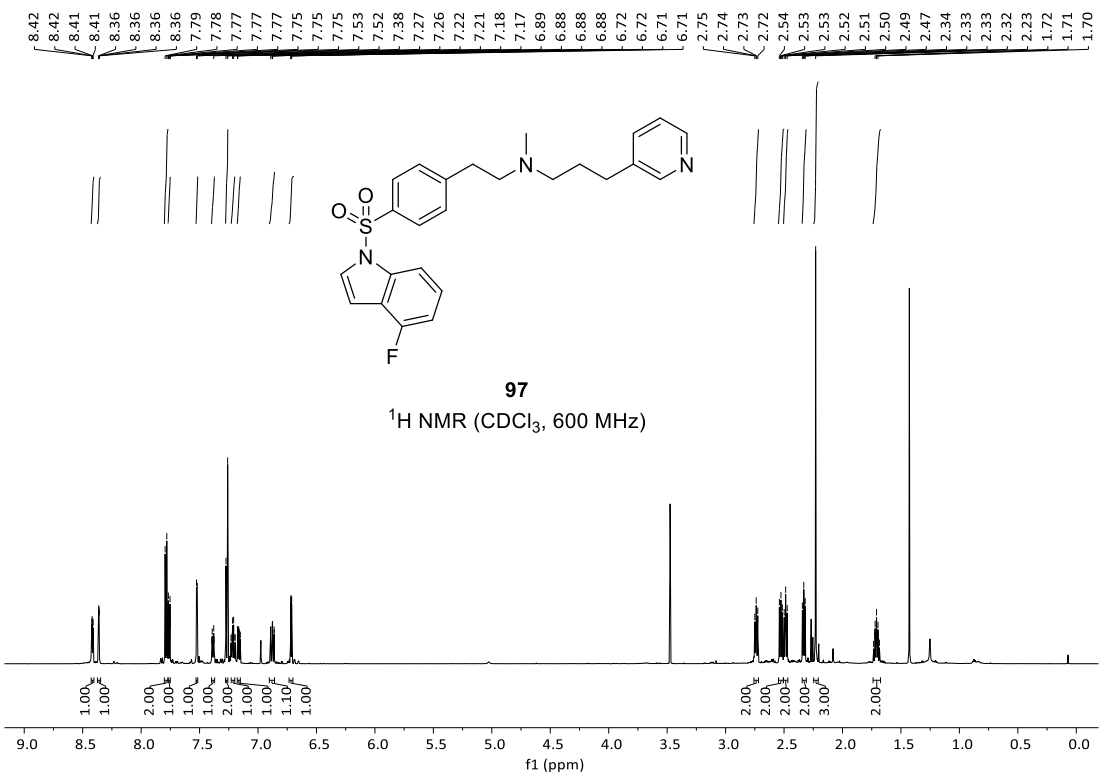

97

^{1}H NMR ($CDCl_3$, 600 MHz)

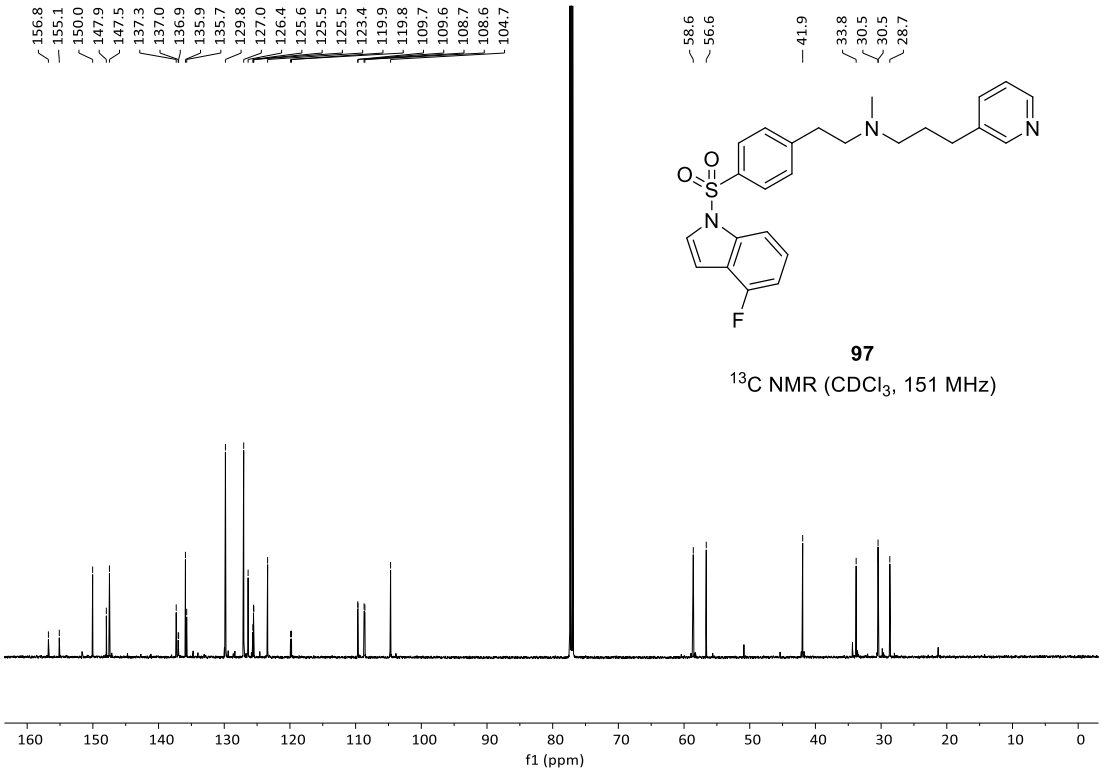

97

^{13}C NMR ($CDCl_3$, 151 MHz)

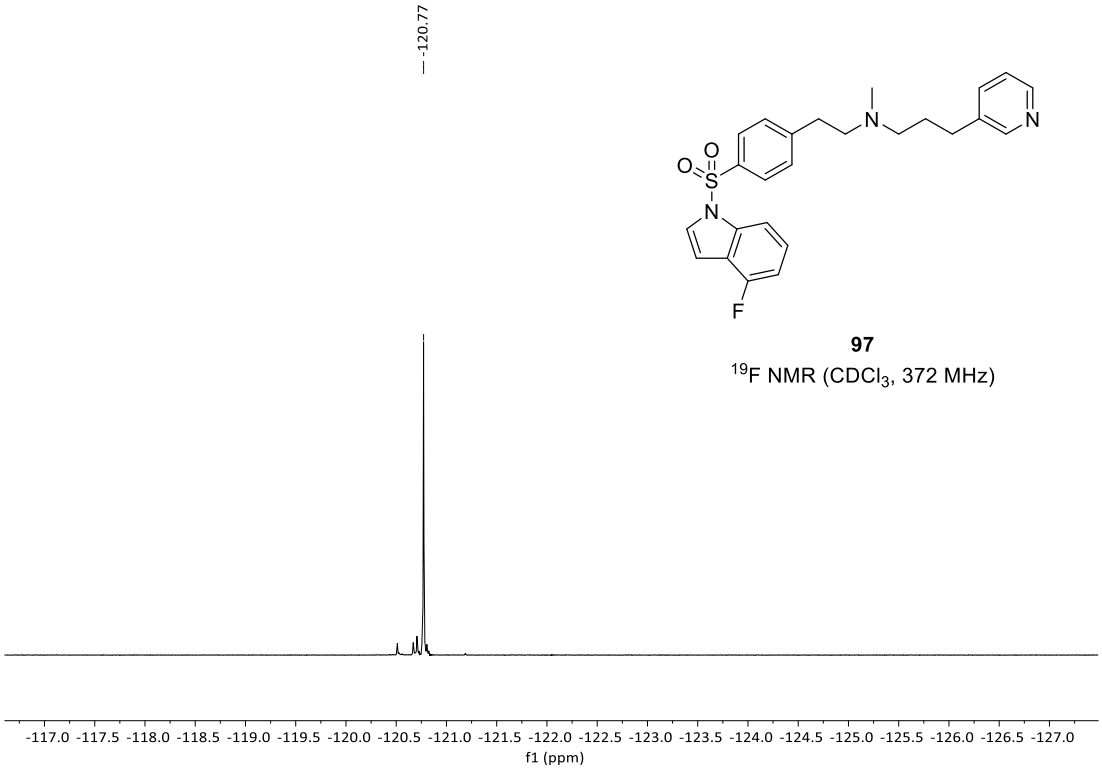

97

^{19}F NMR ($CDCl_3$, 372 MHz)

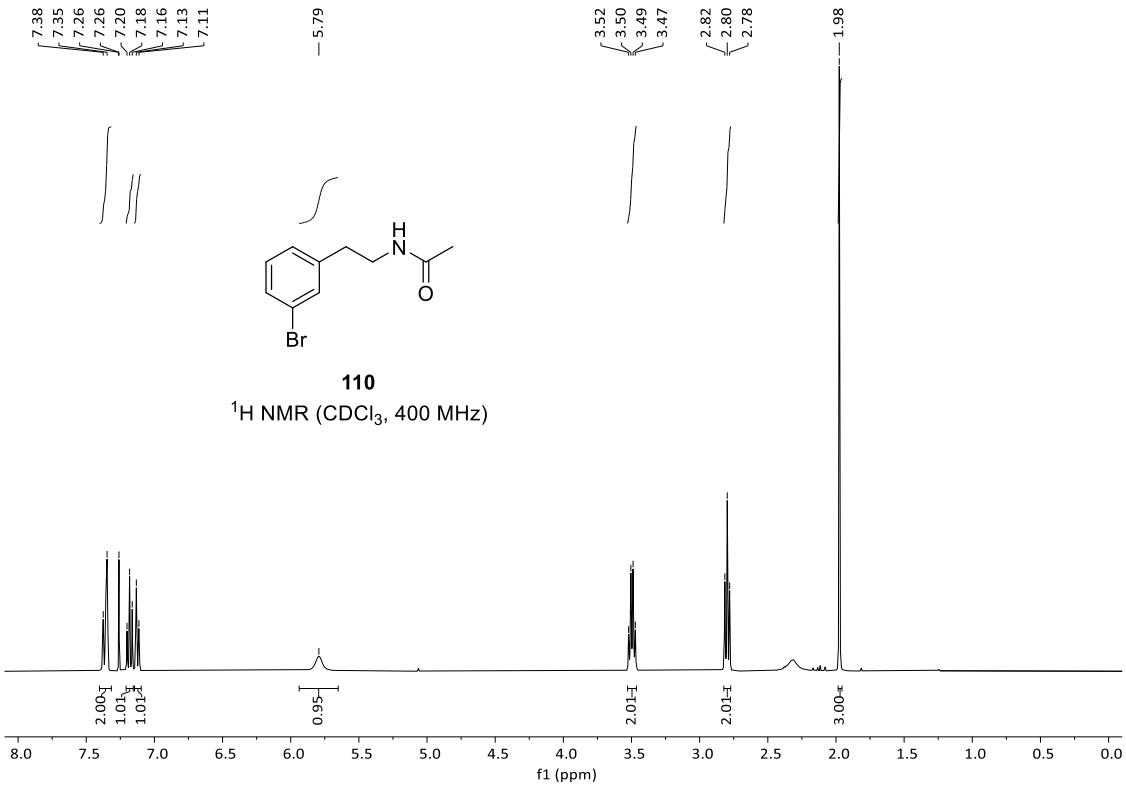

110

^{1}H NMR ($CDCl_3$, 400 MHz)

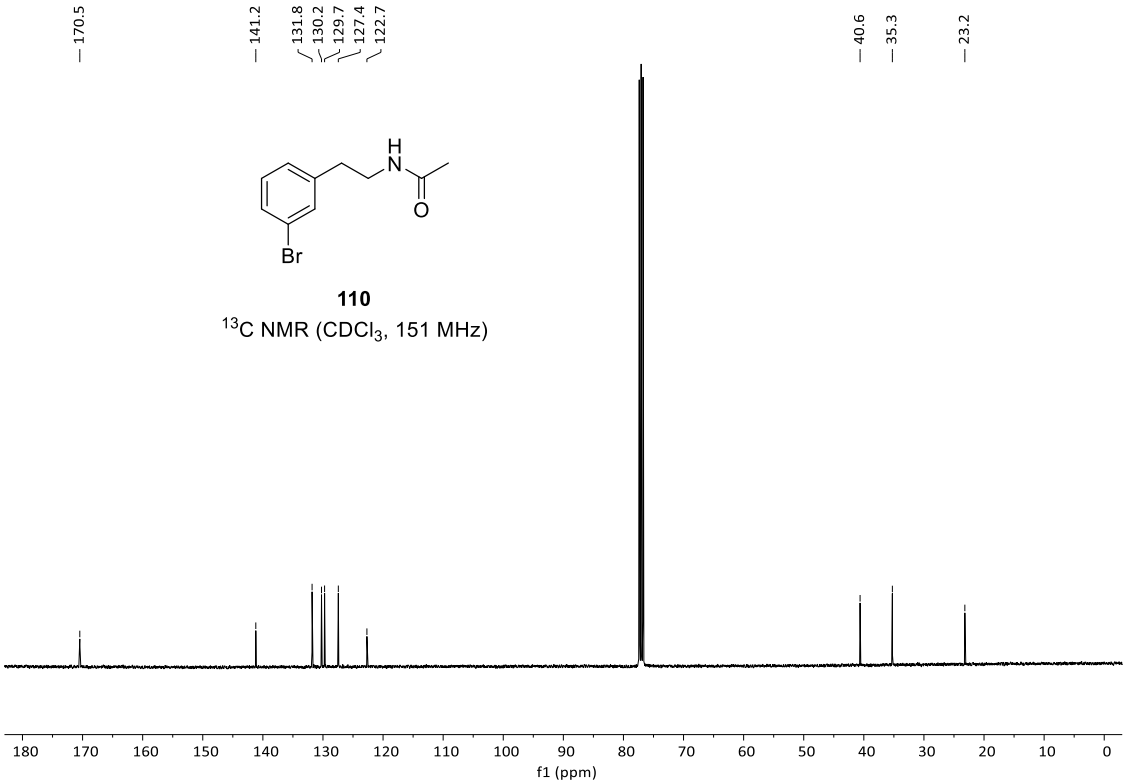

110

^{13}C NMR ($CDCl_3$, 151 MHz)

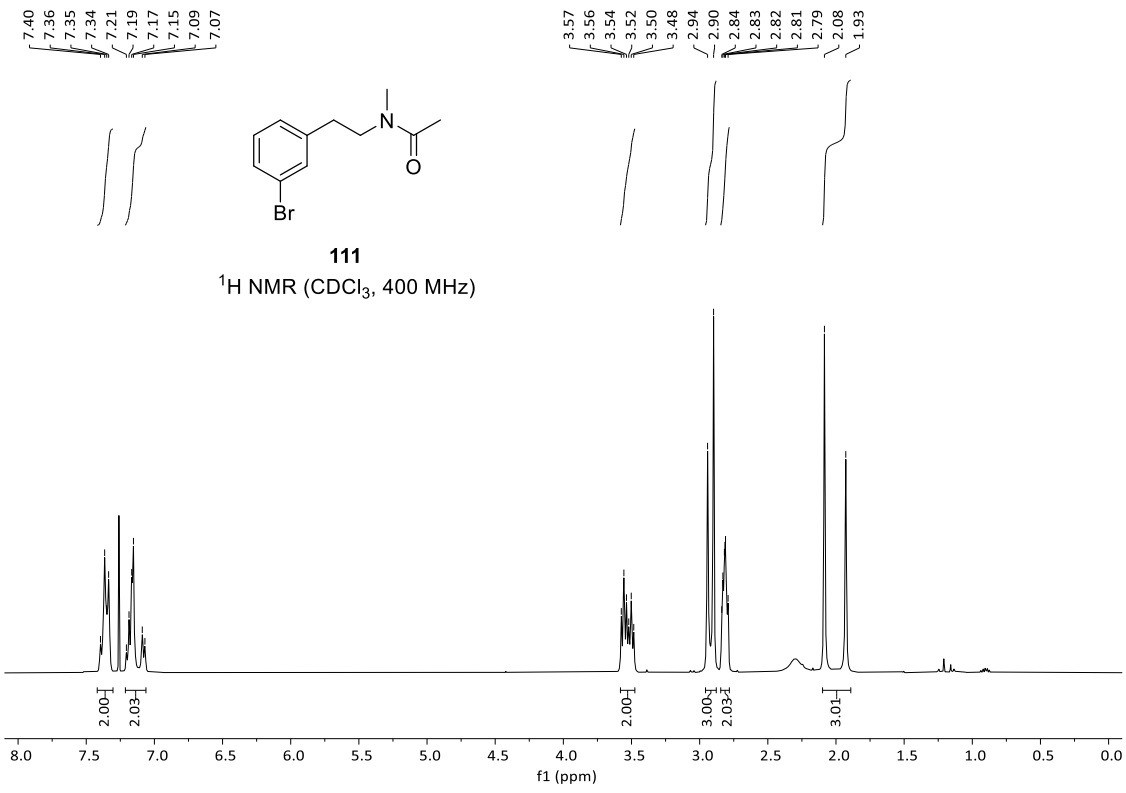

111

^{1}H NMR ($CDCl_3$, 400 MHz)

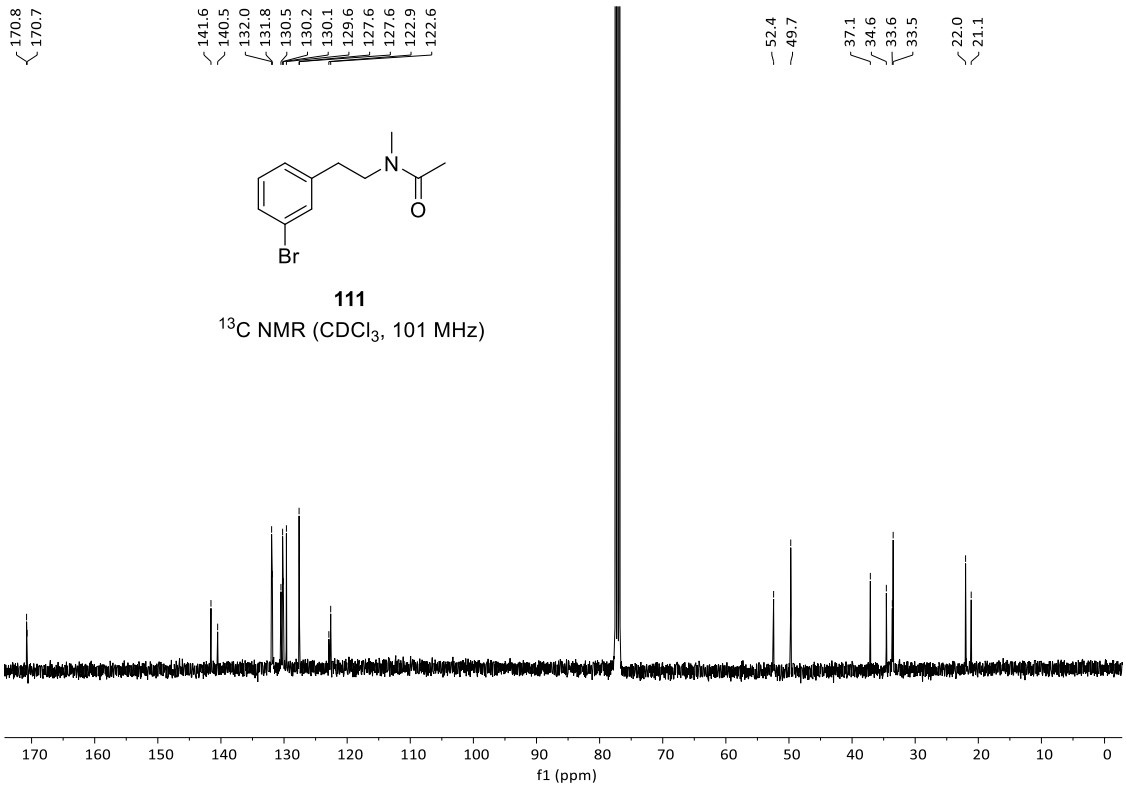

111

^{13}C NMR ($CDCl_3$, 101 MHz)

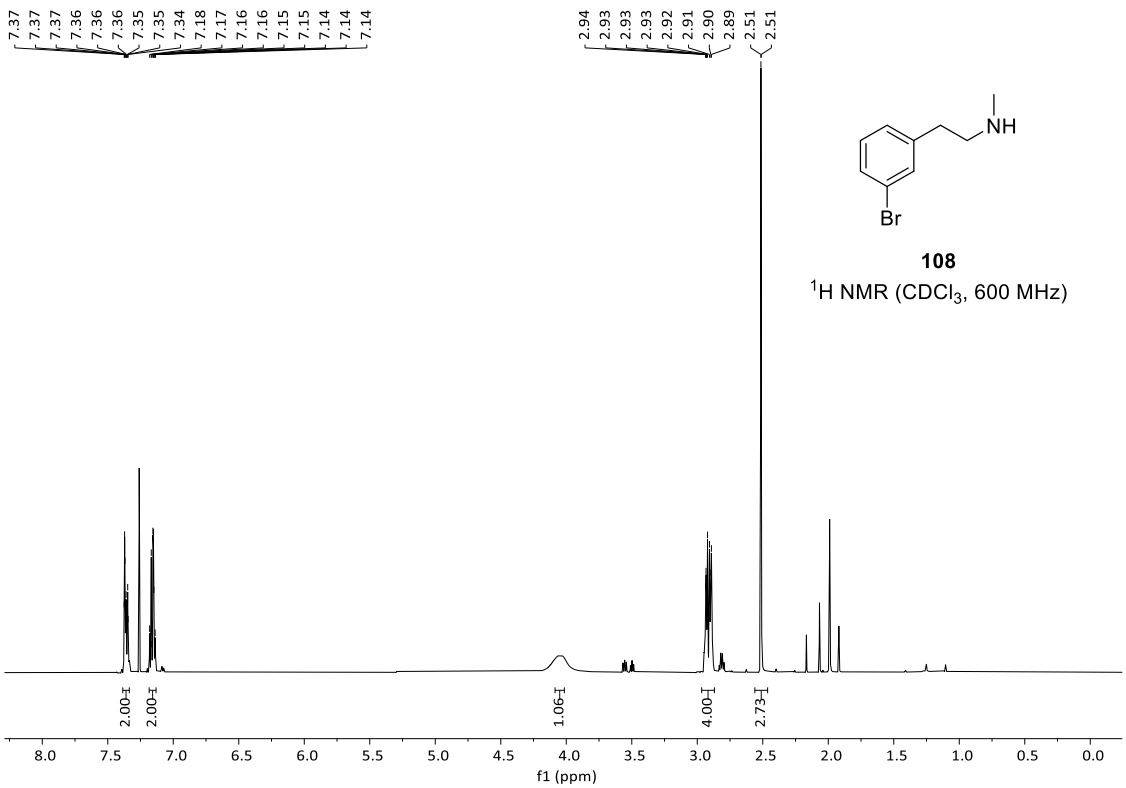

108

^{1}H NMR ($CDCl_3$, 600 MHz)

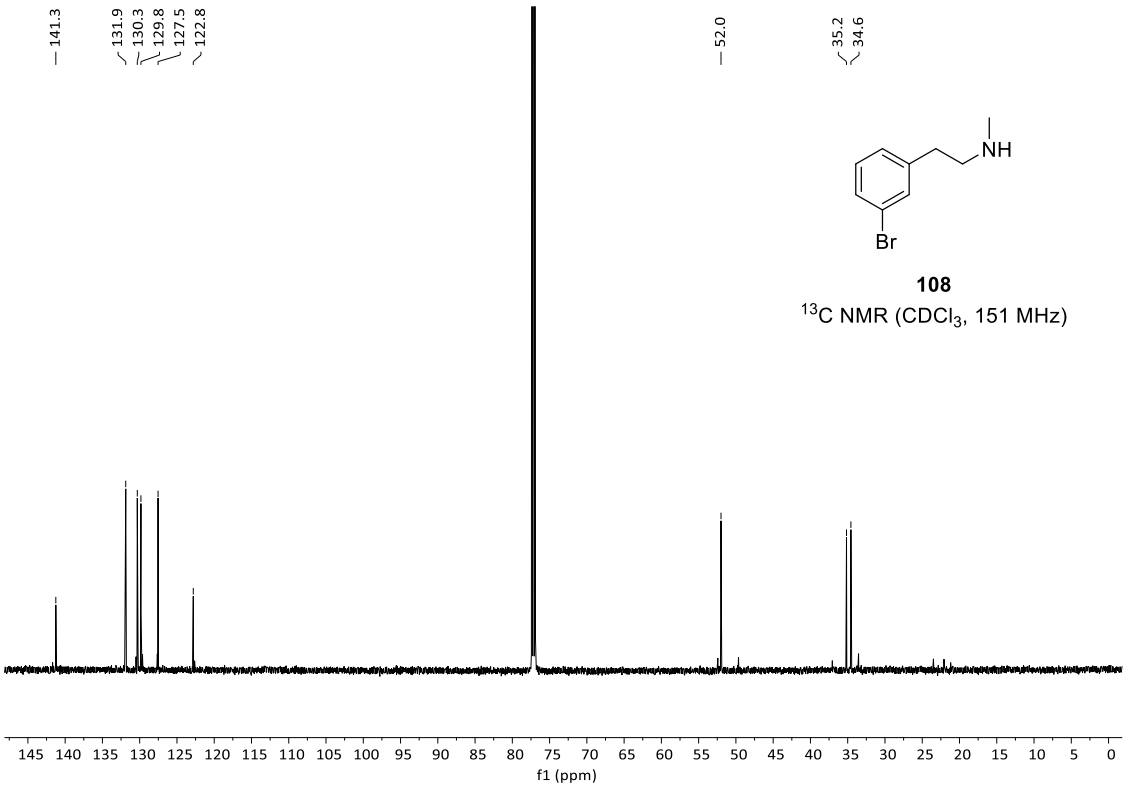

108

^{13}C NMR ($CDCl_3$, 151 MHz)

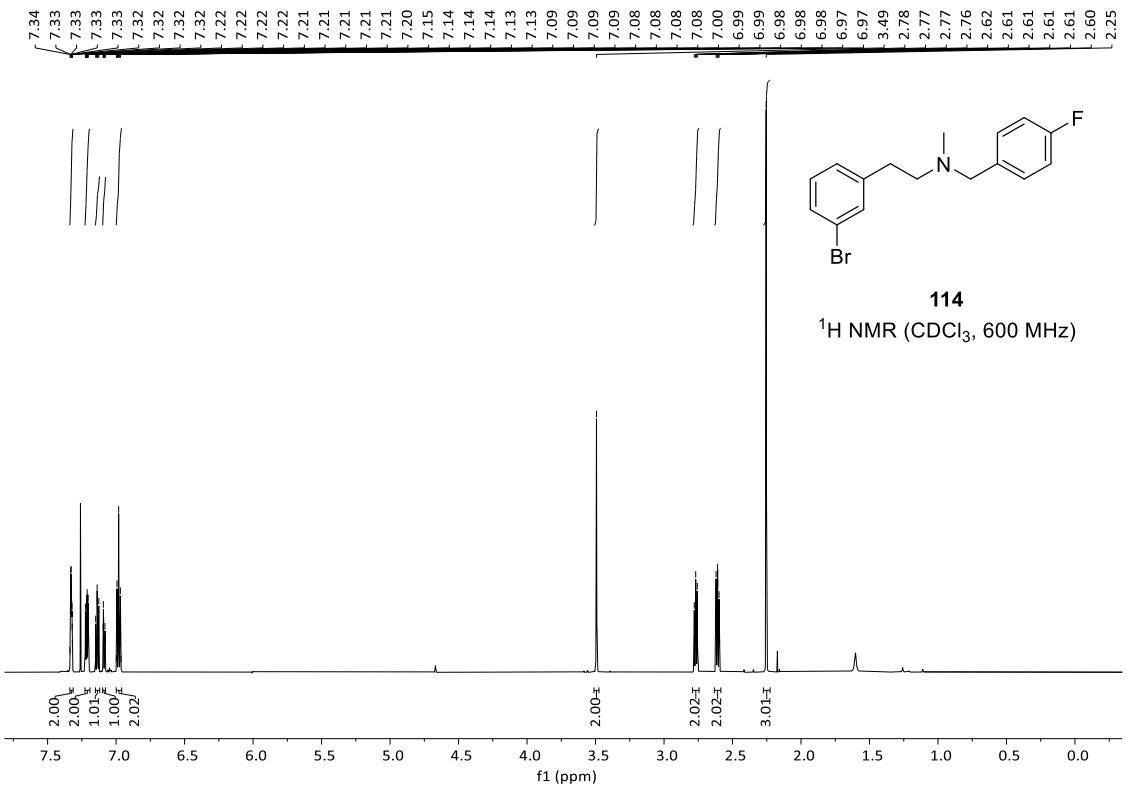

114

^{1}H NMR ($CDCl_3$, 600 MHz)

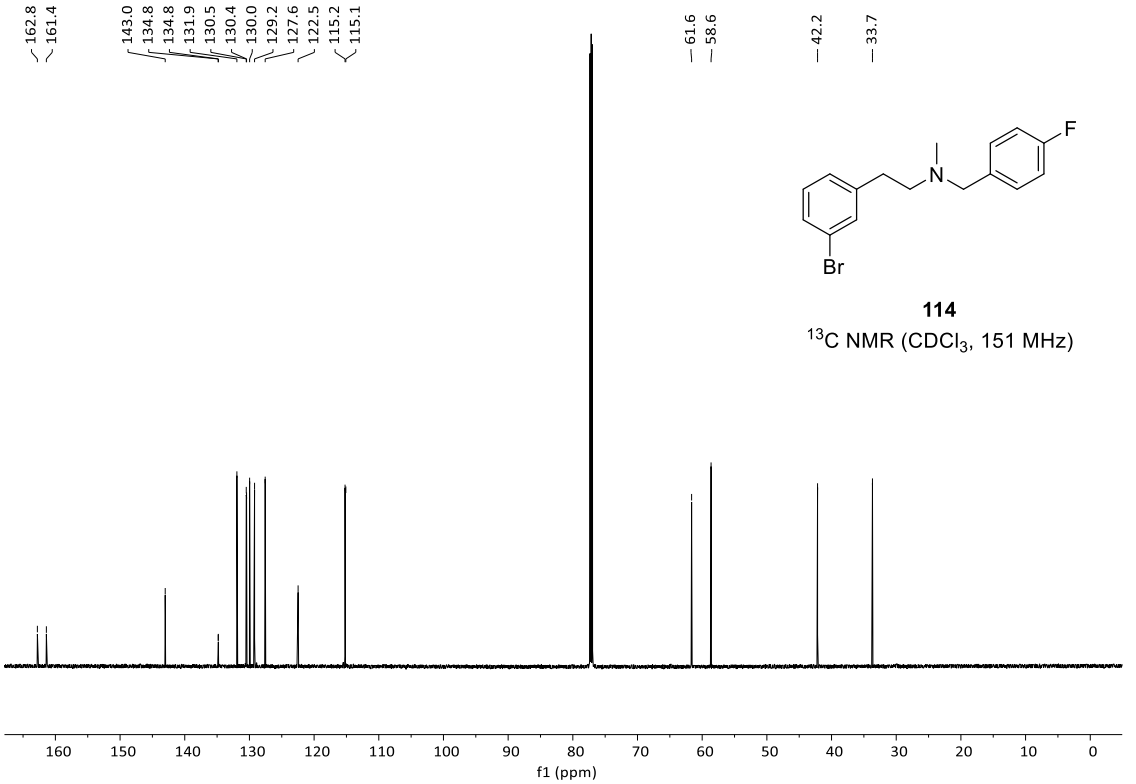

114

^{13}C NMR ($CDCl_3$, 151 MHz)

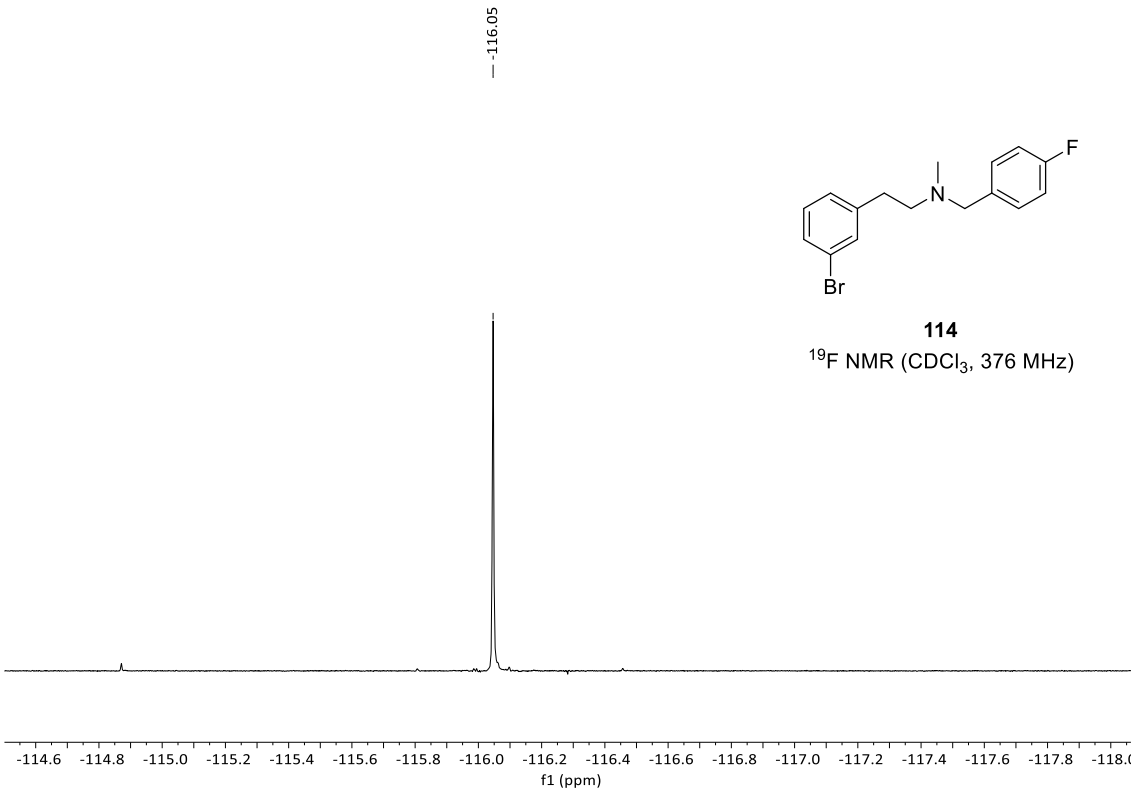

114

^{19}F NMR ($CDCl_3$, 376 MHz)

EC_{50} Data

Activity of 32a against L. major, L. amazonensis, and L. mexicana

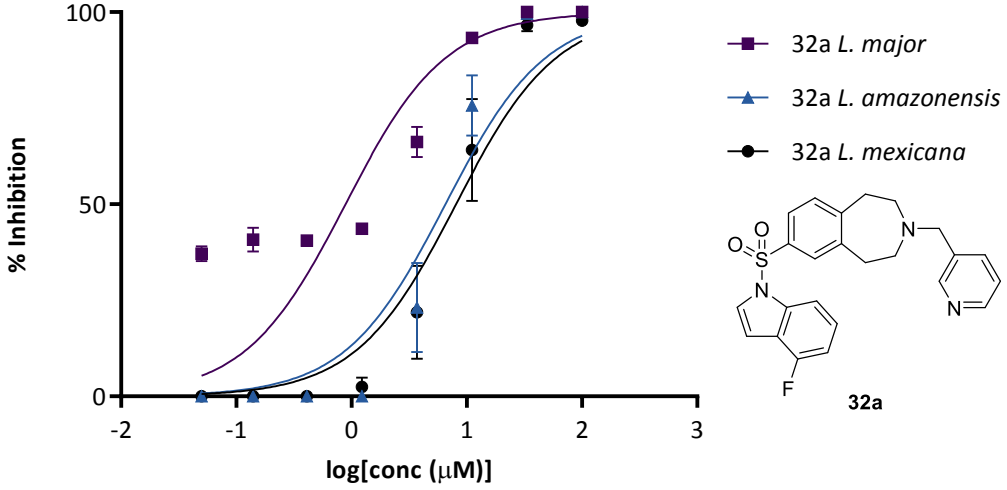

Activity of 33a against L. major, L. amazonensis, and L. mexicana

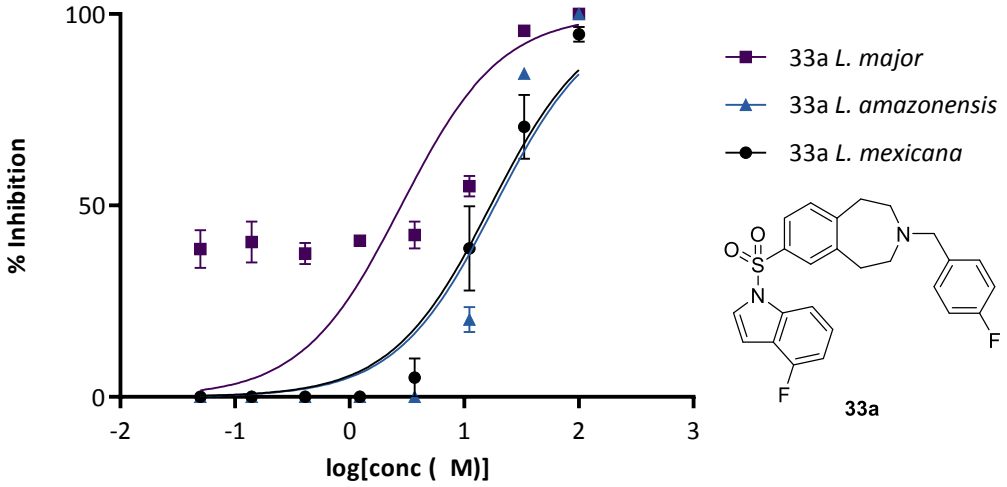

Activity of 56 against L. major, L. amazonensis, and L. mexicana

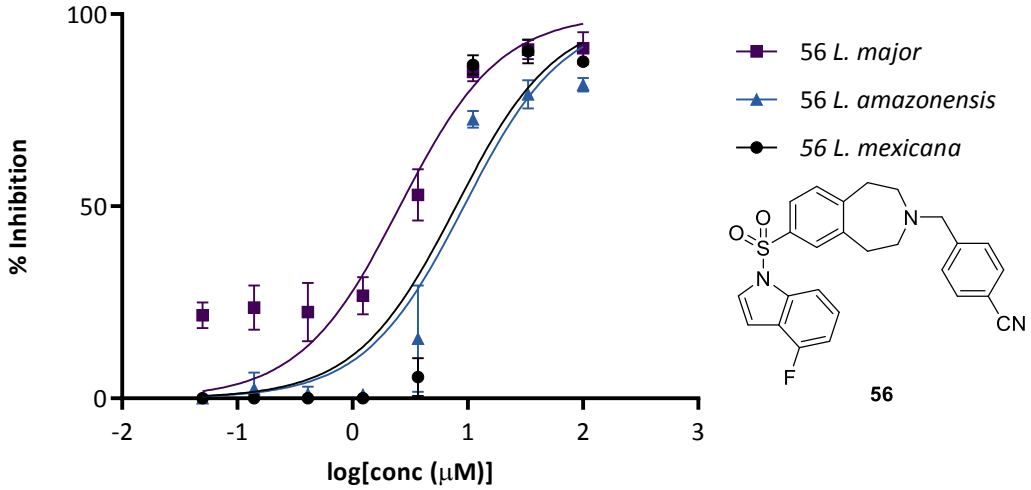

Activity of 74 against L. major, L. amazonensis, and *L. mexicana*

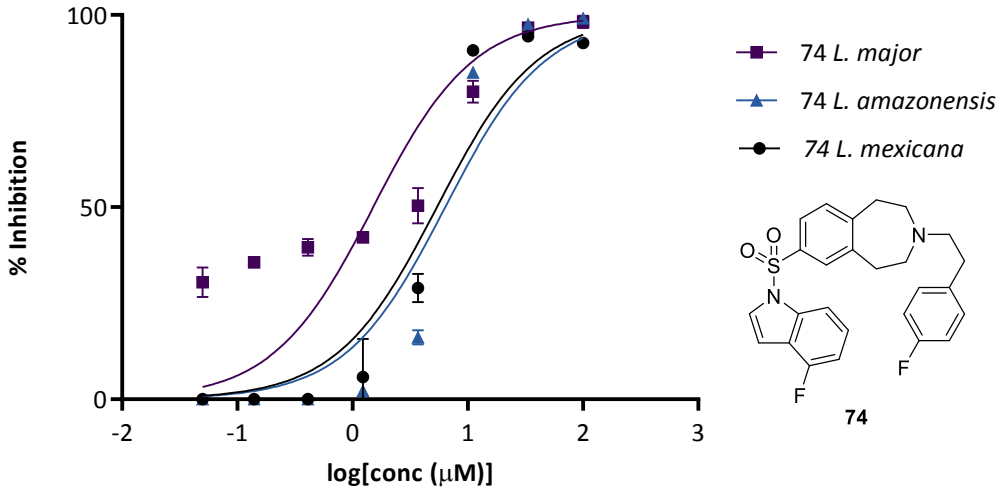

Activity of 70 against *L. major, L. amazonensis,* and *L. mexicana*

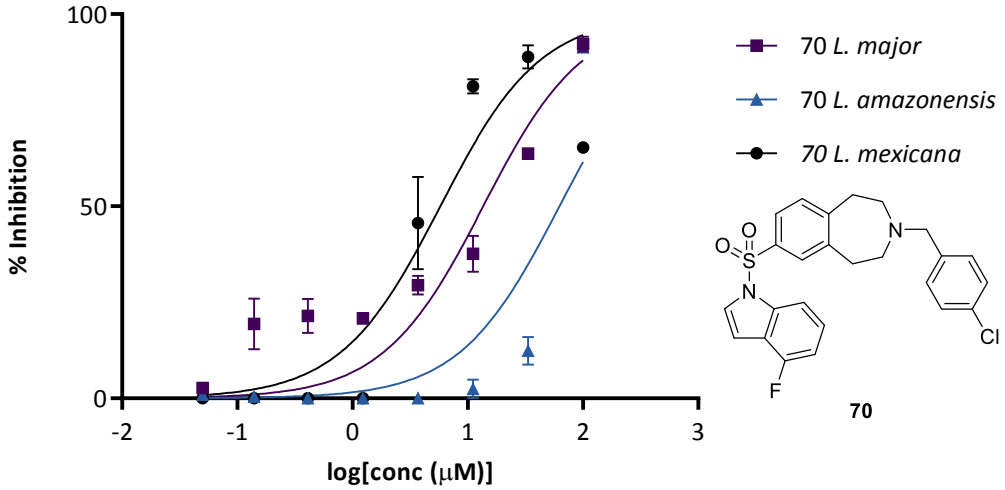

70

Activity of 66 against *L. major, L. amazonensis,* and *L. mexicana*

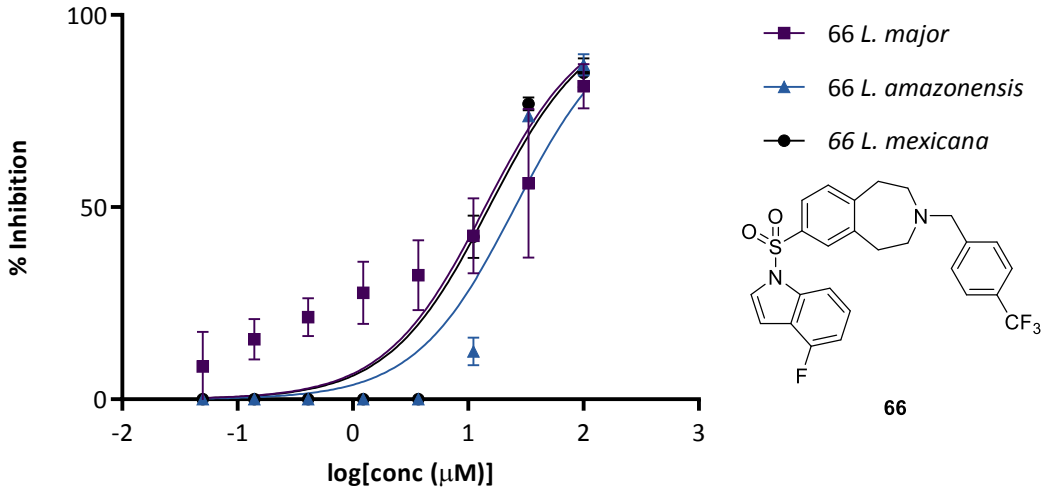

66

Activity of 69 against *L. major, L. amazonensis,* and *L. mexicana*

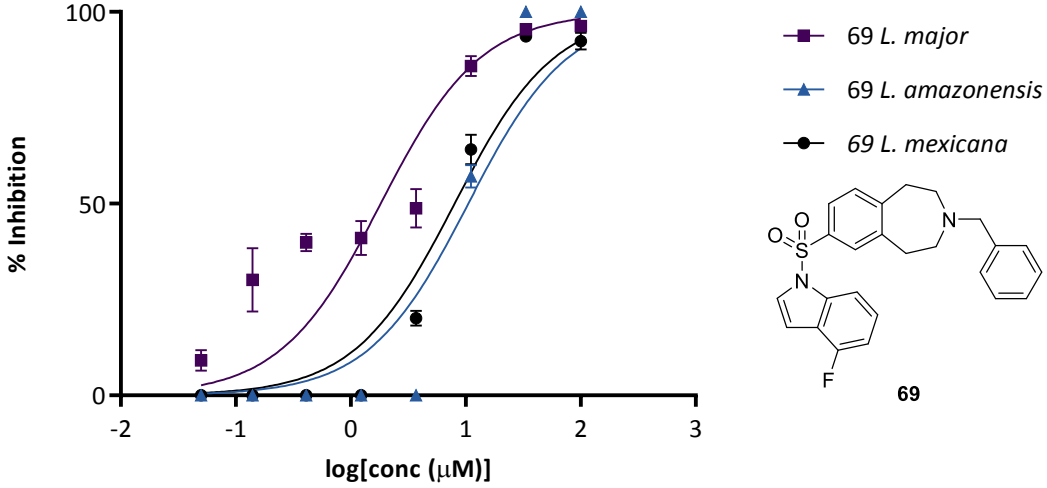

Activity of 65 against *L. major, L. amazonensis,* and *L. mexicana*

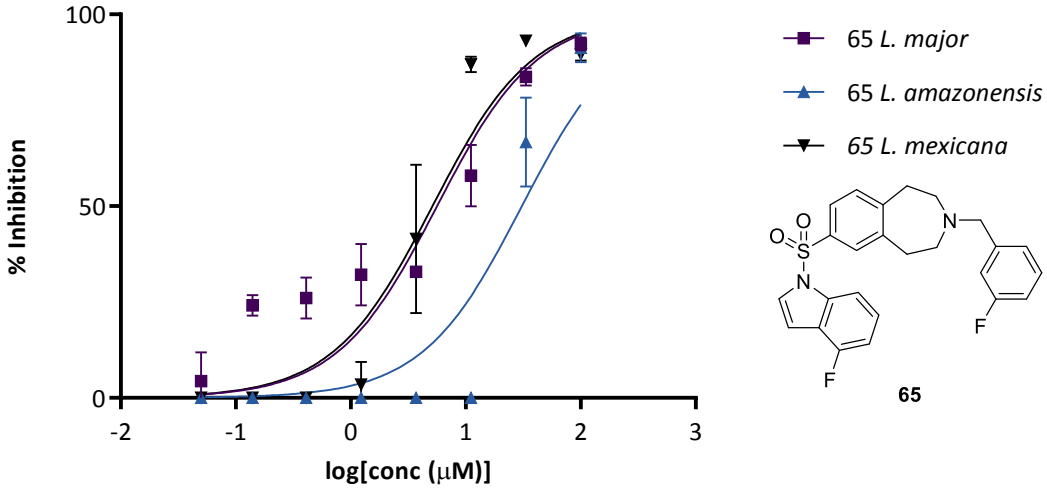

Activity of 67 against *L. major, L. amazonensis*, and *L. mexicana*

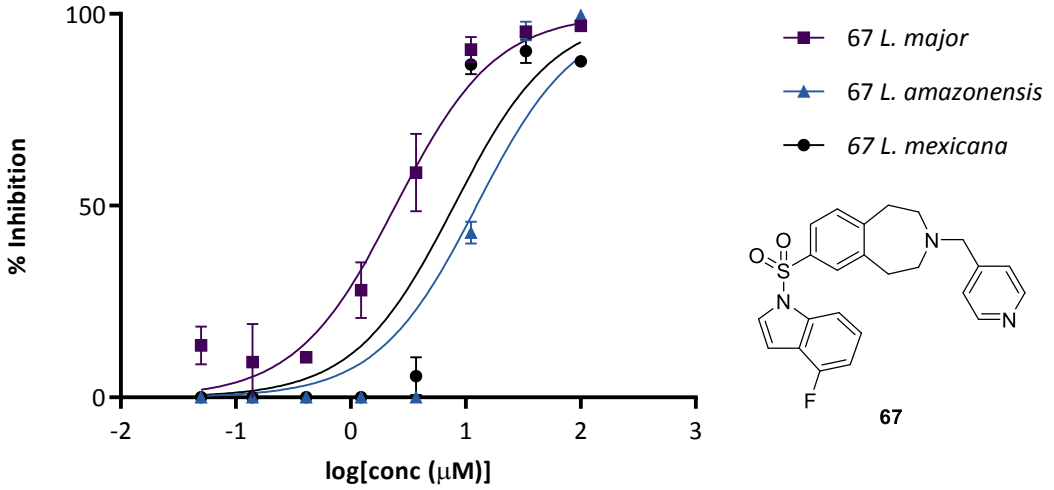

67

Activity of 71 against *L. major, L. amazonensis,* and *L. mexicana*

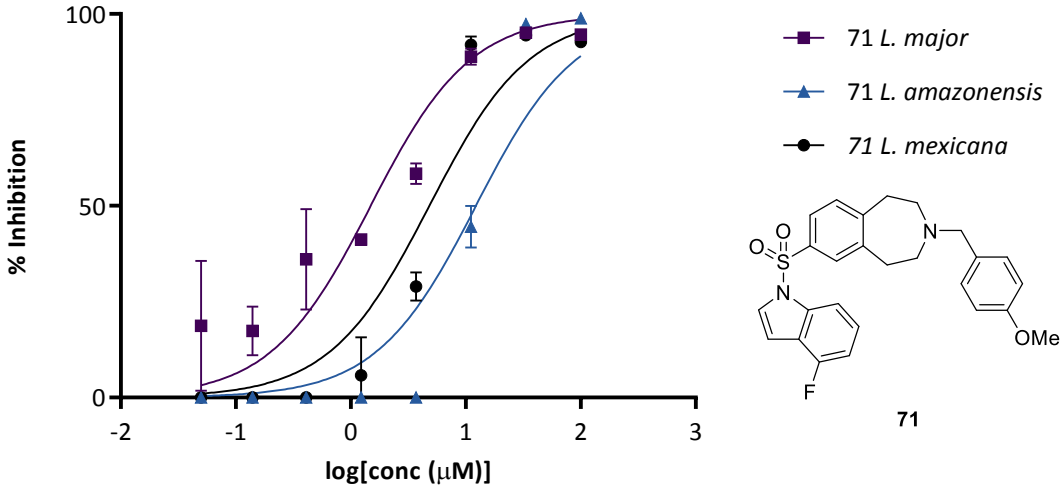

71

Activity of 68 against *L. major, L. amazonensis,* and *L. mexicana*

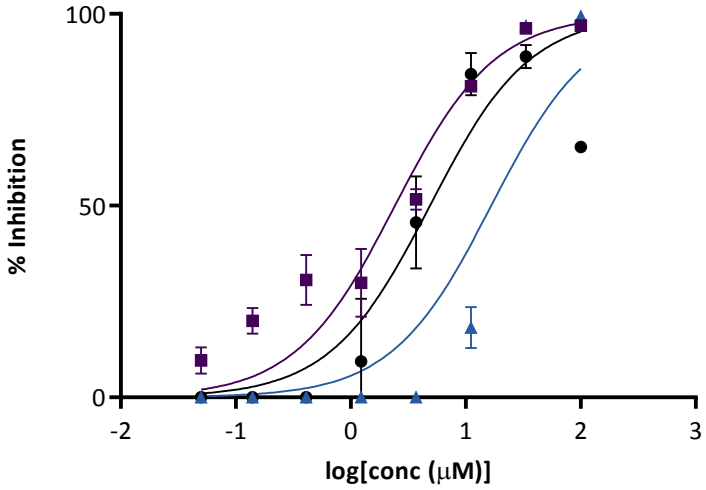

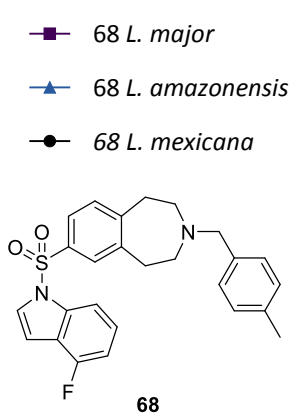

68

Activity of 93 against *L. major and L. amazonensis*

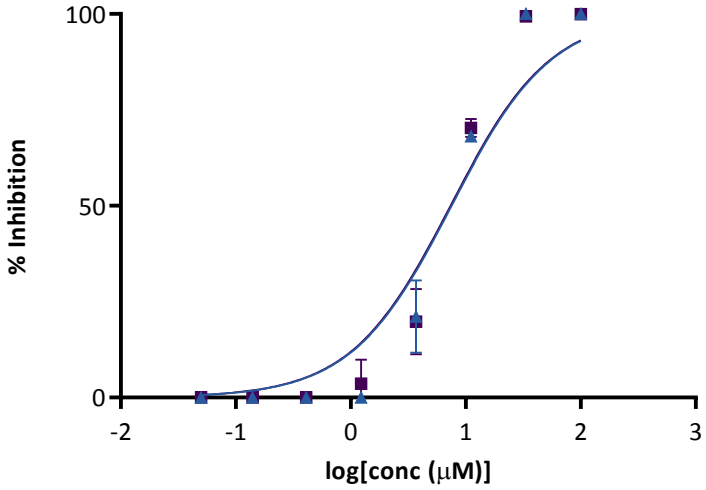

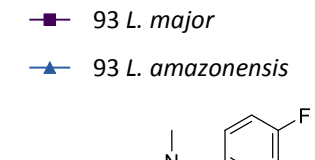

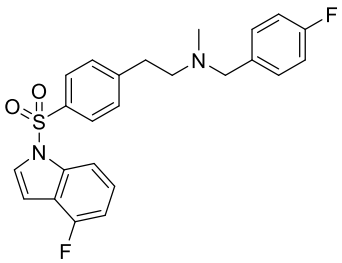

93

Activity of 92 against *L. major and L. amazonensis*

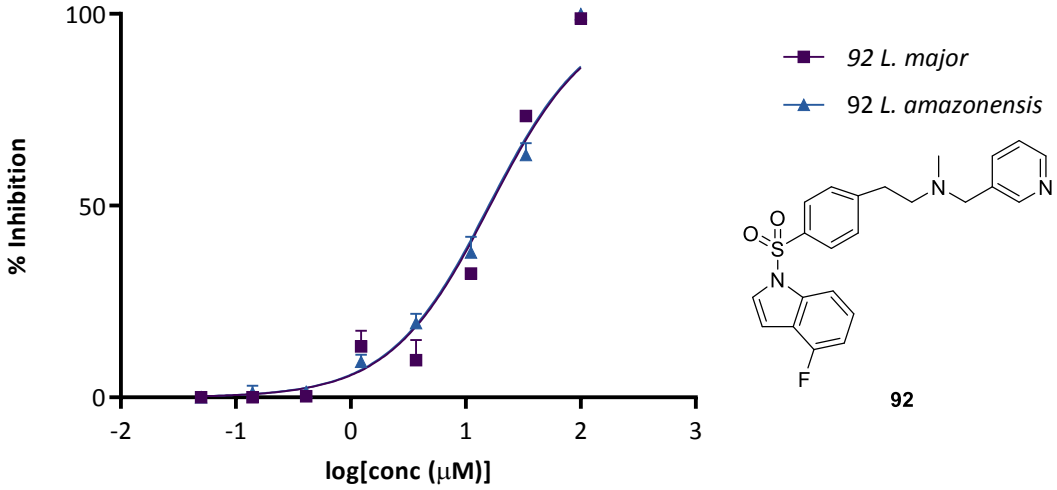

92

Activity of 94 against *L. major and L. amazonensis*

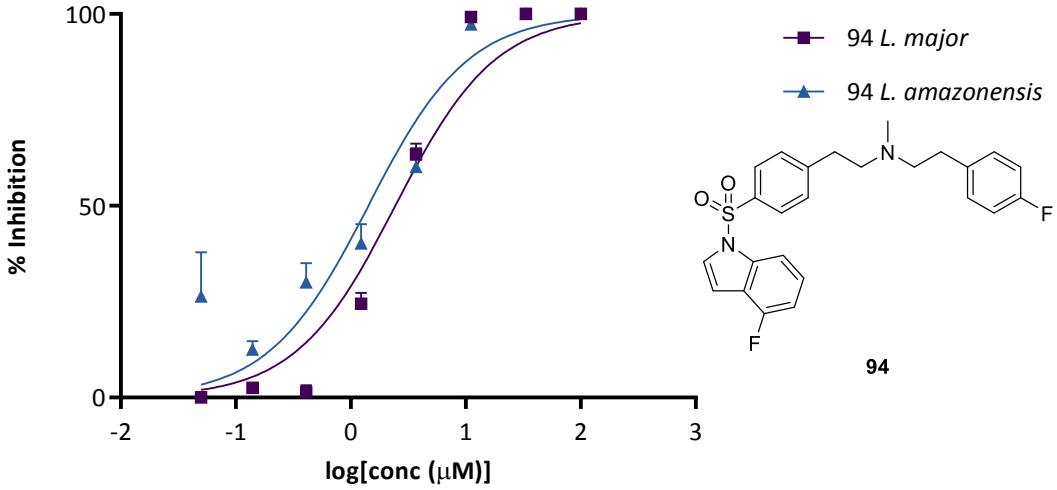

94

Activity of 96 against *L. major and L. amazonensis*

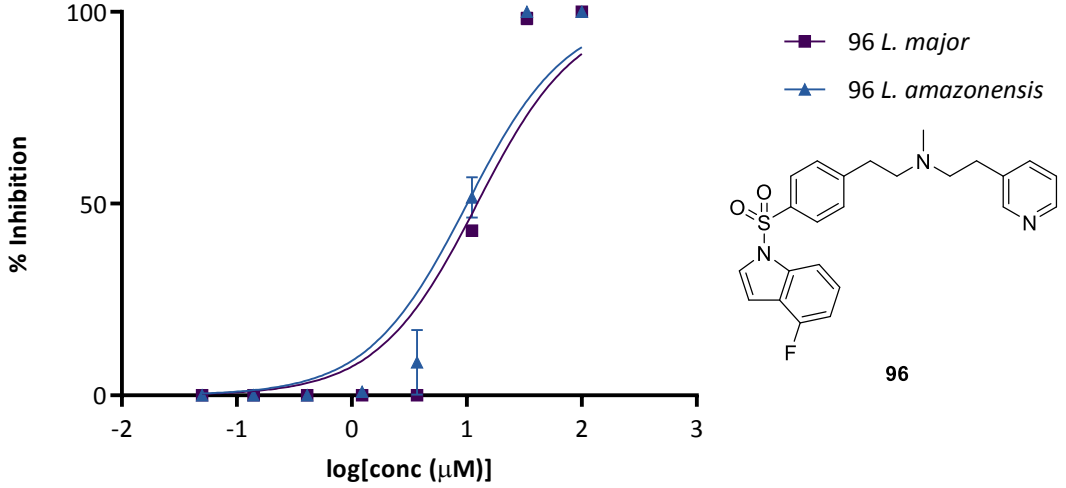

96

Activity of 95 against *L. major and L. amazonensis*

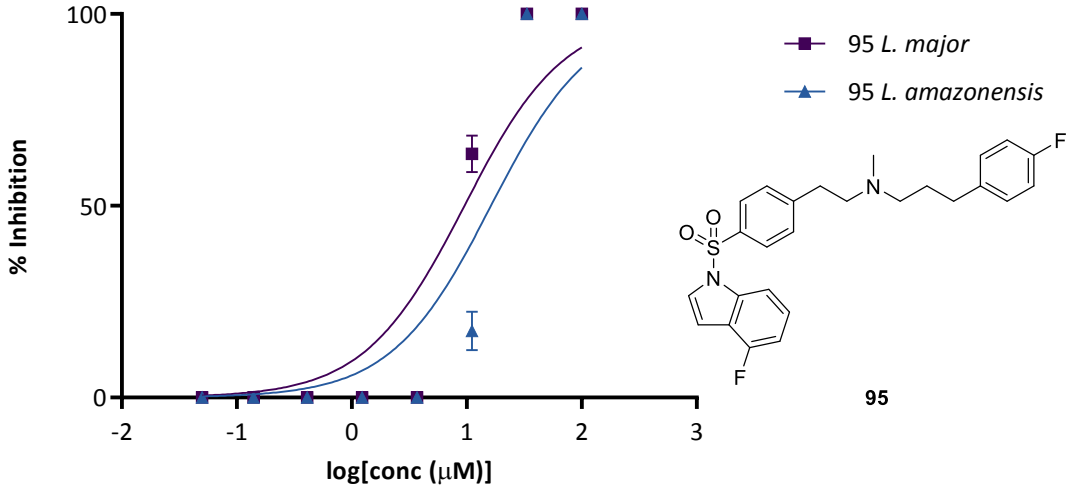

95

Activity of 97 against *L. major and L. amazonensis*

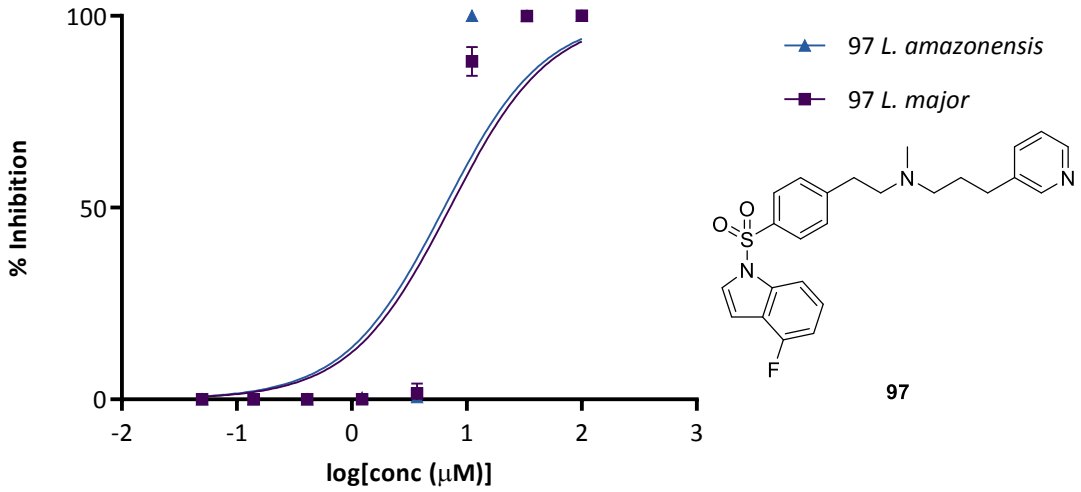

97

Activity of 33a against *L. major* WT, *ΔLCB2*, and *pX* promastigotes

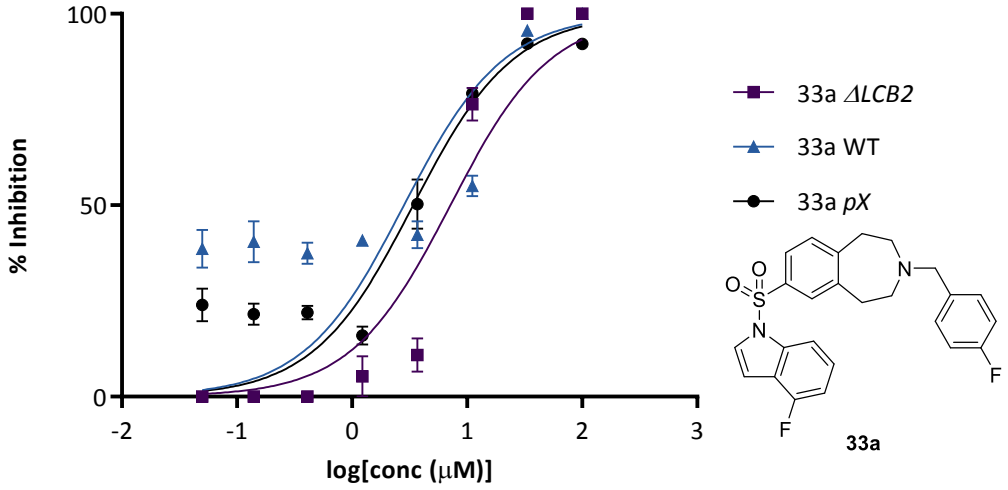

33a

Activity of 32a against *L. major* WT, Δ*LCB2*, and *pX* promastigotes

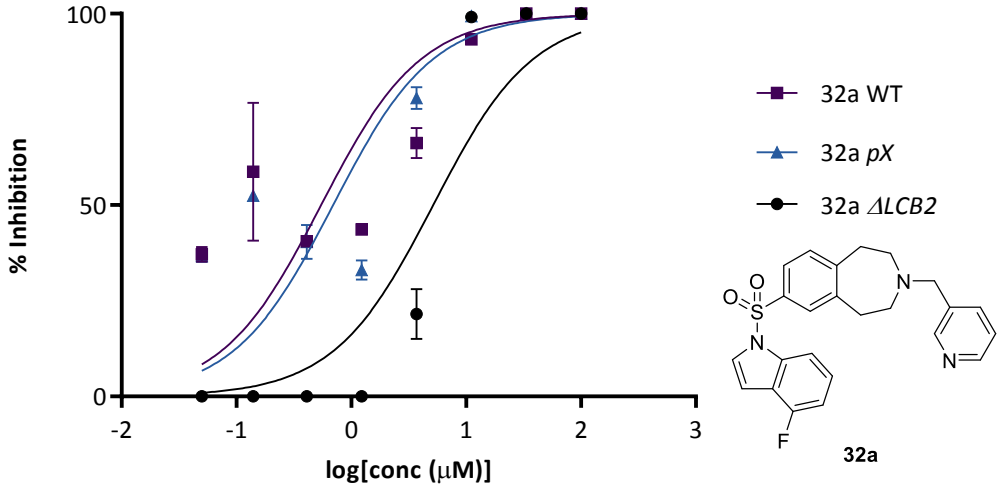

Activity of 74 against *L. major* WT, Δ*LCB2*, and *pX* promastigotes

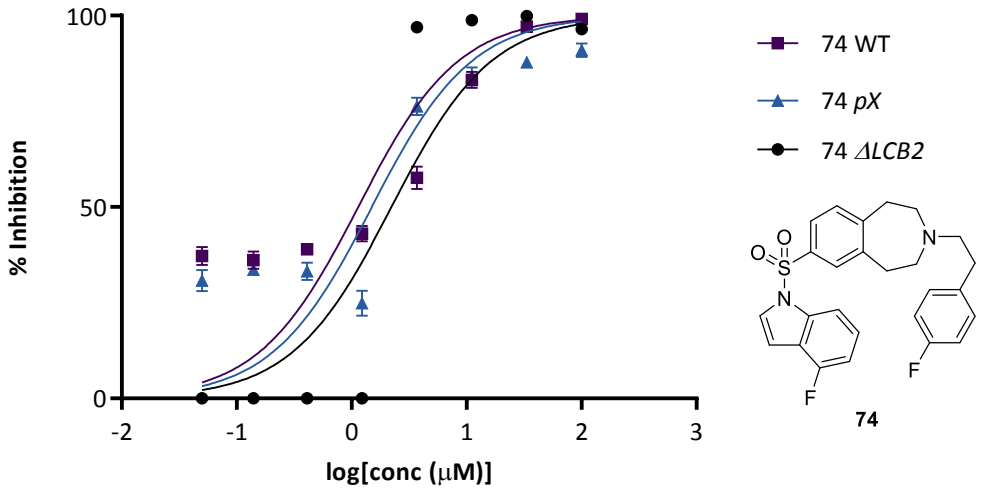

Activity of 71 against *L. major* WT, ◢*LCB2*, and *pX* promastigotes